A posteriori error estimates and stopping criteria for solvers using the domain decomposition method and with local time stepping

Sarah Ali Hassan

THÈSE

présenté à

L'UNIVERSITÉ PIERRE ET MARIE CURIE-PARIS 6

École doctorale : Sciences Mathématiques de Paris Centre (ED 386)

Par

Sarah ALI HASSAN

Pour obtenir le grade de

DOCTEUR de l'UNIVERSITÉ PIERRE ET MARIE CURIE-PARIS 6

Spécialité : Mathématiques Appliquées

Estimations d'erreur a posteriori et critères d'arrêt pour des solveurs par décomposition de domaine et avec des pas de temps locaux

Directeur de thèse : Martin VOHRALÍK

Co-directeurs de thèse : Caroline JAPHET et Michel KERN

Soutenue le : 26 juin 2017

Devant la commission d'examen formée de :

M. Emmanuel CREUSÉ	Université Lille 1	Rapporteur
M. Jan Martin NORDBOTTEN	Université de Bergen	Rapporteur
M. Frédéric NATAF	Université Paris VI	Président du jury
M. Laurent LOTH	ANDRA	Examinateur
M. Pascal OMNES	CEA	Examinateur
Mme Caroline JAPHET	Université Paris XIII	Co-directeur de thèse
M. Michel KERN	Inria Paris	Co-directeur de thèse
M. Martin VOHRALÍK	Inria Paris	Directeur de thèse

DOCTORAL DISSERTATION

presented at

UNIVERSITY OF PIERRE AND MARIE CURIE-PARIS 6

Doctoral school: Mathematical Sciences of Central Paris (ED 386)

By

Sarah ALI HASSAN

To obtain the degree of

DOCTOR of UNIVERSITY PIERRE AND MARIE CURIE-PARIS 6

Speciality: Applied Mathematics

A posteriori error estimates and stopping criteria for solvers using the domain decomposition method and with local time stepping

Thesis advisor: Martin VOHRALÍK

Thesis co-advisors: Caroline JAPHET and Michel KERN

Defended on: June 26th, 2017

In front of the examination committee consisting of:

M. Emmanuel CREUSÉ	The University of Lille 1	Reviewer
M. Jan Martin NORDBOTTEN	The University of Bergen	Reviewer
M. Frédéric NATAF	The University of Paris VI	Chairman
M. Laurent LOTH	ANDRA	Examiner
M. Pascal OMNES	CEA	Examiner
Mme Caroline JAPHET	The University of Paris XIII	Thesis co-advisor
M. Michel KERN	Inria Paris	Thesis co-advisor
M. Martin VOHRALÍK	Inria Paris	Thesis advisor

Résumé

Cette thèse développe des estimations d'erreur a posteriori et critères d'arrêt pour les méthodes de décomposition de domaine avec des conditions de transmission de Robin optimisées entre les interfaces. Différents problèmes sont considérés: l'équation de Darcy stationnaire puis l'équation de la chaleur, discrétisées par les éléments finis mixtes avec un schéma de Galerkin discontinu de plus bas degré en temps pour le second cas. Pour l'équation de la chaleur, une méthode de décomposition de domaine globale en temps, avec mêmes ou différents pas de temps entre les différents sous domaines, est utilisée. Ce travail est finalement étendu à un modèle diphasique en utilisant une méthode de volumes finis centrés par maille en espace. Pour chaque modèle, un problème d'interface est résolu itérativement, où chaque itération nécessite la résolution d'un problème local dans chaque sous-domaine, et les informations sont ensuite transmises aux sous-domaines voisins. Pour les modèles instationnaires, les problèmes locaux dans les sous-domaines sont instationnaires et les données sont transmises par l'interface espace-temps.

L'objectif de ce travail est, pour chaque modèle, de borner l'erreur entre la solution exacte et la solution approchée à chaque itération de l'algorithme de décomposition de domaine. Différentes composantes d'erreur en jeu de la méthode sont identifiées, dont celle de l'algorithme de décomposition de domaine, de façon à définir un critère d'arrêt efficace pour cette méthode. En particulier, pour l'équation de Darcy stationnaire, on bornera l'erreur par un estimateur de décomposition de domaine ainsi qu'un estimateur de discrétisation en espace. On ajoutera à la borne de l'erreur un estimateur de discrétisation en temps pour l'équation de la chaleur et pour le modèle diphasique. L'estimation a posteriori répose sur des techniques de reconstructions de pressions et de flux conformes respectivement dans les espaces H^1 et $\mathbf{H}(\mathrm{div})$ et sur la résolution de problèmes locaux de Neumann dans des bandes autour des interfaces de chaque sous-domaine pour les flux. Ainsi, des critères pour arrêter les itérations de l'algorithme itératif de décomposition de domaine sont développés. Des simulations numériques pour des problèmes académiques ainsi qu'un problème plus réaliste basé sur des données industrielles sont présentées pour illustrer l'efficacité de ces techniques. En particulier, différents pas de temps entre les sous-domaines sont considérés pour cet exemple.

Mots-clés : Écoulement et transport en milieu poreux, éléments finis mixtes, décomposition de domaine en espace, décomposition de domaine globale en temps, discrétisation conforme et non-conforme en temps, pas de temps locaux, conditions d'interface de Robin, estimation d'erreur a posteriori, critère d'arrêt, problème local de Neumann

Abstract

This work contributes to the developpement of a posteriori error estimates and stopping criteria for domain decomposition methods with optimized Robin transmission conditions on the interface between subdomains. We study several problems. First, we tackle the steady diffusion equation using the mixed finite element subdomain discretization. Then the heat equation using the mixed finite element method in space and the discontinuous Galerkin scheme of lowest order in time is investigated. For the heat equation, a global-in-time domain decomposition method is used for both conforming and nonconforming time grids allowing for different time steps in different subdomains. This work is then extended to a two-phase flow model using a finite volume scheme in space. For each model, the multidomain formulation can be rewritten as an interface problem which is solved iteratively. Here at each iteration, local subdomain problems are solved, and information is then transferred to the neighboring subdomains. For unsteady problems, the subdomain problems are time-dependent and information is transferred via a space-time interface.

The aim of this work is to bound the error between the exact solution and the approximate solution at each iteration of the domain decomposition algorithm. Different error components, such as the domain decomposition error, are identified in order to define efficient stopping criteria for the domain decomposition algorithm. More precisely, for the steady diffusion problem, the error of the domain decomposition method and that of the discretization in space are estimated separately. In addition, the time error for the unsteady problems is identified. Our a posteriori estimates are based on the reconstruction techniques for pressures and fluxes respectively in the spaces H^1 and $\mathbf{H}(\mathrm{div})$. For the fluxes, local Neumann problems in bands arround the interfaces extracted from the subdomains are solved. Consequently, an effective criterion to stop the domain decomposition iterations is developed. Numerical experiments, both academic and more realistic with industrial data, are shown to illustrate the efficiency of these techniques. In particular, different time steps in different subdomains for the industrial example are used.

Keywords: Flow and transport in porous media, mixed finite element method, domain decomposition in space, global-in-time domain decomposition, conforming and nonconforming time grids, local time steps, Robin interface conditions, a posteriori error estimate, stopping criteria, local Neumann problem

Acknowledgements

First and foremost I would like to thank God, for providing me with the strength to carry out this thesis, and without whose blessings I could never have completed it. Thank you for everything and the fact that I am now here to acknowledge the people to whom I am deeply indebted for their direct or indirect contributions to this work.

I would like to say a big thank you to Luís Neves de Almeida, the director of the Mathematics applied to Biological and Medical Sciences Master's course at Paris 6, and who was my supervisor during my master internship. He is the one who encouraged me to contact Martin Vohralík to do a Ph.D thesis.

I owe my deepest gratitude to my supervisor Martin Vohralík, director of the Serena team at INRIA Paris. It has been an honor, as well as a pleasure, to work with you. Thank you, Martin, for the continuous and excellent guidance, patience, ideas, and immense knowledge that you gave me thoughout my Ph.D.

I would like to express my warmest gratitude to my co-supervisor, Caroline Japhet, especially for sharing her specialist knowledge of the domain decomposition method and for the continuous support and optimism she gave me. This thesis would have been so much more difficult to complete without you, Caroline.

I would also like to thank Michel Kern, my co-supervisor for the useful discussions we had, and the help he provided during the CEMRACS summer school, which led to the fourth chapter of this thesis.

I am very grateful to ANDRA, the French national radioactive waste management agency, who funded this thesis over three years.

Three years ago, I would never have imagined that I would be capable of writing my thesis in English. That I was able to do so is largely due to the efforts of Richard James, and I would like offer him my special thanks.

I cannot fail to mention here, the valuable contribution Elyes Ahmed made to the fourth chapter, at the CEMRACS summer school. Thanks Elyes!

I would like to acknowledge all the members of Pomdapi team, which later became the Serena team, who provided such a friendly atmosphere at work: Jean E. Roberts, Jérôme Jaffré, François Clément, Pierre Weis, Géraldine Pichot, Vincent Martin, Iain Smears, Fatma Cheikh, Nabil Birgle, Mohamed Hedi Riahi, Émilie Joannopoulos, Clément Franchini. Special thanks goes to Zuki Tang with whom I shared an office at Inria Rocquencourt, and another special thanks goes to Jad Dabaghi, Patrik Daniel, and Khadija Talali with whom I shared an office (as well as a lot of food!) at Inria Paris. Thanks for the help of our team assistants, who supported me during my thesis, Nathalie Bonte, Cindy Crossouard, Virginie Collette, and Kevin Bonny.

My family's support has played a major role...

I would like to thank my mother-in-law, Mariam, for her encouragement and her prayers. Please, accept my thanks! I would also thank my father-in-law Houssein, Ayat, Mouhamad, and Karim for their kindness. Your kind wishes mean a great deal to me.

I'd like to thank my grandparents "Jedo" Mahmoud and "Teta" Najwa for their love, and my grandmother's non-stop questioning, for the last three years, about when I will finish. I wonder what she is going to ask about, now i have in fact finished.

I express my special thanks to my two lovely brothers Ali and Moustapha and Moustapha's wife Zaineb and their lovely little daughter Sarah. Thank you for your constant support and encouragement.

My lovely patient husband, dear Mayssam, I owe you thanks for all the years you have been by my side and always believed in me. I am very thankful that I have you in my life and appreciate all you have done for me. Without your love, presence, support, comfort, understanding, guidance, prayers, and encouragement, this thesis would not have been possible. My gratitude and deepest appreciation go to you, Mayssam.

My beloved parents, Mum Zeinab Chahine and Dad Mehdi Ali Hassan, I am forever indebted to you, for all the continuous love, support, sacrifices, prayers, and encouragement that you have given me throughout my life, to make me the person I am today. I am eternally grateful you, Mum and Dad.

Mum, thank you for coming to Paris twice to support me, and once for my defense. Thank you also for the delicious strawberry jam and Za'atar you made for me. The best moments in my life are when you are beside me. Because I have you, Mum, I have everything.
Dad, you told me, "Never be afraid because you are my daughter." Dad you knew that I could achieve this thesis, and you already prepared my gift for this day. Now I have finished, I want to thank you for being my rock, and for asking me to send you my programming code to find the bug when I had one. I remember how we laughed because we both knew that you, never having written any code, wouldn't ever find it!

Mum, Dad, Mayssam, and I followed and shared the same dream. This thesis was really done by all four of us together. Mum, Mayssam, and I dedicate this thesis to you Dad, the most special person in our life...

For

Mehdi Moustapha Ali Hassan

(as you always like to sign your name)

Contents

List of Figures

List of Tables

Introduction

Motivation

Radioactive materials are nowadays used for scientific research, electricity production, in medecine, in national defense, and in many other fields. All these activities produce radioactive waste. An important question is how to dispose radioactive waste safely and without overwhelming cost for future generations?

The radioactive waste must be confined and isolated until the radioactivity has decayed to a level that no longer poses a threat to the environment. ANDRA, the french national radioactive waste management agency, (l'Agence nationale pour la gestion de déchets radioactifs), which funded this thesis, is a public institution founded in 1991. The purpose of this agency is to ensure a safe long-term management of all radioactive waste produced in France. In order to provide safe nuclear waste management solutions, ANDRA classifies this waste according two main criteria:

- First, the level of activity (quantity of radiation), classified in 4 levels: very low level, low level, intermediate level, high level.
- Second, the period of radioactivity, which can be from a few seconds to hundreds of thousands of years. Here the waste is classified in 2 levels: short lived (31 years or less) and long lived (more than 31 years).

Cigéo (Centre industriel de stockage géologique), the industrial centre of geological storage founded by ANDRA, is a deep repository for long lived and high level radioactive waste, see Figure 1 for more details of the site (figure from www.anfra.fr). The waste is first encapsulated in sealed steel casks, see Figure 2, and then stored in underground areas, about 500 meters deep, in geologically stable formations, embedded in an impermeable clay layer so that the radioactive waste will remain isolated for hundreds of thousands of years. Until now, this deep storage has been the only long-term solution for managing this type of high level waste without putting the environment at risk.

One of the most important issues for storing nuclear waste is water resource management, since water may corrode the sealed steel casks and create a risk of leakage and underground pollution. For this reason ANDRA carries out simulations to predict the behavior of nuclear waste underground over periods of thousands of years to monitor the state of casks over time. More precisely, ANDRA has to perform many numerical simulations to quantify flow and solute transfer from the repository to the surrounding geological environment. Simulations have to take into account many physical processes with different space-time scales: from the waste packages to the geological

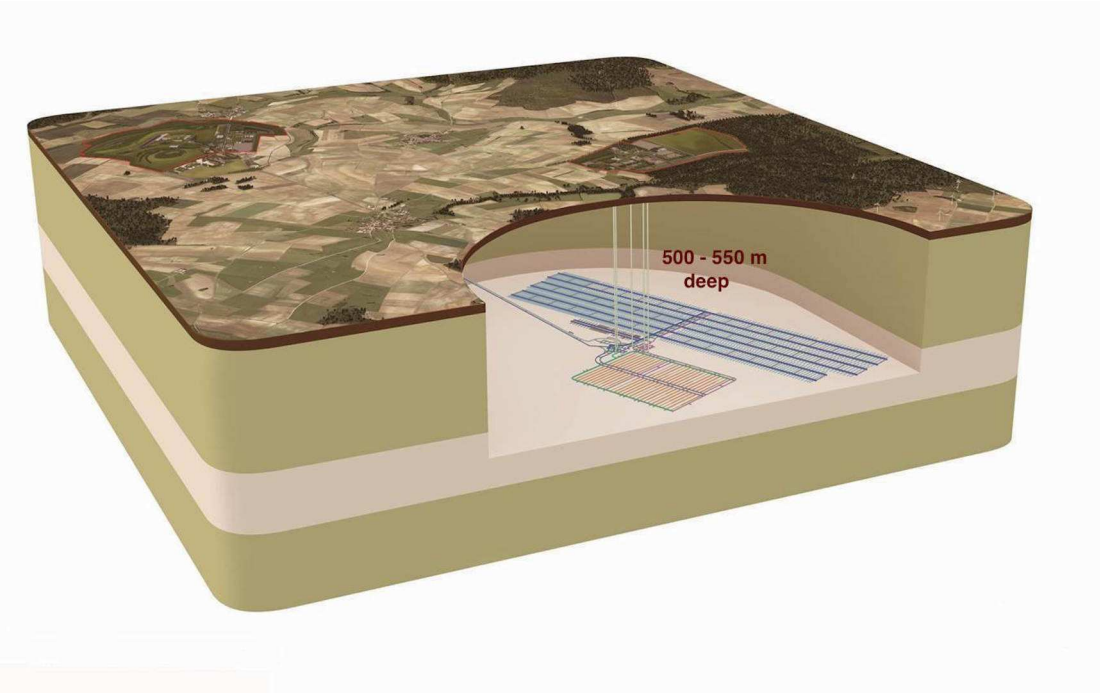

Figure 1: View of the installations of the Cigéo projet (approximately $5\text{km}^2 \times 5\text{km}^2$ underground zone)

media (from centimeters to tens of kilometers) on very large time (up to one million years).
In this work, we aim to simulate different types of flow in porous media, which is of great importance to ANDRA. The mathematical models used for the simulations are introduced in the next section.

Mathematical models

We consider mathematical models for a single phase and simplified two-phase fluid flow in porous media, (see e.g. [19, 48] and the references therein). The first model is described by the Darcy law together with the equation of conservation of mass for steady flow (see e.g. [99]). It is written in the form of a partial differential equation as follows:

$$\mathbf{u} = -\boldsymbol{S}\nabla p, \quad \text{in } \Omega, \tag{1a}$$

$$\nabla \cdot \mathbf{u} = f, \quad \text{in } \Omega, \tag{1b}$$

where Ω is the domain, f is the source term, $\mathbf{u}$ is the Darcy velocity, p is the pressure head, and $\boldsymbol{S}$ is the permeability tensor (where the fluid density is supposed to be constant). This gives a complete problem after adding an appropriate boundary condition.

The second model considered is the Darcy law together with the mass balance

Figure 2: Sealed steel cask of nuclear Waste (Height:1.3m, diameter: 43 cm, approximate weight: 500kg)

equation for the unsteady fluid flow:

$$\mathbf{u} = -\boldsymbol{S}\nabla p, \quad \text{in } \Omega \times (0,T), \tag{2a}$$

$$\phi \frac{\partial p}{\partial t} + \nabla \cdot \mathbf{u} = f, \qquad \text{in } \Omega \times (0,T), \tag{2b}$$

where ϕ is the porosity, T is the final time; an appropriate boundary condition and an initial condition need to be added.

For such a model, the computational domain and data are:

- with very different spatial lengths, starting from one meter to thousands of meters, leading to very different scales in space.
- with a set of sub-areas with very different physical properties such as different materials in each area, leading to a very large heterogeneity in the geological medium in space. Consequently, the phenomena may occur on different time scales depending on the physical properties of the area.

Remark. *Equation* (2) *may also be interpreted as a first step for solving the balance equation for the transport of contaminant (quantity of a dissolved species in a fluid phase measured by its concentration):*

$$\phi \frac{\partial c}{\partial t} + \nabla \cdot (-\boldsymbol{D}(\mathbf{u})\nabla c + c\mathbf{u}) + \phi \lambda c = g, \quad \textit{in } \Omega \times (0,T),$$

where $\mathbf{u}$ *is the Darcy velocity,* c *is the concentration of a contaminant dissolved in water,* $\boldsymbol{D}(\mathbf{u})$ *is the diffusion-dispersion tensor, and* λ *is the radioactive decay coefficient. More precisely, if one uses operator splitting [100] to solve* (3) *with possibly different numerical time schemes for advection and diffusion, then one solves an advection equation and a diffusion equation of type* (2).

The third model is a simplified two-phase flow with phase appearance and disappearance. We will consider a flow between one or more rock types in a porous medium with continuous or discontinuous capillary pressure. The mathematical form studied in Chapter 4 is exposed in [39, 63] as follows:

$$\partial_t u - \nabla\cdot(\lambda(u,\mathbf{x})\nabla\pi(u,\mathbf{x})) = f, \quad \text{in } \Omega\times(0,T), \tag{3a}$$

$$u(\cdot,0) = u_0, \quad \text{in } \Omega, \tag{3b}$$

$$\pi(u,\cdot) = g, \quad \text{on } \partial\Omega\times(0,T), \tag{3c}$$

where the unknown scalar $u \in [0,1]$ is the gas saturation (and therefore (1-u) is the water saturation), u_0 is the initial gas saturation, f is the source term, g is a non-homogeneous Dirichlet boundary condition, the function $\pi(u,\mathbf{x})$ is the capillary pressure:

$$\pi(u,\mathbf{x}) : [0,1]\times\Omega\to\mathbb{R}, \tag{4}$$

and $\lambda(u,\mathbf{x})$ is the global mobility of the gas:

$$\lambda(u,\mathbf{x}) : [0,1]\times\Omega\to\mathbb{R}. \tag{5}$$

For simplicity, we consider only Dirichlet boundary condition on $\partial\Omega$. This is a nonlinear degenerate parabolic problem with nonlinear and discontinuous transmission condition on the interface.

The problems proposed above give rise to large sparse systems of linear algebraic equations which can be solved by different methods.

In the following section, different methods are presented.

Finding a suitable method to solve the model problem

Consider for motivation the problem (2). On each time step of a usual discontinuous Galerkin scheme in time and a finite element discretization in space, it leads to a linear system $\mathbb{A}\mathbf{X} = \mathbf{B}$. When attempting to solve this system, doing the operation $\mathbf{X} = \mathbb{A}^{-1}\mathbf{B}$ is impossible as the size of the matrix $\mathbb{A}$ is typically prohibitively large. Several methods are used in practice:

• Direct methods [53]: for example, the $\mathbb{L}\mathbb{U}$ factorization. These methods are robust in the sense that we obtain the solution in a time which can be estimated a priori and give typically high precision (depending, though, on rounding errors that are influenced by the problem complexity) relatively easily. The disadvantage of these methods is that they require great deal of computer memory, and they are not well suited to parallelization.

• Iterative methods [143]: for example, Krylov methods (conjugate gradients, GMRES, etc.). The advantages of these methods are that they enable parallelization and require little memory space. Unfortunately, they may lack robustness since they may take a long time to converge or may not converge at all.

• Domain decomposition methods [57, 125, 135, 150], where the subdomains are constructed with some control over the size of each subdomain. These methods solve the problem in a subdomain directly or iteratively, and they ensure the connection on the interface iteratively. They are naturally parallel and typically more robust than purely iterative methods, though less robust than direct methods.

For highly heterogeneous problems such as (1), (2), or (3) with very different space and/or time scales, the third method, the domain decomposition method proposed above, is well suited. In this context, as the conservation of mass is crucial for ANDRA's applications, the conservative cell-centered techniques for discretization in space such as mixed finite element methods or finite volume methods are used, see [36, 45, 69, 142]. In particular, a mixed finite element method will be used in Chapters 1, 2, 3 and a finite volume method will be used in Chapter 4.
On the other hand, together with the solvers and discretizations proposed above, the theory of a posteriori estimates could be used to monitor the error and to improve the efficiency of the method through defining an adaptive stopping criterion for the algorithm or adaptive mesh refinement.
This thesis is based on coupling these two suitable methods, domain decomposition and a posteriori estimates, for which we introduce the state of the art below.

Bibliography and previous studies

Domain decomposition methods

Domain decomposition methods are a family of methods which allow to solve problems naturally on parallel machines. Referring to the books [57, 125, 135, 150] and the references therein of Domain decomposition methods, we mention the main classes of domain decomposition algorithms which can be used: Schwarz, Dirichlet–Neumann, Neumann–Neumann/FETI. Schwarz iterative method is used throughout this work and Dirichlet–Neumann iterative method is introduced in Chapter 1 in order to show the difference between the interface operator for these two methods.

• The Dirichlet–Neumann iterative methods lead to two problems at each iteration. The first problem is solved in one subdomain with the Dirichlet condition at the interface between the subdomains, while the second problem is the solved on the other subdomain, with the Neumann condition applied at the interface. This interface problem can be defined in terms of the Steklov–Poincaré operator (interface operator) that we introduce briefly in Chapter 1. This interface operator enforce the classical Dirichlet–Neumann transmission conditions between subdomains. For the origins of this method, see the seminal paper of Przemieniecki [133], see also [5, 27, 33, 134, 160], and [80] for a review. The discrete counterpart of the Steklov–Poincaré operator (namely, the Schur complement matrix) leads to an interface problem solved by an iterative method. Neumann–Neumann preconditioner is used to accelerate the convergence of such methods, where local Neumann boundary problems are solved in the subdomains, see [30, 54, 129]. For a decomposition into many subdomains, the Balancing Domain Decomposition (BDD) [49, 122, 123] propagate information globally between subdomains to make the method scalable (i.e.

the condition number is almost independent of the number of subdomains) and ensure the consistency of the Neumann problems. In [60, 82], the authors extended the Steklov–Poincaré operator to parabolic problems with uniform time grids between the subdomains. The time-dependent Steklov–Poincaré operator leading to a "space-time" domain decomposition method was given and analysed in [94, 95], in particular with different time grids in different subdomains.

• Schwarz methods: introduced by H. A. Schwarz [144] in which an iterative method (called the Schwarz alternating method) is proposed to prove existence and uniqueness of the solution of Laplace's equation in irregular overlapping domains (composed of a disk and a rectangle which intersect). In the context of numerical methods adapted to parallel computer architectures for solving partial differential equations (PDEs), P.-L. Lions [119] introduces a parallelizable nonoverlapping version of the Schwarz method based on Robin transmission conditions (see also [117, 118]). This approach is a strong basis of domain decomposition methods, in particular the Optimized Schwarz method introduced in [101, 102, 103, 104], which is used throughout this thesis. This method uses Robin or Ventcell transmission conditions on the interfaces with optimized coefficients in order to improve the convergence rates of the algorithm. Such transmission conditions are approximations of the exact artificial conditions [83, 126] and are quite different from the "low frequency" approximations [88] and reduce dramatically the convergence factor of the method. An overview of the Optimized Schwarz method is given in [71], completed by an extension to a diffusion problem with discontinuous coefficient in [72]. As mixed finite elements is the central numerical method used in this thesis, we refer to [59] (respectively [94, 98]) for the classical Schwarz algorithm with Robin (the Optimized Schwarz method with Ventcell) transmission conditions in the mixed formulations context.

For parabolic equations two approaches can be adopted:

• One possibility is to discretize in time first using an implicit scheme and then employ the Schwarz method in order to solve the steady problems at each time step. In this case, it is necessary to use the same time discretization in each subdomain. The main drawback of this method is that it is very costly in parallel computing, as information has to be transferred at each time discretization step and on each domain decomposition iteration.
• Another possibility is to use the space-time domain decomposition method. This method consists in discretizing differently the time interval for each subdomain according to its physical properties. We solve on each subdomain the time-dependent problem over all the time interval, and then space-time boundary information is exchanged on the space-time interfaces between subdomains at each iteration of the iterative method. This method allows us to use different numerical schemes in time (and eventually in space) in different subdomains. The communication cost is then reduced since the data is transferred over the whole time interval once for each DD iteration.

In this thesis the space-time domain decomposition method is used.

In [79, 84], the authors introduce such an approach based on classical transmissions conditions. To accelerate the convergence of this method, it has been proposed in [75, 76, 124] to use optimized transmission conditions on each space-time interface. This method is called the Optimized Schwarz Waveform Relaxation (OSWR) method. In [21, 73, 124], the authors analysed the optimization of the Robin or Ventcell parameters and in [28, 91, 105] the optimization was extended to discontinuous coefficients. Extensions to heterogeneous problems and non-matching time grids were introduced in [29, 74]. The discontinuous Galerkin (DG) method for the time discretization of the OSWR was introduced in [29, 90, 92, 93] to cope with non-conforming time grids. A suitable time projection between subdomains was obtained by a projection algorithm in order to exchange data on the space-time interfaces, see [77, 78]. The mixed formulation was extended in the context of operator splitting (see [94, 95, 96, 97, 98]).
The domain decomposition methods presented above can be written into an interface problem on the interfaces between subdomains. More precisely, for space-time DD methods, the multidomain problem is transformed into an interface problem on the space-time interfaces between subdomains. The discrete counterpart of the interface problem is solved iteratively using the Jacobi iterative method. A Krylov method such as GMRES can also be used to accelerate the convergence (see [94] in the mixed finite elements context).

A posteriori error estimates

A posteriori error estimates represent a powerful methodology and have become an important research domain; we refer for instance to the books [9, 138, 153] and the references therein. Recall that with a priori error estimates, we estimate the error as a functions of mesh size and an unknown constant depending on the unknown exact solution p which cannot generally be computed. This estimation is typically as follows:

$$|||p - p_h||| \leq C(p)h^l, \tag{6}$$

where h is the mesh size, $l \geq 0$ is the order of the method, and C depends on the exact solution p. Thus $C(p)h^l$ is typically not a computable upper bound. Unlike the a priori error estimates, the a posteriori error estimates are based on bounding the error by a completely computable upper bound. Indeed, the error between the exact solution and the approximate solution in an energy norm is estimated by an a posteriori error estimate which depends on the approximate known solution and known constants only. For an optimal a posteriori error estimate, several important properties have to be satisfied:

- the estimator provides a guaranteed upper bound which is fully computable and features no unknown constant, i.e.

$$|||p - p_h||| \leq \eta(\mathcal{T}_h, p_h, \mathbf{u}_h), \tag{7}$$

  where $\mathcal{T}_h$ is the mesh and p_h and $\mathbf{u}_h$ are the known approximations (in the context of problem (1)),

- the ratio of the estimated upper bound and of the error goes to one in the limit:

$$I_{\text{eff}} := \frac{\eta(\mathcal{T}_h, p_h, \mathbf{u}_h)}{|||p - p_h|||} \to 1, \tag{8}$$

- the local components of the estimator $\eta_K(h_K, p_h|_K, \mathbf{u}_h|_K)$ where $\eta(\mathcal{T}_h, p_h, \mathbf{u}_h) = \left\{ \sum_{K \in \mathcal{T}_h} \left(\eta_K(h_K, p_h|_K, \mathbf{u}_h|_K)\right)^2 \right\}^{\frac{1}{2}}$ must not overestimate the local error in the sense that they must provide a lower bound of the local error, up to a multiplicative constant C_L. This property is called local efficiency:

$$C_L \eta_K(h_K, p_h|_K, \mathbf{u}_h|_K) \leq |||p - p_h|||_K, \tag{9}$$

- the estimators η_K have to be computable locally in each element K of the mesh $\mathcal{T}_h$,

- the estimates have to distinguish the different error components.

In this thesis, and as mentioned before, locally conservative methods such as the lowest-order mixed finite elements or cell-centered finite volume methods are employed. Several studies on a posteriori error estimates for the mixed finite element methods have been carried out. They began with Alonso [13] and Braess and Verfürth [32], followed by other work such as [2, 8, 43, 62, 111, 114, 120, 159, 162]. Then, in [139] the authors give a guaranteed but potentially costly bound for a heterogeneous diffusion tensor, without local efficiency. A posteriori error estimates are also studied in [108] with an undetermined constant in the upper bound. In [137] the authors give a posteriori error estimates for the case where the approximate solutions are conforming in the sense that $\mathbf{u}_h \in \mathbf{H}(\text{div}, \Omega)$ and $p_h \in H^1(\Omega)$. Finally, [156] presents a guaranteed and fully computable upper bound and local efficiency on the energy norm between the exact solution and the approximate solution for the steady diffusion equation in extension of the results from the lowest-order mixed finite element case [154]. This upper bound is only based on a conforming potential reconstruction because the approximate flux is equilibrated and satisfies $\mathbf{u}_h \in \mathbf{H}(\text{div}, \Omega)$. As the approximate solution of p is piecewise constant in each mesh element, following Arnold and Brezzi [17], Arbogast and Chen [15], and other references such as [34, 47, 147], a new approximate solution $\tilde{p}_h$ which improves the approximation of p is used. Indeed, an a posteriori error estimate for $p - \tilde{p}_h$ is given, as $\tilde{p}_h$ is more regular than p_h while being higher-degree polynomial function. The flux of this postprocessing $-\boldsymbol{S}\nabla\tilde{p}_h$ is equal to $\mathbf{u}_h$ in the lowest-order case and the mean value of $\tilde{p}_h$ is equal to p_h on each mesh element. Then, in order to obtain a H^1-conforming potential reconstruction, called s_h, we use the averaging operator $\mathscr{I}_{\text{av}}$ applied on $\tilde{p}_h$ following [3, 37, 61, 107] and the references therein.

For unsteady problems, several works have also been carried out. In [67], Ern and Vohralík derive a fully computable upper bound for the energy norm augmented by a dual norm of the time derivative following Verfürth [152]. They give a unified framework for the heat equation using different numerical schemes covering nonconforming methods such as mixed finite element methods, various finite volume

schemes, and discontinuous Galerkin schemes in space and an implicit Euler scheme in time. A posteriori estimates for conforming finite element methods are also derived. This upper bound, global-in-space and in time, is established using estimates which are based on a H^1-conforming potential reconstruction in space, continuous and piecewise affine in time, and where the mean value of the potential reconstruction has to be linked to the approximate discrete solution on each mesh element. It is also based on an $\mathbf{H}(\mathrm{div},\Omega)$-conforming and locally conservative flux reconstruction in space, which is piecewise constant in time. In the case of the mixed finite element method, it is not necessary to build the flux reconstruction since this is already available from the method. The ideas underlying these flux and potential reconstructions, presented in [67], are inspired from the estimator reconstructions given for the steady problem [10, 31, 64, 66, 109, 112, 121, 132, 154, 155, 156, 157], and the references therein, as at each time step of the unsteady problem, a steady diffusion problem is solved.

The a posteriori error estimates presented in this thesis are based on [156] for the steady diffusion equation and on [65, 67] for the unsteady diffusion case. The crucial difference is that the Robin domain decomposition method does not conserve the conformity of the flux, nor the conformity of the potential, on the interface. We first have to build a flux reconstruction which is globally conforming and locally conservative in each mesh element. The potential reconstruction in the domain and on the interface is built following the studies proposed above. Secondly, as the domain decomposition method intervenes in our work, one of the most important questions that we will study is the following: can we distinguish the domain decomposition error from the discretization one?

Coupling domain decomposition and a posteriori error estimates

In [130], the authors are interested in the steady diffusion equation where the domain of computation is divided into different subdomains and where different numerical methods can be used in different subdomains (different discretization mesh can also be used in each subdomain giving rise to nonmatching grids on the space interface between the subdomains). The coupling of these method is done through the mortar technique where the interfaces are partitioned by a coarse mesh. An equilibrated flux reconstruction is designed in this context, and it can be seen as a pathway towards flux reconstruction in domain decomposition methods. Indeed, the challenge is to obtain a reconstructed flux which is globally $\mathbf{H}(\mathrm{div},\Omega)$-conforming and locally conservative. Under an assumption on the approximate flux, to be weakly continuous across the interface a reconstructed flux is obtained by solving well-posed local Neumann problems using mixed finite element methods. It was shown that under the assumptions proposed by the authors, the Neumann boundary conditions are in equilibrium with the source term, which leads to well-posed problems. Different error components are distinguished: the discretization error of the subdomains and the interface errors coming from the mortar technique.

In [141], a posteriori analysis is introduced for the case of a linear elasticity problem which is approximated by the finite element method and a non-overlapping

domain decomposition method such as FETI or BDD. The authors derive an upper bound for the error where different error components are distinguished: a discretization error component and a domain decomposition component. Thus an a posteriori stopping criterion for the iterative method is derived. In their article, the authors use the potential solution provided by the Neumann–Neumann DD method to obtain a natural potential reconstruction. Indeed, local problems with Dirichlet conditions on the interface are first solved using the finite element method resulting in a natural potential reconstruction. Then local Neumann problems in the subdomains, with conforming Neumann conditions on the interface, are solved using BDD in order to obtain the Neumann compatibility. From that, the authors distinguish the errors coming from the DD method and the error coming from the discretization method. The DD component distinguished through the properties of the finite element method is the difference between the approximate potential solution given by the local Neumann problem and the natural potential reconstruction given by the Dirichlet problems. This approach seems to be only possible in the presence of the two types (Dirichlet and Neumann) of local problems solved on each DD iteration.

Different related a posteriori error estimates have also recently been proposed: multiscale discretizations [1, 87, 110, 113, 128], discretizations with mortar coupling for the Galerkin methods and mixed finite element methods [22, 159, 161], and for multinumerics [23, 50].

The above-described approaches open up the possibility of distinguishing the errors of the DD method in the posteriori estimates, for the Robin DD method in the mixed finite elements context, which is studied throughout this thesis. In this DD method, there is no assumption such as that given in [130] and there is no continuity neither of the potential nor for the flux on the interface, during the DD iterations.

Aims of this thesis

In this thesis, we start from the a posteriori analysis for the diffusion equation and the heat equation studied respectively in [130] and [67] for the mixed finite element method. We aim to extend the a posteriori analysis to the case of the Robin transmission conditions method and then distinguish and separate the different components of the error in the upper bound at each Jacobi or GMRES domain decomposition iteration. We also aim to extend this theory to the case of:
• different time grids used in each subdomain for the heat equation,
• the two phase flow problem with phase appearance and disappearance, where the problem at hand is nonlinear (degenerate), so that a new error component stemming from iterative linearization appears.
Once the estimators have been obtained, we need to answer to the following questions:

- Is the error between the exact solution and numerical solution precisely controlled?
- Can we distinguish all the error components?
- Can we stop the iterations of the domain decomposition method before a usual

stopping criterion in order to save useless iterations and computing time?

Outline

This thesis is organized as follows:

In Chapter 1, we introduce the steady diffusion equation (1) with different boundary conditions. The optimized Schwarz domain decomposition method is then used to solve local subdomain problems iteratively and then transfer information to the neighbouring subdomains. The mixed finite element discretization is employed and described since local mass conservation is required. Numerical results comparing the one-domain solution and the solution resulting from the domain decomposition method are presented for unstructured triangle meshes and for anisotropic and heterogeneous diffusion tensors.

In Chapter 2 we derive a posteriori error estimates for problem (1) introduced in Chapter 1. We derive a fully computable upper bound for the error between the exact solution p of the partial differential equation and the approximate numerical solution p_h^{k+1} in an energy norm, at each iteration $k+1$ of the DD algorithm. The estimates are based on the reconstruction techniques for pressures and fluxes as described below. In order to build the potential reconstructions, the following steps are taken (see Figure 3): we first construct a postprocessing $\tilde{p}_h^{k+1}$ of p_h^{k+1} at each iteration of the DD algorithm. This postprocessing is more regular than the piecewise constant p_h^{k+1}, being piecewise quadratic, but it does not lie in the space $H^1(\Omega)$. For this reason we next construct a conforming potential $\overline{s}_{h,i}^{k+1} \in H^1(\Omega_i)$ independently on each subdomain Ω_i, as well as a global conforming potential reconstruction $s_h^{k+1} \in H^1(\Omega)$. We also have to

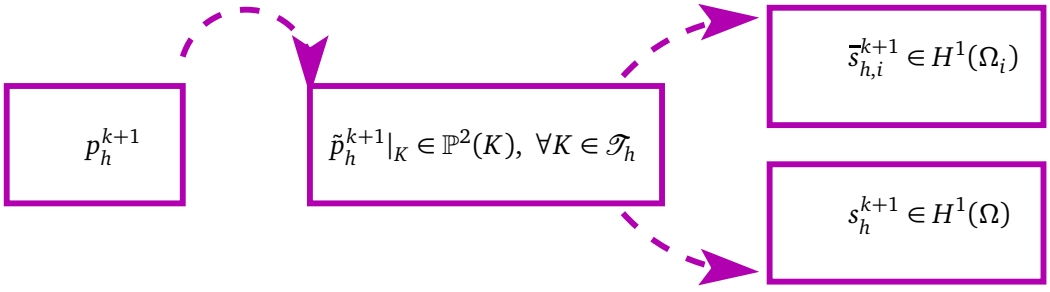

Figure 3: Steps to build a potential reconstruction

construct a conforming reconstruction flux $\boldsymbol{\sigma}_h^{k+1} \in \mathbf{H}(\mathrm{div}, \Omega)$ which verifies the local conservation with the source term in each mesh element. We have managed to separate our estimators into two categories: estimators due to the discretization in space and estimators due to the domain decomposition. Splitting our estimators into two parts led us to define an a posteriori stopping criterion for the DD algorithm instead of the usual domain decomposition stopping criterion. This a posteriori stopping criterion is satisfied as soon as the domain decomposition error components do not contribute significantly to the overall estimates. Numerical results for the Jacobi iterative method and the GMRES method show how this technique saves unnecessary iterations.

In Chapter 3 the unsteady diffusion equation (2) is introduced. As time scales vary by several degrees of magnitude between different domains in our targeted applications, the classical domain decomposition method which consists in discretizing the problem in time, and then applying a domain decomposition algorithm to solve the stationary problem on each time step, is not well suited here. Namely, when the same time step is applied for all subdomains, it may become prohibitively small in terms of the overall cost. For this reason, we propose to use the global-in-time domain decomposition method where the scales over times are adjusted (independent time discretization) for each subdomain. Here, local subdomain problems in time are solved independently in each subdomain, then data is transferred between the neighbouring subdomain through the space-time interface, see [95] and the references therein. In this chapter, the heat equation is discretized using the lowest-order mixed finite element method in space and the lowest-order discontinuous Galerkin scheme in time. Different error components are identified using the a posteriori error estimates. Bounding the error between the exact solution and the approximate solution in an energy norm, the domain decomposition, the discretization in time, and the discretization in space components are identified for the conforming time grids. An a posteriori stopping criterion is defined allowing to save numerous domain decomposition iterations. The a posteriori estimates presented here are based on:

- a potential reconstruction, H^1-conforming (piecewise second-order polynomial) in space and continuous piecewise affine in time, together with a link between the mean values of the potential reconstruction and the approximate discrete solution following [67],
- a locally conservative flux reconstruction, $\mathbf{H}(\mathrm{div}, \Omega)$-conforming (Raviart–Thomas of lowest order) in space and piecewise constant in time.

We also extend our theory for the nonconforming time grids in different subdomains, where the transfer of data between the neighbouring subdomain is done through a suitable projection. Then, an extension of the a posteriori estimates to the case of nonconforming time grids is introduced. Numerical results illustrating a nuclear waste repository are presented both for conforming and nonconforming time grids.

In Chapter 4, we extend the a posteriori error estimates and stopping criteria to the domain decomposition method for the two-phase flow problem (3). The work described in this chapter was carried out in the context of the CEMRACS 2016 summer school, in the collaboration with Elyes Ahmed, Caroline Japhet, Michel Kern, and Martin Vohralík. The aim of this projet was to extend the approach we adopted for a posteriori error estimates and stopping criteria presented in Chapter 3 to a nonlinear degenerate parabolic problem in order to obtain significant gains in the total number of iterations of the global-in-time domain decomposition method. This work is motivated by ANDRA's Cigéo project and is part of the ANR project DEDALES. The nonlinear two-phase (water/gas) flow model problem in a porous medium is discretized by a cell-centered finite volume scheme in space with backward Euler temporal stepping. A guaranteed and fully computable upper bound is proven and different error components are distinguished: discretization in space, discretization in time, domain decomposition, and linearization, leading to a posteriori stopping criteria of both the linearization and the DD algorithm.

Chapter 1

Domain decomposition method for steady diffusion problems in mixed formulation

Contents

In this section, we describe the Dirichlet-to-Neumann formulation as well as the optimized Schwarz method [71, 102, 103, 104] in the mixed formulation following [94, 95]. For the latter, the difference with [94, 95] is that the method is presented for unstructured meshes and some numerical results as shown for full and heteregeneous diffusion tensor.

1.1 The diffusion equation

This chapter presents the mathematical model (1) for a single phase fluid in a porous medium based on Darcy's equation:

$$\mathbf{u} = -\boldsymbol{S}\nabla p \quad \text{in} \quad \Omega, \tag{1.1a}$$
$$\nabla\cdot\mathbf{u} = f \quad \text{in} \quad \Omega, \tag{1.1b}$$
$$p = g_{\mathrm{D}} \quad \text{on} \quad \Gamma^{\mathrm{D}}, \tag{1.1c}$$
$$-\mathbf{u}\cdot\boldsymbol{n} = g_{\mathrm{N}} \quad \text{on} \quad \Gamma^{\mathrm{N}}. \tag{1.1d}$$

In this problem, $\mathbf{u}$ is the Darcy fluid velocity and p is the fluid pressure head. We consider here $\Omega \subset \mathbb{R}^d$, $d = 2,3$, a polygonal (polyhedral if $d = 3$) domain (open, bounded, and a connected set), and $\partial\Omega = \Gamma^{\mathrm{D}} \cup \Gamma^{\mathrm{N}}$ is the boundary of the domain with:

$-$ Γ^{D}: the boundary with a Dirichlet condition $g_{\mathrm{D}} \in H^{\frac{1}{2}}(\Gamma^{\mathrm{D}}) \cap C^0(\overline{\Gamma}^{\mathrm{D}})$.
$-$ Γ^{N}: the boundary with a Neumann condition $g_{\mathrm{N}} \in L^2(\Gamma^{\mathrm{N}})$.
We suppose that $|\Gamma^{\mathrm{D}}| > 0$. An example of domain Ω is given in Figure 1.1.

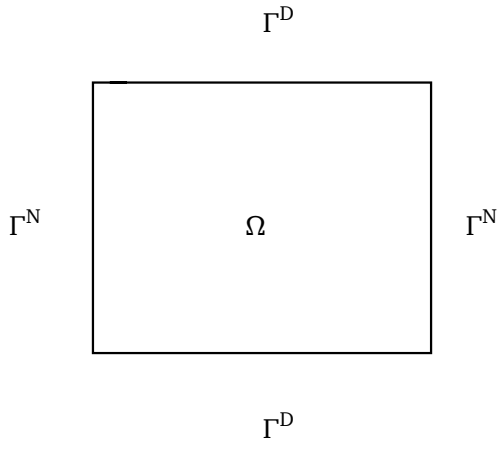

Figure 1.1: Global domain Ω

Furthermore, $f \in L^2(\Omega)$ is the source term, $\boldsymbol{n}$ is the outward unit normal vector to $\partial\Omega$ and $\boldsymbol{S}$ is a symmetric, bounded, and uniformly positive definite tensor whose terms are functions in $L^\infty(\Omega)$. In particular, when $d = 2$, $\boldsymbol{S}$ is written as:

$$\mathbf{x} \in \Omega, \qquad \boldsymbol{S}(\mathbf{x}) = \begin{pmatrix} S_{11}(\mathbf{x}) & S_{12}(\mathbf{x}) \\ S_{12}(\mathbf{x}) & S_{22}(\mathbf{x}) \end{pmatrix}. \tag{1.2}$$

In order to make use of parallel computing, we use domain decomposition methods, which decompose Ω into non-overlapping subdomains Ω_i, $i \in [\![1, \mathcal{N}]\!]$, where $\mathcal{N}$ denotes the total number of subdomains:

$$\overline{\Omega} = \bigcup_{i=1}^{\mathcal{N}} \overline{\Omega}_i. \tag{1.3}$$

We denote by $\Gamma_{i,j}$ the interface between two adjacent subdomains Ω_i and Ω_j, and by $\boldsymbol{n}_i$ the outer normal vector to Ω_i. The second order elliptic problem (1.1) will in particular be reduced to smaller problems on each subdomain with appropriate coupling conditions. We assume that this decomposition is geometrically conforming in the sense that the intersection of the closure of two different subdomains is either a common vertex, or a common edge, or a common face, or an empty set. In the following section, we introduce some function spaces which will be used to define the method.

1.2 Presentation of some function spaces

We present here some basic function spaces following [4, 12, 136, 148]. For a given non-empty domain $D \subset \Omega$, and a real number l, $1 \leq l \leq \infty$, we employ the standard functional notations $L^l(D)$ and $\mathbf{L}^l(D) := [L^l(D)]^d$ of Lebesgue spaces. We denote by $(\cdot,\cdot)_D$ the scalar product for $L^2(D)$ and $\mathbf{L}^2(D)$, associated with the norm $\|\cdot\|_{L^2(D)}$, and by $|D|$ the Lebesgue measure of D. Let $\langle\cdot,\cdot\rangle_\gamma$ be the scalar product for the $d-1$ dimensional $L^2(\gamma)$ on $\gamma = \partial D$ or its subset.
Let $H^1(D)$ be the Sobolev space defined as:

$$H^1(D) := \{v \in L^2(D);\ \nabla v \in \mathbf{L}^2(D)\}, \tag{1.4}$$

with the associated norm:

$$\|v\|^2_{H^1(D)} := \|v\|^2_{L^2(D)} + \|\nabla v\|^2_{L^2(D)}. \tag{1.5}$$

Next, $\mathbf{H}(\mathrm{div}, D)$ is the space of vector functions whose weak divergence is square integrable:

$$\mathbf{H}(\mathrm{div}, D) := \{\mathbf{v} \in \mathbf{L}^2(D);\ \nabla\cdot\mathbf{v} \in L^2(D)\}, \tag{1.6}$$

associated with the following norm:

$$\|\mathbf{v}\|^2_{\mathbf{H}(\mathrm{div},D)} := \|\mathbf{v}\|^2_{L^2(D)} + \|\nabla\cdot\mathbf{v}\|^2_{L^2(D)}. \tag{1.7}$$

As Ω is decomposed into subdomains (1.3), we introduce local spaces which are the restrictions of these previous spaces on each subdomain, by assuming that $D = \Omega_i$, $\forall i \in [\![1, \mathcal{N}]\!]$:

$$M_i := L^2(\Omega_i), \tag{1.8a}$$
$$\mathbf{W}_i := \mathbf{H}(\mathrm{div}, \Omega_i). \tag{1.8b}$$

Recall that if $\mathbf{v} \in \mathbf{H}(\mathrm{div}, D)$, then in general $\mathbf{v}\cdot\boldsymbol{n} \notin L^2(\partial D)$, but verify $\mathbf{v}\cdot\boldsymbol{n} \in H^{-\frac{1}{2}}(\partial D)$. For the coupling (Robin) conditions considered in the sequel, we need a greater regularity [59]. Thus we define the following space:

$$\overline{\mathbf{W}}_i := \{\mathbf{v} \in \mathbf{W}_i;\ \mathbf{v}\cdot\boldsymbol{n}_i \in L^2(\partial\Omega_i)\}. \tag{1.9}$$

We define from the Neumann condition on Γ^{N} the following sets:

$$\mathbf{W}_i^{g_{\mathrm{N}}} := \{\mathbf{v} \in \overline{\mathbf{W}}_i;\ \mathbf{v}\cdot\boldsymbol{n}_i = g_{\mathrm{N}} \text{ on } \Gamma^{\mathrm{N}} \cap \partial\Omega_i\}, \tag{1.10a}$$
$$\mathbf{W}_i^0 := \{\mathbf{v} \in \overline{\mathbf{W}}_i;\ \mathbf{v}\cdot\boldsymbol{n}_i = 0 \text{ on } \Gamma^{\mathrm{N}} \cap \partial\Omega_i\}. \tag{1.10b}$$

The space $\overline{\mathbf{W}}_i$ is associated with the following norm:

$$\|\mathbf{v}\|^2_{\overline{\mathbf{W}}_i} := \|\mathbf{v}\|^2_{L^2(\Omega_i)} + \|\nabla\cdot\mathbf{v}\|^2_{L^2(\Omega_i)} + \|\mathbf{v}\cdot\boldsymbol{n}_i\|^2_{L^2(\partial\Omega_i)}, \tag{1.11}$$

for Robin boundary conditions on $\partial\Omega_i$.

For the sake of simplicity, we will first consider a decomposition of Ω into two non-overlapping subdomains ($\mathcal{N} = 2$) and then the case of multiple subdomains will be presented.

1.3 The two-subdomain DD case in the mixed formulation

In this section, we introduce two equivalent formulations of problem (1.1) using domain decomposition methods: the Dirichlet-to-Neumann formulation and the Robin-to-Robin formulation. The Dirichlet-to-Neumann method is based on physical transmission conditions, whereas the Robin-to-Robin method is based on Robin transmission conditions. For simplicity, we present these methods for the two-subdomain case, where $\mathcal{N} = 2$. For example, starting from Figure 1.1, we decompose Ω into two non-overlapping subdomains Ω_1 and Ω_2 as illustrated in Figure 1.2. We denote the interface by $\Gamma_{1,2}$. As the problems in the subdomains are locally similar in native to the original problem, we will be able to solve all of them using the same solver.

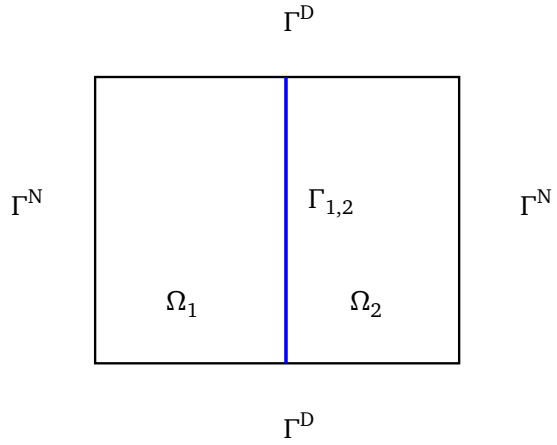

Figure 1.2: Partition of the domain Ω into two subdomains Ω_1 and Ω_2

Links with the global formulation

Theorem 1.1 (Continuity of traces in $H^1(\Omega)$)**.** *Let Ω be a domain divided into two subdomains: $\overline{\Omega} = \overline{\Omega}_1 \cup \overline{\Omega}_2$, $\Omega_1 \cap \Omega_2 = \emptyset$, and $\Gamma_{1,2} = \partial\Omega_1 \cap \partial\Omega_2$. For $p \in H^1(\Omega)$, let $p_i = p_{|\Omega_i}$, $i = 1, 2$. Then (see [116, 135]),*

$$p \in H^1(\Omega) \iff \begin{cases} p_i \in H^1(\Omega_i),\ i = 1, 2, \\ p_1 = p_2 \text{ on } \Gamma \text{ in the } H^{1/2}(\Gamma_{1,2}) \subset L^2(\Gamma_{1,2}) \text{ sense.} \end{cases}$$

Theorem 1.2 (Continuity of normal traces in $\mathbf{H}(\mathrm{div}, \Omega)$)**.** *Let Ω as in Theorem 1.1. For $\mathbf{u} \in \mathbf{H}(\mathrm{div}, \Omega)$, let $\mathbf{u}_i = \mathbf{u}_{|\Omega_i}$, $i = 1, 2$. Then (see [116, 135]),*

$$\mathbf{u} \in \mathbf{H}(\mathrm{div}, \Omega) \iff \begin{cases} \mathbf{u}_i \in \mathbf{H}(\mathrm{div}, \Omega_i),\ i = 1, 2, \\ \mathbf{u}_1 \cdot \boldsymbol{n}_1 = \mathbf{u}_2 \cdot \boldsymbol{n}_1 \text{ on } \Gamma_{1,2} \text{ in the } ({H_{00}}^{1/2}(\Gamma_{1,2}))' \text{ sense,} \end{cases}$$

where for a smooth interface $\Gamma_{1,2}$, the space $({H_{00}}^{1/2}(\Gamma_{1,2}))'$ denotes the dual space of ${H_{00}}^{1/2}(\Gamma_{1,2})$. Recall that the space ${H_{00}}^{1/2}(\Gamma_{1,2})$ consists of those elements $v \in H^{1/2}(\Gamma_{1,2})$ whose extension $\tilde{v}$ of v by zero to all $\partial\Omega_i$ belongs to $H^{1/2}(\partial\Omega_i)$ [116].

1.3.1 Multidomain formulation with physical transmission conditions

The problem (1.1) can be reformulated as an equivalent multidomain problem consisting of the following subdomain problems, $\forall i = 1,2$:

$$\begin{aligned} \mathbf{u}_i &= -\boldsymbol{S}\nabla p_i && \text{in} && \Omega_i, && (1.12a)\\ \nabla\cdot\mathbf{u}_i &= f && \text{in} && \Omega_i, && (1.12b)\\ p_i &= g_{\mathrm{D}} && \text{on} && \Gamma^{\mathrm{D}}\cap\partial\Omega_i, && (1.12c)\\ -\mathbf{u}_i\cdot\boldsymbol{n}_i &= g_{\mathrm{N}} && \text{on} && \Gamma^{\mathrm{N}}\cap\partial\Omega_i, && (1.12d) \end{aligned}$$

together with the transmission conditions on the interface, based on Theorems 1.1 and 1.2:

$$\begin{aligned} p_1 &= p_2 && \text{on} && \Gamma_{1,2}, && (1.13a)\\ \mathbf{u}_1\cdot\boldsymbol{n}_1 &= \mathbf{u}_2\cdot\boldsymbol{n}_1 && \text{on} && \Gamma_{1,2}. && (1.13b) \end{aligned}$$

Recall that $\boldsymbol{n}_1$ is the normal vector on $\Gamma_{1,2}$ pointing from Ω_1 to Ω_2 with $\boldsymbol{n}_2 = -\boldsymbol{n}_1$. Equations (1.13a)–(1.13b) are the physical transmission conditions for the flux $\mathbf{u}$ and the pressure head p on the interface $\Gamma_{1,2}$. These equations ensure the continuity of the global solution p and the continuity of the normal trace of $\mathbf{u}$ on $\Gamma_{1,2}$.
For this method, an interface operator is used to reformulate the multidomain problem as a problem where the unkowns are located only on the interface. This operator is called the Steklov–Poincaré (Dirichlet-to-Neumann) operator, see e.g. [135].

The Steklov–Poincaré (Dirichlet-to-Neumann) operator

In order to solve the split formulation (1.12) with the transmission conditions (1.13) on the interface, we introduce the problem in Ω_i, $i = 1,2$, as:

$$\begin{aligned} \mathbf{u}_i &= -\boldsymbol{S}\nabla p_i && \text{in} && \Omega_i, && (1.14a)\\ \nabla\cdot\mathbf{u}_i &= f && \text{in} && \Omega_i, && (1.14b)\\ p_i &= g_{\mathrm{D}} && \text{on} && \Gamma^{\mathrm{D}}\cap\partial\Omega_i, && (1.14c)\\ -\mathbf{u}_i\cdot\boldsymbol{n}_i &= g_{\mathrm{N}} && \text{on} && \Gamma^{\mathrm{N}}\cap\partial\Omega_i, && (1.14d)\\ p_i &= \lambda && \text{on} && \Gamma_{1,2}, && (1.14e) \end{aligned}$$

where λ is a given function on $\Gamma_{1,2}$. Therefore, if $(p_1,\mathbf{u}_1)$ and $(p_2,\mathbf{u}_2)$ are the solutions of (1.14), for $i = 1$ and $i = 2$ respectively, then $p_1 = \lambda = p_2$ on $\Gamma_{1,2}$, and thus the condition (1.13a) is satisfied. Let $\mathscr{V}_i = L^2(\Omega_i)\times L^2(\Gamma^{\mathrm{D}}\cap\partial\Omega_i)\times L^2(\Gamma^{\mathrm{N}}\cap\partial\Omega_i)$, $i = 1,2$. We introduce the following linear operator for $i = 1,2$:

$$\begin{array}{rccc} \boldsymbol{S}_i^{\mathrm{DtN}} & : & L^2(\Gamma_{1,2})\times\mathscr{V}_i & \to & L^2(\Gamma_{1,2}) \\ & & (\xi_i,\mathscr{F}_i) & \mapsto & \mathbf{u}_i\cdot\boldsymbol{n}_i|_{\Gamma_{1,2}}, \end{array} \qquad (1.15)$$

where $(p_i,\mathbf{u}_i)$ is the solution of problem (1.14) in the $L^2(\Omega_i)\times\mathbf{W}_i^{g_{\mathrm{N}}}$ space. Here $\mathscr{F}_i = (f|_{\Omega_i}, g_{\mathrm{D}}|_{\Gamma^{\mathrm{D}}\cap\partial\Omega_i}, g_{\mathrm{N}}|_{\Gamma^{\mathrm{N}}\cap\partial\Omega_i})$ represents all the physical source terms except the one on the interface which is represented separately by the given function λ. From the definition of $\boldsymbol{S}_i^{\mathrm{DtN}}$, the second condition (1.13b) can be written as:

$$\boldsymbol{S}_1^{\mathrm{DtN}}(\lambda,\mathscr{F}_1) + \boldsymbol{S}_2^{\mathrm{DtN}}(\lambda,\mathscr{F}_2) = 0. \qquad (1.16)$$

By linearity, $\boldsymbol{S}_i^{\mathrm{DtN}}$ can be separated into two parts. The first part depends on λ and the second part depends on the source term and the boundary conditions denoted by $\mathscr{F}_i$:

$$\sum_{i=1}^{2} \boldsymbol{S}_i^{\mathrm{DtN}}(\lambda, 0) = -\sum_{i=1}^{2} \boldsymbol{S}_i^{\mathrm{DtN}}(0, \mathscr{F}_i). \tag{1.17}$$

In other words, for $i = 1, 2$, $\mathbf{u}_i$ can be written as:

$$\mathbf{u}_i = \mathbf{u}_i^0 + \mathbf{u}_i^\star, \tag{1.18}$$

where $\mathbf{u}_i^0$ and $\mathbf{u}_i^\star$ are respectively the solutions of the following problems:

$$\begin{aligned}
\mathbf{u}_i^0 &= -\boldsymbol{S}\nabla p_i^0 && \text{in} && \Omega_i, && (1.19a)\\
\nabla\cdot\mathbf{u}_i^0 &= 0 && \text{in} && \Omega_i, && (1.19b)\\
p_i^0 &= 0 && \text{on} && \Gamma^{\mathrm{D}} \cap \partial\Omega_i, && (1.19c)\\
-\mathbf{u}_i^0 \cdot \boldsymbol{n}_i &= 0 && \text{on} && \Gamma^{\mathrm{N}} \cap \partial\Omega_i, && (1.19d)\\
p_i^0 &= \lambda && \text{on} && \Gamma_{1,2}, && (1.19e)
\end{aligned}$$

and

$$\begin{aligned}
\mathbf{u}_i^\star &= -\boldsymbol{S}\nabla p_i^\star && \text{in} && \Omega_i, && (1.20a)\\
\nabla\cdot\mathbf{u}_i^\star &= f && \text{in} && \Omega_i, && (1.20b)\\
p_i^\star &= g_{\mathrm{D}} && \text{on} && \Gamma^{\mathrm{D}} \cap \partial\Omega_i, && (1.20c)\\
-\mathbf{u}_i^\star \cdot \boldsymbol{n}_i &= g_{\mathrm{N}} && \text{on} && \Gamma^{\mathrm{N}} \cap \partial\Omega_i, && (1.20d)\\
p_i^\star &= 0 && \text{on} && \Gamma_{1,2}. && (1.20e)
\end{aligned}$$

Therefore, we can rewrite the problem (1.12)–(1.13) as the following equivalent interface problem:

$$\boldsymbol{S}^{\mathrm{DtN}}\lambda = \boldsymbol{\chi}, \tag{1.21}$$

where

$$\boldsymbol{\chi} = -\sum_{i=1}^{2} \mathbf{u}_i^\star \cdot \boldsymbol{n}_i, \tag{1.22}$$

and

$$\boldsymbol{S}^{\mathrm{DtN}}\lambda = \sum_{i=1}^{2} \mathbf{u}_i^0 \cdot \boldsymbol{n}_i. \tag{1.23}$$

Another method is to rewrite (1.13) as equivalent Robin conditions and then use a Robin-to-Robin interface operator.

1.3.2 Multidomain formulation with Robin transmission conditions

The physical conditions (1.13a)–(1.13b) introduced previously can be replaced by other equivalent conditions, namely Robin transmission conditions [59, 95]:

$$\begin{aligned}
-\beta_{1,2}\mathbf{u}_1 \cdot \boldsymbol{n}_1 + p_1 &= -\beta_{1,2}\mathbf{u}_2 \cdot \boldsymbol{n}_1 + p_2 && \text{on} && \Gamma_{1,2}, && (1.24a)\\
-\beta_{2,1}\mathbf{u}_2 \cdot \boldsymbol{n}_2 + p_2 &= -\beta_{2,1}\mathbf{u}_1 \cdot \boldsymbol{n}_2 + p_1 && \text{on} && \Gamma_{1,2}, && (1.24b)
\end{aligned}$$

where $\beta_{1,2} > 0$ and $\beta_{2,1} > 0$ are fixed parameters; a Robin condition is a combination of Dirichlet and Neumann conditions.

Proof. First, observe that the implication (1.13a)–(1.13b)⇒(1.24a)–(1.24b) is obvious. Next, we know that $\boldsymbol{n}_2 = -\boldsymbol{n}_1$. Thus, we multiply (1.24a) by $\beta_{2,1}$ and (1.24b) by $\beta_{1,2}$ respectively, and then subtract (1.24b) from (1.24a). We obtain:

$$\beta_{2,1}p_1 - \beta_{1,2}p_2 = \beta_{2,1}p_2 - \beta_{1,2}p_1.$$

Therefore, as $\beta_{1,2} + \beta_{2,1} \neq 0$, then $(\beta_{1,2} + \beta_{2,1})(p_1 - p_2) = 0 \iff p_1 = p_2$ on $\Gamma_{1,2}$. By replacing p_1 by p_2 in the equation (1.24a), we obtain $\mathbf{u}_1 \cdot \boldsymbol{n}_1 = \mathbf{u}_2 \cdot \boldsymbol{n}_1$.

□

The Robin-to-Robin operator

In order to solve the split formulation (1.12) with the Robin transmission conditions (1.24a)–(1.24b) on the interface, we introduce the problem for Ω_i, $i = 1, 2$, and where $j = 3 - i$, as follows:

$$\begin{aligned}
\mathbf{u}_i = -\boldsymbol{S}\nabla p_i \quad &\text{in} \quad \Omega_i, && \text{(1.25a)}\\
\nabla\cdot\mathbf{u}_i = f \quad &\text{in} \quad \Omega_i, && \text{(1.25b)}\\
p_i = g_{\mathrm{D}} \quad &\text{on} \quad \Gamma^{\mathrm{D}} \cap \partial\Omega_i, && \text{(1.25c)}\\
-\mathbf{u}_i \cdot \boldsymbol{n}_i = g_{\mathrm{N}} \quad &\text{on} \quad \Gamma^{\mathrm{N}} \cap \partial\Omega_i, && \text{(1.25d)}\\
-\beta_{i,j}\mathbf{u}_i \cdot \boldsymbol{n}_i + p_i = \xi_i \quad &\text{on} \quad \Gamma_{1,2}, && \text{(1.25e)}
\end{aligned}$$

where ξ_i is a given function on $\Gamma_{1,2}$. Then, for $i = 1, 2$, we introduce the following operator:

$$\begin{array}{rccc}
\boldsymbol{S}_i^{\mathrm{RtR}} & : & L^2(\Gamma_{1,2}) \times \mathscr{V}_i & \to & L^2(\Gamma_{1,2}) \\
 & & (\xi_i, \mathscr{F}_i) & \mapsto & -\beta_{j,i}\mathbf{u}_i \cdot \boldsymbol{n}_j|_{\Gamma_{1,2}} + p_i,
\end{array} \tag{1.26}$$

where $\mathbf{u}_i$ and p_i are the solutions of (1.25) and $\mathscr{F}_i = (f|_{\Omega_i}, g_{\mathrm{D}}|_{\Gamma^{\mathrm{D}}\cap\partial\Omega_i}, g_{\mathrm{N}}|_{\Gamma^{\mathrm{N}}\cap\partial\Omega_i})$ represents all the physical source terms except the one on the interface, which is represented separately by the function ξ_i. From the definition of $\boldsymbol{S}_i^{\mathrm{RtR}}$, the problem (1.12) with the Robin transmission conditions (1.24a)–(1.24b) can be written in the equivalent form:

$$\begin{aligned}
\xi_1 = \boldsymbol{S}_2^{\mathrm{RtR}}(\xi_2, \mathscr{F}_2) \quad &\text{on} \quad \Gamma_{1,2}, && \text{(1.27a)}\\
\xi_2 = \boldsymbol{S}_1^{\mathrm{RtR}}(\xi_1, \mathscr{F}_1) \quad &\text{on} \quad \Gamma_{1,2}, && \text{(1.27b)}
\end{aligned}$$

or in compact form,

$$\boldsymbol{S}^{\mathrm{RtR}} \begin{pmatrix} \xi_1 \\ \xi_2 \end{pmatrix} = \boldsymbol{\chi}_{\mathrm{R}} \quad \text{on} \quad \Gamma_{1,2}, \tag{1.28}$$

where $\boldsymbol{S}^{\mathrm{RtR}} := \boldsymbol{I} - \tilde{\boldsymbol{S}}^{\mathrm{RtR}}$, and

$$\tilde{\boldsymbol{S}}^{\mathrm{RtR}} \begin{pmatrix} \xi_1 \\ \xi_2 \end{pmatrix} = \begin{pmatrix} \boldsymbol{S}_2^{\mathrm{RtR}}(\xi_2, 0) \\ \boldsymbol{S}_1^{\mathrm{RtR}}(\xi_1, 0) \end{pmatrix}, \quad \boldsymbol{\chi}_{\mathrm{R}} = \begin{pmatrix} \boldsymbol{S}_2^{\mathrm{RtR}}(0, \mathscr{F}_2) \\ \boldsymbol{S}_1^{\mathrm{RtR}}(0, \mathscr{F}_1) \end{pmatrix}. \tag{1.29}$$

In this work, we use the domain decomposition method based on Robin transmission conditions since the parameters $\beta_{1,2}$ and $\beta_{2,1}$ can be optimized to improve the convergence rate of the iterative scheme [71, 102, 103, 104]. This method is known as the Optimized Schwarz Method, see [71] for an overview of this method.

1.4 The case of many subdomains using the Optimized Schwarz Method

In this section, we present the optimized Schwarz method to the multidomain case [57, 51, 71, 102, 103, 104]. More precisely, the interface problem is based on [51]. We now suppose that Ω is decomposed into more than two subdomains as in (1.3), such that Ω_i is a polygon for $d=2$ (polyhedron if $d=3$). For all $i \in [\![1, \mathcal{N}]\!]$, let:

$$\Gamma_i^{\mathrm{N}} = \Gamma^{\mathrm{N}} \cap \partial\Omega_i \quad \text{and} \quad \Gamma_i^{\mathrm{D}} = \Gamma^{\mathrm{D}} \cap \partial\Omega_i. \tag{1.30}$$

Let B^i be the set of neighbors of the subdomain Ω_i that share at least one edge with Ω_i (face for $d=3$), let $\tilde{B}^i$ be the set of neighbors of the subdomain Ω_i that share at least one vertex with Ω_i, and let $|B^i|$ and $|\tilde{B}^i|$ be the cardinality of these sets. Using this notation, we introduce:

$$\Gamma_{i,j} = \partial\Omega_i \cap \partial\Omega_j, \quad \forall j \in B^i, \tag{1.31}$$

$$\Gamma_i = \underset{j\in B^i}{\cup} \Gamma_{i,j}, \tag{1.32}$$

and

$$\partial\Omega_i = \Gamma_i^{\mathrm{N}} \cup \Gamma_i^{\mathrm{D}} \cup \Gamma_i. \tag{1.33}$$

We also introduce the spaces:

$$L^p(\Gamma_i) = \prod_{j\in B^i} L^p(\Gamma_{i,j}) \text{ and } L^p(\Gamma) = \prod_{i=1}^{\mathcal{N}} L^p(\Gamma_i). \tag{1.34}$$

Let $\beta_{i,j} > 0$, $j \in B^i$, $i \in [\![1, \mathcal{N}]\!]$ be the Robin parameters. Then, solving the subdomain problem for $i \in [\![1, \mathcal{N}]\!]$:

$$\mathbf{u}_i = -\boldsymbol{S}\nabla p_i \quad \text{in} \quad \Omega_i, \tag{1.35a}$$

$$\nabla\cdot\mathbf{u}_i = f \quad \text{in} \quad \Omega_i, \tag{1.35b}$$

$$p_i = g_{\mathrm{D}} \quad \text{on} \quad \Gamma_i^{\mathrm{D}}, \tag{1.35c}$$

$$-\mathbf{u}_i\cdot\boldsymbol{n}_i = g_{\mathrm{N}} \quad \text{on} \quad \Gamma_i^{\mathrm{N}}, \tag{1.35d}$$

$$-\beta_{i,j}\mathbf{u}_i\cdot\boldsymbol{n}_i + p_i = -\beta_{i,j}\mathbf{u}_j\cdot\boldsymbol{n}_i + p_j \quad \text{on} \quad \Gamma_{i,j},\ \forall j \in B^i, \tag{1.35e}$$

is equivalent to solving the original problem (1.1). As shown on the two-subdomain case (1.24), the two Robin conditions on $\Gamma_{i,j}$ are:

$$-\beta_{i,j}\mathbf{u}_i\cdot\boldsymbol{n}_i + p_i = -\beta_{i,j}\mathbf{u}_j\cdot\boldsymbol{n}_i + p_j \quad \text{on} \quad \Gamma_{i,j}, \tag{1.36a}$$

$$-\beta_{j,i}\mathbf{u}_j\cdot\boldsymbol{n}_j + p_j = -\beta_{j,i}\mathbf{u}_i\cdot\boldsymbol{n}_j + p_i \quad \text{on} \quad \Gamma_{i,j}. \tag{1.36b}$$

In order to introduce the Robin-to-Robin operator, we first make the following remark:

Remark 1.3. *Note that the condition* (1.36b) *is the Robin condition of the subdomain problem in* Ω_j, $j \in B^i$. *Using* $\boldsymbol{n}_j = -\boldsymbol{n}_i$, *the right-hand side in* (1.36b) *can also be written as:*

$$\beta_{j,i}\mathbf{u}_i\cdot\boldsymbol{n}_i + p_i \text{ on } \Gamma_{i,j}. \tag{1.37}$$

Now, in (1.37), *if* $p_i \in L^2(\Omega_i)$, *then* $p_i|_{\Gamma_{i,j}} \notin L^2(\Gamma_{i,j})$ *and is defined through the Robin condition in* Ω_i: $-\beta_{i,j}\mathbf{u}_i\cdot\boldsymbol{n}_i + p_i = \xi_{i,j}$, *that is*

$$p_i|_{\Gamma_{i,j}} = \xi_{i,j} + \beta_{i,j}\mathbf{u}_i\cdot\boldsymbol{n}_i. \tag{1.38}$$

As in the previous section, let $\mathscr{V}_i = L^2(\Omega_i) \times L^2(\Gamma_i^{\mathrm{D}}) \times L^2(\Gamma_i^{\mathrm{N}})$ for $i \in [\![1, \mathscr{N}]\!]$. We now introduce the subproblem solution operator for Ω_i, $i \in [\![1, \mathscr{N}]\!]$, as follows:

$$\begin{array}{rccc} \mathscr{M}_i & : & L^2(\Gamma_i) \times \mathscr{V}_i & \to & L^2(\Gamma_i) \times L^2(\Omega_i) \times \mathbf{W}_i^{g_{\mathrm{N}}} \\ & & (\boldsymbol{\xi}_i, \boldsymbol{\mathscr{F}}_i) & \mapsto & (\boldsymbol{\xi}_i, p_i, \mathbf{u}_i), \end{array} \tag{1.39}$$

where $\boldsymbol{\xi}_i = \left(\xi_{i,j}\right)_{j \in B^i}$, $\boldsymbol{\mathscr{F}}_i = (f|_{\Omega_i}, g_{\mathrm{D}}|_{\Gamma_i^{\mathrm{D}}}, g_{\mathrm{N}}|_{\Gamma_i^{\mathrm{N}}})$, and where $(p_i, \mathbf{u}_i)$ is the solution of the following problem in Ω_i:

$$\mathbf{u}_i = -\boldsymbol{S} \nabla p_i \quad \text{in} \quad \Omega_i, \tag{1.40a}$$
$$\nabla \cdot \mathbf{u}_i = f \quad \text{in} \quad \Omega_i, \tag{1.40b}$$
$$p_i = g_{\mathrm{D}} \quad \text{on} \quad \Gamma_i^{\mathrm{D}}, \tag{1.40c}$$
$$-\mathbf{u}_i \cdot \boldsymbol{n}_i = g_{\mathrm{N}} \quad \text{on} \quad \Gamma_i^{\mathrm{N}}, \tag{1.40d}$$
$$-\beta_{i,j} \mathbf{u}_i \cdot \boldsymbol{n}_i + p_i = \xi_{i,j} \quad \text{on} \quad \Gamma_{i,j}, \ \forall j \in B^i. \tag{1.40e}$$

Using Remark 1.3, we also introduce:

$$\begin{array}{rccc} \mathscr{R}_i & : & L^2(\Gamma_i) \times L^2(\Omega_i) \times \mathbf{W}_i^{g_{\mathrm{N}}} & \to & L^2(\Gamma_i) \\ & & (\boldsymbol{\xi}_i, p_i, \mathbf{u}_i) & \mapsto & \left(\beta_{j,i} \mathbf{u}_i \cdot \boldsymbol{n}_i + (\xi_{i,j} + \beta_{i,j} \mathbf{u}_i \cdot \boldsymbol{n}_i)\right)_{j \in B^i}. \end{array} \tag{1.41}$$

We now introduce the Robin-to-Robin operator defined as:

$$\boldsymbol{S}_i^{\mathrm{RtR}} = \mathscr{R}_i \circ \mathscr{M}_i \ : \ L^2(\Gamma_i) \times \mathscr{V}_i \ \to \ L^2(\Gamma_i). \tag{1.42}$$

In the case $\mathscr{N} = 2$, this operator is the one of the previous section.
Then, the subproblems (1.35e) lead to the equivalent interface problem:

Find $(\boldsymbol{\xi}_1, \ldots, \boldsymbol{\xi}_{\mathscr{N}}) \in L^2(\Gamma_1) \times \ldots \times L^2(\Gamma_{\mathscr{N}})$ such that:

$$(\boldsymbol{\xi}_i)_j = (\boldsymbol{S}_j^{\mathrm{RtR}}(\boldsymbol{\xi}_j, \boldsymbol{\mathscr{F}}_j))_i, \quad \forall j \in B^i, \quad \forall i \in [\![1, \mathscr{N}]\!]. \tag{1.43}$$

Using $\mathscr{M}_j(\boldsymbol{\xi}_j, \boldsymbol{\mathscr{F}}_j) = \mathscr{M}_j(\boldsymbol{\xi}_j, \mathbf{0}) + \mathscr{M}_j(\mathbf{0}, \boldsymbol{\mathscr{F}}_j)$ and the linearity of $\mathscr{R}_i$, we obtain:

$$\begin{aligned} \boldsymbol{S}_j^{\mathrm{RtR}}(\boldsymbol{\xi}_j, \boldsymbol{\mathscr{F}}_j) &= \mathscr{R}_j(\mathscr{M}_j(\boldsymbol{\xi}_j, \boldsymbol{\mathscr{F}}_j)) \\ &= \mathscr{R}_j(\mathscr{M}_j(\boldsymbol{\xi}_j, \mathbf{0})) + \mathscr{R}_j(\mathscr{M}_j(\mathbf{0}, \boldsymbol{\mathscr{F}}_j)) \\ &= \boldsymbol{S}_j^{\mathrm{RtR}}(\boldsymbol{\xi}_j, \mathbf{0}) + \boldsymbol{S}_j^{\mathrm{RtR}}(\mathbf{0}, \boldsymbol{\mathscr{F}}_j). \end{aligned} \tag{1.44}$$

Hence, (1.43) can be rewritten as:

$$(\boldsymbol{\xi}_i)_j - (\boldsymbol{S}_j^{\mathrm{RtR}}(\boldsymbol{\xi}_j, \mathbf{0}))_i = (\boldsymbol{S}_j^{\mathrm{RtR}}(\mathbf{0}, \boldsymbol{\mathscr{F}}_j))_i, \quad \forall j \in B^i, \quad \forall i \in [\![1, \mathscr{N}]\!]. \tag{1.45}$$

Finally, our interface problem is:

$$\boldsymbol{S}^{\mathrm{RtR}} \boldsymbol{\xi} = \boldsymbol{\chi}_{\mathrm{R}}. \tag{1.46}$$

The interface problem is usually solved by iterative methods, for example: Jacobi, GMRES. For the sake of simplicity, the Jacobi iterative method is explained in the following section but a numerical result for GMRES will be presented.

1.4.1 Local solver of the Jacobi method

The Jacobi algorithm applied to the interface problem (1.46) is equivalent to solving iteratively local subdomain problems and then transfer information to the neighboring subdomain, at each iteration. More precisely, let Ω_i be a subdomain of Ω, and let k be the iteration index. Then, applying the Jacobi algorithm to (1.46) leads to the following algorithm: for $k \geq 0$, at iteration $k+1$, we are looking for the solutions p_i^{k+1} and $\mathbf{u}_i^{k+1}$ in subdomain Ω_i such that:

$$\mathbf{u}_i^{k+1} = -\boldsymbol{S}\nabla p_i^{k+1} \quad \text{in} \quad \Omega_i, \tag{1.47a}$$

$$\nabla\cdot\mathbf{u}_i^{k+1} = f \quad \text{in} \quad \Omega_i, \tag{1.47b}$$

$$p_i^{k+1} = g_{\mathrm{D}} \quad \text{on} \quad \Gamma_i^{\mathrm{D}}, \tag{1.47c}$$

$$-\mathbf{u}_i^{k+1}\cdot\boldsymbol{n}_i = g_{\mathrm{N}} \quad \text{on} \quad \Gamma_i^{\mathrm{N}}, \tag{1.47d}$$

$$-\beta_{i,j}\mathbf{u}_i^{k+1}\cdot\boldsymbol{n}_i + p_i^{k+1} = g_{\mathrm{R},j}^{k} \quad \text{on} \quad \Gamma_{i,j},\ \forall j \in B^i, \tag{1.47e}$$

where $g_{\mathrm{R},j}^{k} := -\beta_{i,j}\mathbf{u}_j^k\cdot\boldsymbol{n}_i + p_j^k$ for $k \geq 1$ is the information coming from the neighboring subdomain Ω_j, $j \in B^i$, at step k of the Jacobi algorithm. More precisely, p_j^k and $\mathbf{u}_j^k$ were computed at iteration k on Ω_j. This algorithm starts from an initial guess $g_{\mathrm{R},j}^0$ which is a given function in $L^2(\Gamma_{i,j})$, $j \in B^i$, $1 \leq i \leq \mathcal{N}$ (see [59] for the convergence analysis).

Remark 1.4. *Note that the continuity of the normal traces $\mathbf{u}_i\cdot\boldsymbol{n}_i = \mathbf{u}_j\cdot\boldsymbol{n}_i$ and of the pressure $p_i = p_j$ will be verified only at convergence of the DD algorithm.*

In order to derive a posteriori error estimates and an acceleration technique by defining a stopping criterion, we first make a discretization of the problem. In the next section, we detail the discretization using the mixed finite element method at step $k+1$ of the domain decomposition method.

1.5 The local solver in the mixed finite element formulation

We first write the weak formulation of problem (1.47).

1.5.1 Continuous problem: weak mixed formulation

In order to write the variational formulation in the mixed form for the problem (1.47) at iteration $k+1$ of the DD algorithm, we use the following spaces defined in Section 1.2: M_i, $\mathbf{W}_i$, $\overline{\mathbf{W}}_i$, $\mathbf{W}_i^{g_{\mathrm{N}}}$, and $\mathbf{W}_i^0$. We first multiply the equation (1.47a) by a test function $\mathbf{v}_i \in \mathbf{W}_i^0$ and then integrate over Ω_i. Green's formula is then applied:

$$\int_{\Omega_i} (\boldsymbol{S}^{-1}\mathbf{u}_i^{k+1})\cdot\mathbf{v}_i\,\mathrm{d}\mathbf{x} = \int_{\Omega_i} p_i^{k+1}\nabla\cdot\mathbf{v}_i\,\mathrm{d}\mathbf{x} - \int_{\partial\Omega_i} p_i^{k+1}\mathbf{v}_i\cdot\boldsymbol{n}_i\,\mathrm{d}\gamma, \tag{1.48}$$

so that,

$$\begin{aligned}\int_{\Omega_i} (\boldsymbol{S}^{-1}\mathbf{u}_i^{k+1})\cdot\mathbf{v}_i\,\mathrm{d}\mathbf{x} - \int_{\Omega_i} p_i^{k+1}\nabla\cdot\mathbf{v}_i\,\mathrm{d}\mathbf{x} = &-\int_{\Gamma_i^{\mathrm{D}}} p_i^{k+1}\mathbf{v}_i\cdot\boldsymbol{n}_i\,\mathrm{d}\gamma - \int_{\Gamma_i^{\mathrm{N}}} p_i^{k+1}\mathbf{v}_i\cdot\boldsymbol{n}_i\,\mathrm{d}\gamma \\ &- \sum_{j\in B^i}\int_{\Gamma_{i,j}} p_i^{k+1}\mathbf{v}_i\cdot\boldsymbol{n}_i\,\mathrm{d}\gamma.\end{aligned} \tag{1.49}$$

In equation (1.49), we do not know the value of p_i^{k+1} on $\Gamma_{i,j}$ and we do not know how to reformulate it in the mixed formulation as $p_i \in M_i$. Therefore, we will use Robin condition (1.47e), and replace p_i^{k+1} on $\Gamma_{i,j}$ by:

$$p_i^{k+1} = \beta_{i,j}\mathbf{u}_i^{k+1}\cdot\boldsymbol{n}_i + g_{\mathrm{R},j}^k.$$

Also, using the fact that $\mathbf{v}_i \in \mathbf{W}_i^0$, thus $\mathbf{v}_i\cdot\boldsymbol{n} = 0$ on Γ^{N}, we obtain:

$$\begin{aligned}\int_{\Omega_i}(\boldsymbol{\mathcal{S}}^{-1}\mathbf{u}_i^{k+1})\cdot\mathbf{v}_i\,\mathrm{d}\mathbf{x} + \sum_{j\in B^i}\int_{\Gamma_{i,j}}(\beta_{i,j}\mathbf{u}_i^{k+1}\cdot\boldsymbol{n}_i)(\mathbf{v}_i\cdot\boldsymbol{n}_i)\,\mathrm{d}\gamma - \int_{\Omega_i}p_i^{k+1}\nabla\cdot\mathbf{v}_i\,\mathrm{d}\mathbf{x} = \\ -\int_{\Gamma_i^{\mathrm{D}}}g_{\mathrm{D}}\mathbf{v}_i\cdot\boldsymbol{n}_i\,\mathrm{d}\gamma - \sum_{j\in B^i}\int_{\Gamma_{i,j}}g_{\mathrm{R},j}^k\mathbf{v}_i\cdot\boldsymbol{n}_i\,\mathrm{d}\gamma, \qquad \forall\mathbf{v}_i\in\mathbf{W}_i^0.\end{aligned} \tag{1.50}$$

Problem (1.50) is the weak formulation of the local problem in Ω_i. In order to write the DD algorithm, we give below the computation of the second term on the right-hand side of (1.50), for $j \in B^i$:

$$\begin{aligned}\int_{\Gamma_{i,j}}g_{\mathrm{R},j}^k\mathbf{v}_i\cdot\boldsymbol{n}_i\,\mathrm{d}\gamma &= \int_{\Gamma_{i,j}}(-\beta_{i,j}\mathbf{u}_j^k\cdot\boldsymbol{n}_i + p_j^k)\mathbf{v}_i\cdot\boldsymbol{n}_i\,\mathrm{d}\gamma \\ &= \int_{\Gamma_{i,j}}-\beta_{i,j}(\mathbf{u}_j^k\cdot\boldsymbol{n}_i)\mathbf{v}_i\cdot\boldsymbol{n}_i\,\mathrm{d}\gamma + \int_{\Gamma_{i,j}}p_j^k\mathbf{v}_i\cdot\boldsymbol{n}_i\,\mathrm{d}\gamma,\end{aligned} \tag{1.51}$$

where $\mathbf{u}_j^k\cdot\boldsymbol{n}_i$ and p_j^k, defined on the interface $\Gamma_{i,j}$, were computed at iteration k and coming from the neighboring subdomain Ω_j. In (1.51), the term $\displaystyle\int_{\Gamma_{i,j}}p_j^k\mathbf{v}_i\cdot\boldsymbol{n}_i\,\mathrm{d}\gamma$ is computed using the transmission condition of Ω_j on $\Gamma_{i,j}$:

$$\int_{\Gamma_{i,j}}p_j^k\mathbf{v}_i\cdot\boldsymbol{n}_i\mathrm{d}\gamma = \int_{\Gamma_{i,j}}(\beta_{j,i}\mathbf{u}_j^k\cdot\boldsymbol{n}_j + g_{\mathrm{R},i}^{k-1})\mathbf{v}_i\cdot\boldsymbol{n}_i\mathrm{d}\gamma. \tag{1.52}$$

Consequently, using (1.51), (1.52), and $\boldsymbol{n}_j = -\boldsymbol{n}_i$, we have:

$$\langle g_{\mathrm{R},j}^k, \mathbf{v}_i\cdot\boldsymbol{n}_i\rangle_{\Gamma_{i,j}} = \int_{\Gamma_{i,j}}\beta_{i,j}(\mathbf{u}_j^k\cdot\boldsymbol{n}_j)\mathbf{v}_i\cdot\boldsymbol{n}_i\,\mathrm{d}\gamma + \int_{\Gamma_{i,j}}(\beta_{j,i}\mathbf{u}_j^k\cdot\boldsymbol{n}_j + g_{\mathrm{R},i}^{k-1})\mathbf{v}_i\cdot\boldsymbol{n}_i\,\mathrm{d}\gamma. \tag{1.53}$$

Equation (1.50) together with (1.53) correspond to the k^{th} iteration of the Jacobi algorithm applied to the interface problem (1.46).

Remark 1.5. *For a basis function $\mathbf{v}_i$ associated to an edge on $\Gamma_{i,j}$ (in particular $\mathbf{v}_i = 0$ on $\partial\Omega_i\backslash\Gamma_{i,j}$), the term $\displaystyle\int_{\Gamma_{i,j}}p_j^k\mathbf{v}_i\cdot\boldsymbol{n}_i\mathrm{d}\gamma$ can be computed either by (1.52) or using (1.49) (replacing i by j and replacing $k+1$ by k):*

$$\int_{\Gamma_{i,j}}p_j^k\mathbf{v}_i\cdot\boldsymbol{n}_i\,\mathrm{d}\gamma = -\int_{\Gamma_{i,j}}p_j^k\mathbf{v}_i\cdot\boldsymbol{n}_j\,\mathrm{d}\gamma = \int_{\Omega_j}(\boldsymbol{\mathcal{S}}^{-1}\mathbf{u}_j^k)\cdot\mathbf{v}_i\,\mathrm{d}\mathbf{x} - \int_{\Omega_j}p_j^k\nabla\cdot\mathbf{v}_i\,\mathrm{d}\mathbf{x}. \tag{1.54}$$

Next, we multiply the equation (1.47b) by a test function $q_i \in M_i$ and we integrate over Ω_i. We obtain:

$$\int_{\Omega_i} \nabla\cdot\mathbf{u}_i^{k+1} q_i \,\mathrm{d}\mathbf{x} = \int_{\Omega_i} f\, q_i \,\mathrm{d}\mathbf{x}, \qquad \forall q_i \in M_i. \tag{1.55}$$

The dual mixed variational formulation of problem (1.47) can be written as: find $\mathbf{u}_i^{k+1} \in \mathbf{W}_i^{g_\mathrm{N}}$ and $p_i^{k+1} \in M_i$ such that:

$$(\boldsymbol{S}^{-1}\mathbf{u}_i^{k+1}, \mathbf{v}_i)_{\Omega_i} + \sum_{j\in B^i} \langle \beta_{i,j}\mathbf{u}_i^{k+1}\cdot\boldsymbol{n}_i, \mathbf{v}_i\cdot\boldsymbol{n}_i\rangle_{\Gamma_{i,j}} - (p_i^{k+1}, \nabla\cdot\mathbf{v}_i)_{\Omega_i} = \boldsymbol{\ell}_i^k(\mathbf{v}_i), \quad \forall \mathbf{v}_i \in \mathbf{W}_i^0, \tag{1.56a}$$

$$(\nabla\cdot\mathbf{u}_i^{k+1}, q_i)_{\Omega_i} = (f, q_i)_{\Omega_i}, \ \ \forall q_i \in M_i, \tag{1.56b}$$

where $\boldsymbol{\ell}_i^k$ is a linear form defined as:

$$\boldsymbol{\ell}_i^k : \mathbf{W}_i^0 \longmapsto \mathbb{R}, \quad \boldsymbol{\ell}_i^k(\mathbf{v}) = -\langle g_\mathrm{D}, \mathbf{v}\cdot\boldsymbol{n}_i\rangle_{\Gamma_i^\mathrm{D}} - \sum_{j\in B^i} \langle g_{\mathrm{R},j}^k, \mathbf{v}\cdot\boldsymbol{n}_i\rangle_{\Gamma_{i,j}}, \tag{1.57}$$

and where $\langle g_{\mathrm{R},j}^k, \mathbf{v}\cdot\boldsymbol{n}_i\rangle_{\Gamma_{i,j}}$ is defined by (1.53), for $j \in B^i$. Note that, in general, $\langle \beta_{i,j}\mathbf{u}_i^{k+1}\cdot\boldsymbol{n}_i, \mathbf{v}_i\cdot\boldsymbol{n}_i\rangle_{\Gamma_{i,j}}$ does not make sense because $\mathbf{v}_i\cdot\boldsymbol{n}_i \in H^{-\frac{1}{2}}(\partial\Omega_i)$ and $\mathbf{u}_i^{k+1}\cdot\boldsymbol{n}_i \in H^{-\frac{1}{2}}(\partial\Omega_i)$. But in our case, $\langle \beta_{i,j}\mathbf{u}_i^{k+1}\cdot\boldsymbol{n}_i, \mathbf{v}_i\cdot\boldsymbol{n}_i\rangle_{\Gamma_{i,j}}$ is well defined because we suppose $\mathbf{v}_i\cdot\boldsymbol{n}_i \in L^2(\partial\Omega_i)$ and $\mathbf{u}_i^{k+1}\cdot\boldsymbol{n}_i \in L^2(\partial\Omega_i)$, using the space $\overline{\mathbf{W}}_i$, $\mathbf{v}_i \in \mathbf{W}_i^0 \subset \overline{\mathbf{W}}_i$. Therefore, we have more regularity and the integral is defined in the $L^2(\partial\Omega_i)$ sense. We introduce the following bilinear forms $\mathbf{a}_i$ and $\mathbf{b}_i$:

$$\mathbf{a}_i : \mathbf{W}_i^{g_\mathrm{N}} \times \mathbf{W}_i^0 \longmapsto \mathbb{R}, \quad \mathbf{a}_i(\mathbf{u}, \mathbf{v}) = (\boldsymbol{S}^{-1}\mathbf{u}, \mathbf{v})_{\Omega_i} + \sum_{j\in B^i} \langle \beta_{i,j}\mathbf{u}\cdot\boldsymbol{n}_i, \mathbf{v}\cdot\boldsymbol{n}_i\rangle_{\Gamma_{i,j}}, \tag{1.58a}$$

$$\mathbf{b}_i : \mathbf{W}_i^0 \times M_i \longmapsto \mathbb{R}, \quad \mathbf{b}_i(\mathbf{v}, p) = (p, \nabla\cdot\mathbf{v})_{\Omega_i}. \tag{1.58b}$$

The new form of the abstract variational formulation (1.56) for the mixed problem (1.47) is: find $\mathbf{u}_i^{k+1} \in \mathbf{W}_i^{g_\mathrm{N}}$ and $p_i^{k+1} \in M_i$ such that:

$$\mathbf{a}_i(\mathbf{u}_i^{k+1}, \mathbf{v}_i) - \mathbf{b}_i(\mathbf{v}_i, p_i^{k+1}) = \boldsymbol{\ell}_i^k(\mathbf{v}_i), \qquad \forall \mathbf{v}_i \in \mathbf{W}_i^0, \tag{1.59a}$$

$$\mathbf{b}_i(\mathbf{u}_i^{k+1}, q_i) = (f, q_i)_{\Omega_i}, \qquad \forall q_i \in M_i. \tag{1.59b}$$

1.5.2 Discrete problem: approximation by the mixed finite element method

Many different numerical methods for the discretization of partial differential equations can be used to approximate their solution. The conservative cell-centered techniques, as the mixed finite element method, mixed hybrid finite element method, or finite volume method are suitable here because they give the conservation of mass which is essential in our application. In this work, we will use the mixed finite element method with the lowest-order Raviart–Thomas–Nédélec space [136, 142]. Therefore, the scalar variable p is approximated in L^2 by a constant in each element of the mesh, and the vector function $\mathbf{u}$ is approximated in $\mathbf{H}(\mathrm{div})$ by functions such that the divergence is constant on each element and the normal trace is constant over the edges

in two dimensions and faces in three dimensions. Having the weak mixed formulation (1.59), we can apply the mixed finite element method, by replacing the spaces M_i and $\mathbf{W}_i$ by their finite-dimensional subspaces $M_{h,i}$ and $\mathbf{W}_{h,i}$.

1.5.2.1 Triangulation and notation

We define $\mathcal{T}_h := \bigcup_{i=1}^{\mathcal{N}} \mathcal{T}_{h,i}$, where $\mathcal{T}_{h,i}$ is a regular triangulation, $\forall i \in [\![1,\mathcal{N}]\!]$, of the polygonal subdomain Ω_i, such that $\Omega_i = \bigcup_{K\in\mathcal{T}_{h,i}} K$, with card($\mathcal{T}_{h,i}$) the number of triangles (tetrahedra if d=3) in the i-th subdomain. We suppose that $\mathcal{T}_{h,i}$ is a matching mesh, i.e., such that if $K, K' \in \mathcal{T}_{h,i}$, $K \neq K'$, then $K \cap K'$ is either an empty set or a common vertex or edge or face. For simplicity, we also assume that $\mathcal{T}_h$ is conforming. We denote the set of all faces (edges if $d = 2$) of $\mathcal{T}_{h,i}$ by $\mathcal{E}_{h,i}$, and the set of all faces of K by $\mathcal{E}_K$. $\mathcal{E}_{h,i}^{\text{int}}$ is the set of interior faces, $\mathcal{E}_{h,i}^{\text{ext}} = \mathcal{E}_{h,i}^{\Gamma^{\text{D}}} \cup \mathcal{E}_{h,i}^{\Gamma^{\text{N}}}$ is the set of boundary faces on $\partial\Omega \cap \partial\Omega_i$, and $\mathcal{E}_h^{\Gamma_{i,j}}$ is the set of sides on $\Gamma_{i,j}$. We then set $\mathcal{E}_{h,i} := (\bigcup_{j\in B^i} \mathcal{E}_h^{\Gamma_{i,j}}) \cup \mathcal{E}_{h,i}^{\text{int}} \cup \mathcal{E}_{h,i}^{\text{ext}}$. Let h_K denote the diameter of K and let h_i be the largest diameter of all triangles (tetrahedra if d=3) in $\mathcal{T}_{h,i}$, i.e., $h_i = \max_{K\in\mathcal{T}_{h,i}} h_K$. The set of vertices will be denoted by $\mathcal{V}_h$; it is decomposed into interior vertices $\mathcal{V}_h^{\text{int}}$, vertices located on the boundaries $\mathcal{V}_h^{\Gamma^{\text{D}}}$, $\mathcal{V}_h^{\Gamma^{\text{N}}}$, or $\mathcal{V}_h^{\Gamma^{\text{D}}\cap\Gamma^{\text{N}}} := \mathcal{V}_h^{\Gamma^{\text{D}}} \cap \mathcal{V}_h^{\Gamma^{\text{N}}}$ and vertices located on the interface $\Gamma_{i,j}$ denoted by $\mathcal{V}_h^{\Gamma_{i,j}}$, $i < j,\ \ i,j \in [\![1,\mathcal{N}]\!]$. We denote the set of verticies $\mathbf{a} \subset \partial\Gamma_{i,j}$ by $\mathcal{V}_h^{\partial\Gamma_{i,j}}$, and the set of verticies $\mathbf{a} \subset \Gamma_{i,j}\backslash(\partial\Gamma_{i,j})$ by $\mathcal{V}_h^{\Gamma_{i,j}\backslash(\partial\Gamma_{i,j})}$. Let $I_{\mathbf{a}}$ be the set of interfaces $\Gamma_{i,j}$ that share the vertex $\mathbf{a} \in \mathcal{V}_h^{\partial\Gamma_{i,j}}$, i.e.:

$$I_{\mathbf{a}} := \{\Gamma_{i,j} : i < j,\ \ i,j \in [\![1,\mathcal{N}]\!], \mathbf{a} \in \mathcal{V}_h^{\partial\Gamma_{i,j}}\}, \tag{1.60}$$

as shown in Figure 1.3 for the case of a decomposition of Ω into four subdomains, where $I_{\mathbf{a}} = \{\Gamma_{1,2},\ \Gamma_{1,3},\ \Gamma_{2,4},\ \Gamma_{3,4},\ \}$. Let $|I_{\mathbf{a}}|$ be the cardinality of this set and $I_{\mathbf{a}}^r$ the r^{th} interface in $I_{\mathbf{a}}$ sharing $\mathbf{a}$.

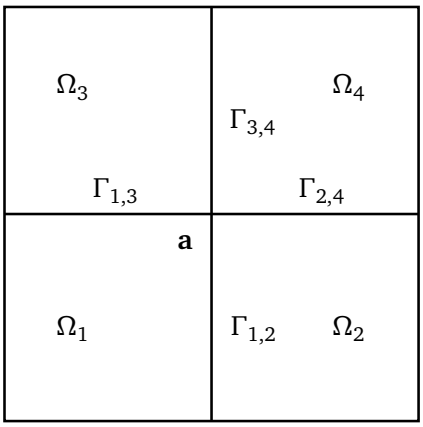

Figure 1.3: Intersection of the interfaces $\Gamma_{1,2}$, $\Gamma_{1,3}$, $\Gamma_{2,4}$, and $\Gamma_{3,4}$ at vertex $\mathbf{a}$

We denote the set of all the elements sharing the node $\mathbf{a}$ by $\mathscr{T}_{\mathbf{a}}$:

$$\begin{aligned}\mathscr{T}_{\mathbf{a}} &:= \{K \in \mathscr{T}_h;\ \mathbf{a} \in K\} \\ &= \bigcup_{i=1}^{\mathscr{N}} \{K \in \mathscr{T}_{h,i};\ \mathbf{a} \in K\} \\ &= \bigcup_{i=1}^{\mathscr{N}} \mathscr{T}_{\mathbf{a}}^{i},\end{aligned} \tag{1.61}$$

where $\mathscr{T}_{\mathbf{a}}^{i}$ is the set of all elements in the subdomain Ω_i sharing the node $\mathbf{a}$. $|\mathscr{T}_{\mathbf{a}}|$ and $|\mathscr{T}_{\mathbf{a}}^{i}|$ are the number of such elements. In the example of Figure 1.4, we have :

$$\mathscr{T}_{\mathbf{a}} = \bigcup_{i=1}^{4} \mathscr{T}_{\mathbf{a}}^{i} = \{K_1,\ K_2\} \cup \{K_3,\ K_4\} \cup \{K_5,\ K_6\} \cup \{K_7,\ K_8\}.$$

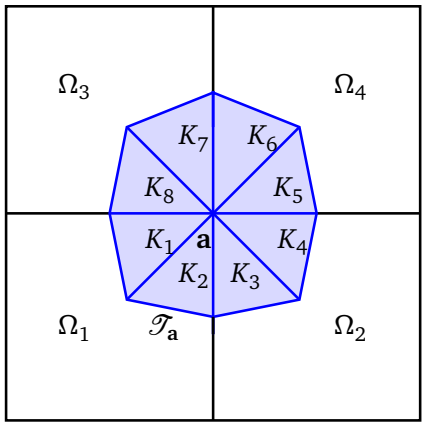

Figure 1.4: Patch $\mathscr{T}_{\mathbf{a}}$ of the elements which share the node $\mathbf{a}$

As we suppose that Ω_i is polygonal, for each integrable function f defined on Ω_i, we have:

$$\int_{\Omega_i} f(\mathbf{x})\,\mathrm{d}\mathbf{x} = \sum_{K \in \mathscr{T}_{h,i}} \int_K f(\mathbf{x})\,\mathrm{d}\mathbf{x}. \tag{1.62}$$

1.5.2.2 Finite-dimensional spaces for the mixed finite element method

Let $M_{h,i} \times \mathbf{W}_{h,i} \subset L^2(\Omega_i) \times \mathbf{H}(\mathrm{div}, \Omega_i)$ be the Raviart–Thomas–Nédélec mixed finite element space of order 0.

▹ $M_{h,i}$ **space**

$M_{h,i}$ is the space of functions $p_{h,i}$ in $L^2(\Omega_i)$ such that:

$$M_{h,i} := \{p_{h,i} \in L^2(\Omega_i);\ \forall K \in \mathscr{T}_{h,i},\ p_{h,i|K} \in \mathbb{P}^0(K)\}, \tag{1.63}$$

where $\mathbb{P}^0(K)$ is the space of polynomials of degree 0, i.e., which are constant in K. The dimension of this space is dim $M_{h,i}$= Card $(\mathscr{T}_{h,i})$= number of elements in $\mathscr{T}_{h,i}$.

– A basis of $M_{h,i}$ is the polynomial function of degree 0, defined on each element, and denoted by $\{\chi_K\}_{K\in\mathscr{T}_{h,i}}$, where:

$$\chi_K(\mathbf{x}) = \begin{cases} 1 & if \quad \mathbf{x}\in K, \\ 0 & \text{otherwise.} \end{cases} \tag{1.64}$$

– The approximate scalar solution $p_{h,i} \in M_{h,i}$ has a unique representation:

$$p_{h,i}(\mathbf{x}) = \sum_{K\in\mathscr{T}_{h,i}} p_K \chi_K(\mathbf{x}) \quad \text{for} \quad \mathbf{x}\in\Omega_i, \tag{1.65}$$

where p_K are the unknowns over the element K for all $K \in \mathscr{T}_{h,i}$, also called the degrees of freedom of the pressure head.

▹ $\mathbf{W}_{h,i}$ space

We first define the Raviart–Thomas–Nédélec vectorial field space of degree zero on a given simplex. It has dimension $(d+1)$ in $\mathbb{R}^d$ and is defined locally over an element $K \in \mathscr{T}_{h,i}$:

$$\mathbf{RTN}_0(K) := [\mathbb{P}_0(K)]^d + \mathbf{x}\mathbb{P}_0(K), \qquad \mathbf{x}\in\mathbb{R}^d. \tag{1.66}$$

For $d = 2$, a vector field $\mathbf{v}_h \in \mathbf{RTN}_0(K)$ in a point $\mathbf{x}$ of K where $\mathbf{x}\in\mathbb{R}^2$ can be written as:

$$\mathbf{v}_h = \begin{pmatrix} a_K \\ b_K \end{pmatrix} + d_K \begin{pmatrix} x \\ y \end{pmatrix}; \quad \text{where } (a_K, b_K, d_K)\in\mathbb{R}^3, \tag{1.67}$$

and for $d = 3$, $\mathbf{v}_h$ is written as:

$$\mathbf{v}_h = \begin{pmatrix} a_K \\ b_K \\ c_K \end{pmatrix} + d_K \begin{pmatrix} x \\ y \\ z \end{pmatrix}; \quad \text{where } (a_K, b_K, c_K, d_K)\in\mathbb{R}^4. \tag{1.68}$$

To have the property of continuity of the normal traces over the edges of the mesh $\mathscr{T}_{h,i}$ we use the space $\mathbf{W}_{h,i} \subset \mathbf{H}(\mathrm{div}, \Omega_i)$ defined as follows:

$$\mathbf{W}_{h,i} = \mathbf{RTN}_0(\mathscr{T}_{h,i}) := \{\mathbf{u}_{h,i} \in \mathbf{H}(\mathrm{div}, \Omega_i) \,:\, \mathbf{u}_{h,i\,|K} \in \mathbf{RTN}_0(K), \quad \forall K \in \mathscr{T}_{h,i}\}. \tag{1.69}$$

The most important properties of this space are:
• dim $\mathbf{W}_{h,i}$= card $(\mathscr{E}_{h,i})$=number of all the sides of $\mathscr{T}_{h,i}$,
• $\nabla\cdot\mathbf{u}_{h,i\,|K} \in \mathbb{P}_0(K) \quad \forall K \in \mathscr{T}_{h,i}$,
• $\mathbf{u}_{h,i}\cdot\boldsymbol{n}_e \in \mathbb{P}_0(e)$, $\forall\ e \in \mathscr{E}_{h,i}$.

– Let K and K' be two adjacent triangles (tetrahedrons if d=3) that share the edge e (face if d=3). We call $\mathbf{x}_{K,e}$ the vertex opposite to edge e (face if d=3) in triangle K (tetrahedron if d=3), and $\mathbf{x}_{K',e}$ the vertex opposite to edge e (face if d=3) in triangle K' (tetrahedron if d=3). We fix the normal $\boldsymbol{n}_e$ on e, and we suppose that it is oriented from K to K', see Figure 1.5. There is a basis function of the space $\mathbf{RTN}_0(\mathscr{T}_{h,i})$, associated with the edge $e \in \mathscr{E}_{h,i}^{\mathrm{int}}$ (face if d=3), defined on $K\cup K'$, and denoted ψ_e:

$$\psi_e(\mathbf{x}) = \frac{1}{d|K|}\overrightarrow{\mathbf{x}_{K,e}\mathbf{x}} = \frac{1}{d|K|}(\mathbf{x}-\mathbf{x}_{K,e}) \qquad \text{for } \mathbf{x}\in K, \tag{1.70a}$$

$$\psi_e(\mathbf{x}) = \frac{1}{d|K'|}\overrightarrow{\mathbf{x}\mathbf{x}_{K',e}} = \frac{1}{d|K'|}(\mathbf{x}_{K',e} - \mathbf{x}) \quad \text{for } \mathbf{x} \in K', \tag{1.70b}$$

$$\psi_e(\mathbf{x}) = 0 \quad \text{otherwise}, \tag{1.70c}$$

see Figure 1.6 for a representation of ψ_e on K, in 2D.

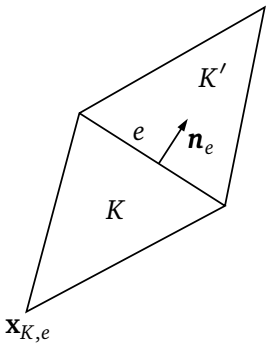

Figure 1.5: The normal of the edge e of the triangle K

Let $e \subset \partial\Omega \cup \partial\Omega_i$, and let $\boldsymbol{n}_e = \boldsymbol{n}$ be the normal on the edge e, where $\boldsymbol{n}$ is the exterior normal of Ω. In this case, $\psi_e(\mathbf{x})$ is equal to (1.70a) if $\mathbf{x} \in K$ and (1.70c) otherwise.

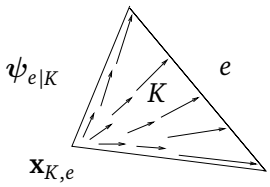

Figure 1.6: Flux through the edge e of the triangle K

Some consequence of ψ_e:

• For the basis $\{\psi_e\}_{e\in\mathscr{E}_{h,i}}$ of the space $\mathbf{W}_{h,i}$, we have:

$$\int_{e'} \psi_e \cdot \boldsymbol{n}_{e'} \mathrm{d}\gamma = \delta_{e,e'}, \quad e,\ e' \in \mathscr{E}_{h,i}. \tag{1.71}$$

In fact, if $e = e'$:

$$\langle \psi_e \cdot \boldsymbol{n}_e, 1\rangle_e = \int_e \psi_e \cdot \boldsymbol{n}_e \,\mathrm{d}\gamma = \langle \psi_e \cdot \boldsymbol{n}_K, 1\rangle_{\partial K} = (\nabla\cdot\psi_e, 1)_K = (\frac{1}{|K|}, 1)_K = 1,$$

and $\psi_e \cdot \boldsymbol{n}_{e'} = 0$ if $e', e \in \mathscr{E}_K$ and $e' \neq e$.
• Because of $\langle \psi_{e|K} \cdot \boldsymbol{n}_e, 1\rangle_e = \langle \psi_{e|K'} \cdot \boldsymbol{n}_e, 1\rangle_e = 1$, the normal trace is continuous through the edge e. Thus, the jump is zero $[\psi_e \cdot \boldsymbol{n}_e] = 0$.

– The approximate vector solution $\mathbf{u}_{h,i} \in \mathbf{W}_{h,i}$ has a unique representation as follows:

$$\mathbf{u}_{h,i}(\mathbf{x}) = \sum_{e\in\mathscr{E}_{h,i}} u_e \psi_e(\mathbf{x}), \quad \text{for } \mathbf{x} \in \Omega_i, \tag{1.72}$$

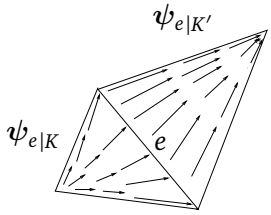

Figure 1.7: Flux through edge e in K and K'

where u_e are the degrees of freedom and are defined as the normal flux, which is an approximation of the vector flow $\mathbf{u}_i$ over edge $e \in \mathscr{E}_{h,i}$:

$$u_e = \int_e \mathbf{u}_{h,i} \cdot \boldsymbol{n}_e \mathrm{d}\gamma. \tag{1.73}$$

▹ **Degrees of freedom in $M_{h,i} \times \mathbf{W}_{h,i}$**

For a single mesh element K (for $d = 2$), the local degrees of freedom of $\mathbf{W}_{h,i}$ are represented by the arrows over the edges. The degree of freedom of $M_{h,i}$ is represented by the bullet in the triangle, as illustrated in Figure 1.8.

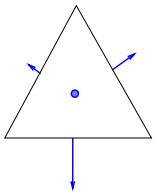

Figure 1.8: Degrees of freedom in $M_{h,i} \times \mathbf{W}_{h,i}$ for a single mesh element

▹ **M_h and $\mathbf{W}_h$ spaces**

We set $M_h := \oplus_{i=1}^{\mathscr{N}} M_{h,i}$ and $\mathbf{W}_h := \oplus_{i=1}^{\mathscr{N}} \mathbf{W}_{h,i}$. As noticed in Remark 1.4, the normal traces of the vectors in $\mathbf{W}_h$ and the pressure in M_h are continuous across the sides between two triangles in each subdomain Ω_i but not across the interfaces in Γ_i at each iteration of the DD algorithm. Only at convergence of the DD algorithm, the continuity of the normal traces and the pressure will be satisfied.

1.5.2.3 Approximation of the local problem

We define the approximation $g_{h,\mathrm{N}}$ of the function g_N as a piecewise constant function on each edge $e \subset \Gamma^\mathrm{N}$:

$$g_{h,\mathrm{N}|e} := \frac{1}{|e|} \int_e g_\mathrm{N} \mathrm{d}\gamma \quad \text{for each } e \subset \Gamma^\mathrm{N} \text{ of length } |e|. \tag{1.74}$$

We define the two following sets:

$$\mathbf{W}_{h,i}^{g_{h,\mathrm{N}}} := \{\mathbf{w}_{h,i} \in \mathbf{W}_{h,i};\ \mathbf{w}_{h,i} \cdot \boldsymbol{n} = g_{h,\mathrm{N}} \quad \text{on} \quad \Gamma_i^\mathrm{N}\}, \tag{1.75a}$$

$$\mathbf{W}_{h,i}^{0} := \{\mathbf{w}_{h,i} \in \mathbf{W}_{h,i};\ \mathbf{w}_{h,i} \cdot \boldsymbol{n} = 0 \quad \text{on} \quad \Gamma_i^\mathrm{N}\}. \tag{1.75b}$$

The discrete counterpart of (1.59) reads: find $\mathbf{u}_{h,i}^{k+1} \in \mathbf{W}_{h,i}^{g_{h,\mathrm{N}}}$ and $p_{h,i}^{k+1} \in M_{h,i}$ such that:

$$\mathbf{a}_i(\mathbf{u}_{h,i}^{k+1}, \mathbf{v}_{h,i}) - \mathbf{b}_i(\mathbf{v}_{h,i}, p_{h,i}^{k+1}) = \boldsymbol{\ell}_i^k(\mathbf{v}_{h,i}), \qquad \forall \mathbf{v}_{h,i} \in \mathbf{W}_{h,i}^0, \tag{1.76a}$$

$$\mathbf{b}_i(\mathbf{u}_{h,i}^{k+1}, q_{h,i}) = (f, q_{h,i})_{\Omega_i}, \qquad \forall q_{h,i} \in M_{h,i}, \tag{1.76b}$$

where the linear form $\boldsymbol{\ell}_i^k$ is defined in (1.57) and the bilinear forms $\mathbf{a}_i$ and $\mathbf{b}_i$ are defined in (1.58). Problem (1.76) can be written as an equivalent linear system that we detail below.

1.5.2.4 System of linear equations

For all $e \in \mathcal{E}_{h,i}$, $e \subset \Gamma_i^{\mathrm{N}}$, the discrete Neumann condition can be written as:

$$u_e^{k+1} = \int_e \mathbf{u}_h^{k+1} \cdot \boldsymbol{n}_e \mathrm{d}\gamma = \int_e g_{\mathrm{N}} \mathrm{d}\gamma = |e| g_{h,\mathrm{N}}. \tag{1.77}$$

Using the basis function as a function test in (1.76):

- $q_{h,i} = \chi_K$, $K \in \Omega_{h,i}$,
- $\mathbf{v}_{h,i} = \boldsymbol{\psi}_{e'}$, $e' \in \mathcal{E}_{h,i}$,

and using (1.65) and (1.72), we obtain the following system of linear equations, where $\{p_K^{k+1}\}_{K \in \mathcal{T}_{h,i}}$ and $\{u_e^{k+1}\}_{e \in \mathcal{E}_{h,i},\, e \notin \Gamma_i^{\mathrm{N}}}$ are the degrees of freedom:

$$\mathbf{a}_i\left(\sum_{e \in \mathcal{E}_{h,i}} u_e^{k+1} \boldsymbol{\psi}_e, \boldsymbol{\psi}_{e'}\right) - \mathbf{b}_i\left(\boldsymbol{\psi}_{e'}, \sum_{K \in \mathcal{T}_{h,i}} p_K^{k+1} \chi_K\right) = \boldsymbol{\ell}_i^k(\boldsymbol{\psi}_{e'}), \quad \forall e' \in \mathcal{E}_{h,i},\ e' \notin \Gamma_i^{\mathrm{N}}, \tag{1.78a}$$

$$\mathbf{b}_i\left(\sum_{e \in \mathcal{E}_{h,i}} u_e^{k+1} \boldsymbol{\psi}_e, \chi_K\right) = (f, \chi_K)_{\Omega_i}, \quad \forall K \in \mathcal{T}_{h,i}, \tag{1.78b}$$

$$u_e^{k+1} = g_{h,\mathrm{N}}|e|, \qquad e \in \mathcal{E}_{h,i},\ e \subset \Gamma_i^{\mathrm{N}}, \tag{1.78c}$$

or equivalently:

$$\sum_{e \in \mathcal{E}_{h,i}} \mathbf{a}_i(\boldsymbol{\psi}_e, \boldsymbol{\psi}_{e'}) u_e^{k+1} - \sum_{K \in \mathcal{T}_{h,i}} \mathbf{b}_i(\boldsymbol{\psi}_{e'}, \chi_K) p_K^{k+1} = \boldsymbol{\ell}_i^k(\boldsymbol{\psi}_{e'}), \quad \forall e' \in \mathcal{E}_{h,i},\ e' \notin \Gamma_i^{\mathrm{N}}, \tag{1.79a}$$

$$\sum_{e \in \mathcal{E}_{h,i}} \mathbf{b}_i(\boldsymbol{\psi}_e, \chi_K) u_e^{k+1} = (f, \chi_K)_{\Omega_i}, \quad \forall K \in \mathcal{T}_{h,i}, \tag{1.79b}$$

$$u_e^{k+1} = g_{h,\mathrm{N}}|e|, \qquad e \in \mathcal{E}_{h,i},\ e \subset \Gamma_i^{\mathrm{N}}. \tag{1.79c}$$

where $\boldsymbol{\ell}_i^k$ is defined in (1.57) as follows:

$$\boldsymbol{\ell}_i^k : \mathbf{W}_i^0 \longmapsto \mathbb{R}, \quad \boldsymbol{\ell}_i^k(\boldsymbol{\psi}_{e'}) = -\langle g_{\mathrm{D}}, \boldsymbol{\psi}_{e'} \cdot \boldsymbol{n}_i \rangle_{\Gamma_i^{\mathrm{D}}} - \sum_{j \in B^i} \langle g_{\mathrm{R},j}^k, \boldsymbol{\psi}_{e'} \cdot \boldsymbol{n}_i \rangle_{\Gamma_{i,j}}, \quad \forall k \geq 0. \tag{1.80}$$

Here, $g_{\mathrm{R},j}^0$ is a given initial guess on $\Gamma_{i,j}$ and $\langle g_{\mathrm{R},j}^k, \boldsymbol{\psi}_{e'} \cdot \boldsymbol{n}_i \rangle_{\Gamma_{i,j}}$, for $j \in B^i$ and $k \geq 1$, is the discrete counterpart of (1.53) when $e' \subset \Gamma_{i,j}$:

$$\langle g_{\mathrm{R},j}^k, \boldsymbol{\psi}_{e'} \cdot \boldsymbol{n}_i \rangle_{\Gamma_{i,j}} = \int_{\Gamma_{i,j}} \beta_{i,j} (\mathbf{u}_{h,j}^k \cdot \boldsymbol{n}_j) \boldsymbol{\psi}_{e'} \cdot \boldsymbol{n}_i \, \mathrm{d}\gamma + \int_{\Gamma_{i,j}} (\beta_{j,i} \mathbf{u}_{h,j}^k \cdot \boldsymbol{n}_j + g_{\mathrm{R},i}^{k-1}) \mathrm{d}\gamma, \tag{1.81}$$

and is equal to zero when $e' \not\subset \Gamma_{i,j}$. Equations (1.79a) and (1.79c) lead to:

$$\begin{aligned}
&\sum_{\substack{e\in\mathscr{E}_{h,i}\\ e\not\subset\Gamma_i^{\mathrm{N}}}} u_e^{k+1}\int_{\Omega_i} \boldsymbol{S}^{-1}\boldsymbol{\psi}_e\cdot\boldsymbol{\psi}_{e'}\,\mathrm{d}\mathbf{x}\\
&+\sum_{\substack{e\in\mathscr{E}_{h,i}\\ e\not\subset\Gamma_i^{\mathrm{N}}}} u_e^{k+1}\sum_{j\in B^i}\int_{\Gamma_{i,j}}\beta_{i,j}(\boldsymbol{\psi}_e\cdot\boldsymbol{n}_i)(\boldsymbol{\psi}_{e'}\cdot\boldsymbol{n}_i)\,\mathrm{d}\gamma-\sum_{K\in\mathscr{T}_{h,i}} p_K^{k+1}\int_{\Omega_i}\chi_K\nabla\cdot\boldsymbol{\psi}_{e'}\,\mathrm{d}\mathbf{x}=\\
&-\int_{\Gamma_i^{\mathrm{D}}} g_{\mathrm{D}}\boldsymbol{\psi}_{e'}\cdot\boldsymbol{n}_i\mathrm{d}\gamma-\sum_{j\in B^i}\int_{\Gamma_{i,j}} g_{\mathrm{R},j}^k\boldsymbol{\psi}_{e'}\cdot\boldsymbol{n}_i\mathrm{d}\gamma\\
&-\sum_{\substack{e\in\mathscr{E}_{h,i}\\ e\subset\Gamma_i^{\mathrm{N}}}} g_{h,\mathrm{N}}|e|\int_{\Omega_i}\boldsymbol{S}^{-1}\boldsymbol{\psi}_e\cdot\boldsymbol{\psi}_{e'}\,\mathrm{d}\mathbf{x},\ \forall e'\in\mathscr{E}_{h,i},\ e'\not\subset\Gamma_i^{\mathrm{N}}.
\end{aligned}\tag{1.82}$$

Indeed, note that for $j\in B^i$:

$$\int_{\Gamma_{i,j}}\beta_{i,j}(\boldsymbol{\psi}_e\cdot\boldsymbol{n}_i)(\boldsymbol{\psi}_{e'}\cdot\boldsymbol{n}_i)\,\mathrm{d}\gamma=\begin{cases}\displaystyle\int_e\beta_{i,j}(\boldsymbol{\psi}_e\cdot\boldsymbol{n}_i)^2\,\mathrm{d}\gamma=\frac{\beta_{i,j}}{|e|} & \text{if}\quad e=e'\text{ and }e\subset\Gamma_{i,j},\\ 0 & \text{otherwise,}\end{cases}\tag{1.83}$$

thus, $\displaystyle\sum_{\substack{e\in\mathscr{E}_{h,i}\\ e\subset\Gamma_i^{\mathrm{N}}}} u_e^{k+1}\int_{\Gamma_{i,j}}\beta_{i,j}(\boldsymbol{\psi}_e\cdot\boldsymbol{n}_i)(\boldsymbol{\psi}_{e'}\cdot\boldsymbol{n}_i)\,\mathrm{d}\gamma=0.$

Equations (1.79b) and (1.79c) give:

$$\sum_{\substack{e\in\mathscr{E}_{h,i}\\ e\not\subset\Gamma_i^{\mathrm{N}}}} u_e^{k+1}\int_{\Omega_i}\chi_K\nabla\cdot\boldsymbol{\psi}_e\,\mathrm{d}\mathbf{x}=\int_{\Omega_i} f\,\chi_K\,\mathrm{d}\mathbf{x}-\sum_{\substack{e\in\mathscr{E}_{h,i}\\ e\subset\Gamma_i^{\mathrm{N}}}} g_{h,\mathrm{N}}|e|\int_{\Omega_i}\chi_K\nabla\cdot\boldsymbol{\psi}_e\,\mathrm{d}\mathbf{x},\qquad\forall K\in\mathscr{T}_{h,i}.\tag{1.84}$$

The matrix form of this linear system is:

$$\mathbb{B}_i\mathbf{U}_i^{k+1}+\mathbb{C}_i\mathbf{P}_i^{k+1}=\mathbf{F}_{i,\mathbf{DR}}^k,\tag{1.85a}$$

$$\mathbb{C}_i^T\mathbf{U}_i^{k+1}=-\mathbf{F}_i,\tag{1.85b}$$

where

- $\mathbb{B}_i$ is a positive definite and sparse matrix, of dimension $(n_i^e-n_{Ni}^e)\times(n_i^e-n_{Ni}^e)$ where n_i^e is the number of all edges $e\in\mathscr{T}_{h,i}$ and n_{Ni}^e is the number of Neumann edges, i.e., $e\subset\Gamma_i^{\mathrm{N}}$:

$$\mathbb{B}_i=(\mathbf{a}_i(\boldsymbol{\psi}_e,\boldsymbol{\psi}_{e'}))_{e,e'\in\mathscr{E}_{h,i},\ e,e'\not\subset\Gamma_i^{\mathrm{N}}}.$$

The term $\boldsymbol{\psi}_e\cdot\boldsymbol{\psi}_{e'}$ is a polynomial of degree 2. By the quadrature formula, we have in two space dimensions:

$$\int_{\Omega_i}\boldsymbol{S}^{-1}\boldsymbol{\psi}_e\cdot\boldsymbol{\psi}_{e'}\,\mathrm{d}\mathbf{x}=\sum_{K\in\mathscr{T}_{h,i}}\int_{K/e,e'\subset\partial K}\boldsymbol{S}^{-1}\boldsymbol{\psi}_e\cdot\boldsymbol{\psi}_{e'}\,\mathrm{d}\mathbf{x}=\sum_{K\in\mathscr{T}_{h,i}}\sum_{p=1}^{3}\omega_p[\boldsymbol{S}^{-1}\boldsymbol{\psi}_e(\mathbf{m}_p).\boldsymbol{\psi}_{e'}(\mathbf{m}_p)]\tag{1.86}$$

where $w_p = \dfrac{|K|}{3}$ and $\mathbf{m}_p \in \mathbb{R}^2$ is the middle of the edge $e \subset \partial K$.

- $\mathbf{U}_i^{k+1}$ is the vector of degrees of freedom over the edges if d=2 (faces if d=3), of dimension $(n_i^e - n_{Ni}^e)$:

$$\mathbf{U}_i^{k+1} = (u_e^{k+1})_{e\in\mathscr{E}_{h,i},\, e\notin\Gamma_i^{\mathrm{N}}} = \left(\int_e \mathbf{u}_{h,i}^{k+1}\cdot\boldsymbol{n}_e \mathrm{d}\gamma\right)_{e\in\mathscr{E}_{h,i},\, e\notin\Gamma_i^{\mathrm{N}}},$$

- $\mathbb{C}_i$ is a matrix of dimension $(n_i^e - n_{Ni}^e)\times|\mathscr{T}_{h,i}|$:

$$\mathbb{C}_i = (-\mathbf{b}_i(\psi_e,\chi_K))_{e\in\mathscr{E}_{h,i},\, e\notin\Gamma_i^{\mathrm{N}},\, K\in\mathscr{T}_{h,i}}.$$

To compute the terms of the matrix $\mathbb{C}_i$, we need to compute:

$$\int_{\Omega_i}\chi_K\nabla\cdot\boldsymbol{\psi}_e\,\mathrm{d}\mathbf{x} = \int_K\nabla\cdot\boldsymbol{\psi}_e\,\mathrm{d}\mathbf{x} = \int_{\partial K}\boldsymbol{\psi}_e\cdot\boldsymbol{n}_K\mathrm{d}\gamma = \begin{cases} 0 & \text{if } e\notin\partial K,\\ 1 & \text{if } e\subset\partial K \text{ and } \boldsymbol{n}_K \text{ is outward},\\ -1 & \text{if } e\subset\partial K \text{ and } \boldsymbol{n}_K \text{ is inward}.\end{cases} \tag{1.87}$$

Hence, each column of $\mathbb{C}_i$ contains at most three non-zero elements in two space dimensions.

- $\mathbf{P}_i^{k+1}$ is the vector of degrees of freedom on the triangles, of dimension card$(\mathscr{T}_{h,i})$:

$$\mathbf{P}_i^{k+1} = (p_K^{k+1})_{K\in\mathscr{T}_{h,i}},$$

-$\mathbf{F}_{i,\mathbf{DR}}^k$ is a vector of dimension $(n_i^e - n_{Ni}^e)$:

$$\mathbf{F}_{i,\mathbf{DR}}^k = \left(\boldsymbol{\ell}_i^k(\boldsymbol{\psi}_{e'}) - \sum_{\substack{e\in\mathscr{E}_{h,i}\\ e\subset\Gamma_i^{\mathrm{N}}}} g_{h,\mathrm{N}}|e|\int_{\Omega_i}\boldsymbol{S}^{-1}\boldsymbol{\psi}_e\cdot\boldsymbol{\psi}_{e'}\,\mathrm{d}\mathbf{x}\right)_{e'\in\mathscr{E}_{h,i},e'\notin\Gamma_i^{\mathrm{N}}}, \tag{1.88}$$

- $\mathbf{F}_i$ is a vector of dimension card$(\mathscr{T}_{h,i})$:

$$\mathbf{F}_i = \left((f,\chi_K) - \sum_{\substack{e\in\mathscr{E}_{h,i}\\ e\subset\Gamma_i^{\mathrm{N}}}} g_{h,\mathrm{N}}|e|\int_{\Omega_i}\chi_K\nabla\cdot\boldsymbol{\psi}_e\,\mathrm{d}\mathbf{x}\right)_{K\in\mathscr{T}_{h,i}}.$$

The system (1.85) is the $(k+1)^{\text{th}}$ iteration of the discrete DD algorithm (i.e. the discrete counterpart of (1.47)), where $\mathbf{F}_{i,\mathbf{DR}}^k$ is defined by (1.88), using (1.80).

Remark 1.6. *For simplicity, we have presented one iteration of the discrete counterpart of* (1.46) *solved by the Jacobi iterative method. If GMRES is used instead of the Jacobi method, the discrete corresponding algorithm will uses similar discrete subdomain Robin problems as above.*

1.6 Numerical results

In this section, we present the results of numerical experiments for the MFE method in two cases. The first case is an illustration of the discretization error in the case of one domain Ω, with more general boundary conditions (Robin conditions) than the usual Dirichlet or Neumann conditions. The second case concerns the decomposition of Ω into two subdomains Ω_1 and Ω_2 using the DD method presented in the previous sections. An example of numbering of the vertices, edges, and triangles of the mesh, is shown in Figure 1.9.

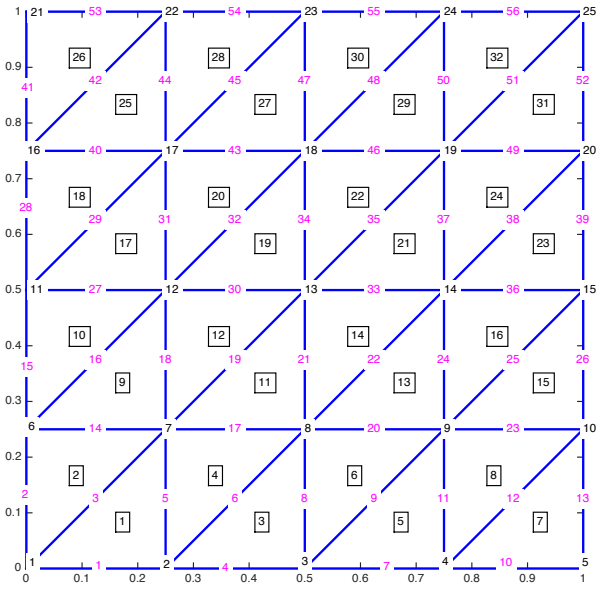

Figure 1.9: Global number of vertices, edges, and triangles for the domain Ω

1.6.1 The MFE method in one domain with different boundary conditions

This first example focuses on using the MFE method to solve the problem (1.1) with Robin boundary condition $-\mathbf{u}\cdot\boldsymbol{n}+p$ on one part of $\partial\Omega$, where on $\Omega=]0,1[\times]0,1[$. We have:

- the diffusion tensor: $\boldsymbol{S}=\begin{pmatrix}3 & 2\\ 2 & 3\end{pmatrix}$,
- the exact solution: $p(x,y)=\sin(2\pi x)\sin(2\pi y)$,
- f =$24\pi^2\sin(2\pi x)\sin(2\pi y)$-$16\pi^2\cos(2\pi x)\cos(2\pi y)$ the corresponding source term,
- $x=0$ the Neumann boundary,
- $x=1$ the Robin boundary,
- $y=0$ and $y=1$ the Dirichlet boundaries,

where the boundary conditions are prescribed by the exact solution.
As explained in the previous sections, the appoximate solution p_h of p by the MFE method is constant on each mesh element, see Figure 1.10 for $|\mathcal{T}_h|=512$ triangles.

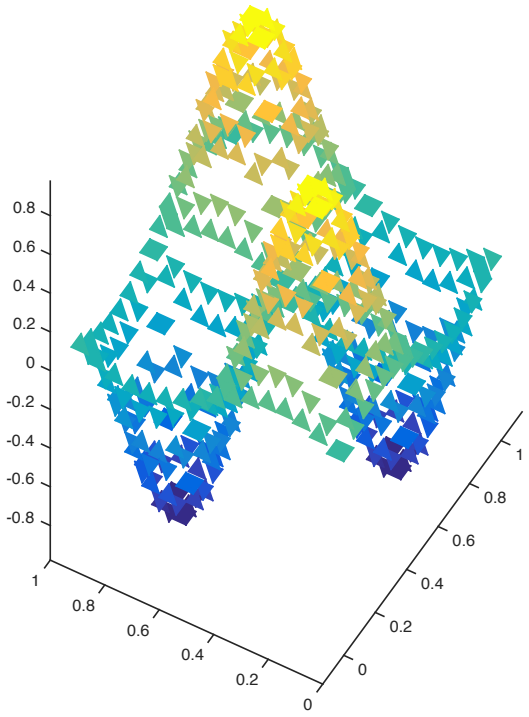

Figure 1.10: Approximation of p by a constant on each triangle, using the lowest-order Raviart–Thomas–Nédélec space

The method used to solve the system of linear equations is a direct method (LU factorization). We can see in Figure 1.11, where $|\mathscr{T}_h| = 131072$, that the approximate solution (on the right) is visually very close to the exact solution represented at the barycenter of each triangle (on the left). In Figure 1.12, we plot for $|\mathscr{T}_h| = 131072$ the distribution of the error between the exact solution p and the approximate solution p_h on the domain Ω, with a uniform mesh. In Figure 1.13, we plot the relative error of the pressure in the L^2 norm as a function of h (on the left), and the relative error of the flux in the $\mathbf{H}(\mathrm{div},\Omega)$ norm as a function of h (on the right). For more precision, we also include Tables 1.1 and 1.2. The convergence rate is very close to the value 1, and thus verifies the following a priori error estimates based on [36, 142]:

$$\|p - p_h\|_{L^2(\Omega)} \approx \mathscr{O}(h),$$

$$\|\mathbf{u} - \mathbf{u}_h\|_{\mathbf{H}(\mathrm{div},\Omega)} \approx \mathscr{O}(h).$$

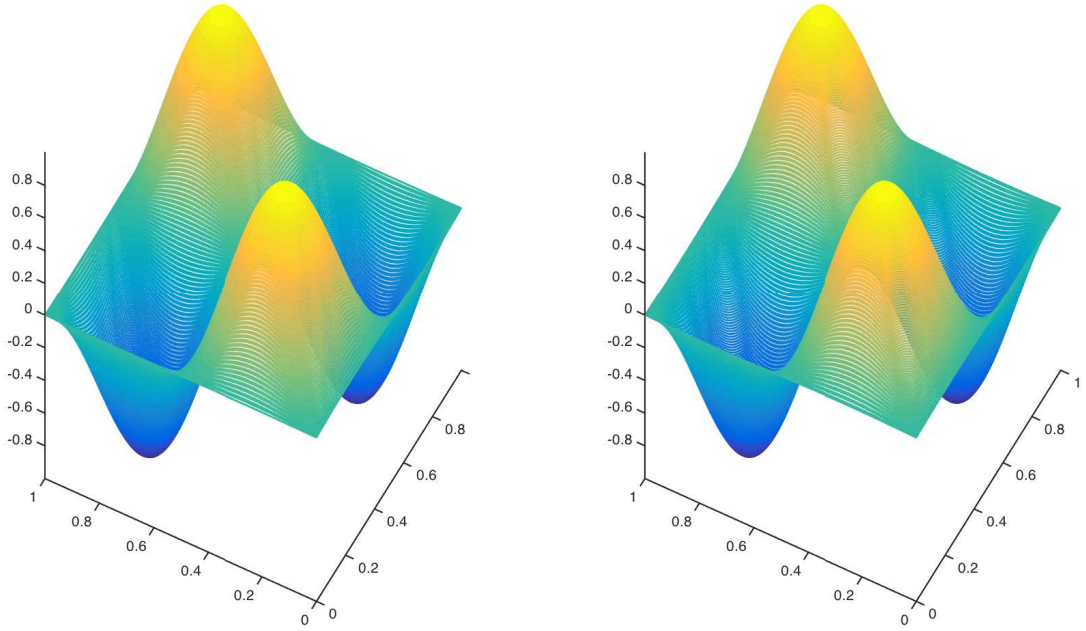

Figure 1.11: Exact solution (on the left) and approximate solution (on the right)

number of edges	number of triangles	$\text{err}_\text{p}=\frac{\|p-p_h\|_{L^2(\Omega)}}{\|p\|_{L^2(\Omega)}}$	convergence rate	h
3136	2048	0.0655		0.0442
12416	8192	0.0327	1.002	0.0221
49408	32768	0.0164	0.9891	0.0110
197120	131072	0.0082	1	0.0055
787456	524288	0.0041	1.0267	0.0028

Table 1.1: Convergence rate of the pressure error for different mesh refinements

number of edges	number of triangles	$\text{err}_\text{u}=\frac{\|\mathbf{u}-\mathbf{u}_h\|_{\mathbf{H}(\text{div},\Omega)}}{\|\mathbf{u}\|_{\mathbf{H}(\text{div},\Omega)}}$	convergence rate	h
3136	2048	0.079		0.0442
12416	8192	0.0396	0.9964	0.0221
49408	32768	0.0198	0.9935	0.0110
197120	131072	0.0099	1	0.0055
787456	524288	0.0049	1.0417	0.0028

Table 1.2: Convergence rate of the flux error for different mesh refinements

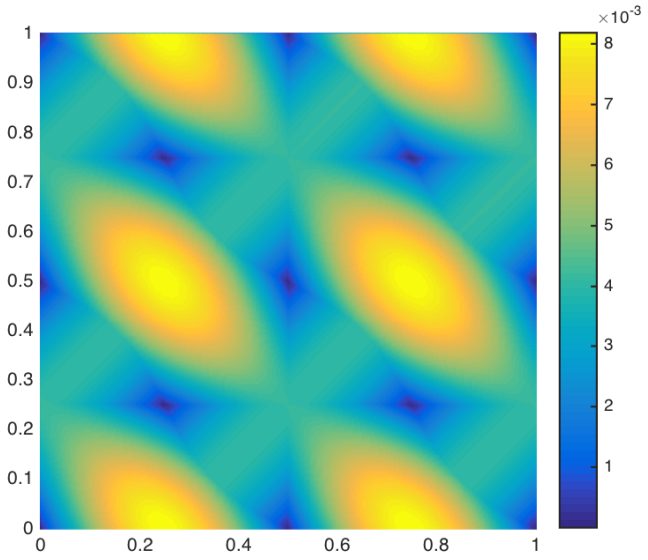

Figure 1.12: Error in the L^2-norm between the exact solution p and the approximate solution p_h

1.6.2 The MFE method in the DD method: Jacobi iterative solver

Let us first consider the domain decomposition of $\Omega =]0,1[\times]0,1[$ into two subdomains $\Omega_1 =]0,0.5[\times]0,1[$ and $\Omega_2 =]0.5,1[\times]0,1[$. The global numbering of the domain Ω becomes an independent numbering in each subdomain, as shown in Figures 1.14–1.15. The same problem defined above is now solved on each subdomain.

In this part, the discrete counterpart of the interface problem (1.46) is solved with the Jacobi algorithm. The DD stopping criteria is when the jump of Robin condition on the interface is less than 1e-10. In Figure 1.16 we show the convergence rate of the pressure error (on the left) and the flux error (on the right). The values of the error are shown in Tables 1.3 and 1.4 again to give more precision. It is clear from Figure 1.17 that the difference between the approximate solution p_h in the monodomain case and the approximate solution $p_{h,\mathrm{DD}}$ in the DD method is very small. We observe that the DD algorithm converges up to the given tolerance 1e-10 to the discrete monodomain solution (the solution of the discrete counterpart of problem 1.1). We can

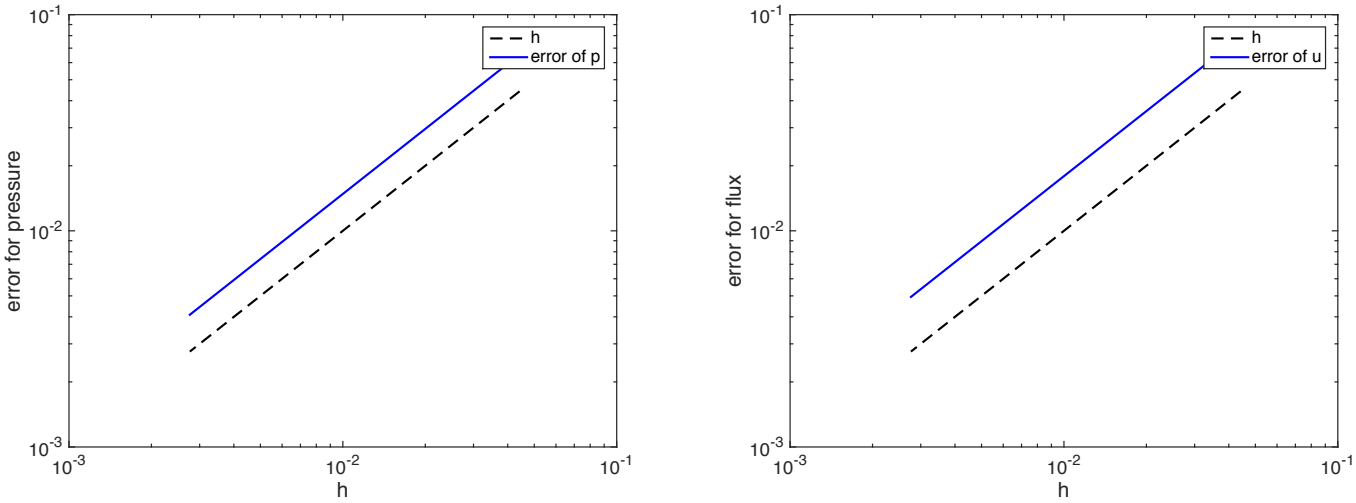

Figure 1.13: Error in the L^2-norm between the exact solution p and the approximate solution p_h (on the left) and error in the $\mathbf{H}(\mathrm{div},\Omega)$ norm between the exact solution $\mathbf{u}$ and the approximate solution $\mathbf{u}_h$ (on the right) for different mesh refinements

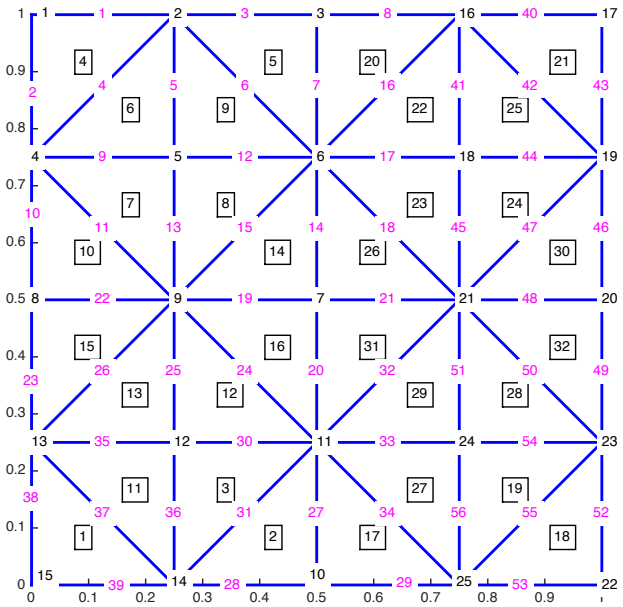

Figure 1.14: Global numbering in the mesh $\mathcal{T}_h$ of Ω

see in Table 1.5 that this difference is also very small for different mesh refinements. For all algebraic and domain decomposition solvers fully converged and without the presence of rounding errors, the approximate solution and the monodomain solution theoretically coincide. In this Chapter, the tolerance in the stopping criterion of the

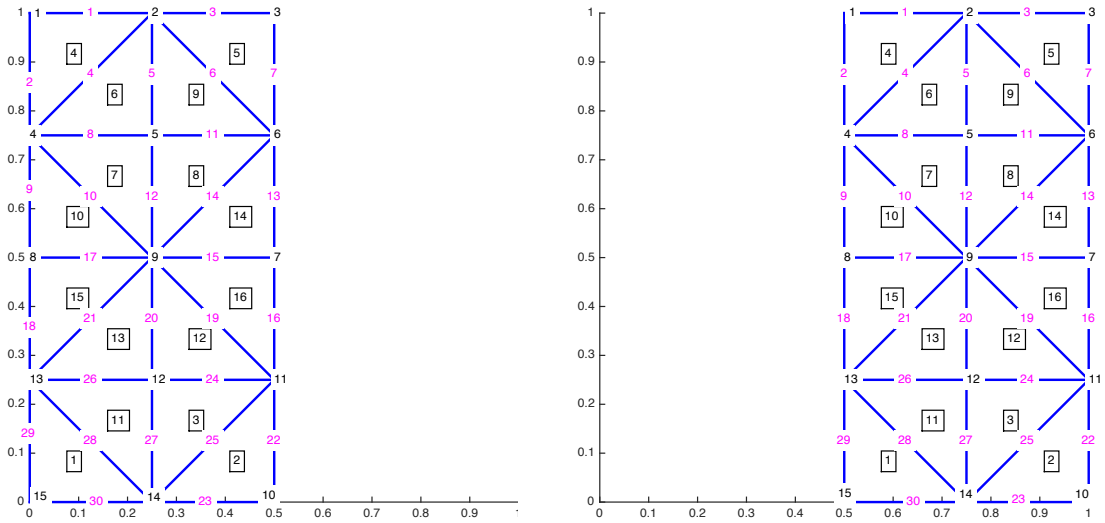

Figure 1.15: Global numbering of the mesh in the subdomain Ω_1 (on the left) and the subdomain Ω_2 (on the right) after domain decomposition

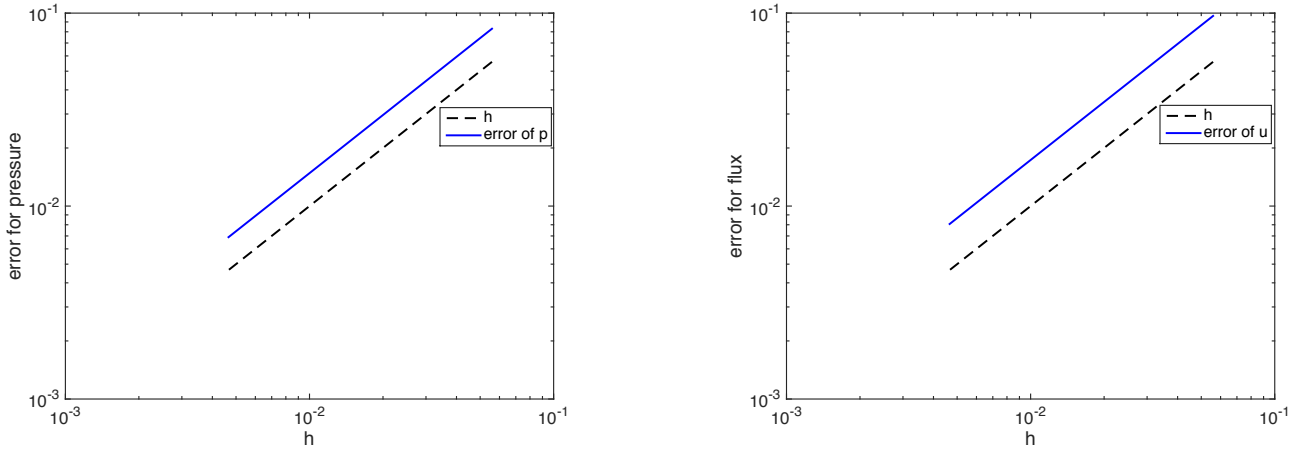

Figure 1.16: Convergence rate of the pressure (on the left) and the flux (on the right) in the DD method for different mesh refinements

DD algorithm is chosen arbitrary equal to 1e-10 which maybe a too much restrictive stopping criterion. In the next chapter, we will develop the theory of a posteriori estimates for the DD method in order to obtain an a posteriori stopping criterion with a lower tolerance, adapted to the problem considered.

no. of edges in Ω_1 /Ω_2	no. of triangles in Ω_1 /Ω_2	$\text{err}_\text{p}=\frac{\sum_{i=1,2}\|p_i - p_{h,i}\|_{L^2(\Omega_i)}}{\|p\|_{L^2(\Omega)}}$	convergence rate	h
1240/1240	800/800	0.083		0.0559
19360/19360	12800/12800	0.0208	0.9996	0.0140
43440/43440	28800/ 28800	0.0138	1.0030	0.0093
59080/ 59080	39200/39200	0.0118	1.0398	0.008
173280 / 173280	115200/ 115200	0.0068	1.0363	0.0047

Table 1.3: Convergence rate of the pressure error for different mesh refinements using the DD method for two subdomains

no. of edges in Ω_1 /Ω_2	no. of triangles in Ω_1 /Ω_2	$\text{err}_\text{u}= \frac{\sum_{i=1,2}\|\mathbf{u}_i - \mathbf{u}_{h,i}\|_{\mathbf{H}(\text{div},\Omega_i)}}{\|\mathbf{u}\|_{\mathbf{H}(\text{div},\Omega)}}$	convergence rate	h
1240/1240	800/800	0.09670		0.0559
19360/19360	12800/12800	0.0242	1.0005	0.0140
43440/43440	28800/ 28800	0.0161	0.9896	0.0093
59080/ 59080	39200/39200	0.0138	1.0412	0.008
173280 / 173280	115200/ 115200	0.0081	1.0017	0.0047

Table 1.4: Convergence rate of the flux error for different mesh refinements using the DD method for two subdomains

h	$\|\|p_{h,\text{DD}} - p_h\|\|_\infty$
0.0559	8.415e-11
0.0140	7.485e-11
0.0093	7.16e-10
0.008	4.12e-9
0.0047	1.989e-10

Table 1.5: Error between the approximate solution p_h in the one domain case and the approximate solution $p_{h,\text{DD}}$ in the DD case (with two subdomains) for different mesh refinements

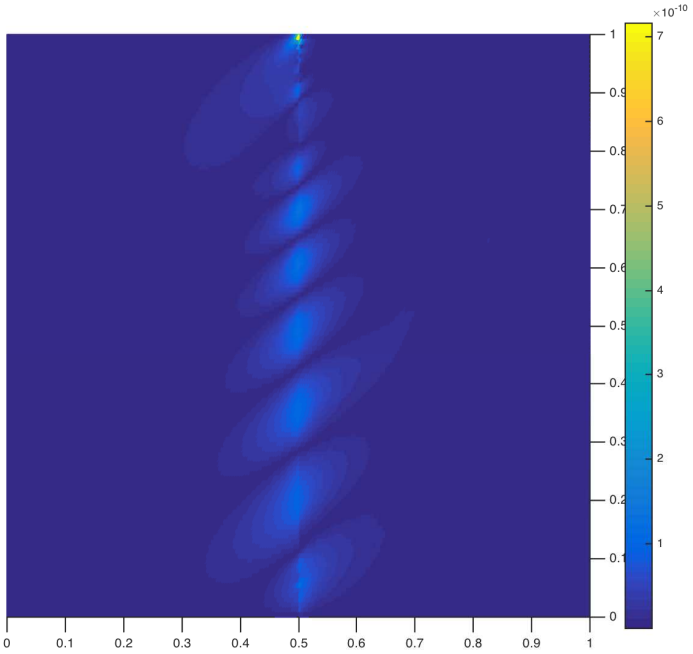

Figure 1.17: Error between the approximate solution p_h in the monodomain case and the approximate solution $p_{h,\mathrm{DD}}$ in the DD method with 28800 triangles in the domains Ω_i, $i = 1, 2$

Chapter 2

Estimates and stopping criteria in steady diffusion case

Contents

In this chapter, we develop a posteriori error estimates for the discretization introduced in the previous chapter. The purpose is to bound the error between the exact solution and the approximate solution, $|||\mathbf{u} - \mathbf{u}_h^{k+1}|||_\star$ and $|||p - p_h^{k+1}|||$, at each iteration $k+1$ of the DD method, by indicators that are completely computed from the approximate solution $(p_h^{k+1}, \mathbf{u}_h^{k+1})$ such that:

$$p_h^{k+1}|_{\Omega_i} := p_{h,i}^{k+1}, \qquad \mathbf{u}_h^{k+1}|_{\Omega_i} := \mathbf{u}_{h,i}^{k+1}, \ \forall i \in [\![1, \mathcal{N}]\!].$$

In order to obtain optimal a posteriori error estimates of p and $\mathbf{u}$ in the mixed finite element method, we first derive a postprocessing of p_h^{k+1}, denoted by $\tilde{p}_h^{k+1}$. This postprocessing improves the approximation of p. In general, our approach is based on

the reconstruction of an equilibrated flux and a potential, following [130, 154, 156]. We also wish to distinguish the different error components, namely the subdomain discretization error and the domain decomposition error as in [141]. This allows us to define suitable stopping criteria. We finally note that our approach is not restricted to the (non-preconditioned) Jacobi iteration. We use this setting only for the clarity of exposition. Any iteration (GMRES, conjugate gradients, etc.) can be used, together with any preconditioning.

Notation

We suppose for simplicity that $g_{\mathrm{D}} \in \mathbb{P}_2(\Gamma^{\mathrm{D}}) \cap C^0(\Gamma^{\mathrm{D}})$ and $g_{\mathrm{N}} \in \mathbb{P}_0(\Gamma^{\mathrm{N}})$. We introduce the broken Sobolev space $H^1(\mathscr{T}_h)$:

$$H^1(\mathscr{T}_h) := \{v \in L^2(\Omega);\, v|_K \in H^1(K), \quad \forall K \in \mathscr{T}_h\}. \tag{2.1}$$

For each interior edge $e \in (\underset{j\in B^i}{\cup} \mathscr{E}_h^{\Gamma_{i,j}}) \cup \mathscr{E}_{h,i}^{\mathrm{int}}$, such that the triangles K and K' share the edge e (the order of K, K' is arbitrary but fixed once and for all), we denote by $\boldsymbol{n}_e$ the normal vector pointing from K to K'. We also introduce the following notation for the jump and the average. For a given function v, its jump is defined as:

$$[\![v]\!] := \begin{cases} v|_K - v|_{K'} & \text{if} \quad e \in (\underset{j\in B^i}{\cup} \mathscr{E}_h^{\Gamma_{i,j}}) \cup \mathscr{E}_{h,i}^{\mathrm{int}}, \\ v|_e - g_{\mathrm{D}} & \text{if} \quad e \in \mathscr{E}_{h,i}^{\Gamma^{\mathrm{D}}}, \end{cases} \tag{2.2}$$

and its average on e is defined as:

$$\{\!\{v\}\!\} := \begin{cases} \frac{1}{2}(v|_K + v|_{K'}) & \text{if} \quad e \in (\underset{j\in B^i}{\cup} \mathscr{E}_h^{\Gamma_{i,j}}) \cup \mathscr{E}_{h,i}^{\mathrm{int}}, \\ \frac{1}{2}(v|_e + g_{\mathrm{D}}) & \text{if} \quad e \in \mathscr{E}_{h,i}^{\mathrm{ext}}. \end{cases} \tag{2.3}$$

In Sections 2.1 and 2.2, we give the ingredients which allow the general a posteriori estimates of Section 2.3. Then in Sections 2.5 and 2.6, we propose a specific construction of these tools based on the discretization and the DD method used in this thesis, to achieve as sharp as possible bounds.

The a posteriori analysis of the domain decomposition method presented below is applied for any locally conservative method, such as the mixed finite element and the cell-centered finite volume schemes.

2.1 Postprocessing of p_h^{k+1} in the lowest-order Raviart–Thomas case

Here, we consider what happens in a given subdomain Ω_i. In the continuous case, there is a direct link between $\mathbf{u}_i$ and p_i, the constitutive law:

$$\mathbf{u}_i = -\boldsymbol{S}\nabla p_i.$$

This link does not hold in the discrete case in the MFE method, i.e. $\mathbf{u}_{h,i} \neq -\boldsymbol{S}\nabla p_{h,i}$. This inspires us to perform a postprocessing $\tilde{p}_{h,i}^{k+1}$ of $p_{h,i}^{k+1}$ at each iteration $k+1$ of the DD algorithm, for all $k \geq 0$. The following postprocessing of $p_{h,i}^{k+1}$ was proposed in [154]: we construct $\tilde{p}_{h,i}^{k+1} \in \mathbb{P}_2(\mathscr{T}_{h,i})$, where $\mathbb{P}_2(\mathscr{T}_{h,i})$ is the space of piecewise polynomials of total degree less than or equal to 2, such that:

$$-\boldsymbol{S}\nabla\tilde{p}_{h,i}^{k+1}|_K = \mathbf{u}_{h,i}^{k+1}|_K, \qquad \forall K \in \mathscr{T}_{h,i}, \tag{2.4a}$$

$$\pi_0(\tilde{p}_{h,i}^{k+1}|_K) = p_{h,i}^{k+1}|_K, \qquad \forall K \in \mathscr{T}_{h,i}, \tag{2.4b}$$

where π_0 is the projection of $\tilde{p}_{h,i}^{k+1}|_K$ on constants:

$$\pi_0(\tilde{p}_{h,i}^{k+1}|_K) := \frac{(\tilde{p}_{h,i}^{k+1}, 1)_K}{|K|}. \tag{2.5}$$

Thus, $\tilde{p}_{h,i}^{k+1}$ is constructed element by element on $\mathscr{T}_{h,i}$. In general, $\tilde{p}_{h,i}^{k+1}$ is not conforming in the sense that $\tilde{p}_{h,i}^{k+1} \notin H^1(\Omega_i)$. It has been shown in [154] that $\tilde{p}_{h,i}^{k+1} \in W_0(\mathscr{T}_{h,i})$, where:

$$W_0(\mathscr{T}_{h,i}) := \{\varphi \in H^1(\mathscr{T}_{h,i});\ \langle[[\varphi]], 1\rangle_e = 0,\ \forall e \in \mathscr{E}_{h,i}^{\text{int}}\}. \tag{2.6}$$

This is the space such that the trace of jumps on the edges are orthogonal to a constant for all edges $e \in \mathscr{E}_{h,i}^{\text{int}}$. In other words, there is a weak continuity, in the sense that the mean of $\tilde{p}_{h,i}^{k+1}$ on the left is equal to the mean on the right of the interior edges of $\mathscr{T}_{h,i}$:

$$\begin{aligned} &\langle[[\tilde{p}_{h,i}^{k+1}]], 1\rangle_e = 0, \quad \forall e \in \mathscr{E}_{h,i}^{\text{int}} \\ \iff &\langle\tilde{p}_{h,i}^{k+1}, 1\rangle_{e\in K} = \langle\tilde{p}_{h,i}^{k+1}, 1\rangle_{e\in K'}, \quad \forall e = K \cap K' \text{ s.t. } K, K' \in \mathscr{T}_{h,i}. \end{aligned} \tag{2.7}$$

If $p_i|_e = g_{\text{D}}$ is a Dirichlet condition on $e \subset \partial\Gamma_i^{\text{D}}$, then $\langle\tilde{p}_{h,i}^{k+1}, 1\rangle_e = \langle g_{\text{D}}, 1\rangle_e$.

Remark 2.1. *In the case of one domain Ω, this postprocessing leads to the continuity of the means of the traces of $\tilde{p}_h^{k+1}$ on interior domain sides. In the case of a decomposition into two or more subdomains, $\tilde{p}_{h,i}^{k+1}$ and $\tilde{p}_{h,j}^{k+1}$ are constructed separately and independently in Ω_i and Ω_j. Hence, there is a priori no reason to have $\langle[[\tilde{p}_h^{k+1}]], 1\rangle_e = 0$ for $e \in \mathscr{E}_h^{\Gamma_{i,j}}$. In general:*

$$\begin{aligned} &\langle[[\tilde{p}_h^{k+1}]], 1\rangle_e \neq 0, \ \forall e \in \mathscr{E}_h^{\Gamma_{i,j}} \\ \iff &\langle\tilde{p}_{h,i}^{k+1}, 1\rangle_e \neq \langle\tilde{p}_{h,j}^{k+1}, 1\rangle_e \ \text{ for } \ e = K \cap K' \ \text{ s.t. } \ K \in \mathscr{T}_{h,i},\ K' \in \mathscr{T}_{h,j}. \end{aligned} \tag{2.8}$$

2.2 Concept of potential and flux reconstructions

The goal of this section is to present our potential and flux reconstructions at each iteration $k+1$ of the DD algorithm, $k \geq 0$, which will be the central tool used in Theorem 2.5 and 2.7.

2.2.1 Potential reconstruction

Definition 2.2 (Potential reconstruction)**.** *We will call a* potential reconstruction *any function s_h^{k+1} constructed from p_h^{k+1}, $\mathbf{u}_h^{k+1}$, as proposed in [58, 130, 154], which satisfies:*

$$s_h^{k+1} \in H^1(\Omega) \cap C^0(\overline{\Omega}), \tag{2.9a}$$

$$s_h^{k+1}|_{\Gamma^{\text{D}}} = g_{\text{D}}. \tag{2.9b}$$

2.2.2 Subdomain potential reconstruction

Definition 2.3 (Subdomain potential reconstruction)**.** *Let $i \in [\![1, \mathcal{N}]\!]$. We will call a* subdomain potential reconstruction *any function $\overline{s}_{h,i}^{k+1}$ constructed from p_h^{k+1}, $\mathbf{u}_h^{k+1}$, which satisfies:*

$$\overline{s}_{h,i}^{k+1} \in H^1(\Omega_i) \cap C^0(\overline{\Omega}_i), \tag{2.10a}$$

$$\overline{s}_{h,i}^{k+1}|_{\Gamma_i^{\mathrm{D}}} = g_{\mathrm{D}}|_{\Gamma_i^{\mathrm{D}}}. \tag{2.10b}$$

In contrast to s_h^{k+1} of Definition 2.2, $\overline{s}_{h,i}^{k+1}$ is constructed locally subdomain by subdomain to capture the nonconformity from the numerical scheme only and not that from the domain decomposition method. Thus, $\overline{s}_{h,i}^{k+1}$ is close to $\tilde{p}_{h,i}^{k+1}$ independently in each subdomain and $\overline{s}_{h,i}^{k+1}|_{\Gamma_{i,j}}$ is close to $\tilde{p}_{h,i}^{k+1}|_{\Gamma_{i,j}}$, $\forall i \in [\![1, \mathcal{N}]\!]$, $j \in B^i$ in the sense that the estimator (2.17) and (2.28) are as small as possible.

2.2.3 Equilibrated flux reconstruction

Definition 2.4 (Equilibrated flux reconstruction)**.** *We will call an* equilibrated flux reconstruction *any function $\boldsymbol{\sigma}_h^{k+1}$ constructed from p_h^{k+1}, $\mathbf{u}_h^{k+1}$, as proposed in [58, 130, 156], which satisfies:*

$$\boldsymbol{\sigma}_h^{k+1} \in \mathbf{H}(\mathrm{div}, \Omega), \tag{2.11a}$$

$$(\nabla \cdot \boldsymbol{\sigma}_h^{k+1}, 1)_K = (f, 1)_K, \qquad \forall K \in \mathscr{T}_h, \tag{2.11b}$$

with

$$-(\boldsymbol{\sigma}_h^{k+1} \cdot \boldsymbol{n}_\Omega, 1)_e = (g_{\mathrm{N}}, 1)_e, \qquad \forall e \in \bigcup_{i=1}^{\mathcal{N}} \mathscr{E}_{h,i}^{\Gamma^{\mathrm{N}}}. \tag{2.12}$$

The construction of $\boldsymbol{\sigma}_h^{k+1}$ is more complex than the construction of s_h^{k+1} because it must satisfy both of the above requirements (2.11a) and (2.11b). We present it in details in Section 2.6.

2.3 General a posteriori error estimates for $\tilde{p}_h \in H^1(\mathscr{T}_h)$ and $\mathbf{u}_h \in \mathbf{L}^2(\Omega)$

Because we use the MFE method inside the Robin-to-Robin domain decomposition method, we obtain:

$$\mathbf{u}_h^{k+1} \notin \mathbf{H}(\mathrm{div}, \Omega), \quad \forall k \geq 0, \text{ in the DD algorithm,}$$

$$p_h^{k+1} \notin H_0^1(\Omega), \quad \nabla p_h^{k+1} \notin \mathbf{H}(\mathrm{div}, \Omega), \quad \text{and} \quad \nabla \cdot (-\boldsymbol{S} \nabla p_h^{k+1}) \neq f,$$

where ∇p_h^{k+1} is the broken (elementwise) gradient. Also, in order to evaluate the energy error between the unknown exact solution and the known approximate solution, p_h^{k+1} does not sum suitable. In fact:

$$\|\boldsymbol{S}^{\frac{1}{2}} \nabla (p - p_h^{k+1})\|^2 = \sum_{K \in \mathscr{T}_h} \|\boldsymbol{S}^{\frac{1}{2}} \nabla (p - p_h^{k+1})\|_K^2 = \|\boldsymbol{S}^{\frac{1}{2}} \nabla p\|^2 \text{ because } p_h^{k+1}|_K \in \mathbb{P}_0(K).$$

That is one of the reasons to introduce the postprocessing $\tilde{p}_h^{k+1}$ of p_h^{k+1} such that $\tilde{p}_h^{k+1}|_K \in \mathbb{P}_2(K)$, $\forall K \in \mathscr{T}_h$. In this section, we present a general framework for

the a posteriori error estimate independently of the discretization method used in each subdomain and based on the results given in [130] and [156]. In particular, this general theory of a posteriori estimates is valid at each iteration $k+1$ of the DD algorithm, for the Robin-to-Robin domain decomposition with the MFE method. We first define the energy semi-norm on $H^1(\mathcal{T}_h)$:

$$|||\varphi|||^2 := \|\boldsymbol{S}^{\frac{1}{2}}\nabla\varphi\|^2, \qquad \varphi \in H^1(\mathcal{T}_h), \tag{2.13}$$

and the energy norm on $\mathbf{L}^2(\Omega)$:

$$|||\mathbf{v}|||_\star^2 := \|\boldsymbol{S}^{-\frac{1}{2}}\mathbf{v}\|^2, \qquad \mathbf{v} \in \mathbf{L}^2(\Omega). \tag{2.14}$$

For $D \subset \Omega$, we denote respectively $c_{\boldsymbol{S},D}$, $C_{\boldsymbol{S},D}$ the smallest and the largest eigenvalue of the tensor $\boldsymbol{S}$ in D. For the forthcoming theorems, we will use the Poincaré inequality: for $K \in \mathcal{T}_h$, and a constant $C_{\mathrm{P},K} := \dfrac{1}{\pi}$ (since K is convex), we have:

$$\|\varphi - \pi_0\varphi\|_K \le C_{\mathrm{P},K} h_K \|\nabla\varphi\|_K, \qquad \forall \varphi \in H^1(K). \tag{2.15}$$

Theorem 2.5 (A posteriori error estimates for the flux)**.** *Let* $\mathbf{u}$ *be the weak solution of the initial problem* (1.1) *and let* $\mathbf{u}_h^{k+1} \in \mathbf{L}^2(\Omega)$ *be an arbitrary approximation, in particular* $\mathbf{u}_h^{k+1}$ *can be solution of the problem* (1.76) *at iteration* $k+1$ *of the Optimized Shwarz (Robin-to-Robin) algorithm. Let* s_h^{k+1} *be the potential reconstruction of Definition 2.2,* $\overline{s}_{h,i}^{k+1}$ *be the subdomain potential reconstruction of Definition 2.3, and* $\boldsymbol{\sigma}_h^{k+1}$ *be the equilibrated flux reconstruction of Definition 2.4. We have:*

$$|||\mathbf{u} - \mathbf{u}_h^{k+1}|||_\star \le \eta^{k+1} := \left\{\sum_{i=1}^{\mathcal{N}} \sum_{K\in\mathcal{T}_{h,i}} \eta_{\mathrm{CR},K}^2\right\}^{\frac{1}{2}} + \left\{\sum_{i=1}^{\mathcal{N}} \sum_{K\in\mathcal{T}_{h,i}} \eta_{\mathrm{DDP},K}^2\right\}^{\frac{1}{2}} + \left\{\sum_{K\in\mathcal{T}_h} \eta_{\mathrm{DDF},K}^2\right\}^{\frac{1}{2}} + \left\{\sum_{K\in\mathcal{T}_h} \eta_{\mathrm{osc},K}^2\right\}^{\frac{1}{2}}, \tag{2.16}$$

where

$$\eta_{\mathrm{CR},K} := |||\mathbf{u}_{h,i}^{k+1} + \boldsymbol{S}\nabla\overline{s}_{h,i}^{k+1}|||_{\star,K} \qquad \text{“constitutive relation”}, \tag{2.17}$$

$$\eta_{\mathrm{DDP},K} := |||\boldsymbol{S}\nabla(\overline{s}_{h,i}^{k+1} - s_{h,i}^{k+1})|||_{\star,K} \qquad \text{“DD potential non conformity”}, \tag{2.18}$$

$$\eta_{\mathrm{DDF},K} := |||\mathbf{u}_h^{k+1} - \boldsymbol{\sigma}_h^{k+1}|||_{\star,K} \qquad \text{“DD flux non conformity”}, \tag{2.19}$$

$$\eta_{\mathrm{osc},K} := C_{\mathrm{P},K} h_K c_{\boldsymbol{S},K}^{-\frac{1}{2}} \|f - \nabla\cdot\boldsymbol{\sigma}_h^{k+1}\|_K \qquad \text{“data oscillation”}. \tag{2.20}$$

For this theorem, we denote I_{eff}^{k+1} *the effectivity index, which is the ratio of the estimated and the actual error at the iteration* $k+1$ *of the DD algorithm, given as:*

$$I_{\mathrm{eff}}^{k+1} := \frac{\eta^{k+1}}{|||\mathbf{u} - \mathbf{u}_h^{k+1}|||_\star}. \tag{2.21}$$

Proof. It follows readily from [130] Section 3, Therorem 3.1, that for the DD method where the flux and the potential are not continuous on the interface we have:

$$|||\mathbf{u}-\mathbf{u}_h^{k+1}|||_\star \leq \eta^{k+1} := \left\{\sum_{K\in\mathcal{T}_h} |||\mathbf{u}_h^{k+1}+\boldsymbol{S}\nabla s_h^{k+1}|||_{\star,K}^2\right\}^{\frac{1}{2}} + \left\{\sum_{K\in\mathcal{T}_h}\eta_{\mathrm{DDF},K}^2\right\}^{\frac{1}{2}} + \left\{\sum_{K\in\mathcal{T}_h}\eta_{\mathrm{osc},K}^2\right\}^{\frac{1}{2}}. \tag{2.22}$$

Moreover, we have:

$$\begin{aligned}
\sum_{K\in\mathcal{T}_h} |||\mathbf{u}_h^{k+1}+\boldsymbol{S}\nabla s_h^{k+1}|||_{\star,K}^2 &= \sum_{i=1}^{\mathcal{N}}\sum_{K\in\mathcal{T}_{h,i}} |||\mathbf{u}_{h,i}^{k+1}+\boldsymbol{S}\nabla s_{h,i}^{k+1}|||_{\star,K}^2 \\
&= \sum_{i=1}^{\mathcal{N}}\sum_{K\in\mathcal{T}_{h,i}} |||\mathbf{u}_{h,i}^{k+1}+\boldsymbol{S}\nabla \overline{s}_{h,i}^{k+1}-\boldsymbol{S}\nabla \overline{s}_{h,i}^{k+1}+\boldsymbol{S}\nabla s_{h,i}^{k+1}|||_{\star,K}^2 \\
&\leq \sum_{i=1}^{\mathcal{N}}\sum_{K\in\mathcal{T}_{h,i}} (|||\mathbf{u}_{h,i}^{k+1}+\boldsymbol{S}\nabla \overline{s}_{h,i}^{k+1}|||_{\star,K} + |||\boldsymbol{S}\nabla \overline{s}_{h,i}^{k+1}-\boldsymbol{S}\nabla s_{h,i}^{k+1}|||_{\star,K})^2 \\
&= \sum_{i=1}^{\mathcal{N}}\sum_{K\in\mathcal{T}_{h,i}} (\eta_{\mathrm{CR},K}+\eta_{\mathrm{DDP},K})^2.
\end{aligned} \tag{2.23}$$

Using the triangle inequality on the space l^2 on $\mathbb{R}^{|\mathcal{T}_h|}$, we obtain the same terms as in (2.16):

$$\begin{aligned}
\left\{\sum_{K\in\mathcal{T}_h} |||\mathbf{u}_h^{k+1}+\boldsymbol{S}\nabla s_h^{k+1}|||_{\star,K}^2\right\}^{\frac{1}{2}} &\leq \left\{\sum_{K\in\mathcal{T}_h}(\eta_{\mathrm{CR},K}+\eta_{\mathrm{DDP},K})^2\right\}^{\frac{1}{2}} \\
&\leq \left\{\sum_{i=1}^{\mathcal{N}}\sum_{K\in\mathcal{T}_{h,i}}\eta_{\mathrm{CR},K}^2\right\}^{\frac{1}{2}} + \left\{\sum_{i=1}^{\mathcal{N}}\sum_{K\in\mathcal{T}_{h,i}}\eta_{\mathrm{DDP},K}^2\right\}^{\frac{1}{2}}.
\end{aligned} \tag{2.24}$$

□

Lemma 2.6. *Theorem 2.5 bounds the error in each subdomain due to the discretization and the error on the interface due to the decomposition of the domain. The discretization error estimator η_{disc} (also called subdomain estimator) is:*

$$\eta_{\mathrm{disc}} := \left\{\sum_{i=1}^{\mathcal{N}}\sum_{K\in\mathcal{T}_{h,i}}\eta_{\mathrm{CR},K}^2\right\}^{\frac{1}{2}} + \left\{\sum_{K\in\mathcal{T}_h}\eta_{\mathrm{osc},K}^2\right\}^{\frac{1}{2}} \tag{2.25}$$

and the domain decomposition estimator η_{DD} (also called the interface estimator) is:

$$\eta_{\mathrm{DD}} := \left\{\sum_{i=1}^{\mathcal{N}}\sum_{K\in\mathcal{T}_{h,i}}\eta_{\mathrm{DDP},K}^2\right\}^{\frac{1}{2}} + \left\{\sum_{K\in\mathcal{T}_h}\eta_{\mathrm{DDF},K}^2\right\}^{\frac{1}{2}}. \tag{2.26}$$

Theorem 2.7 (A posteriori error estimates for the potential)**.** *Let p be the weak solution of the problem (1.1) and let $\tilde{p}_h^{k+1}\in H^1(\mathcal{T}_h)$ be an arbitrary solution, in particular $\tilde{p}_h^{k+1}$ can be the postprocessing of p_h^{k+1} solution of the problem (1.76) at iteration $k+1$ of the Optimized Schwarz algorithm described in Section 2.1. Let $\mathbf{u}_h^{k+1}=-\boldsymbol{S}\nabla\tilde{p}_h^{k+1}$. Let s_h^{k+1} be*

the potential reconstruction of Definition 2.2, $\overline{s}_{h,i}^{k+1}$ be the subdomain potential reconstruction of Definition 2.3, and $\boldsymbol{\sigma}_h^{k+1}$ be the equilibrated flux reconstruction of Definition 2.4. We have:

$$|||p - \tilde{p}_h^{k+1}||| \leq \tilde{\eta}^{k+1} := \left\{\sum_{i=1}^{\mathcal{N}} \sum_{K\in\mathcal{T}_{h,i}} \eta_{\mathrm{NCP},K}^2\right\}^{\frac{1}{2}} + \left\{\sum_{i=1}^{\mathcal{N}} \sum_{K\in\mathcal{T}_{h,i}} \eta_{\mathrm{DDP},K}^2\right\}^{\frac{1}{2}} + \left\{\sum_{K\in\mathcal{T}_h} \eta_{\mathrm{DDF},K}^2\right\}^{\frac{1}{2}} + \left\{\sum_{K\in\mathcal{T}_h} \eta_{\mathrm{osc},K}^2\right\}^{\frac{1}{2}}, \tag{2.27}$$

where $\eta_{\mathrm{NCP},K}$ is the "potential non conformity" estimator:

$$\eta_{\mathrm{NCP},K} := |||\tilde{p}_{h,i}^{k+1} - \overline{s}_{h,i}^{k+1}|||_K, \tag{2.28}$$

$\eta_{\mathrm{osc},K}$ is defined in (2.20), $\eta_{\mathrm{DDP},K}$ is defined in (2.18), and $\eta_{\mathrm{DDF},K}$ is defined in (2.19). For this theorem, we denote I_{eff}^{k+1} the effectivity index, which is the ratio of the estimated and the actual error at the iteration $k+1$ of the DD algorithm, given as:

$$I_{\mathrm{eff}}^{k+1} := \frac{\tilde{\eta}^{k+1}}{|||p - \tilde{p}_h^{k+1}|||}. \tag{2.29}$$

Proof. It follows readily from [130] Section 3 Therorem 3.3 that for the DD method where the flux and the potential are not continuous in the interface we have:

$$|||p - \tilde{p}_h^{k+1}||| \leq \tilde{\eta}^{k+1} := \left\{\sum_{K\in\mathcal{T}_h} |||\tilde{p}_h^{k+1} - s_h^{k+1}|||_K{}^2\right\}^{\frac{1}{2}} + \left\{\sum_{K\in\mathcal{T}_h} |||\boldsymbol{S}\nabla\tilde{p}_h^{k+1} + \boldsymbol{\sigma}_h^{k+1}|||_{\star,K}{}^2\right\}^{\frac{1}{2}} + \left\{\sum_{K\in\mathcal{T}_h} \eta_{\mathrm{osc},K}^2\right\}^{\frac{1}{2}}. \tag{2.30}$$

Note that $|||\boldsymbol{S}\nabla\tilde{p}_h^{k+1} + \boldsymbol{\sigma}_h^{k+1}|||_{\star,K}$ can be divided into two parts:

$$|||\boldsymbol{S}\nabla\tilde{p}_h^{k+1} + \boldsymbol{\sigma}_h^{k+1}|||_{\star,K} \leq |||\boldsymbol{S}\nabla\tilde{p}_h^{k+1} + \mathbf{u}_h^{k+1}|||_{\star,K} + |||\mathbf{u}_h^{k+1} - \boldsymbol{\sigma}_h^{k+1}|||_{\star,K}. \tag{2.31}$$

The first term above disappears by assumption. Inserting now the subdomain potential reconstruction $\overline{s}_{h,i}^{k+1}$ we obtain:

$$\begin{aligned}\sum_{K\in\mathcal{T}_h} \eta_{\mathrm{NCP},K}^2 &= \sum_{i=1}^{\mathcal{N}} \sum_{K\in\mathcal{T}_{h,i}} |||\tilde{p}_{h,i}^{k+1} - \overline{s}_{h,i}^{k+1} + \overline{s}_{h,i}^{k+1} - s_{h,i}^{k+1}|||_K^2 \\ &\leq \sum_{i=1}^{\mathcal{N}} \sum_{K\in\mathcal{T}_{h,i}} (|||\tilde{p}_{h,i}^{k+1} - \overline{s}_{h,i}^{k+1}|||_K + |||\overline{s}_{h,i}^{k+1} - s_{h,i}^{k+1}|||_K)^2.\end{aligned} \tag{2.32}$$

Thus,

$$\sum_{K\in\mathcal{T}_h} \eta_{\mathrm{NCP},K}^2 \leq \sum_{i=1}^{\mathcal{N}} \sum_{K\in\mathcal{T}_{h,i}} (\eta_{\mathrm{NCP},K} + \eta_{\mathrm{DDP},K})^2. \tag{2.33}$$

Using the triangle inequality on the space l^2 on $\mathbb{R}^{|\mathcal{T}_h|}$, we obtain the same terms as in (2.27):

$$\left\{\sum_{K\in\mathcal{T}_h}\eta^2_{\mathrm{NCP},K}\right\}^{\frac{1}{2}} \leq \left\{\sum_{i=1}^{\mathcal{N}}\sum_{K\in\mathcal{T}_{h,i}}\eta^2_{\mathrm{NCP},K}\right\}^{\frac{1}{2}} + \left\{\sum_{i=1}^{\mathcal{N}}\sum_{K\in\mathcal{T}_{h,i}}\eta^2_{\mathrm{DDP},K}\right\}^{\frac{1}{2}}. \tag{2.34}$$

□

Lemma 2.8. *Theorem 2.7 bounds the error in the subdomains due to the discretization error and the error on the interface due to the decomposition of the domain. The discretization estimator η_{disc} (also called the subdomain error estimator) is:*

$$\eta_{\mathrm{disc}} := \left\{\sum_{i=1}^{\mathcal{N}}\sum_{K\in\mathcal{T}_{h,i}}\eta^2_{\mathrm{NCP},K}\right\}^{\frac{1}{2}} + \left\{\sum_{K\in\mathcal{T}_h}\eta^2_{\mathrm{osc},K}\right\}^{\frac{1}{2}}, \tag{2.35}$$

and the domain decomposition estimator η_{DD} is defined in (2.26).

Remark 2.9. *In the MFE method for a single domain, we do not need to construct $\boldsymbol{\sigma}_h$ because the approximate flux $\mathbf{u}_h$ is equilibrated and in $\mathbf{H}(\mathrm{div},\Omega)$, see (1.76b). Thus, $\eta_{\mathrm{DDF},K} = |||\mathbf{u}_h - \boldsymbol{\sigma}_h|||_{\star,K} = 0$, $\forall K \in \mathcal{T}_h$. In the two or more subdomains case, $\eta_{\mathrm{DDF},K}$ will be equal to 0 in the triangles not touching the interface $\Gamma_{i,j}$, for the construction of $\boldsymbol{\sigma}_h$ given below.*

2.4 Properties of $\mathbf{u}_h^{k+1}$ and p_h^{k+1} in Ω at each iteration of the DD algorithm

At iteration $k+1$ of the DD algorithm for the Robin-to-Robin domain decomposition using the MFE method, we have the two following Robin conditions on the interface $\Gamma_{i,j}$:

$$-\beta_{i,j}\mathbf{u}_{h,i}^{k+1}\cdot\boldsymbol{n}_i + p_{h,i}^{k+1} = -\beta_{i,j}\mathbf{u}_{h,j}^{k}\cdot\boldsymbol{n}_i + p_{h,j}^{k} \qquad \text{on } \Gamma_{i,j}, \tag{2.36a}$$

$$-\beta_{j,i}\mathbf{u}_{h,j}^{k+1}\cdot\boldsymbol{n}_j + p_{h,j}^{k+1} = -\beta_{j,i}\mathbf{u}_{h,i}^{k}\cdot\boldsymbol{n}_j + p_{h,i}^{k} \qquad \text{on } \Gamma_{i,j}. \tag{2.36b}$$

However, the physical quantities are not conserved at each iteration on $\Gamma_{i,j}$:

$$\mathbf{u}_{h,i}^{k+1}|_e\cdot\boldsymbol{n}_i \neq \mathbf{u}_{h,j}^{k+1}|_e\cdot\boldsymbol{n}_i, \quad \forall e\in\Gamma_{i,j}$$

and

$$p_{h,i}^{k+1}|_e \neq p_{h,j}^{k+1}|_e, \quad \forall e\in\Gamma_{i,j}.$$

The continuity of the normal component of the flux is only obtained at convergence. Indeed, at each iteration $k+1$ of the DD algorithm, the MFE method gives locally $\mathbf{u}_{h,i}^{k+1}\in\mathbf{H}(\mathrm{div},\Omega_i)$ for all $i\in[\![1,\mathcal{N}]\!]$. Thus, $\mathbf{u}_h^{k+1}\notin\mathbf{H}(\mathrm{div},\Omega)$. For this reason, we will construct a flux $\boldsymbol{\sigma}_h^{k+1}$ that satisfies both conditions (2.11a) and (2.11b) in Section 2.6. We also need to build a potential reconstruction s_h^{k+1} and a subdomain potential reconstruction $\overline{s}_{h,i}^{k+1}$. Once $\boldsymbol{\sigma}_h^{k+1}$, s_h^{k+1}, and $\overline{s}_{h,i}^{k+1}$ have been constructed at each iteration, we can compute the error estimators in Theorems 2.5 and 2.7.

2.5 Potential reconstructions for the Robin DD in the MFE method

2.5.1 Potential reconstruction

In order to build the potential reconstruction s_h^{k+1} which is $H^1(\Omega)$-conforming as indicated in Section 2.2.1, we first introduce the averaging operator (interpolation operator) acting on the nodes of the mesh:

$$\mathscr{I}_{\rm av} : \mathbb{P}_m(\mathscr{T}_h) \longrightarrow \mathbb{P}_m(\mathscr{T}_h) \cap H^1(\Omega), \tag{2.37}$$

where $\mathbb{P}_m(\mathscr{T}_h)$ is the space of polynomials of maximal degree m on each $K \in \mathscr{T}_h$. This operator $\mathscr{I}_{\rm av}$ associates to a piecewise m-th order discontinous polynomial $\varphi_h \in \mathbb{P}_m(\mathscr{T}_h)$ a piecewise m-th order continuous polynomial on Ω ($H^1(\Omega)$-conforming), equal to $g_{\rm D}$ on $\Gamma^{\rm D}$. The value of the function $\mathscr{I}_{\rm av}(\varphi_h)$ is prescribed at each Lagrangian node $\mathbf{a}$ by the average of the values of φ_h at this node:

$$\mathscr{I}_{\rm av}(\varphi_h)(\mathbf{a}) = \frac{1}{|\mathscr{T}_\mathbf{a}|} \sum_{K \in \mathscr{T}_\mathbf{a}} \varphi_{h|K}(\mathbf{a}), \tag{2.38}$$

where $\mathscr{T}_\mathbf{a}$ is the set of all the elements sharing the node $\mathbf{a}$, see (1.61). In particular, if $m = 2$ and $d = 2$, the Lagrangian nodes are the vertices of triangles and the nodes in the midpoints of the edges. At the Dirichlet boundary nodes $\mathbf{a}_{\rm D}$, the value of $\mathscr{I}_{\rm av}(\varphi_h)$ is set to $g_{\rm D}(\mathbf{a}_{\rm D})$.

In our case, we take $\tilde{p}_h^{k+1} \in \mathbb{P}_2(\mathscr{T}_h)$ from (2.4) and we define the pontential reconstruction at iteration $k+1$ as follows:

$$s_h^{k+1} := \mathscr{I}_{\rm av}(\tilde{p}_h^{k+1}) \in H^1(\Omega). \tag{2.39}$$

2.5.2 Subdomain potential reconstruction

As explained in Remark 2.1, the means of the traces of $\tilde{p}_h^{k+1}$ on the edges belonging the interface are not continuous during the DD algorithm:

$$\langle [[\tilde{p}_h^{k+1}]], 1 \rangle_e \neq 0, \quad \forall e \in \mathscr{E}_h^{\Gamma_{i,j}}. \tag{2.40}$$

The purpose of this section is to construct a subdomain potential reconstruction which is different from $\mathscr{I}_{\rm av}$ of (2.38) at the beginning of the DD algorithm because of (2.40), but close to $\mathscr{I}_{\rm av}$ at convergence of the DD algorithm where both the subdomain potential reconstruction and $\mathscr{I}_{\rm av}$ satisfy $\langle [[\tilde{p}_h^{k+1}]], 1 \rangle_e = 0, \ \ \forall e \in \mathscr{E}_h^{\Gamma_{i,j}}$. To do so, we first bound the mean value $\dfrac{|\langle [[\tilde{p}_h^{k+1}]], 1 \rangle_e|}{|e|}$ from above as follows:

$$0 \leq \frac{|\langle [[\tilde{p}_h^{k+1}]], 1 \rangle_e|}{|e|} \leq \frac{\langle |[[\tilde{p}_h^{k+1}]]|, 1 \rangle_e}{|e|}. \tag{2.41}$$

We next define weights on edges (faces) and vertices belonging the interface at each iteration $k+1$ of the DD algorithm as follows:

Definition 2.10 (Weights on edges belonging to the interface)**.** *We define the weight of the edge (face) $e \in \mathscr{E}_h^{\Gamma_{i,j}}$ using (2.41) by:*

$$\overline{w}_e^{k+1} := \left(\frac{|\langle [[\tilde{p}_h^{k+1}]], 1 \rangle_e|}{\langle |[[\tilde{p}_h^{k+1}]]|, 1 \rangle_e} \right)^3. \tag{2.42}$$

We know that at convergence, when $k \to \infty$ we obtain $\langle [[\tilde{p}_h^{k+1}]], 1 \rangle_e \to 0$, and so $|\langle [[\tilde{p}_h^{k+1}]], 1 \rangle_e| \to 0$. Thus, at convergence we have:

$$\overline{w}_e^{k+1} = 0. \tag{2.43}$$

Conversely, $\overline{w}_e^{k+1}$ is typically close to 1 at the beginning of the DD algorithm, and altogether:

$$0 \leq \overline{w}_e^{k+1} \leq 1. \tag{2.44}$$

Definition 2.11 (Weights on Lagrangian nodes belonging to the interface)**.** *Using the notation (1.60), we define the weight on the Lagrangian node $\mathbf{a} \in \mathscr{V}_h^{\Gamma_{i,j}}$ located on the interface, in two space dimensions for simplicity, by:*

$$\overline{w}_{\mathbf{a}}^{k+1} := \begin{cases} \dfrac{1}{2}(\overline{w}_e^{k+1} + \overline{w}_{e'}^{k+1}) & \text{if } \mathbf{a} \in \mathscr{V}_h^{\Gamma_{i,j} \setminus (\partial\Gamma_{i,j})} \text{ where } e, e' \in \mathscr{E}_h^{\Gamma_{i,j}} \ / \ e \cap e' = \mathbf{a}, \\ \dfrac{1}{|I_{\mathbf{a}}|} \displaystyle\sum_{r=1}^{|I_{\mathbf{a}}|} \overline{w}_{e_r}^{k+1} & \text{if } \mathbf{a} \in \mathscr{V}_h^{\partial\Gamma_{i,j}} \text{ where } \mathbf{a} \in e_r \subset I_{\mathbf{a}}^r, \end{cases} \tag{2.45}$$

where we recall that $I_{\mathbf{a}}^r$ is the r^{th} interface in $I_{\mathbf{a}}$ that shares $\mathbf{a}$. We note that $\overline{w}_{\mathbf{a}}^{k+1}$ has similar properties to $\overline{w}_e^{k+1}$. It is close to 1 at the beginning of the DD algorithm and close to 0 at convergence.

Remark 2.12. *In the case of the standard averaging operator $\mathscr{I}_{\text{av}}$ from (2.37), the weights are distributed uniformly on each element $K \in \mathscr{T}_{\mathbf{a}}$ sharing the node $\mathbf{a}$, being equal to $\dfrac{1}{|\mathscr{T}_{\mathbf{a}}|}$, see (2.38). Recall that for a given vertex $\mathbf{a}$ on the interface, the patch $\mathscr{T}_{\mathbf{a}}$ is a union of subdomains subpatchs $\mathscr{T}_{\mathbf{a}}^i$, see (1.61). For the subdomain potential reconstruction of Definition 2.3, we now want to define weights so that all elements sharing the same node in the interface do not have the same weight during the iterations of the DD algorithm.*

Definition 2.13 (Weight of verticies $\mathbf{a}$ on the interface for each $\mathscr{T}_{\mathbf{a}}^i$ in $\mathscr{T}_{\mathbf{a}}$)**.** *In order to construct the subdomain potential reconstruction on the subdomain Ω_i, we now define a weight of elements in $\mathscr{T}_{\mathbf{a}}^i$ and the weight of elements in $\mathscr{T}_{\mathbf{a}} \setminus \mathscr{T}_{\mathbf{a}}^i$, for $\mathbf{a}$ belonging the interface. The elements $K \in \mathscr{T}_{\mathbf{a}}^i$ have the same weight $w_{i,\mathbf{a}}^{k+1}$ on the node $\mathbf{a}$:*

$$w_{i,\mathbf{a}}^{k+1} = \frac{1}{|\mathscr{T}_{\mathbf{a}}^i| + (1 - \overline{w}_{\mathbf{a}}^{k+1}) \sum_{j \in \tilde{B}^i} |\mathscr{T}_{\mathbf{a}}^j|}. \tag{2.46}$$

The weight of the elements $K \in \mathscr{T}_{\mathbf{a}} \setminus \mathscr{T}_{\mathbf{a}}^i$ on the node $\mathbf{a}$ is:

$$w_{i,\mathbf{a}}^{k+1}(1 - \overline{w}_{\mathbf{a}}^{k+1}). \tag{2.47}$$

Lemma 2.14. *The sum of the weights (2.46) and (2.47) is equal to 1 on each node $\mathbf{a}$:*

$$w_{i,\mathbf{a}}^{k+1} |\mathscr{T}_{\mathbf{a}}^i| + w_{i,\mathbf{a}}^{k+1}(1 - \overline{w}_{\mathbf{a}}^{k+1}) \sum_{j \in \tilde{B}^i} |\mathscr{T}_{\mathbf{a}}^j| = 1. \tag{2.48}$$

Proof.

$$\begin{aligned} w_{i,\mathbf{a}}^{k+1}|\mathscr{T}_{\mathbf{a}}^{i}| + w_{i,\mathbf{a}}^{k+1}(1-\overline{w}_{\mathbf{a}}^{k+1})\sum_{j\in\tilde{B}^i}|\mathscr{T}_{\mathbf{a}}^{j}| &= w_{i,\mathbf{a}}^{k+1}(|\mathscr{T}_{\mathbf{a}}^{i}| + (1-\overline{w}_{\mathbf{a}}^{k+1})\sum_{j\in\tilde{B}^i}|\mathscr{T}_{\mathbf{a}}^{j}|) \\ &= 1 \quad \text{(from (2.46))}. \end{aligned} \tag{2.49}$$

□

Remark 2.15. *This distribution of the weight on the patch $\mathscr{T}_{\mathbf{a}}$ is the way to obtain weight located only in the elements $K \in \mathscr{T}_{\mathbf{a}}^{i}$ at the begining of the DD algorithm. Indeed, we have $(1-\overline{w}_{\mathbf{a}}^{k+1}) = 0$ and the weight at the node $\mathbf{a}$ for the elements $K \in \mathscr{T}_{\mathbf{a}} \backslash \mathscr{T}_{\mathbf{a}}^{i}$ disappears;*

$$w_{i,\mathbf{a}}^{k+1}(1-\overline{w}_{\mathbf{a}}^{k+1}) = 0. \tag{2.50}$$

Therefore $K \in \mathscr{T}_{\mathbf{a}} \backslash \mathscr{T}_{\mathbf{a}}^{i}$ do not contribute, whereas $w_{i,\mathbf{a}}^{k+1}$ becomes $w_{i,\mathbf{a}}^{k+1} = \dfrac{1}{|\mathscr{T}_{\mathbf{a}}^{i}|}$. Thus,

$$w_{i,\mathbf{a}}^{k+1}|\mathscr{T}_{\mathbf{a}}^{i}| = \frac{1}{|\mathscr{T}_{\mathbf{a}}^{i}|}|\mathscr{T}_{\mathbf{a}}^{i}| = 1. \tag{2.51}$$

At convergence of the DD algorithm, $\overline{w}_{\mathbf{a}}^{k+1} = 0$, which leads to $(1-\overline{w}_{\mathbf{a}}^{k+1}) = 1$. Thus,

$$\begin{aligned} w_{i,\mathbf{a}}^{k+1} &= \frac{1}{|\mathscr{T}_{\mathbf{a}}^{i}| + (1-\overline{w}_{\mathbf{a}}^{k+1})\sum_{j\in\tilde{B}^i}|\mathscr{T}_{\mathbf{a}}^{j}|} \\ &= \frac{1}{|\mathscr{T}_{\mathbf{a}}^{i}| + \sum_{j\in\tilde{B}^i}|\mathscr{T}_{\mathbf{a}}^{j}|} \\ &= \frac{1}{|\mathscr{T}_{\mathbf{a}}|}, \end{aligned} \tag{2.52}$$

and

$$w_{i,\mathbf{a}}^{k+1}(1-\overline{w}_{\mathbf{a}}^{k+1}) = \frac{1}{|\mathscr{T}_{\mathbf{a}}|}. \tag{2.53}$$

Then, at convergence, the weight on a node $\mathbf{a}$ is distributed uniformly on each element $K \in \mathscr{T}_{\mathbf{a}}$ and we return to the case as in (2.38). In particular, we obtain:

$$\begin{aligned} w_{i,\mathbf{a}}^{k+1}|\mathscr{T}_{\mathbf{a}}^{i}| + w_{i,\mathbf{a}}^{k+1}(1-\overline{w}_{\mathbf{a}}^{k+1})\sum_{j\in\tilde{B}^i}|\mathscr{T}_{\mathbf{a}}^{j}| &= \frac{1}{|\mathscr{T}_{\mathbf{a}}|}|\mathscr{T}_{\mathbf{a}}^{i}| + \frac{1}{|\mathscr{T}_{\mathbf{a}}|}\sum_{j\in\tilde{B}^i}|\mathscr{T}_{\mathbf{a}}^{j}| \\ &= \frac{1}{|\mathscr{T}_{\mathbf{a}}|}|\mathscr{T}_{\mathbf{a}}| \\ &= 1. \end{aligned} \tag{2.54}$$

Finally, the subdomain pontential reconstruction $\overline{s}_{h,i}^{k+1}$ at iteration $k+1$ of the DD algorithm is defined as follows:

$$\begin{aligned} &\overline{s}_{h,i}^{k+1}(\mathbf{a}) = w_{i,\mathbf{a}}^{k+1}\sum_{K\in\mathscr{T}_{\mathbf{a}}^{i}}\tilde{p}_{h,i}^{k+1}|_K(\mathbf{a}) + w_{i,\mathbf{a}}^{k+1}(1-\overline{w}_{\mathbf{a}}^{k+1})\sum_{j\in\tilde{B}^i}\sum_{K\in\mathscr{T}_{\mathbf{a}}^{j}}\tilde{p}_{h,j}^{k+1}|_K(\mathbf{a}), \ \ \mathbf{a}\subset\Gamma_i, \\ &\overline{s}_{h,i}^{k+1}(\mathbf{a}) = s_{h,i}^{k+1}(\mathbf{a}), \ \ \text{otherwise.} \end{aligned} \tag{2.55}$$

This construction leads to a subdomain potential reconstruction $\overline{s}_{h,i}^{k+1}$ where at the beginning of the DD method the elements of $\mathscr{T}_{\mathbf{a}}^{i}$ of the subdomain Ω_i contribute more, i.e. with high weights, whereas the elements in $K \in \mathscr{T}_{\mathbf{a}} \backslash \mathscr{T}_{\mathbf{a}}^{i}$ do not contibute because their weights are (close to) zero. At convergence, all elements contribute and have the same weights. Thus, $\overline{s}_{h,i}^{k+1}$ converges to $\mathscr{I}_{\text{av}}(\tilde{p}_{h,i}^{k+1})|_{\Omega_i}$.

2.6 Flux reconstruction for the Robin DD in the MFE method

In this section, we suppose that for all $e \subset \Gamma_{i,j}$, $\boldsymbol{n}_e$ has the same direction as $\boldsymbol{n}_{\Gamma_{i,j}}$, where $\boldsymbol{n}_{\Gamma_{i,j}}$ is set arbitrarily, pointing either from Ω_i to Ω_j, or from Ω_j to Ω_i, with $j \in B^i$, $i < j$, $i \in [\![1, \mathcal{N}]\!]$.

2.6.1 Construction of $\boldsymbol{\sigma}_h^{k+1} \in \mathbf{H}(\mathrm{div}, \Omega)$

Proposition 2.16. *For any decomposition of Ω in many subdomains, we can build a flux reconstruction $\boldsymbol{\sigma}_h^{k+1} \in \mathbf{H}(\mathrm{div}, \Omega)$ by taking the average of the normal trace of the flux, on the left and on the right of each edge $e \in \underset{j\in B^i}{\cup} \mathscr{E}_h^{\Gamma_{i,j}}$:*

$$\boldsymbol{\sigma}_h^{k+1} \cdot \boldsymbol{n}_e = \begin{cases} \{\!\{ \mathbf{u}_h^{k+1} \cdot \boldsymbol{n}_e \}\!\}, & \forall e \in \underset{j\in B^i}{\cup} \mathscr{E}_h^{\Gamma_{i,j}}, \\ \mathbf{u}_{h,i}^{k+1} \cdot \boldsymbol{n}_e, & \forall e \in \mathscr{E}_{h,i}^{\mathrm{int}} \cup \mathscr{E}_{h,i}^{\mathrm{ext}}. \end{cases} \tag{2.56}$$

Using this construction, we obtain $[\![\boldsymbol{\sigma}_h^{k+1} \cdot \boldsymbol{n}_e]\!] = 0$, $\forall\ e \in \mathscr{E}_h$. Thus, we obtain the first required property (2.11a):

$$\boldsymbol{\sigma}_h^{k+1} \in \mathbf{H}(\mathrm{div}, \Omega) \tag{2.57}$$

as well as the third property (2.12).

It remains to verify the balance (2.11b) in all the elements $K \in \mathscr{T}_h$.

Lemma 2.17. *The property (2.11b) does not hold for $\boldsymbol{\sigma}_h$ constructed as in (2.56). Indeed, $\boldsymbol{\sigma}_h$ is not balanced with the source term in the triangles having a face on the interface $\Gamma_{i,j}$, but $\boldsymbol{\sigma}_h$ is balanced in the other triangles of $\mathscr{T}_{h,i}$, $\forall i \in [\![1, \mathcal{N}]\!]$.*

Proof. In the mixed formulation (1.76b), we take the space $M_{h,i}$ of piecewise constant functions. We thus have:

$$(\nabla \cdot \mathbf{u}_h, 1)_K = (f, 1)_K, \quad \forall K \in \mathscr{T}_h. \tag{2.58}$$

This leads to the balance with the term source in every $K \in \mathscr{T}_{h,i}$, $\forall i \in [\![1, \mathcal{N}]\!]$. We note that, with this construction of the flux $\boldsymbol{\sigma}_h^{k+1}$ in the triangles which have no edges on the interface $\Gamma_{i,j}$, (white triangles in Figure 2.1 for a domain decomposition into two subdomains), we do not change the normal traces of the fluxes, thus

$$(\nabla \cdot \boldsymbol{\sigma}_h^{k+1}, 1)_K = (f, 1)_K, \quad \forall K \in \mathscr{T}_{h,i}. \tag{2.59}$$

It remains to verify this property on the triangles (tetrahedra if d=3) that have one side on the interface. Let K be a triangle such that $e_3 \in \Gamma_{i,j}$, see Figure 2.2 for $i = 1$, $j = 2$. Let $\boldsymbol{n}_K$ be the outward normal vector to K and $\boldsymbol{n}_e = \boldsymbol{n}_K$ for $e \in \mathscr{E}_K$.

$$\begin{aligned} (\nabla \cdot \boldsymbol{\sigma}_h^{k+1}, 1)_K &= \sum_{e \in \mathscr{E}_K} \langle \boldsymbol{\sigma}_h^{k+1} \cdot \boldsymbol{n}_K, 1 \rangle_e \\ &= \langle \mathbf{u}_h^{k+1} \cdot \boldsymbol{n}_{e_1}, 1 \rangle_{e_1} + \langle \mathbf{u}_h^{k+1} \cdot \boldsymbol{n}_{e_2}, 1 \rangle_{e_2} + \langle \boldsymbol{\sigma}_h^{k+1} \cdot \boldsymbol{n}_{e_3}, 1 \rangle_{e_3} \\ &= \langle \mathbf{u}_h^{k+1} \cdot \boldsymbol{n}_{e_1}, 1 \rangle_{e_1} + \langle \mathbf{u}_h^{k+1} \cdot \boldsymbol{n}_{e_2}, 1 \rangle_{e_2} + \frac{1}{2} \langle \mathbf{u}_h^{k+1}|_K \cdot \boldsymbol{n}_{e_3} + \mathbf{u}_h^{k+1}|_{K'} \cdot \boldsymbol{n}_{e_3}, 1 \rangle_{e_3} \\ &\quad \text{(in general for the Robin DD: } \langle \mathbf{u}_h^{k+1}|_K \cdot \boldsymbol{n}_{e_3}, 1 \rangle_{e_3} \neq \langle \mathbf{u}_h^{k+1}|_{K'} \cdot \boldsymbol{n}_{e_3}, 1 \rangle_{e_3}) \\ &\neq \sum_{e \in \mathscr{E}_K} \langle \mathbf{u}_h^{k+1} \cdot \boldsymbol{n}_K, 1 \rangle_e = (f, 1)_K. \end{aligned} \tag{2.60}$$

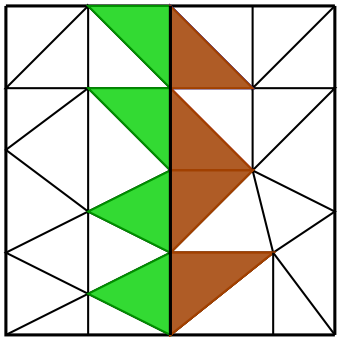

Figure 2.1: Triangles in $\mathcal{T}_h$ having a face on the interface (triangles in color)

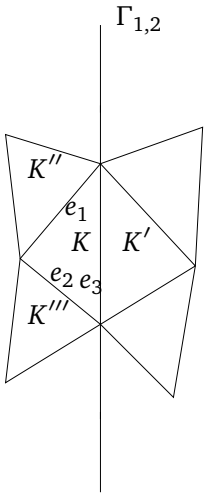

Figure 2.2: Triangles K et K' on each side of the interface

Thus, there is no balance between the normal traces on the edges $\mathscr{E}_K$ of K and the source term f. Therefore, the choice of this flux reconstruction $\boldsymbol{\sigma}_h$ verifies (2.11a) but does not verify (2.11b). □

2.6.2 Improving $\boldsymbol{\sigma}_h^{k+1}$ to obtain the balance with the source term

We will now define an area, called a band, which contains triangles that share an edge or a vertex with $\Gamma_{i,j}$. Inspired by [130], we will construct $\boldsymbol{\sigma}_h^{k+1} \in \mathbf{H}(\mathrm{div}, \Omega)$, which is the solution of a local Neumann problem in the band. We use the MFE method to solve this local problem in order to obtain $\boldsymbol{\sigma}_h^{k+1}$. The crucial point is to find Neumann conditions on the boundary of the band that are in equilibrium with the prescribed source term whereas in [130] the equilibrium is the result of a fixed assumption which is not valid in our case. For simplicity, we first consider the case of the DD where any subdomain touches the boundary $\partial\Omega$. To explain the idea, we start with the two-subdomain case Ω_1 and Ω_2: for $i = 1, 2$, we split Ω_i into two parts Ω_i^{ext} and Ω_i^{int} such that $\overline{\Omega_i^{\mathrm{ext}}} \cup \overline{\Omega_i^{\mathrm{int}}} = \overline{\Omega_i}$. Note that $\Gamma_{1,2} \subset \overline{\Omega_1^{\mathrm{ext}}} \subset \Omega_1$, and also $\Gamma_{1,2} \subset \overline{\Omega_2^{\mathrm{ext}}} \subset \Omega_2$, see Figure 2.3. The band Ω_i^{ext} is made up of triangles that have an edge or a vertex on

the interface $\Gamma_{1,2}$. We also denote Γ_i^b for $i=1,2$ and $b=1,2$ the intersections of $\partial\Omega_i^{\text{ext}}$ with $\partial\Omega_i \cap \partial\Omega$ of nonzero $(d-1)$-dimensional measure.

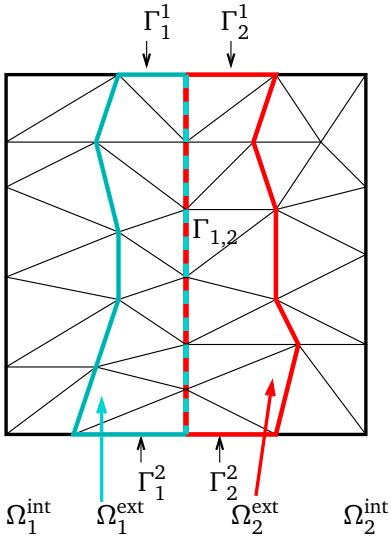

Figure 2.3: The band Ω_1^{ext} (blue) of the subdomain Ω_1 and the band Ω_2^{ext} (red) of the subdomain Ω_2, on each side of the interface $\Gamma_{1,2}$

Starting with $\boldsymbol{\sigma}_h^{k+1}$ given by (2.56), we do not have equilibrium with the source term in the band Ω_i^{ext} for $i=1,2$. On each egde $e \subset \Gamma_{1,2}$ for $i=1,2$, there appears a difference between the normal trace of the original flux and the reconstructed flux. This difference is a constant function on each edge $e \subset \Gamma_{1,2}$ which is as follows:

$$\mathbf{u}_{h,i}^{k+1}\cdot\boldsymbol{n}_e - \{\!\{\mathbf{u}_h^{k+1}\cdot\boldsymbol{n}_e\}\!\} = \boldsymbol{n}_{\Gamma_{1,2}}\cdot\boldsymbol{n}_{\partial\Omega_i^{\text{ext}}}\frac{1}{2}[[\mathbf{u}_h^{k+1}\cdot\boldsymbol{n}_e]], \quad \forall e\subset\Gamma_{1,2}. \tag{2.61}$$

In particular, using the Green's theorem in a given Ω_i^{ext}, we have:

Corollary 2.18. *In the band Ω_i^{ext}, for $i=1,2$, the misfit of mass balance due to the averaging on the interface $\Gamma_{1,2}$ is:*

$$\boldsymbol{n}_{\Gamma_{1,2}}\cdot\boldsymbol{n}_{\partial\Omega_i^{\text{ext}}}\sum_{e\subset\Gamma_{1,2}}\int_e\frac{1}{2}[[\mathbf{u}_h^{k+1}\cdot\boldsymbol{n}_e]]\mathrm{d}\gamma = (f,1)_{\Omega_i^{\text{ext}}} - \langle\{\!\{\mathbf{u}_h^{k+1}\cdot\boldsymbol{n}_{\partial\Omega_i^{\text{ext}}}\}\!\},1\rangle_{\partial\Omega_i^{\text{ext}}}. \tag{2.62}$$

Remark 2.19. *In the case where all the subdomains touch the boundary $\partial\Omega$, we can compute for each band Ω_i^{ext}a correction which is equal to $(f,1)_{\Omega_i^{\text{ext}}} - \langle\{\!\{\mathbf{u}_h^{k+1}\cdot\boldsymbol{n}_{\partial\Omega_i^{\text{ext}}}\}\!\},1\rangle_{\partial\Omega_i^{\text{ext}}}$, and which we distribute on Γ_i^b for $b=1,2$. Then this enables us to have equilibrium in the band Ω_i^{ext}, when $i=1,2$. For example, in Figure 2.3, we add a correction $c_{\Gamma_i^1}^{k+1}$ on Γ_i^1 and $c_{\Gamma_i^2}^{k+1}$ on Γ_i^2 such that:*

$$\sum_{b=1,2} c_{\Gamma_i^b}^{k+1} = (f,1)_{\Omega_i^{\text{ext}}} - \langle\{\!\{\mathbf{u}_h^{k+1}\cdot\boldsymbol{n}_{\partial\Omega_i^{\text{ext}}}\}\!\},1\rangle_{\partial\Omega_i^{\text{ext}}}. \tag{2.63}$$

Note that we do not make a correction on $\partial\Omega_i^{\text{ext}}\cap\partial\Omega_i^{\text{int}}$ or on $\Gamma_{i,j}$, in order to keep the property $\mathbf{H}(\mathrm{div},\Omega_i)$ of $\boldsymbol{\sigma}_h^{k+1}$. We then solve local Neumann problems in the two bands Ω_1^{ext} and Ω_2^{ext} following the process given in the general case, see problem (2.79) in Section 2.6.2.3 below, in order to obtain $\boldsymbol{\sigma}_{h\,|\Omega_i^{\text{ext}}}^{k+1}\cdot\boldsymbol{n}_e$ for all $e\subset\Omega_i^{\text{ext}}$, $\forall i=1,2$. The

disadvantage of this manual method of distribution is that for a general domain decomposition, for many subdomains where at least one of the subdomains does not touch the boundary $\partial\Omega$, it does not work. The difficulty is with subdomains which do not touch $\partial\Omega$, where we can not push the misfit onto the boundary $\partial\Omega$.

A possibility to solve this problem is to use a Balancing (BDD) method [49, 122, 123] where we obtain one unknown in each subdomain by using a coarse grid. This coarse problem with one unknown per subdomain would allow us to obtain the balancing in each subomain. However, we choose to adopt a simpler new method that makes the connection between subdomains in order to rebalance the flux independently of the number of subomains, and can also be applied in the case where at least one subdomain does not touch the boundary. The aim of this method is to find one correction through a simple coarse balancing problem.

2.6.2.1 The two-subdomain case

We first present our general approach for two-subdomains, and then we generalize it for any domain decomposition. In the situation of Figure 2.3, we want to find five corrections to the averaged flux $\{\!\{\mathbf{u}_h^{k+1}\cdot\boldsymbol{n}_{\partial\Omega_i^{\text{ext}}}\}\!\}$ which will lead to equilibrium in each band Ω_1^{ext} and Ω_2^{ext}. We denote these corrections by: $c_{\Gamma_{1,2}}^{k+1}$, $c_{\Gamma_1^1}^{k+1}$, $c_{\Gamma_1^2}^{k+1}$, $c_{\Gamma_2^1}^{k+1}$, and $c_{\Gamma_2^2}^{k+1}$, defined respectively on $\Gamma_{1,2}$, Γ_1^1, Γ_1^2, Γ_2^1 and Γ_2^2, see Figure 2.3, such that:

$$c_{\Gamma_i^b}^{k+1}\approx 0 \text{ for } i=1,2 \text{ and } b=1,2, \tag{2.64a}$$

$$c_{\Gamma_{1,2}}^{k+1}\approx 0. \tag{2.64b}$$

We keep the same value of the flux $\mathbf{u}_h^{k+1}\cdot\boldsymbol{n}_{\partial\Omega_i^{\text{ext}}\cap\partial\Omega_i^{\text{int}}}$ located on $\partial\Omega_i^{\text{ext}}\cap\partial\Omega_i^{\text{int}}$, where i represents the number of the subdomain Ω_i. Thus, we set:

$$c_{\partial\Omega_1^{\text{ext}}\cap\partial\Omega_1^{\text{int}}}^{k+1}:=0, \tag{2.65}$$

$$c_{\partial\Omega_2^{\text{ext}}\cap\partial\Omega_2^{\text{int}}}^{k+1}:=0. \tag{2.66}$$

There are as many balancing conditions as bands Ω_i^{ext}, i.e. as many as the subdomains. In the case of two subdomains, the two balancing conditions to satisfy are:

$$(\boldsymbol{n}_{\Gamma_{1,2}}\cdot\boldsymbol{n}_{\partial\Omega_1^{\text{ext}}})c_{\Gamma_{1,2}}^{k+1}+\sum_{b=1}^{2}c_{\Gamma_1^b}^{k+1}=(f,1)_{\Omega_1^{\text{ext}}}-\langle\{\!\{\mathbf{u}_h^{k+1}\cdot\boldsymbol{n}_{\partial\Omega_1^{\text{ext}}}\}\!\},1\rangle_{\partial\Omega_1^{\text{ext}}}, \tag{2.67a}$$

$$(\boldsymbol{n}_{\Gamma_{1,2}}\cdot\boldsymbol{n}_{\partial\Omega_2^{\text{ext}}})c_{\Gamma_{1,2}}^{k+1}+\sum_{b=1}^{2}c_{\Gamma_2^b}^{k+1}=(f,1)_{\Omega_2^{\text{ext}}}-\langle\{\!\{\mathbf{u}_h^{k+1}\cdot\boldsymbol{n}_{\partial\Omega_2^{\text{ext}}}\}\!\},1\rangle_{\partial\Omega_2^{\text{ext}}}, \tag{2.67b}$$

where $(f,1)_{\Omega_i^{\text{ext}}}-\langle\{\!\{\mathbf{u}_h^{k+1}\cdot\boldsymbol{n}_{\partial\Omega_i^{\text{ext}}}\}\!\},1\rangle_{\partial\Omega_i^{\text{ext}}}$ is the mistfit of mass balance of the averaging in each subdomain for $i=1,2$.

Remark 2.20. *This problem is a non-square linear system with* 5 *single-valued unknowns $c_{\Gamma_1^1}^{k+1}$, $c_{\Gamma_1^2}^{k+1}$, $c_{\Gamma_{1,2}}^{k+1}$, $c_{\Gamma_2^1}^{k+1}$, and $c_{\Gamma_2^2}^{k+1}$ and 2 equations (2.67a) and (2.67b), to ensure that the bands Ω_1^{ext} and Ω_2^{ext} will be in balance with the source term. Moreover, our construction will ensure the continuity of the flux on the interface $\Gamma_{1,2}$ because we reused $c_{\Gamma_{1,2}}^{k+1}$ in the condition (2.67b).*

Rectangular linear system:

Using the notation of Figure 2.3, this non-square linear system reads:

$$\begin{pmatrix} 1 & 1 & 1 & 0 & 0 \\ 0 & 0 & -1 & 1 & 1 \end{pmatrix} \begin{pmatrix} c^{k+1}_{\Gamma^1_1} \\ c^{k+1}_{\Gamma^2_1} \\ c^{k+1}_{\Gamma_{1,2}} \\ c^{k+1}_{\Gamma^1_2} \\ c^{k+1}_{\Gamma^2_2} \end{pmatrix} = \begin{pmatrix} (f,1)_{\Omega^{\text{ext}}_1} - \langle \{\!\{ \mathbf{u}^{k+1}_h \cdot \boldsymbol{n}_{\partial\Omega^{\text{ext}}_1} \}\!\}, 1 \rangle_{\partial\Omega^{\text{ext}}_1} \\ (f,1)_{\Omega^{\text{ext}}_2} - \langle \{\!\{ \mathbf{u}^{k+1}_h \cdot \boldsymbol{n}_{\partial\Omega^{\text{ext}}_2} \}\!\}, 1 \rangle_{\partial\Omega^{\text{ext}}_2} \end{pmatrix}. \tag{2.68}$$

The rectangular matrix contains integers which are 0, 1 or -1. We note that in the second line of the matrix, two new unknowns appear compared to the first line. Thus, these two lines are linearly independent. Consequently, this linear system has an infinite number of solutions. We must choose between all these solutions. For this, we take into account that we do not want the values to differ too greatly from what we had before, i.e., the corrections should be as small as possible, see (2.64). To achieve this, we use the classical least squares algorithm to minimize between all of the solutions, in order to find the nearest solutions to (2.64), in the sense:

$$(c^{k+1}_{\Gamma^1_1})^2 + (c^{k+1}_{\Gamma^2_1})^2 + (c^{k+1}_{\Gamma_{1,2}})^2 + (c^{k+1}_{\Gamma^1_2})^2 + (c^{k+1}_{\Gamma^2_2})^2 = \min. \tag{2.69}$$

The resulting boundary fluxes of this method are as follows:

$$\boldsymbol{\sigma}^{k+1}_h \cdot \boldsymbol{n}_e = \begin{cases} \{\!\{ \mathbf{u}^{k+1}_h \cdot \boldsymbol{n}_e \}\!\} + \dfrac{1}{|\Gamma_{1,2}|} c^{k+1}_{\Gamma_{1,2}}, & \forall e \subset \Gamma_{1,2}, \\ \mathbf{u}^{k+1}_{h,i} \cdot \boldsymbol{n}_e + \dfrac{1}{|\Gamma^b_i|} c^{k+1}_{\Gamma^b_i}, & \forall e \subset \Gamma^b_i,\ \forall i = 1,2 \text{ and } b = 1,2, \\ \mathbf{u}^{k+1}_{h,i} \cdot \boldsymbol{n}_e, & \forall e \subset \partial\Omega^{\text{ext}}_i \cap \partial\Omega^{\text{int}}_i \text{ for } i = 1,2. \end{cases} \tag{2.70}$$

2.6.2.2 The case of many subdomains, not necessarily touching the boundary $\partial\Omega$

The above method can be generalized for many subdomains. We want to find corrections to the averaged flux $\{\!\{ \mathbf{u}^{k+1}_h \cdot \boldsymbol{n}_{\partial\Omega^{\text{ext}}_i} \}\!\}$, which will lead to the equilibrium in each band Ω^{ext}_i, such that:

$$c^{k+1}_{\Gamma^b_i} \approx 0 \qquad \text{for } i \in [\![1, \mathcal{N}]\!] \text{ and } b = 1,2 \text{ such that } |\partial\Omega^{\text{ext}}_i \cap \partial\Omega| > 0, \tag{2.71a}$$

$$c^{k+1}_{\Gamma_{i,j}} \approx 0 \qquad \text{for } i,j \in [\![1, \mathcal{N}]\!],\ i < j \text{ such that } j \in B^i. \tag{2.71b}$$

As previously, we keep the same value of the flux $\mathbf{u}^{k+1}_h \cdot \boldsymbol{n}_{\partial\Omega^{\text{ext}}_i \cap \partial\Omega^{\text{int}}_i}$ located on the boundary $\partial\Omega^{\text{ext}}_i \cap \partial\Omega^{\text{int}}_i$, where i represents as usual the number of the subdomain Ω_i. Thus, we set:

$$c^{k+1}_{\partial\Omega^{\text{ext}}_i \cap \partial\Omega^{\text{int}}_i} := 0 \quad \forall \Omega_i,\ i \in [\![1, \mathcal{N}]\!]. \tag{2.72}$$

There are again as many balancing conditions as bands Ω^{ext}_i and consequently as the number of subdomains. The $\mathcal{N}$ balancing conditions that have to be satisfied, $\forall i \in [\![1, \mathcal{N}]\!]$, are:

$$\sum_{\substack{b=1,2/ \\ |\partial\Omega_i \cap \partial\Omega| > 0}} c^{k+1}_{\Gamma^b_i} + \sum_{j \in B^i} (\boldsymbol{n}_{\Gamma_{i,j}} \cdot \boldsymbol{n}_{\partial\Omega^{\text{ext}}_i}) c^{k+1}_{\Gamma_{i,j}} = (f,1)_{\Omega^{\text{ext}}_i} - \langle \{\!\{ \mathbf{u}^{k+1}_h \cdot \boldsymbol{n}_{\partial\Omega^{\text{ext}}_i} \}\!\}, 1 \rangle_{\partial\Omega^{\text{ext}}_i}, \tag{2.73}$$

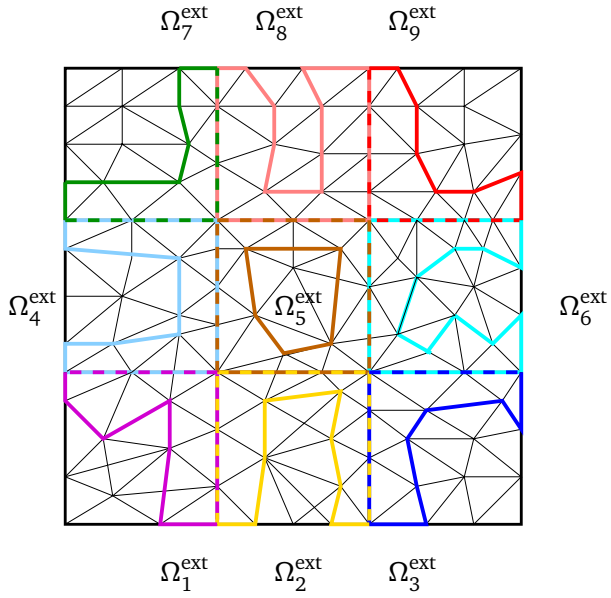

Figure 2.4: Nine bands located close to the interface Γ

where the term

$$(f,1)_{\Omega_i^{ext}} - \langle \{\!\{ \mathbf{u}_h^{k+1} \cdot \boldsymbol{n}_{\partial\Omega_i^{ext}} \}\!\}, 1 \rangle_{\partial\Omega_i^{ext}},\ i \in [\![1, \mathscr{N}]\!] \tag{2.74}$$

is the mistfit of mass balance of the averaging of $\mathbf{u}_h^{k+1} \cdot \boldsymbol{n}_{\partial\Omega_i^{ext}}$ in each subdomain for $i \in [\![1, \mathscr{N}]\!]$. Equations (2.73), for $i \in [\![1, \mathscr{N}]\!]$ lead to a rectangular linear system, that we detail below in the case of the example of nine subdomains given in Figure 2.4.

Rectangular linear system:

In the case of Figure 2.4 (where one of the subdomains does not touch the boundary), equation (2.71a) gives 16 corrections and equation (2.71b) gives 12 corrections. Thus, this problem is a non-square linear system with 28 unknowns (which is very few and independent of the number of mesh elements) and 9 equations (2.73), to ensure the balance in the bands $\Omega_1^{ext}, ..., \Omega_9^{ext}$ with the source term:

$$\begin{pmatrix} 1 & 1 & 0 & 0 & \cdot & \cdot & \cdot \\ 0 & -1 & 1 & 1 & \cdot & \cdot & \cdot \\ \cdot & \cdot & \cdot & \cdot & \cdot & & \\ \cdot & \cdot & \cdot & \cdot & & \cdot & \\ \cdot & \cdot & \cdot & \cdot & & & \cdot \end{pmatrix} \begin{pmatrix} c_{\Gamma_{1,4}}^{k+1} \\ c_{\Gamma_{1,2}}^{k+1} \\ \cdot \\ \cdot \\ \cdot \\ c_{\Gamma_{8,9}}^{k+1} \\ c_{\Gamma_1^1}^{k+1} \\ c_{\Gamma_1^2}^{k+1} \\ \cdot \\ \cdot \\ c_{\Gamma_9^1}^{k+1} \\ c_{\Gamma_9^2}^{k+1} \end{pmatrix} = \begin{pmatrix} (f,1)_{\Omega_1^{ext}} - \langle \{\!\{ \mathbf{u}_h^{k+1} \cdot \boldsymbol{n}_{\partial\Omega_1^{ext}} \}\!\}, 1 \rangle_{\partial\Omega_1^{ext}} \\ (f,1)_{\Omega_2^{ext}} - \langle \{\!\{ \mathbf{u}_h^{k+1} \cdot \boldsymbol{n}_{\partial\Omega_2^{ext}} \}\!\}, 1 \rangle_{\partial\Omega_2^{ext}} \\ (f,1)_{\Omega_3^{ext}} - \langle \{\!\{ \mathbf{u}_h^{k+1} \cdot \boldsymbol{n}_{\partial\Omega_3^{ext}} \}\!\}, 1 \rangle_{\partial\Omega_3^{ext}} \\ (f,1)_{\Omega_4^{ext}} - \langle \{\!\{ \mathbf{u}_h^{k+1} \cdot \boldsymbol{n}_{\partial\Omega_4^{ext}} \}\!\}, 1 \rangle_{\partial\Omega_4^{ext}} \\ (f,1)_{\Omega_5^{ext}} - \langle \{\!\{ \mathbf{u}_h^{k+1} \cdot \boldsymbol{n}_{\partial\Omega_5^{ext}} \}\!\}, 1 \rangle_{\partial\Omega_5^{ext}} \\ (f,1)_{\Omega_6^{ext}} - \langle \{\!\{ \mathbf{u}_h^{k+1} \cdot \boldsymbol{n}_{\partial\Omega_6^{ext}} \}\!\}, 1 \rangle_{\partial\Omega_6^{ext}} \\ (f,1)_{\Omega_7^{ext}} - \langle \{\!\{ \mathbf{u}_h^{k+1} \cdot \boldsymbol{n}_{\partial\Omega_7^{ext}} \}\!\}, 1 \rangle_{\partial\Omega_7^{ext}} \\ (f,1)_{\Omega_8^{ext}} - \langle \{\!\{ \mathbf{u}_h^{k+1} \cdot \boldsymbol{n}_{\partial\Omega_8^{ext}} \}\!\}, 1 \rangle_{\partial\Omega_8^{ext}} \\ (f,1)_{\Omega_9^{ext}} - \langle \{\!\{ \mathbf{u}_h^{k+1} \cdot \boldsymbol{n}_{\partial\Omega_9^{ext}} \}\!\}, 1 \rangle_{\partial\Omega_9^{ext}} \end{pmatrix}. \tag{2.75}$$

The rectangular matrix contains integers which are 0,1 or -1. Each line of this matrix corresponds to one subdomain. With a simple geometric representation, by making the path of the subdomains as shown in Figure 2.5, we remark that there is always at least one new unknown that appears on the next line. Thus, it is not possible to make a linear combination with the previous lines, and the vector lines are linearly independent. Consequently, this linear system has an infinity of solutions. We will

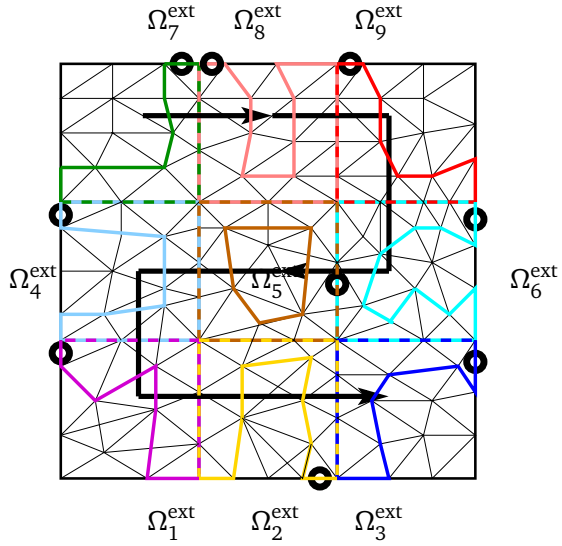

Figure 2.5: Path of the subdomains: each point represents a new unknown compared to the previous subdomains, following the path: Ω_7, Ω_8, Ω_9, Ω_6, Ω_5, Ω_4, Ω_1, Ω_2, Ω_3

again make a choice of these unknowns taking into account that we do not want the values to differ too greatly from what we had before, see (2.71). We use the classical least squares algorithm to minimize between all of the solutions, in order to find the nearest solution to (2.71) in the sense:

$$\sum_{\substack{i=1/\\ |\partial\Omega_i\cap\partial\Omega|>0}}^{\mathcal{N}}\sum_{b=1}^{2}(c_{\Gamma_i^b}^{k+1})^2+\sum_{i=1/j\in B^i,\,i<j}^{\mathcal{N}}(c_{\Gamma_{i,j}}^{k+1})^2=\min. \tag{2.76}$$

The resulting boundary fluxes of this method are as follows:

$$\boldsymbol{\sigma}_h^{k+1}\cdot\boldsymbol{n}_e=\begin{cases}\{\!\{\mathbf{u}_h^{k+1}\cdot\boldsymbol{n}_e\}\!\}+\dfrac{1}{|\Gamma_{i,j}|}c_{\Gamma_{i,j}}^{k+1}, & \forall e\subset\Gamma_{i,j},\ j\in B^i,\ i<j,\ i\in[\![1,\mathcal{N}]\!],\\ \mathbf{u}_{h,i}^{k+1}\cdot\boldsymbol{n}_e+\dfrac{1}{|\Gamma_i^b|}c_{\Gamma_i^b}^{k+1}, & \forall e\subset\Gamma_i^b \text{ for } i\in[\![1,\mathcal{N}]\!] \text{ and } b=1,2\\ & \text{such that } |\partial\Omega_i^{ext}\cap\partial\Omega|>0,\\ \mathbf{u}_{h,i}^{k+1}\cdot\boldsymbol{n}_e, & \forall e\subset\partial\Omega_i^{ext}\cap\partial\Omega_i^{int},\ i=1,..,\mathcal{N}.\end{cases} \tag{2.77}$$

2.6.2.3 Solving local Neumann problem in each band

These boundary fluxes, once computed, lead to the mass balance on each domain Ω_i^{ext}, $\forall i\in[\![1,\mathcal{N}]\!]$, see (2.73). Thus, we can solve a well-posed local Neumann problem in each band, which actually redistributes the boundary corrections.

Definition 2.21 (Spaces of local Neumann problem)**.** *Inspired by [130] Section 3.3.3, we define for $i \in [\![1,\mathcal{N}]\!]$ the spaces on Ω_i^{ext}:*

$$\begin{aligned}
\mathbf{W}_{h,z,\Omega_i^{\text{ext}}} = \Bigg\{ & \mathbf{v}_h^{k+1} \in \mathbf{W}_{h,i}(\Omega_i^{\text{ext}}) : \\
& \mathbf{v}_h^{k+1}\cdot\boldsymbol{n}_{\Omega_i^{\text{ext}}} = z + \left\{ \boldsymbol{n}_{\partial\Omega_i^{\text{ext}}}\cdot\boldsymbol{n}_{\Gamma_{i,j}} \frac{c_{\Gamma_{i,j}}^{k+1}}{|\Gamma_{i,j}|},\ \text{if } z\neq 0 \right\},\ j\in B^i, \\
& \mathbf{v}_h^{k+1}\cdot\boldsymbol{n}_{\Omega_i^{\text{ext}}} = z + \left\{ \frac{c_{\Gamma_i^b}^{k+1}}{|\Gamma_i^b|},\ \text{if } z\neq 0 \right\},\ \text{for } b=1,2 \text{ such that } |\partial\Omega_i^{\text{ext}}\cap\partial\Omega|>0, \\
& \mathbf{v}_h^{k+1}\cdot\boldsymbol{n}_{\Omega_i^{\text{ext}}} = z \text{ on } \partial\Omega_i^{\text{ext}}\cap\partial\Omega_i^{\text{int}} \Bigg\}.
\end{aligned} \tag{2.78}$$

We also define the space $M_{h,i}(\Omega_i^{\text{ext}})$, which is the restriction of $M_{h,i}$ on Ω_i^{ext}.

Definition 2.22 (Local Neumann problem)**.** *Find $\boldsymbol{\sigma}_h^{k+1}{}_{|\Omega_i^{\text{ext}}} \in \mathbf{W}_{h,\{\!\{\mathbf{u}_h^{k+1}\cdot\boldsymbol{n}_{\Omega_i^{\text{ext}}}\}\!\},\Omega_i^{\text{ext}}}$ and $q_h^{k+1}\in M_{h,i}(\Omega_i^{\text{ext}})$ such that $(q_h^{k+1},1)_{|\Omega_i^{\text{ext}}}=0$, $\forall i\in[\![1,\mathcal{N}]\!]$, solution of the following mixed problem:*

$$(\boldsymbol{S}^{-1}(\boldsymbol{\sigma}_h^{k+1}-\mathbf{u}_h^{k+1}),\mathbf{v}_h)_{\Omega_i^{\text{ext}}} - (q_h^{k+1},\nabla\cdot\mathbf{v}_h)_{\Omega_i^{\text{ext}}} = 0, \quad \forall \mathbf{v}_h\in\mathbf{W}_{h,0,\Omega_i^{\text{ext}}}, \tag{2.79a}$$

$$(\nabla\cdot\boldsymbol{\sigma}_h^{k+1},w_h)_{\Omega_i^{\text{ext}}} = (f,w_h)_{\Omega_i^{\text{ext}}}, \quad \forall w_h\in M_{h,i}(\Omega_i^{\text{ext}}), \quad \text{where } (w_h,1)_{|\Omega_i^{\text{ext}}}=0. \tag{2.79b}$$

Remark 2.23. *If we introduce $\tilde{\boldsymbol{\sigma}}_h{}^{k+1}$ defined in Ω_i^{ext} as the difference between the reconstructed equilibreated flux $\boldsymbol{\sigma}_h^{k+1}$ and the mixed finite element approximate flux $\mathbf{u}_h^{k+1}$, $\tilde{\boldsymbol{\sigma}}_h{}^{k+1}|_{\Omega_i^{\text{ext}}} := \boldsymbol{\sigma}_h^{k+1}|_{\Omega_i^{\text{ext}}} - \mathbf{u}_h^{k+1}|_{\Omega_i^{\text{ext}}}$, then $(\tilde{\boldsymbol{\sigma}}_h{}^{k+1},q_h^{k+1})|_{\Omega_i^{\text{ext}}}$ is the approximation by the MFE method of the following local Neumann problem on Ω_i^{ext}, $\forall i\in[\![1,\mathcal{N}]\!]$:*

$$-\nabla\cdot(\boldsymbol{S}\nabla q_h^{k+1}) = f - \nabla\cdot\mathbf{u}_h{}^{k+1} \qquad \text{in} \quad \Omega_i^{\text{ext}}, \tag{2.80a}$$

$$-\boldsymbol{S}\nabla q_h^{k+1}\cdot\boldsymbol{n}_{\partial\Omega_i^{\text{ext}}} = \boldsymbol{n}_{\partial\Omega_i^{\text{ext}}}\cdot\boldsymbol{n}_{\Gamma_{i,j}}\frac{c_{\Gamma_{i,j}}^{k+1}}{|\Gamma_{i,j}|} \qquad \text{on } \Gamma_{i,j},\ \forall j\in B^i \tag{2.80b}$$

$$-\boldsymbol{S}\nabla q_h^{k+1}\cdot\boldsymbol{n}_{\Omega_i^{\text{ext}}} = \frac{c_{\Gamma_i^k}^{k+1}}{|\Gamma_i^b|} \qquad \text{on } \Gamma_i^b \text{ for } b=1,2 \text{ such that } |\partial\Omega_i^{\text{ext}}\cap\partial\Omega|>0, \tag{2.80c}$$

$$-\boldsymbol{S}\nabla q_h^{k+1}\cdot\boldsymbol{n}_{\Omega_i^{\text{ext}}} = 0 \qquad \text{on } \partial\Omega_i^{\text{ext}}\cap\partial\Omega_i^{\text{int}}, \tag{2.80d}$$

$$(q_h^{k+1},1)_{\Omega_i^{\text{ext}}} = 0. \tag{2.80e}$$

Lemma 2.24. *A necessary condition for the existence of a solution to a Neumann problem is that the source term f and boundary data satisfy the compatibility condition. Here, problem (2.79), $i\in[\![1,\mathcal{N}]\!]$, satisfy the Neumann compatibility.*

Proof. It is easy to show that the Neumann conditions on the boundary are in equilibrium with the source term (i.e. the data) , from the $\mathcal{N}$ equilibrium conditions imposed.

This is, however, immediate from (2.73):

$$\sum_{\substack{b=1/\\ |\Gamma_i^b\cap\partial\Omega|>0}}^{2}(\langle\{\!\{\mathbf{u}_h^{k+1}\cdot\boldsymbol{n}_{\Omega_i^{\text{ext}}}\}\!\},1\rangle_{\Gamma_i^b}+c_{\Gamma_i^b}^{k+1})+\langle\{\!\{\mathbf{u}_h^{k+1}\cdot\boldsymbol{n}_{\Omega_i^{\text{ext}}}\}\!\},1\rangle_{\partial\Omega_i^{\text{ext}}\cap\partial\Omega_i^{\text{int}}}$$
$$+\sum_{j\in B^i}(\langle\{\!\{\mathbf{u}_h^{k+1}\cdot\boldsymbol{n}_{\Omega_i^{\text{ext}}}\}\!\},1\rangle_{\Gamma_{i,j}}+c_{\Gamma_{i,j}}^{k+1})$$
$$=\langle\{\!\{\mathbf{u}_h^{k+1}\cdot\boldsymbol{n}_{\partial\Omega_i^{\text{ext}}}\}\!\},1\rangle_{\partial\Omega_i^{\text{ext}}}+\underbrace{\sum_{j\in B^i}c_{\Gamma_{i,j}}^{k+1}+\sum_{\substack{b=1/\\ |\Gamma_i^b\cap\partial\Omega|>0}}^{2}c_{\Gamma_i^b}^{k+1}}_{=(f,1)_{\Omega_i^{\text{ext}}}-\langle\{\!\{\mathbf{u}_h^{k+1}\cdot\boldsymbol{n}_{\partial\Omega_i^{\text{ext}}}\}\!\},1\rangle_{\partial\Omega_i^{\text{ext}}}\text{ from (2.73)}}=(f,1)_{\Omega_i^{\text{ext}}}. \tag{2.81}$$

□

Remark 2.25. *Following the notation, problem (2.79) is equivalent to the constrained minimisation problem. In other words, the reconstructed equilibrated flux $\boldsymbol{\sigma}_h^{k+1}|_{\Omega_i^{\text{ext}}}$ that we find in each band Ω_i^{ext} is that among all $\mathbf{v}_h^{k+1}\in\mathbf{W}_{h,\{\!\{\mathbf{u}_h^{k+1}\cdot\boldsymbol{n}_{\Omega_i^{\text{ext}}}\}\!\},\Omega_i^{\text{ext}}}$ which satisfies $\nabla\cdot\mathbf{v}_h^{k+1}=\pi_0(f)$ and minimizes the distance to the flux $\mathbf{u}_h^{k+1}\notin\mathbf{H}(\text{div},\Omega)$:*

$$\boldsymbol{\sigma}_h^{k+1}{}_{|\Omega_i^{\text{ext}}}=\underset{\mathbf{v}_h\in\mathbf{W}_{h,\{\!\{\mathbf{u}_h^{k+1}\cdot\boldsymbol{n}_{\Omega_i^{\text{ext}}}\}\!\},\Omega_i^{\text{ext}}},\ \nabla\cdot\mathbf{v}_h=\pi_0(f)}{\arg\min}|||\mathbf{u}_h^{k+1}-\mathbf{v}_h|||_{\star,\Omega_i^{\text{ext}}}. \tag{2.82}$$

We thus found the best flux $\boldsymbol{\sigma}_h^{k+1}$ for the estimator $\eta_{\text{DDF},K}$ defined in (2.19).

2.7 Numerical results

In this section, we give some numerical illustrations of the a posteriori error estimators of Theorems 2.5 and 2.7. In this example, Ω is decomposed into nine subdomains. The nine bands where the local Neumann problem are solved are illustrated in Figure 2.6 (on the right).

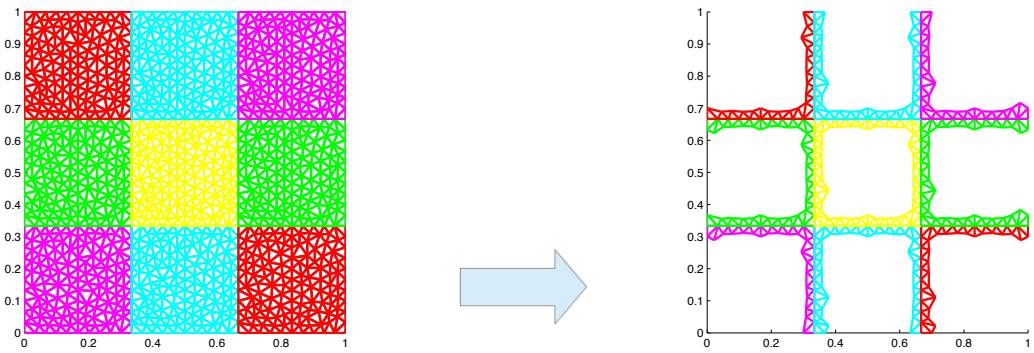

Figure 2.6: DD with 9 subdomains (on the left) and the bands Ω_i^{ext} (on the right)

2.7.1 Example 1 with the Jacobi solver

We take the same example as in Chapter 1 where on $\Omega =]0,1[\times]0,1[$, we have:

- The diffusion tensor: $\boldsymbol{S} = \begin{pmatrix} 3 & 2 \\ 2 & 3 \end{pmatrix}$,
- The exact solution: $p(x,y) = \sin(2\pi x)\sin(2\pi y)$,
- $f = 24\pi^2 \sin(2\pi x)\sin(2\pi y) - 16\pi^2 \cos(2\pi x)\cos(2\pi y)$ is the corresponding source term,
- $x = 0$ is the Neumann boundary,
- $x = 1$ is the Robin boundary,
- $y = 0$ and $y = 1$ are the Dirichlet boundaries.

The number of triangles in the domain $\Omega = \bigcup_{i=1}^{9} \Omega_i$ after discretization is 115 200. The Robin parameters are optimized following [72].

Number of triangles in Ω	115 200
Number of subdomains	9
Subdomain solver	Direct
DD solver	Jacobi
Original DD stopping criterion	1e-12
A posteriori stopping criterion	$\eta_{\text{DD}} \leq 0.1\eta_{\text{disc}}$
Total number of iterations	209
Number of iterations with the a posteriori stopping criterion	47
Unnecessary iterations	162

Table 2.1: Example 1 with the Jacobi solver

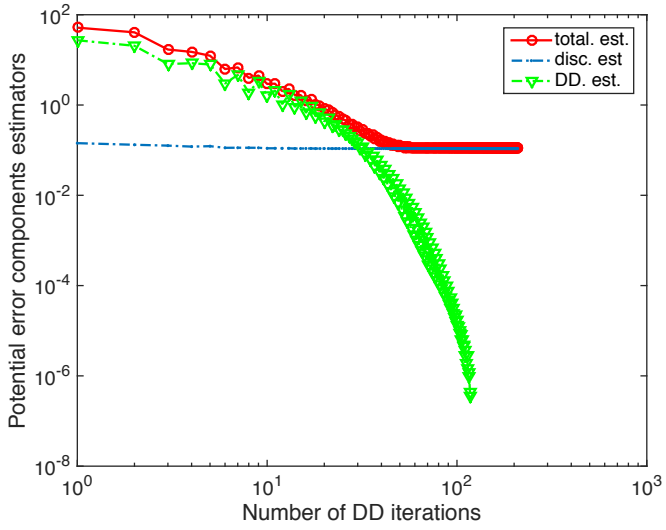

Figure 2.7: Example 1: error component estimates with the Jacobi solver

In Figure 2.7, we plot the evolution of η_{DD}, η_{disc}, of Theorem 2.7 and of their sum as a function of the number of iterations of the DD Jacobi solver. The original DD stopping criteria is when the residual of the jump of the Robin condition is lower

than 1e-12 on the interface as mentioned in Table 2.1. At the beginning we see that η_{DD} dominates up to roughly 35 iterations and then gets smaller compared to η_{disc} and then vanishes. A stopping criterion for the iterative solver that we propose instead is when the domain decomposition error does not contribute significantly to the overall error, i.e., $\eta_{\mathrm{DD}} \leq \gamma \eta_{\mathrm{disc}}$, with $\gamma \approx 0.1$. Here, we can stop the iterations at 47, and avoid 162 unnecessary iterations. We also plot the energy error and the total estimator as

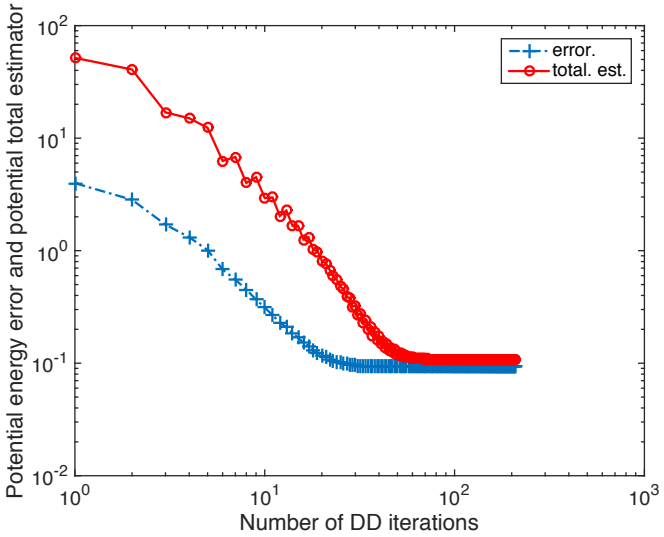

Figure 2.8: Example 1: energy error and total estimator with the Jacobi solver

a function of the number of iterations, see Figure 2.8. Consequently, we can obtain the effectivity index I_{eff}^{k+1} defined in (2.29) at each iteration of the DD algorithm, see Figure 2.9. We observe that the effectivity index is close to the optimal value of 1.

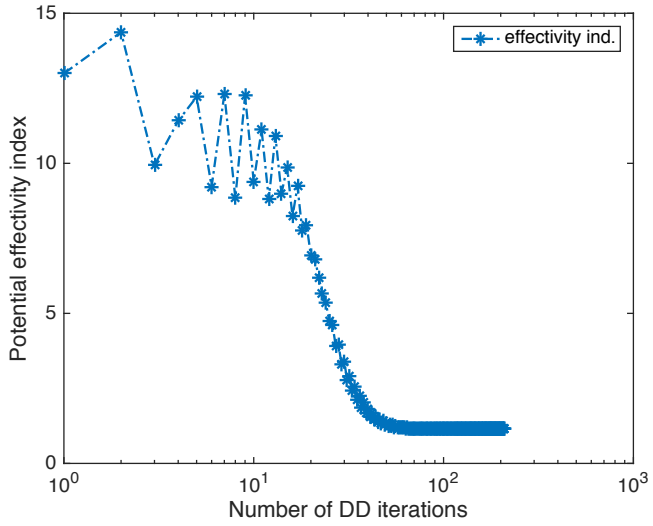

Figure 2.9: Example 1: effectivity index with the Jacobi solver

Below, we give a general description of what happens at iteration 4 and at iteration 47 of the Jacobi algorithm.

At iteration 4

We can see in Figure 2.10 that we have a discontinuous approximation solution p_h^4 on the interface. Thus, at iteration 4, we intuitively can not stop the iterations because the error on the interface is very large. In Figure 2.11, we can see that estimator distribution η_{DD} (on the right) on a uniform mesh is very much concentrated around the interface, whereas η_{disc} (on the left) is rather uniform and smaller. Consequently, the sum of the estimators η_{disc} and η_{DD}, see Figure 2.12 (on the left), overestimates importantly the potential energy error, which is less concentrated around the interface.

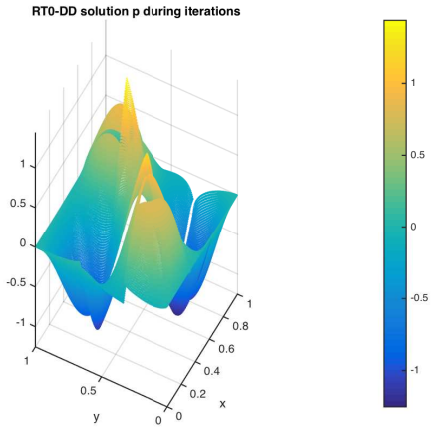

Figure 2.10: Example 1: pressure at the 4th iteration with the Jacobi solver

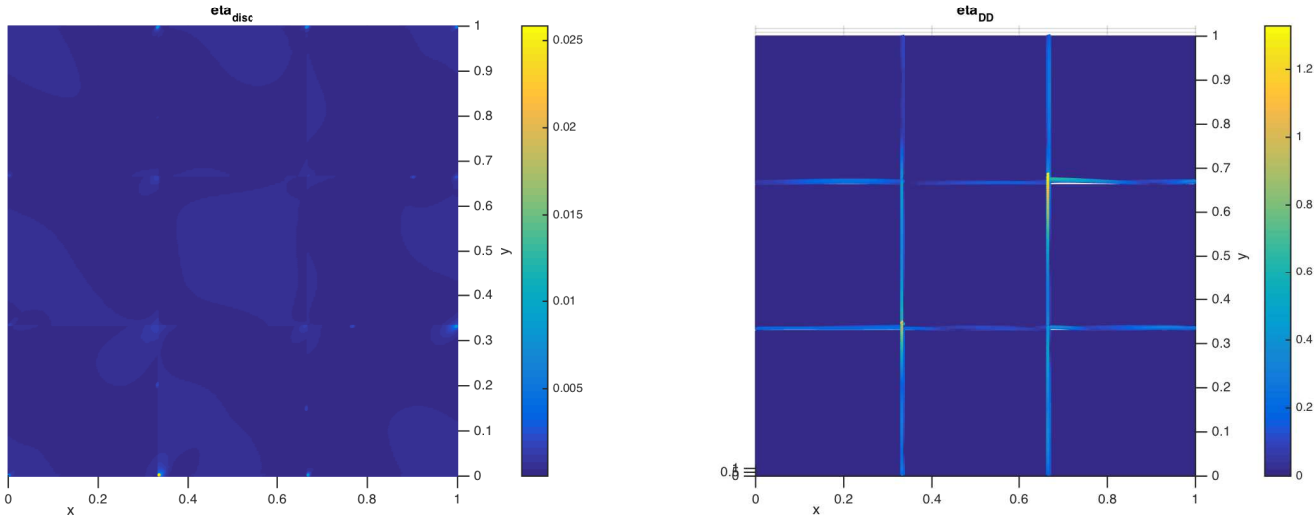

Figure 2.11: Example 1: the two components of the a posteriori estimates η_{disc} (on the left) and η_{DD} (on the right) on each element K of Ω at the 4th iteration with the Jacobi solver

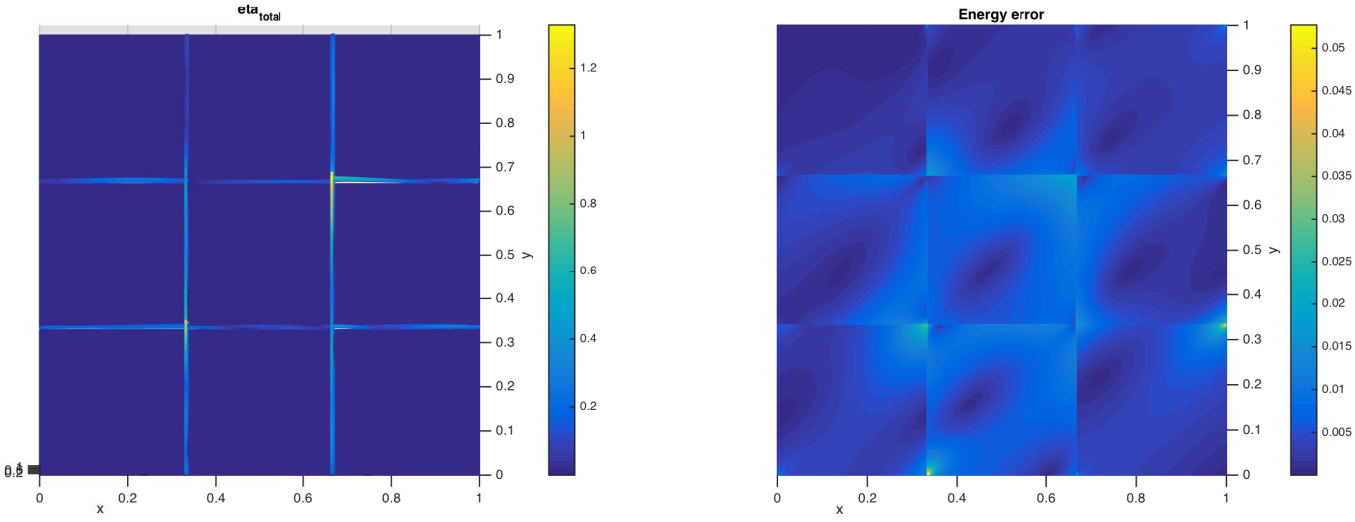

Figure 2.12: Example 1: the total error estimator (on the left) and the distribution of the energy error (on the right) at the 4th iteration with the Jacobi solver

At iteration 47

At iteration 47, the solution p_h^{47} does not present any visually discontinuity, see Figure 2.13. Figure 2.14 shows that the elements contributions of η_{disc} are about 5e-4 and distributed rather uniformly on the hole domain, while η_{DD} is about 10^{-3} and distributed only around the interfaces. Thus, if we sum the values of η_{DD} and η_{disc}, we remark that η_{disc} dominates. Consequently, we can see in Figure 2.15 (on the left) that the total error estimator distribution is very close to the error distribution of η_{disc}. Finally, we see that the energy error distribution shown on Figure 2.15 (on the right) matches well with the total error estimator distribution, see Figure 2.15 (on the left).

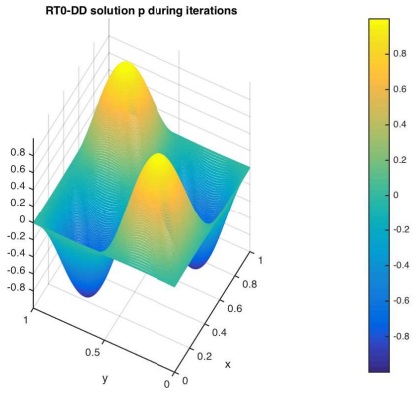

Figure 2.13: Example 1: pressure at the 47th iteration with the Jacobi solver

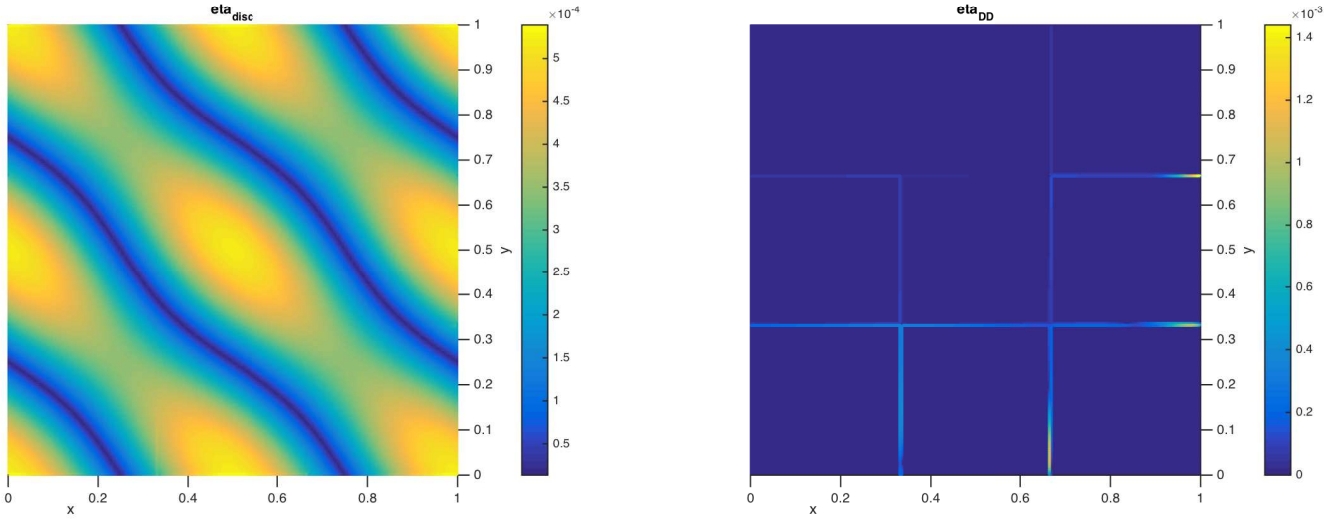

Figure 2.14: Example 1: the two components of the a posteriori estimates η_{disc} (on the left) and η_{DD} (on the right) on each element K of Ω, at the 47th iteration with the Jacobi solver

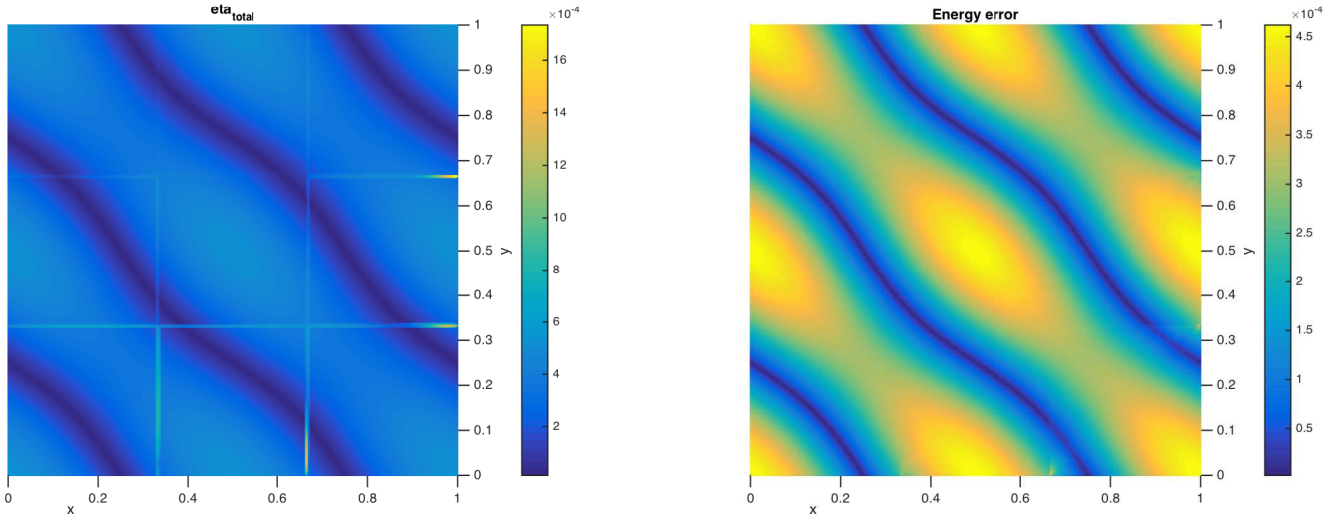

Figure 2.15: Example 1: the total error estimator (on the left) and the distribution of the energy error (on the right) at the 47th iteration with the Jacobi solver

Convergence rates

In Figure 2.16 we plot the convergence rates of the total potential estimator, η_{NCP} and η_{osc} at different discretizations. These convergence rates are part of the factors which play role in the efficiency of the method. We can see that the convergence rate of "total. est.", which corresponds to $\tilde{\eta}$ in (2.27), and η_{NCP} is h as for the solution p of the lowest-order Raviart–Thomas method. We can remark that the convergence rate of η_{osc} is h^2.

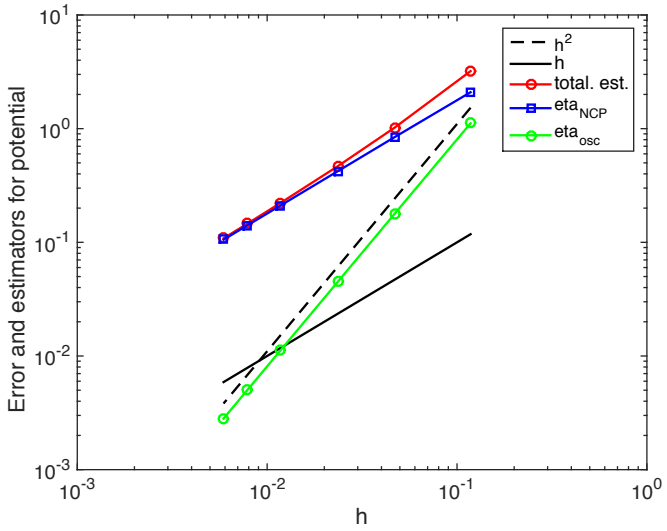

Figure 2.16: Example 1: convergence rate of the different estimators

2.7.2 Example 1 with the GMRES solver

We take the same example as before but using the GMRES solver now, see Table 2.2. One particular advantage of the GMRES solver is that we can make less iterations than Jacobi. As shown in Figure 2.17, η_{DD} dominates up to roughly 12 iterations and then gets small compare to η_{disc} and then vanishes. A resulting stopping criterion is when $\eta_{\text{DD}} \leq \gamma \eta_{\text{disc}}$, with $\gamma \approx 0.1$. Here, we can stop the DD algorithm at iteration 17, and thus save 44 unnecessary iterations. We also plot the energy error and the total estimator as a function of the number of iterations, see Figure 2.18. Consequently, we can obtain the effectivity index I_{eff}^{k+1} defined in (2.29) at each iteration of the DD algorithm, see Figure 2.19. We observe that the effectivity index is close to the optimal value of 1.

Number of triangles in Ω	115 200
Number of subdomains	9
Subdomain solver	Direct
DD solver	GMRES
Original DD stopping criterion	1e-12
A posteriori stopping criterion	$\eta_{\text{DD}} \leq 0.1\eta_{\text{disc}}$
Total number of iterations	61
Number of iterations with the a posteriori stopping criterion	17
Unnecessary iterations	44

Table 2.2: Example 1 with the GMRES solver

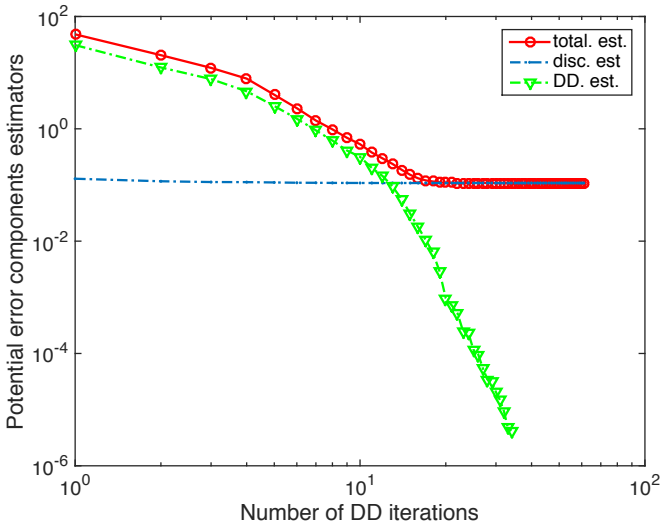

Figure 2.17: Example 1: error component estimates with the GMRES solver

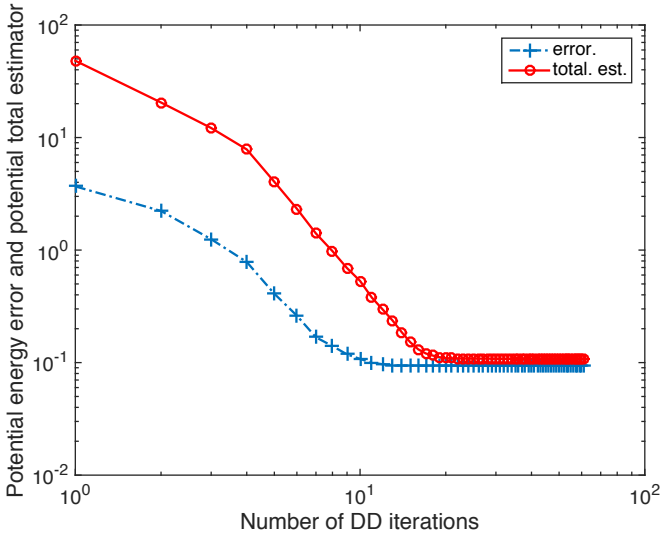

Figure 2.18: Example 1: energy error and total estimator with the GMRES solver

2.7.3 Example 2 with the GMRES solver

The second example focuses on the resolution of the problem (1.1) by the MFE method, where $\Omega = [0,1] \times [0,1]$ and:

- the exact solution is $p(x,y) = x(1-x)y(1-y)$,
- the diffusion tensor is

$$\boldsymbol{S} := \begin{cases} 15 - 10\sin(10\pi x)\sin(10\pi y)\boldsymbol{I}\,, & x,y \in (0,1/2) \text{ or } x,y \in (1/2,1), \\ 15 - 10\sin(2\pi x)\sin(2\pi y)\boldsymbol{I}\,, & \text{otherwise}, \end{cases} \tag{2.83}$$

where $\boldsymbol{I}$ is the identity matrix (2 by 2),

- $\partial\Omega$ is the Dirichlet boundary.

We consider a domain decomposition of Ω into 4 subdomains $\Omega = \bigcup_{i=1}^{4} \Omega_i$. In this

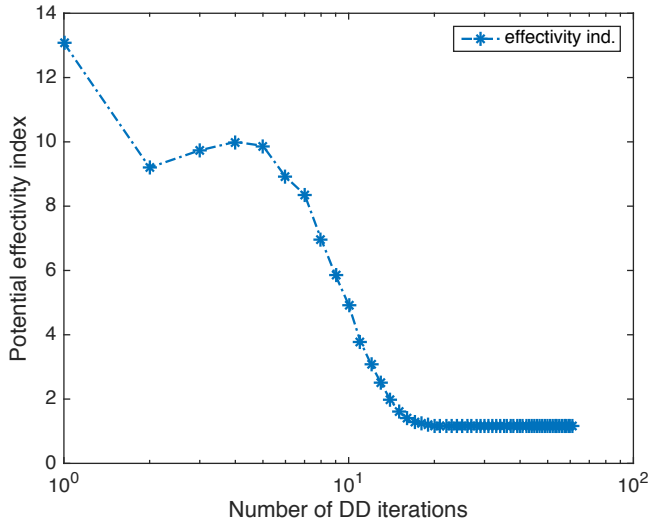

Figure 2.19: Example 1: effectivity index with the GMRES solver

Number of triangles in Ω	12800
Number of subdomains	4
Subdomain solver	Direct
DD solver	GMRES
Original DD stopping criteria	1e-11
A posteriori stopping criteria	$\eta_{\text{DD}} \leq 0.1\eta_{\text{disc}}$
Total number of iterations	40
Number of iterations with a posteriori stopping iteration	6
Unnecessary iterations	34

Table 2.3: Example 2 with the GMRES solver

example, we can see from Figure 2.20 that we can stop the iterations at 6, and so save 34 unnecessary iterations. We also plot the energy error and the total estimator as a function of the number of iterations, see Figure 2.21. We observe that the effectivity index is close to the optimal value of 1, see Figure 2.22.

At iteration 6

At iteration 6, we remark that the DD error is located on the interface, see Figure 2.23 (on the right). We can see in Figure 2.24 (on the left) that the total error estimator distribution is very close to the error distribution of η_{disc} in Figure 2.23 (on the left). Finally, we see that the energy error distribution Figure 2.24 (on the right) matches well with the total error estimator distribution, see Figure 2.24 (on the left).

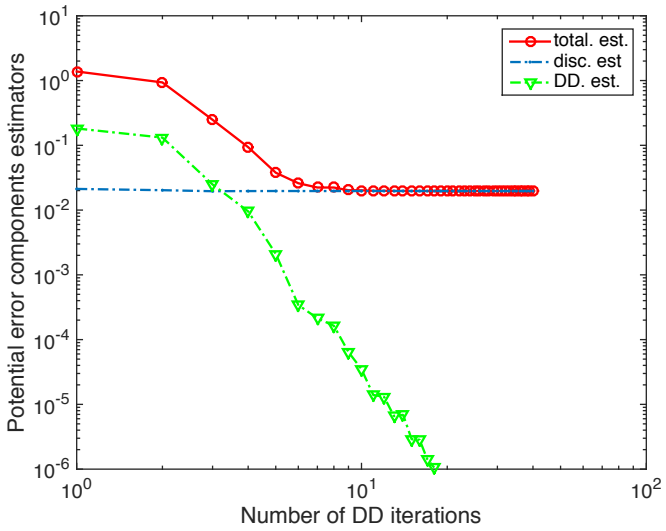

Figure 2.20: Example 2: error component estimates with the GMRES solver

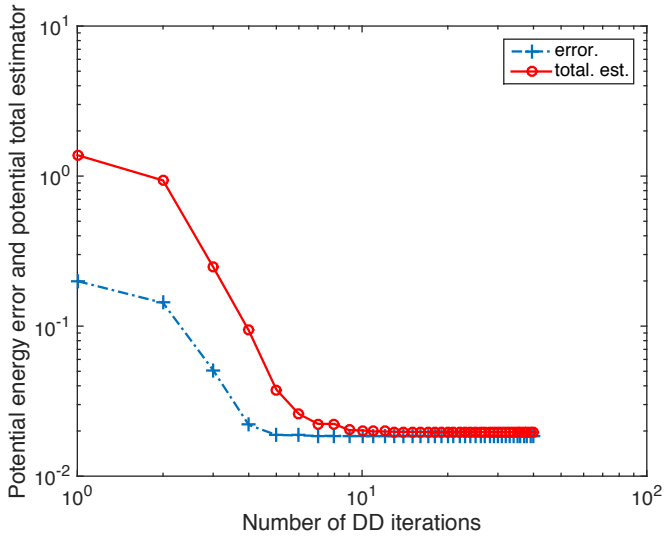

Figure 2.21: Example 2: energy error and total estimator with the GMRES solver

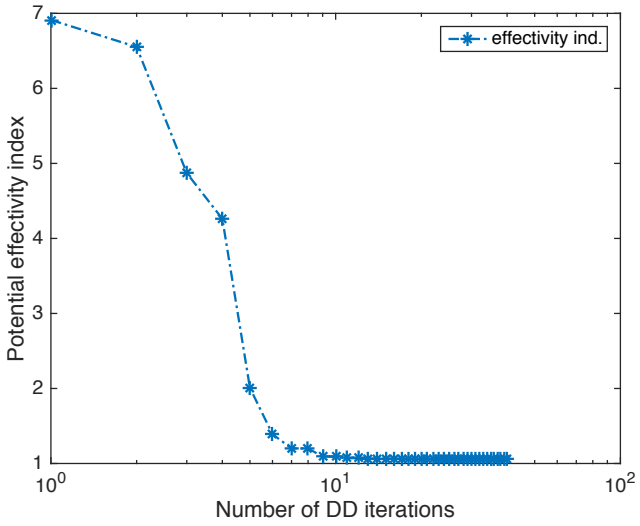

Figure 2.22: Example 2: effectivity index with the GMRES solver

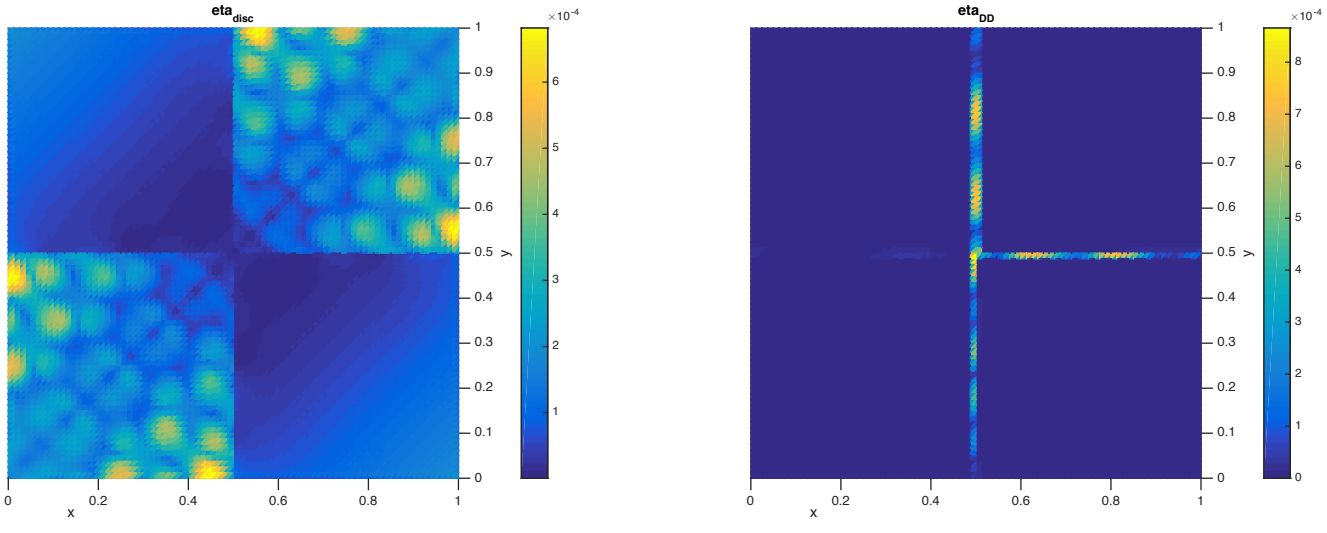

Figure 2.23: Example 2: the two components of the a posteriori estimates η_{disc} (on the left) and η_{DD} (on the right) on each element K of Ω at the 6th iteration with the GMRES solver

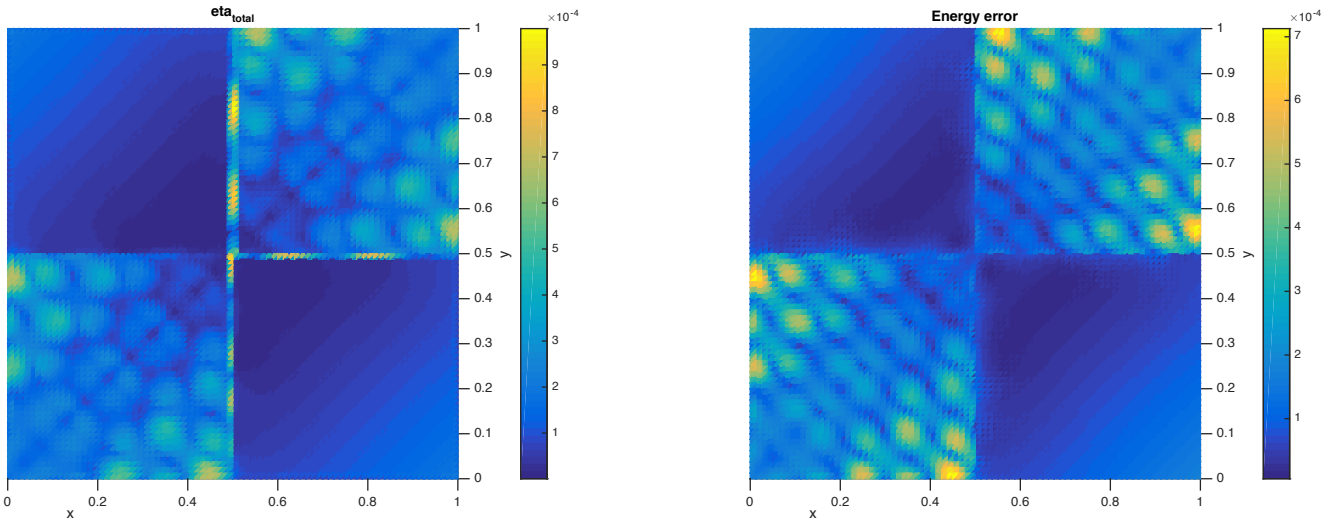

Figure 2.24: Example 2: the total error estimator (on the left) and the distribution of the energy error (on the right) at the 6th iteration with the GMRES solver

Chapter 3

Estimates and stopping criteria in unsteady diffusion case

Contents

In this chapter, we first present the heat equation and its mixed variational formulation. We intend to approximate it iteratively using the Optimized Schwarz method [21, 76] for the DD method which is global in time. This in particular allows to

use different time steps in different subdomains [26, 29, 74, 85, 86, 92, 93, 95, 96]. As in Chapter 2, we are interested in a posteriori error estimates in a MFE discretization. Using the space-time energy norm given in [65, 67], we bound the error $|||p - p_{h\tau}^{k+1}|||$ between the exact solution and the approximate solution at each iteration $k+1$ of the space-time DD method. The indicators which bound the error are completely calculable and constructed from the approximate solution $(p_{h\tau}^{k+1}, \mathbf{u}_{h\tau}^{k+1})$. We first construct a postprocessing $\tilde{p}_{h\tau}^{k+1}$, from which we then construct a potential reconstruction $s_{h\tau}^{k+1}$ at each iteration of the DD algorithm, following [67]. We also construct a subdomain potential reconstruction $\overline{s}_{h\tau,i}^{k+1}$ for each subdomain Ω_i, $\forall i \in [\![1, \mathcal{N}]\!]$, at each iteration of the DD algorithm, following the idea presented in Chapter 2, so as to distinguish the error from $H_0^1(\Omega)$-nonconformity and from domain decomposition. Then, using the same idea of extracting bands and solving local Neumann problems as presented in Chapter 2 to evaluate the error in the $\mathbf{H}(\mathrm{div}, \Omega)$-nonconformity, we build a flux reconstruction $\boldsymbol{\sigma}_h^{k+1,n}$ at each iteration of the DD algorithm and at each time step n. Then,the discretization error, the time discretization error, and the domain decomposition error are distinguished. Numerical results are shown both for the Jacobi iterative method and the GMRES method, to illustrate the efficiency of our a posteriori estimates.

3.1 The heat equation

We consider the following heat equation with final time $T > 0$ and $f \in L^2(\Omega \times (0,T))$: Find the potential p and the flux $\mathbf{u}$ such that:

$$\mathbf{u} = -\boldsymbol{S}\nabla p \quad \text{in} \quad \Omega \times (0,T), \tag{3.1a}$$

$$\frac{\partial p}{\partial t} + \nabla\cdot\mathbf{u} = f \quad \text{in} \quad \Omega \times (0,T), \tag{3.1b}$$

$$p = g_{\mathrm{D}} \quad \text{on} \quad \Gamma^{\mathrm{D}} \times (0,T), \tag{3.1c}$$

$$-\mathbf{u}\cdot\boldsymbol{n} = g_{\mathrm{N}} \quad \text{on} \quad \Gamma^{\mathrm{N}} \times (0,T), \tag{3.1d}$$

$$p(\cdot,0) = p_0 \quad \text{in} \quad \Omega, \tag{3.1e}$$

where $\boldsymbol{S} \in [L^\infty(\Omega \times (0,T))]^{d\times d}$ is the diffusion tensor that we suppose piecewise constant on the mesh $\mathcal{T}_h$ of Ω and constant in time for simplicity, $g_{\mathrm{N}} \in L^2(\Gamma^{\mathrm{N}} \times (0,T))$ is the Neumann boundary condition, $g_{\mathrm{D}} \in H^{\frac{1}{2}}(\Gamma^{\mathrm{D}} \times (0,T)) \cap C^0((\overline{\Gamma}^{\mathrm{D}}) \times (0,T))$ is the Dirichlet boundary condition, and $p_0 \in H^1(\Omega)$ is the initial condition where $p_0|_{\Gamma^{\mathrm{D}}} = g_{\mathrm{D}}(\cdot,0)|_{\Gamma^{\mathrm{D}}}$. Here, Γ^{D} and Γ^{N} are connected subsets of $\partial\Omega$ such that $\Gamma^{\mathrm{D}} \cup \Gamma^{\mathrm{N}} = \partial\Omega$.

3.2 The global-in-time Optimized Schwarz method using OSWR

In this section, we present the interface problem for the heat equation following [51, 95]. We suppose that Ω is decomposed into $\mathcal{N}$ subdomains as in (1.3). The original problem (3.1) is equivalent to solving the subdomain problems for $i = [\![1, \mathcal{N}]\!]$:

$$\mathbf{u}_i = -\boldsymbol{S}\nabla p_i \quad \text{in} \quad \Omega_i \times (0,T), \tag{3.2a}$$

$$\frac{\partial p_i}{\partial t} + \nabla\cdot\mathbf{u}_i = f \quad \text{in} \quad \Omega_i \times (0,T), \tag{3.2b}$$

$$p_i = g_{\mathrm{D}} \quad \text{on} \quad \Gamma_i^{\mathrm{D}} \times (0,T), \tag{3.2c}$$
$$-\mathbf{u}_i \cdot \boldsymbol{n} = g_{\mathrm{N}} \quad \text{on} \quad \Gamma_i^{\mathrm{N}} \times (0,T), \tag{3.2d}$$
$$-\beta_{i,j}\mathbf{u}_i \cdot \boldsymbol{n}_i + p_i = -\beta_{i,j}\mathbf{u}_j \cdot \boldsymbol{n}_i + p_j \quad \text{on} \quad \Gamma_{i,j} \times (0,T), \ \forall j \in B^i, \tag{3.2e}$$
$$p(\cdot,0) = p_0(\cdot) \quad \text{in} \quad \Omega_i. \tag{3.2f}$$

In order to write (3.2) as an equivalent interface problem (see [51] and Chapter 1), we first introduce the following spaces:

$$L_T(\Gamma_i) = \prod_{j \in B^i} H^1(0,T;L^2(\Gamma_{i,j})), \tag{3.3a}$$
$$\mathscr{V}_{T,i} = L^2(0,T;L^2(\Omega_i)) \times L^2(0,T;L^2(\Gamma_i^{\mathrm{D}})) \times L^2(0,T;L^2(\Gamma_i^{\mathrm{N}})) \times H^1(\Omega_i) \text{ for } i \in [\![1,\mathscr{N}]\!] \tag{3.3b}$$

and we recall the following subspaces introduced in Chapter 1:

$$\overline{\mathbf{W}}_i := \{\mathbf{v} \in \mathbf{H}(\mathrm{div},\Omega_i);\ \mathbf{v}\cdot\boldsymbol{n}_i \in L^2(\partial\Omega_i)\}, \tag{3.4a}$$
$$\mathbf{W}_i^{g_{\mathrm{N}}} := \{\mathbf{v} \in \overline{\mathbf{W}}_i;\ \mathbf{v}\cdot\boldsymbol{n}_i = g_{\mathrm{N}}(\cdot,t) \text{ on } \Gamma^{\mathrm{N}} \cap \partial\Omega_i\}, \tag{3.4b}$$

a.e. for a given $t \in (0,T)$. Note that the coefficients $\beta_{i,j} \in L^\infty(\Gamma_{i,j})$ do not depend on time, being fixed for each interface edge.
We now introduce the subproblem solution operator for Ω_i, $i \in [\![1,\mathscr{N}]\!]$, as follows:

$$\begin{array}{rccc} \mathscr{M}_i & : & L_T(\Gamma_i) \times \mathscr{V}_{T,i} & \to & L_T(\Gamma_i) \times H^1(0,T;L^2(\Omega_i)) \times L^2(0,T;\mathbf{W}_i^{g_{\mathrm{N}}}) \\ & & (\boldsymbol{\xi}_i, \boldsymbol{\mathscr{F}}_i) & \mapsto & (\boldsymbol{\xi}_i, p_i, \mathbf{u}_i), \end{array} \tag{3.5}$$

where $\boldsymbol{\xi}_i = \left(\xi_{i,j}\right)_{j\in B^i}$, $\boldsymbol{\mathscr{F}}_i = (f|_{\Omega_i}, g_{\mathrm{D}}|_{\Gamma_i^{\mathrm{D}}}, g_{\mathrm{N}}|_{\Gamma_i^{\mathrm{N}}}, p_0|_{\Omega_i})$, and where $(p_i,\mathbf{u}_i)$ is the solution of the following problem in $\Omega_i \times (0,T)$:

$$\mathbf{u}_i = -\boldsymbol{S}\nabla p_i \quad \text{in} \quad \Omega_i \times (0,T), \tag{3.6a}$$
$$\frac{\partial p_i}{\partial t} + \nabla\cdot\mathbf{u}_i = f \quad \text{in} \quad \Omega_i \times (0,T), \tag{3.6b}$$
$$p_i = g_{\mathrm{D}} \quad \text{on} \quad \Gamma_i^{\mathrm{D}} \times (0,T), \tag{3.6c}$$
$$-\mathbf{u}_i \cdot \boldsymbol{n} = g_{\mathrm{N}} \quad \text{on} \quad \Gamma_i^{\mathrm{N}} \times (0,T), \tag{3.6d}$$
$$-\beta_{i,j}\mathbf{u}_i \cdot \boldsymbol{n}_i + p_i = \xi_{i,j} \quad \text{on} \quad \Gamma_{i,j} \times (0,T), \ \forall j \in B^i, \tag{3.6e}$$
$$p(\cdot,0) = p_0 \quad \text{in} \quad \Omega_i. \tag{3.6f}$$

We also introduce:

$$\begin{array}{rccc} \mathscr{R}_i : & L_T(\Gamma_i) \times H^1(0,T;L^2(\Omega_i)) \times L^2(0,T;\mathbf{W}_i^{g_{\mathrm{N}}}) & \to & L_T(\Gamma_i) \\ & (\boldsymbol{\xi}_i, p_i, \mathbf{u}_i) & \mapsto & \left(\beta_{j,i}\mathbf{u}_i\cdot\boldsymbol{n}_i + (\xi_{i,j} + \beta_{i,j}\mathbf{u}_i\cdot\boldsymbol{n}_i)\right)_{j\in B^i}, \end{array} \tag{3.7}$$

and the Robin-to-Robin operator defined as follows:

$$\boldsymbol{S}_i^{\mathrm{RtR}} := \mathscr{R}_i \circ \mathscr{M}_i \ : \ L_T(\Gamma_i) \times \mathscr{V}_{T,i} \to L_T(\Gamma_i). \tag{3.8}$$

Then, problems (3.2) for $i \in [\![1,\mathscr{N}]\!]$ lead to the equivalent space-time interface problem:

Find $(\boldsymbol{\xi}_1,\ldots,\boldsymbol{\xi}_{\mathscr{N}}) \in L_T(\Gamma_1) \times \ldots \times L_T(\Gamma_{\mathscr{N}})$ such that:

$$(\boldsymbol{\xi}_i)_j = (\boldsymbol{S}_j^{\mathrm{RtR}}(\boldsymbol{\xi}_j, \boldsymbol{\mathscr{F}}_j))_i, \quad \forall j \in B^i, \quad \forall i \in [\![1,\mathscr{N}]\!]. \tag{3.9}$$

Using $\mathscr{M}_j(\boldsymbol{\xi}_j,\boldsymbol{\mathscr{F}}_j)=\mathscr{M}_j(\boldsymbol{\xi}_j,\mathbf{0})+\mathscr{M}_j(\mathbf{0},\boldsymbol{\mathscr{F}}_j)$ and the linearity of $\mathscr{R}_i$, we obtain:

$$\begin{aligned}\boldsymbol{S}_j^{\mathrm{RtR}}(\boldsymbol{\xi}_j,\boldsymbol{\mathscr{F}}_j)=\mathscr{R}_j(\mathscr{M}_j(\boldsymbol{\xi}_j,\boldsymbol{\mathscr{F}}_j))&=\mathscr{R}_j(\mathscr{M}_j(\boldsymbol{\xi}_j,\mathbf{0}))+\mathscr{R}_j(\mathscr{M}_j(\mathbf{0},\boldsymbol{\mathscr{F}}_j))\\&=\boldsymbol{S}_j^{\mathrm{RtR}}(\boldsymbol{\xi}_j,\mathbf{0})+\boldsymbol{S}_j^{\mathrm{RtR}}(\mathbf{0},\boldsymbol{\mathscr{F}}_j).\end{aligned}\tag{3.10}$$

Hence, (3.9) can be rewritten as:

$$(\boldsymbol{\xi}_i)_j-(\boldsymbol{S}_j^{\mathrm{RtR}}(\boldsymbol{\xi}_j,\mathbf{0}))_i=(\boldsymbol{S}_j^{\mathrm{RtR}}(\mathbf{0},\boldsymbol{\mathscr{F}}_j))_i,\quad\forall j\in B^i,\quad\forall i\in[\![1,\mathscr{N}]\!].\tag{3.11}$$

Our interface problem is written in compact form, as in Chapter 1, as follows:

$$\boldsymbol{S}^{\mathrm{RtR}}\boldsymbol{\xi}=\boldsymbol{\chi}_{\mathrm{R}}.\tag{3.12}$$

The Robin parameters $\beta_{i,j}$ can be chosen to improve the convergence rates, see [21, 71, 94, 95, 102, 103]. The space-time interface problem can be solved by the Jacobi iterative method or another methods, e.g. GMRES, and lead to a global-in-time Optimized Schwarz method. The Jacobi algorithm applied to the interface problem corresponds to the well-known Optimized Schwarz waveform relaxation (OSWR) algorithm [21, 76] recalled in the next section.

3.3 Local solver of the OSWR method for the heat equation

Applying the Jacobi algorithm to the space-time interface problem (3.12) leads to the following algorithm:
Find the solutions p_i^{k+1} and $\mathbf{u}_i^{k+1}$ in subdomain Ω_i, at iteration $k+1$, for $k\geq 0$, such that:

$$\mathbf{u}_i^{k+1}=-\boldsymbol{S}\nabla p_i^{k+1}\quad\text{in}\quad\Omega_i\times(0,T),\tag{3.13a}$$

$$\frac{\partial p_i^{k+1}}{\partial t}+\nabla\cdot\mathbf{u}_i^{k+1}=f\quad\text{in}\quad\Omega_i\times(0,T),\tag{3.13b}$$

$$p_i^{k+1}=g_{\mathrm{D}}\quad\text{on}\quad\Gamma_i^{\mathrm{D}}\times(0,T),\tag{3.13c}$$

$$-\mathbf{u}_i^{k+1}\cdot\boldsymbol{n}=g_{\mathrm{N}}\quad\text{on}\quad\Gamma_i^{\mathrm{N}}\times(0,T),\tag{3.13d}$$

$$-\beta_{i,j}\mathbf{u}_i^{k+1}\cdot\boldsymbol{n}_i+p_i^{k+1}=g_{\mathrm{R},j}^k\quad\text{on}\quad\Gamma_{i,j}\times(0,T),\ \forall j\in B^i,\tag{3.13e}$$

$$p(\cdot,0)=p_0\quad\text{in}\quad\Omega_i,\tag{3.13f}$$

where $g_{\mathrm{R},j}^k:=-\beta_{i,j}\mathbf{u}_j^k\cdot\boldsymbol{n}_i+p_j^k$ for $k\geq 1$ is the information coming from the neighboring subdomain Ω_j, $j\in B^i$, at step k of the Jacobi algorithm. This algorithm starts from initial guesses $g_{\mathrm{R},j}^0$ which are given functions in $H^1(0,T;L^2(\Gamma_{i,j}))$, $j\in B^i$, $1\leq i\leq\mathscr{N}$, (see [95] for the convergence analysis and well-posedness).

3.4 Local solver of the heat equation in the mixed finite element formulation

Let Ω_i be a subdomain of Ω, $i=[\![1,\mathscr{N}]\!]$. Let $k+1$ be the iteration index of the global-in-time DD method. We are looking for the solutions p_i^{k+1} and $\mathbf{u}_i^{k+1}$ in subdomain Ω_i

at iteration $k+1$. Based on the variational formulation of the diffusion equation given in Chapter 1, the weak formulation of the heat problem (3.1) at step $k+1$ is written as: for a.e. $t \in (0,T)$, find $\mathbf{u}_i^{k+1}(\cdot,t) \in \mathbf{W}_i^{g_N}$ and $p_i^{k+1}(\cdot,t) \in M_i$ such that:

$$\mathbf{a}_i(\mathbf{u}_i^{k+1},\mathbf{v}_i) - \mathbf{b}_i(\mathbf{v}_i,p_i^{k+1}) = \boldsymbol{\ell}_i^k(\mathbf{v}_i), \qquad \forall \mathbf{v}_i \in \mathbf{W}_i^0,\ \forall t \in (0,T), \tag{3.14a}$$

$$(\frac{\partial p^{k+1}}{\partial t}, q_i)_{\Omega_i} + \mathbf{b}_i(\mathbf{u}_i^{k+1},q_i) = (f,q_i)_{\Omega_i}, \qquad \forall q_i \in M_i,\ \forall t \in (0,T), \tag{3.14b}$$

$$\left(p^{k+1}(\cdot,0),q_i\right)_{\Omega_i} = (p_0^{k+1},q_i), \quad \forall q_i \in M_i, \tag{3.14c}$$

where the bilinear forms $\mathbf{a}_i$ and $\mathbf{b}_i$, and the linear form $\boldsymbol{\ell}_i^k$ are defined in Chapter 1 Section 1.5. Note that the exact solution of the flux in Ω_i is $\mathbf{u}_i \in \mathbf{L}^2(0,T;\mathbf{W}_i^{g_N})$. The exact solution of the potential is such that $p_i \in L^2(0,T;M_i)$.

3.5 Discretization using MFE in space and an implicit scheme in time

The local problem (3.14) in each subdomain is discretized in space by the MFE method presented in Section 1.5 Chapter 1 and using the discontinuous Galerkin method of order zero in time (DG0) [26, 92, 93, 95, 149] or, equivalently for piecewise-constant-in-time source term f, the backward Euler scheme.

Let $\{t^n\}_{0\le n\le N}$ be a sequence of discrete times such that

$$t^0 = 0 < t^1 < \cdots < t^n < \cdots < t^N = T.$$

Let $\mathcal{T}_\tau$ be the partition of the time interval $(0,T)$ into subintervals $I_n := (t^{n-1},t^n]$ and let $\tau^n := t^n - t^{n-1}$ for all $1 \le n \le N$. At time $t^0 = 0$, we approximate the initial condition. We suppose for simplicity that the triangulation $\mathcal{T}_{h,i}$ on the polygonal subdomain Ω_i, $\forall i \in [\![1,\mathcal{N}]\!]$, is the same at each time step, where $\mathcal{T}_{h,i} = \mathcal{T}_h|_{\Omega_i}$. For simplicity, we present in Figure 3.1 the case of a decomposition of Ω into two subdomains in 2D, where the space-time interface $\Gamma_{1,2} \times (0,T)$ is a plane.

Notations

Let E be a space of functions defined on Ω and let $v(\cdot,t)$ be a function taking its values in E. We denote $P_\tau^0(E)$ the vector space such that $v(\mathbf{x},\cdot)$ is piecewise constant in time:

$$P_\tau^0(E) := \{v_\tau : (0,T) \to E;\ \text{where } v_\tau \text{ is constant on } I_n,\ 1 \le n \le N\}. \tag{3.15}$$

Then a function in $P_\tau^0(E)$ is defined by the N functions $\{v^n := v_\tau(\cdot,t)|_{I_n}\}_{1\le n\le N}$ in E. In the following, for each subdomain Ω_i, $p_{\tau,i}$ is a function in $P_\tau^0(L^2(\Omega_i))$ such that $p_{\tau,i}(\cdot,0) = p_0$, and $\mathbf{u}_{\tau,i}$ is a function in $P_\tau^0(\mathbf{W}_i^{g_N})$. We also introduce the notations:

$$p_i^n = p_{\tau,i}|_{I_n} \ \text{ and } \ \mathbf{u}_i^n = \mathbf{u}_{\tau,i}|_{I_n}.$$

In addition, and especially for Definition 3.3 bellow for the a posteriori estimates, we denote $P_\tau^1(E)$ the vector space such that $v_\tau(\mathbf{x},\cdot)$ is continuous and piecewise affine in time:

$$P_\tau^1(E) := \{v_\tau : (0,T) \to E;\ \ v_\tau \in C^0(0,T),\ v_\tau \text{ is affine on } I_n,\ 1 \le n \le N\}. \tag{3.16}$$

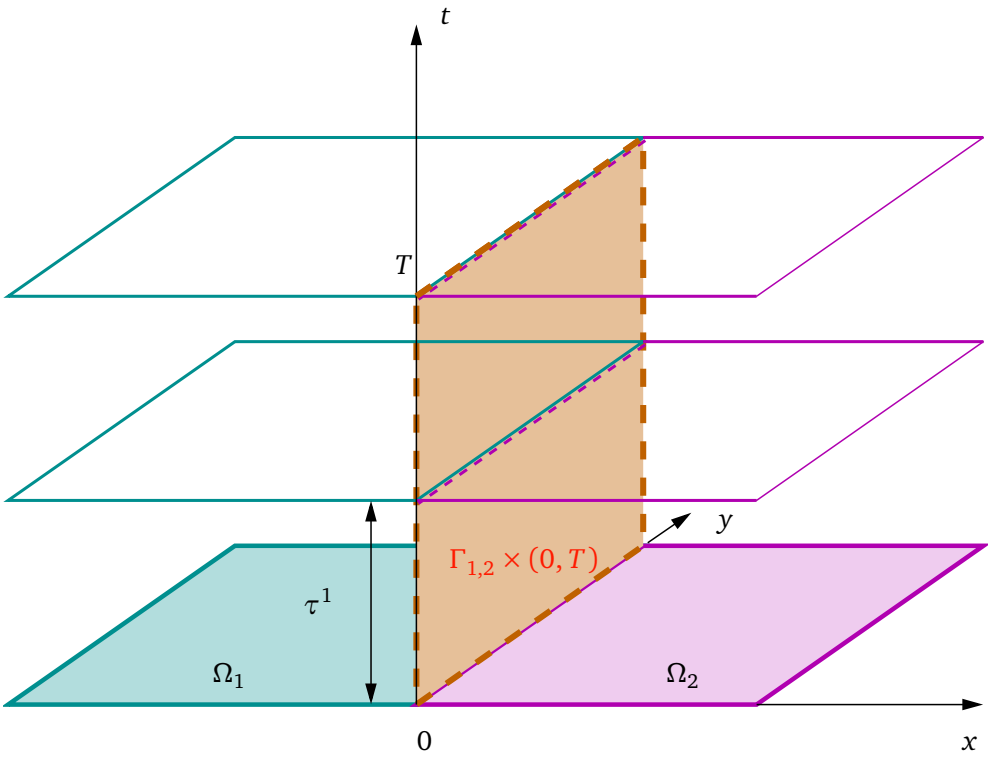

Figure 3.1: The space-time interface $\Gamma_{1,2} \times (0,T)$ between two subdomains Ω_1 and Ω_2 (in 2D)

Note that a function in $P_\tau^1(E)$ is defined by $N+1$ functions $\{v^n := v_\tau(\cdot,t^n)\}_{0\le n\le N}$. Observe that if $v_\tau \in P_\tau^1(E)$, then $\partial_t v_\tau \in P_\tau^0(E)$ is such that :

$$\partial_t v^n := \partial_t v_\tau|_{I_n} = \frac{1}{\tau^n}(v^n - v^{n-1}),\ 1 \le n \le N, \tag{3.17}$$

where v^0 is given in E.

Semi discrete in time interface problem

In order to introduce the semi-discrete in time counterpart of (3.9), we first introduce the following space:

$$L_\tau(\Gamma_i) = P_\tau^0\left(\prod_{j\in B^i} L^2(\Gamma_{i,j})\right), \tag{3.18a}$$

$$\mathcal{W}_{T,\tau,i} = P_\tau^0(L^2(\Omega_i)) \times P_\tau^0(L^2(\Gamma_i^{\mathrm{D}})) \times P_\tau^0(L^2(\Gamma_i^{\mathrm{N}})) \times H^1(\Omega_i) \text{ for } i \in [\![1,\mathcal{N}]\!], \tag{3.18b}$$

and the following notation for $n = 1,..,N$:

$$\tilde{f}^n := \frac{1}{\tau^n}\int_{I_n} f(\cdot,t)\mathrm{d}t, \qquad \tilde{g}_{\mathrm{D}}^n := \frac{1}{\tau^n}\int_{I_n} g_{\mathrm{D}}(\cdot,t)\mathrm{d}t, \qquad \tilde{g}_{\mathrm{N}}^n := \frac{1}{\tau^n}\int_{I_n} g_{\mathrm{N}}(\cdot,t)\mathrm{d}t.$$

We define $\tilde{f} \in P_\tau^0(L^2(\Omega))$, $\tilde{g}_{\mathrm{D}} \in P_\tau^0(L^2(\Gamma_i^{\mathrm{D}}))$, and $\tilde{g}_{\mathrm{N}} \in P_\tau^0(L^2(\Gamma_i^{\mathrm{N}}))$ such that:

$$\tilde{f}|_{I_n} := \tilde{f}^n, \quad \tilde{g}_{\mathrm{D}}|_{I_n} := \tilde{g}_{\mathrm{D}}^n, \text{ and } \quad \tilde{g}_{\mathrm{N}}|_{I_n} := \tilde{g}_{\mathrm{N}}^n, \ 1 \le n \le N. \tag{3.19}$$

We now introduce the semi-discrete in time subproblem solution operator for Ω_i, $i \in [\![1, \mathcal{N}]\!]$, as follows:

$$\begin{array}{rccl} \mathscr{M}_{\tau,i} & : & L_\tau(\Gamma_i) \times \mathscr{V}_{T,\tau,i} & \to & L_\tau(\Gamma_i) \times P^0_\tau(L^2(\Omega_i)) \times P^0_\tau(\mathbf{W}_i^{\tilde{g}_{\mathrm{N}}^n}) \\ & & (\boldsymbol{\xi}_{\tau,i}, \boldsymbol{\mathscr{F}}_{\tau,i}) & \mapsto & (\boldsymbol{\xi}_{\tau,i}, p_{\tau,i}, \mathbf{u}_{\tau,i}), \end{array} \tag{3.20}$$

where $\boldsymbol{\xi}_{\tau,i} = \left(\xi_{\tau,i,j}\right)_{j\in B^i}$, $\xi^n_{i,j} = \xi_{\tau,i,j}|_{I_n}$, $\boldsymbol{\mathscr{F}}_{\tau,i} = (\tilde{f}|_{\Omega_i}, \tilde{g}_{\mathrm{D}}|_{\Gamma_i^{\mathrm{D}}}, \tilde{g}_{\mathrm{N}}|_{\Gamma_i^{\mathrm{N}}}, p_0|_{\Omega_i})$, and where $(p_{\tau,i}\mathbf{u}_{\tau,i})$ is the solution of the following problem in Ω_i, for $n = 1, ..., N$:

$$\mathbf{u}_i^n = -\boldsymbol{S}\nabla p_i^n \quad \text{in} \quad \Omega_i, \tag{3.21a}$$

$$\frac{p_i^n - p_i^{n-1}}{\tau^n} + \nabla\cdot\mathbf{u}_i^n = \tilde{f}^n \qquad \text{in} \quad \Omega_i, \tag{3.21b}$$

$$p_i^n = \tilde{g}_{\mathrm{D}}^n \qquad \text{on} \quad \Gamma_i^{\mathrm{D}}, \tag{3.21c}$$

$$-\mathbf{u}_i^n \cdot \boldsymbol{n} = \tilde{g}_{\mathrm{N}}^n \qquad \text{on} \quad \Gamma_i^{\mathrm{N}}, \tag{3.21d}$$

$$-\beta_{i,j}\mathbf{u}_i^n \cdot \boldsymbol{n}_i + p_i^n = \xi_{i,j}^n \qquad \text{on} \quad \Gamma_{i,j}, \ \forall j \in B^i, \tag{3.21e}$$

$$p_i^0 = p_0 \qquad \text{in} \quad \Omega_i. \tag{3.21f}$$

We also introduce:

$$\begin{array}{rccl} \mathscr{R}_{\tau,i} & : & L_\tau(\Gamma_i) \times P^0_\tau(L^2(\Omega_i)) \times P^0_\tau(\mathbf{W}_i^{\tilde{g}_{\mathrm{N}}^n}) & \to & L_\tau(\Gamma_i) \\ & & (\boldsymbol{\xi}_{\tau,i}, p_{\tau,i}, \mathbf{u}_{\tau,i}) & \mapsto & \left(\beta_{j,i}\mathbf{u}_{\tau,i}\cdot\boldsymbol{n}_i + (\xi_{\tau,i,j} + \beta_{i,j}\mathbf{u}_{\tau,i}\cdot\boldsymbol{n}_i)\right)_{j\in B^i}, \end{array} \tag{3.22}$$

and the Robin-to-Robin operator defined as follows:

$$\boldsymbol{S}^{\mathrm{RtR}}_{\tau,i} = \mathscr{R}_{\tau,i} \circ \mathscr{M}_{\tau,i} \ : \ L_\tau(\Gamma_i) \times \mathscr{V}_{T,\tau,i} \to L_\tau(\Gamma_i). \tag{3.23}$$

The semi-discrete counterpart in time of (3.9) can be written as follows:
Find $(\boldsymbol{\xi}_{\tau,1}, \ldots, \boldsymbol{\xi}_{\tau,\mathcal{N}}) \in L_\tau(\Gamma_1) \times \ldots \times L_\tau(\Gamma_{\mathcal{N}})$ such that: For $\boldsymbol{\xi}_{\tau,i} = \left(\xi_{\tau,i,j}\right)_{j\in B^i}$ where $\xi_{\tau,i,j} \in P^0_\tau(L^2(\Gamma_{i,j}))$:

$$\left((\boldsymbol{\xi}_{\tau,i})_j - (\boldsymbol{S}^{\mathrm{RtR}}_{\tau,j}(\boldsymbol{\xi}_{\tau,j}, \boldsymbol{\mathscr{F}}_{\tau,j}))_i \right)\Big|_{I_n} = 0, \quad \forall n = 1, ..., N, \quad \forall j \in B^i, \quad \forall i \in [\![1, \mathcal{N}]\!]. \tag{3.24}$$

Note that we have used a formulation that is also directly valid for different time grids on different subdomains that we shall adress in Section 3.10. Then, applying the MFE method to (3.24), and using the Jacobi algorithm to solve the resulting discrete problem is equivalent to the fully discrete problem that we give in detail in the next section (see (3.30)).

Local fully discrete problem at iteration $k+1$

We define $\tilde{g}^n_{h,\mathrm{N}} := \dfrac{1}{\tau^n}\displaystyle\int_{I_n} g_{h,\mathrm{N}}(\cdot, t)\mathrm{d}t$ where $g_{h,\mathrm{N}|e}$ is the approximation of the function g_{N} as a piecewise constant on each $e \subset \Gamma^{\mathrm{N}}$: $g_{h,\mathrm{N}|e} := \dfrac{1}{|e|}\displaystyle\int_e g_{\mathrm{N}}\mathrm{d}\gamma$ for each $e \subset \Gamma^{\mathrm{N}}$ of length $|e|$.
The fully discrete problem at iteration $k+1$, in the subdomain Ω_i, $\forall i \in [\![1, \mathcal{N}]\!]$, is:

Find $\mathbf{u}_{h,i}^{k+1,n} \in \mathbf{W}_{h,i}^{\tilde{g}_{h,\mathrm{N}}^n}$ and $p_{h,i}^{k+1,n} \in M_{h,i}$ on the interval I_n, for $n = 1,..,N$, such that:

$$\mathbf{a}_i(\mathbf{u}_{h,i}^{k+1,n}, \mathbf{v}_{h,i}) - \mathbf{b}_i(\mathbf{v}_{h,i}, p_{h,i}^{k+1,n}) = \tilde{\boldsymbol{\ell}}_i^{k,n}(\mathbf{v}_{h,i}), \qquad \forall \mathbf{v}_{h,i} \in \mathbf{W}_{h,i}^0, \tag{3.25a}$$

$$\frac{1}{\tau^n}(p_{h,i}^{k+1,n} - p_{h,i}^{k+1,n-1}, q_{h,i})_{\Omega_i} + \mathbf{b}_i(\mathbf{u}_{h,i}^{k+1,n}, q_{h,i}) = (\tilde{f}^n, q_{h,i})_{\Omega_i}, \quad \forall q_{h,i} \in M_{h,i}, \tag{3.25b}$$

$$\left(p_{h,i}^{k+1,0}, q_{h,i}\right)_{\Omega_i} = (p_0, q_{h,i}), \qquad \forall q_{h,i} \in M_i, \tag{3.25c}$$

where the linear form $\tilde{\boldsymbol{\ell}}_i^{k,n}$ is defined as:

$$\tilde{\boldsymbol{\ell}}_i^{k,n} : \mathbf{W}_{h,i}^0 \longmapsto \mathbb{R}, \quad \tilde{\boldsymbol{\ell}}_i^{k,n}(\mathbf{v}_{h,i}) = -\langle \tilde{g}_{\mathrm{D}}^n, \mathbf{v}_{h,i} \cdot \boldsymbol{n}_i \rangle_{\Gamma_i^{\mathrm{D}}} - \sum_{j \in B^i} \langle \tilde{g}_{\mathrm{R},j}^{k,n}, \mathbf{v}_{h,i} \cdot \boldsymbol{n}_i \rangle_{\Gamma_{i,j}}, \tag{3.26}$$

where

$$\tilde{g}_{\mathrm{R},j}^{k,n} := \frac{1}{\tau^n} \int_{I_n} g_{\mathrm{R},j}^k(\cdot, t)\, \mathrm{d}t. \tag{3.27}$$

Here, $\tilde{g}_{\mathrm{R},j}^{0,n}$ is a given initial guess on $\Gamma_{i,j}$ and $\langle \tilde{g}_{\mathrm{R},j}^{k,n}, \psi_{e'} \cdot \boldsymbol{n}_i \rangle_{\Gamma_{i,j}}$, for $k \geq 1$ and the basis function $\psi_{e'}$ on $e' \in \Gamma_{i,j}$, is given by:

$$\langle \tilde{g}_{\mathrm{R},j}^{k,n}, \psi_{e'} \cdot \boldsymbol{n}_i \rangle_{\Gamma_{i,j}} = \int_{\Gamma_{i,j}} \beta_{i,j}(\mathbf{u}_{h,j}^{k,n} \cdot \boldsymbol{n}_j)\psi_{e'} \cdot \boldsymbol{n}_i \, \mathrm{d}\gamma + \int_{\Gamma_{i,j}} (\beta_{j,i}\mathbf{u}_{h,j}^{k,n} \cdot \boldsymbol{n}_j + \tilde{g}_{\mathrm{R},i}^{k-1,n})\mathrm{d}\gamma, \tag{3.28}$$

and is equal to zero when $e' \notin \Gamma_{i,j}$. Therefore, (3.25) can now be written as:
Find $\mathbf{u}_{h,i}^{k+1,n} \in \mathbf{W}_{h,i}^{\tilde{g}_{h,\mathrm{N}}^n}$ and $p_{h,i}^{k+1,n} \in M_{h,i}$ on the interval I_n, for $n = 1,..,N$, such that:

$$\mathbf{a}_i(\mathbf{u}_{h,i}^{k+1,n}, \mathbf{v}_{h,i}) - \mathbf{b}_i(\mathbf{v}_{h,i}, p_{h,i}^{k+1,n}) = \tilde{\boldsymbol{\ell}}_i^{k,n}(\mathbf{v}_{h,i}), \qquad \forall \mathbf{v}_{h,i} \in \mathbf{W}_{h,i}^0, \tag{3.29a}$$

$$(p_{h,i}^{k+1,n}, q_{h,i})_{\Omega_i} + \tau^n \mathbf{b}_i(\mathbf{u}_{h,i}^{k+1,n}, q_{h,i}) = \tau^n (\tilde{f}^n, q_{h,i})_{\Omega_i} + (p_{h,i}^{k+1,n-1}, q_{h,i})_{\Omega_i}, \quad \forall q_{h,i} \in M_{h,i}, \tag{3.29b}$$

$$(p_{h,i}^{k+1,0}, q_{h,i})_{\Omega_i} = (p_0, q_{h,i}), \qquad \forall q_{h,i} \in M_{h,i}. \tag{3.29c}$$

Remark 3.1. *Note that using the rectangle quadrature rule, $\tilde{f}^n$, $\tilde{g}_{\mathrm{D}}^n$, and $\tilde{g}_{h,\mathrm{N}}^n$ can be approximated by:*

$$\tilde{f}^n \approx f(\cdot, t^n),$$
$$\tilde{g}_{\mathrm{D}}^n \approx g_{\mathrm{D}}(\cdot, t^n),$$
$$\tilde{g}_{h,\mathrm{N}}^n \approx g_{h,\mathrm{N}}(\cdot, t^n).$$

In the present case of conforming grids in time, $\tilde{g}_{\mathrm{R},j}^{k,n}$ can be approximated by:

$$\tilde{g}_{\mathrm{R},j}^{k,n} \approx g_{\mathrm{R},j}^k(\cdot, t^n).$$

In such setting, the discontinuous Galerkin method of order zero in time is equivalent to the backward Euler scheme.

Matrix representation of the discrete problem at iteration $k+1$

The matrix form of problem (3.29) for $n = 1, .., N$ and $i = 1, ..., \mathcal{N}$ is written as:

$$\begin{pmatrix} \mathbb{B}_i & \mathbb{C}_i \\ \tau^n \mathbb{C}_i^T & -\mathbb{M}_i \end{pmatrix} \begin{pmatrix} \mathbf{U}_i^{k+1,n} \\ \mathbf{P}_i^{k+1,n} \end{pmatrix} = \begin{pmatrix} \mathbf{F}_{i,\mathbf{DR}}^{k,n} \\ -\tau^n \mathbf{F}_i^n - \mathbb{M}_i \mathbf{P}_i^{k+1,n-1} \end{pmatrix}, \tag{3.30}$$

with the initial conditon $\mathbb{M}_i \mathbf{P}_i^{k+1,0} = \mathbf{P}_{0,i}$, where:
• $\mathbb{M}_i$ is a $|\mathcal{T}_{h,i}| \times |\mathcal{T}_{h,i}|$ diagonal matrix, where $(\mathbb{M}_i)_{v,v} = |K_v|$ is the area of the v^{th} triangle in $\mathcal{T}_{h,i}$,
• $\mathbb{B}_i$ and $\mathbb{C}_i$ are defined in Chapter 1,
• $\mathbf{P}_{0,i} = \left(\frac{1}{|K|} \int_K p_0 \right)_{K \in \mathcal{T}_{h,i}}$ can be approximated by a quadrature rule,
• $\mathbf{U}_i^{k+1,n}$ is a vector of the d.o.f. on edges at time t^n,
• $\mathbf{P}_i^{k+1,n}$ is a vector of the d.o.f. on triangles at time t^n,
• $\mathbf{P}_i^{k+1,n-1}$ is a vector of the d.o.f. on triangles at time t^{n-1},
• $\mathbf{F}_i^n$ and $\mathbf{F}_{i,\mathbf{DR}}^{k,n}$ are as defined as in Chapter 1 by remplacing f by $\tilde{f}^n$, g_{D} by $\tilde{g}_{\mathrm{D}}^n$, $g_{h,\mathrm{N}}$ by $\tilde{g}_{h,\mathrm{N}}^n$, and $\boldsymbol{\ell}_i^k$ by $\tilde{\boldsymbol{\ell}}_i^{k,n}$:

$$\mathbf{F}_i^n = \left((\tilde{f}^n, \chi_K) - \sum_{\substack{e \in \mathcal{E}_{h,i} \\ e \subset \Gamma_i^{\mathrm{N}}}} \tilde{g}_{h,\mathrm{N}}^n |e| \int_{\Omega_i} \chi_K \nabla \cdot \psi_e \, \mathrm{d}\mathbf{x} \right)_{K \in \mathcal{T}_{h,i}},$$

$$\mathbf{F}_{i,\mathbf{DR}}^{k,n} = \left(\tilde{\boldsymbol{\ell}}_i^{k,n}(\psi_{e'}) - \sum_{\substack{e \in \mathcal{E}_{h,i} \\ e \subset \Gamma_i^{\mathrm{N}}}} \tilde{g}_{h,\mathrm{N}}^n |e| \int_{\Omega_i} \boldsymbol{S}^{-1} \psi_e \cdot \psi_{e'} \, \mathrm{d}\mathbf{x} \right)_{e' \in \mathcal{E}_{h,i} \setminus \Gamma^{\mathrm{N}}}.$$

Notation

Let $(p_{h\tau}^{k+1}, \mathbf{u}_{h\tau}^{k+1})$ denote the solution of problems (3.29) at the iteration $k+1$ of the DD algorithm, when the DD algorithm has been stopped. Then, we set for all $1 \le n \le N$:

$$p_h^{k+1,n} := p_{h\tau}^{k+1}|_{I_n} \text{ and } \mathbf{u}_h^{k+1,n} := \mathbf{u}_{h\tau}^{k+1}|_{I_n} \tag{3.31}$$

and for $i = 1, ..., \mathcal{N}$:

$$p_{h\tau,i}^{k+1} := p_{h\tau}^{k+1}|_{\Omega_i} \text{ and } \mathbf{u}_{h\tau,i}^{k+1} := \mathbf{u}_{h\tau}^{k+1}|_{\Omega_i}. \tag{3.32}$$

Let $(p_{h\tau}, \mathbf{u}_{h\tau})$ be the solution at convergence of the DD algorithm.

Remark 3.2. *Systems (3.30), $n = 1, .., N$, $i = 1, ..., \mathcal{N}$, are the $(k+1)^{\text{th}}$ iteration of the fully discrete DD algorithm (in space and in time). They correspond to the discrete counterpart of problems (3.14) or equivalently, the discrete counterpart of (3.12) solved with the Jacobi algorithm. Note that the Jacobi algorithm can be replaced by another iterative method such as GMRES.*
Using the MFE method in space and the DG0 method in time, the fully discrete DD algorithm (using the Jacobi or the GMRES method) converges to $(p_{h\tau}, \mathbf{u}_{h\tau})$, see [94, 95].

3.6 Concept of potential and flux reconstruction for the heat equation

The main idea of our estimation is to construct at each iteration $k+1$, $k \geq 0$, of the global-in-time DD algorithm:
• An H^1-conforming potential reconstruction in space, continuous and piecewise affine in time.
• An $\mathbf{H}(\mathrm{div})$-conforming and locally conservative flux reconstruction in space, piecewise constant in time.
These reconstructions will be the central tools used in Theorem 3.6. The error is measured in the energy norm augmented by a dual norm of the time derivative [65, 67].

We first introduce a postprocessing as described in Section 2.1 of Chapter 2 for the steady diffusion case. More precisely, for the heat equation, we construct $\tilde{p}_{h,i}^{k+1,n} \in \mathbb{P}_2(\mathcal{T}_{h,i})$ at each iteration $k+1$, at each time step n and for each subdomain, such that:

$$-\boldsymbol{S}\nabla\tilde{p}_{h,i}^{k+1,n}|_K = \mathbf{u}_{h,i}^{k+1,n}|_K, \qquad \forall K \in \mathcal{T}_{h,i}, \tag{3.33a}$$

$$\pi_0(\tilde{p}_{h,i}^{k+1,n}|_K) = p_{h,i}^{k+1,n}|_K, \qquad \forall K \in \mathcal{T}_{h,i}, \tag{3.33b}$$

where $\tilde{p}_{h\tau,i}^{k+1}|_{I_n} := \tilde{p}_{h,i}^{k+1,n}$ and $\tilde{p}_h^{k+1,n}|_{\Omega_i} := \tilde{p}_{h,i}^{k+1,n}$.

3.6.1 Potential reconstruction

Definition 3.3 (Potential reconstruction)**.** *We will call a* potential reconstruction *any function $s_{h\tau}^{k+1}$ constructed from $p_{h\tau}^{k+1}$, $\mathbf{u}_{h\tau}^{k+1}$, as proposed in [67], which satisfies the two following conditions:*

$$s_{h\tau}^{k+1} \in P_\tau^1(H^1(\Omega) \cap C^0(\overline{\Omega})), \tag{3.34a}$$

$$s_{h\tau}^{k+1}|_{\Gamma^{\mathrm{D}}} = g_{\mathrm{D}}, \tag{3.34b}$$

and at each time step n, $0 \leq n \leq N$,

$$(s_h^{k+1,n}, 1)_K = (\tilde{p}_h^{k+1,n}, 1)_K, \ \ \forall K \in \mathcal{T}_h, \tag{3.35}$$

where $\tilde{p}_h^{k+1,n}$ is built in (3.33) form $p_h^{k+1,n}$, $\mathbf{u}_h^{k+1,n}$. In the follows, we will also use the following notations:

$$s_h^{k+1,n} := s_{h\tau}^{k+1}|_{I_n}, \qquad s_{h\tau,i}^{k+1} := s_{h\tau}^{k+1}|_{\Omega_i}, \qquad \textit{and} \qquad s_{h,i}^{k+1,n} := s_{h\tau,i}^{k+1}|_{I_n}.$$

3.6.2 Subdomain potential reconstruction

Definition 3.4 (Subdomain potential reconstruction)**.** *We will call a* subdomain potential reconstruction *any function $\overline{s}_{h\tau,i}^{k+1}$ constructed from $p_{h\tau,i}^{k+1}$, $\mathbf{u}_{h\tau,i}^{k+1}$, which satisfies:*

$$\overline{s}_{h\tau,i}^{k+1} \in P_\tau^1(H^1(\Omega_i) \cap C^0(\overline{\Omega}_i)), \ \ \forall i \in [\![1, \mathcal{N}]\!], \tag{3.36a}$$

$$\overline{s}_{h\tau,i}^{k+1}|_{\Gamma_i^{\mathrm{D}}} = g_{\mathrm{D}}|_{\Gamma_i^{\mathrm{D}}}, \tag{3.36b}$$

and at each time step n, $0 \le n \le N$,

$$(\overline{s}_{h,i}^{k+1,n}, 1)_K = (\tilde{p}_{h,i}^{k+1,n}, 1)_K, \quad \forall K \in \mathcal{T}_{h,i}, \tag{3.37}$$

where $\overline{s}_{h,i}^{k+1,n} := \overline{s}_{h\tau,i}^{k+1}|_{I_n}$.

In contrast to $s_{h\tau}^{k+1}$ of Definition 3.3, $\overline{s}_{h\tau,i}^{k+1}$ is constructed locally subdomain by subdomain to capture only the nonconformity from the numerical scheme only and not that from the domain decomposition method. Thus, $\overline{s}_{h\tau,i}^{k+1}$ is close to $\tilde{p}_{h\tau,i}^{k+1}$ independently in each subdomain and $\overline{s}_{h\tau,i}^{k+1}|_{\Gamma_{i,j}}$ is close to $\tilde{p}_{h\tau,i}^{k+1}|_{\Gamma_{i,j}}$, $\forall i \in [\![1, \mathcal{N}]\!]$, $j \in B^i$ in the sense that the estimator (3.50b), (3.50d), and (3.50g) are as small as possible.

3.6.3 Equilibrated flux reconstruction

Definition 3.5 (Equilibrated flux reconstruction)**.** *We will call an* equilibrated flux reconstruction *any function $\boldsymbol{\sigma}_{h\tau}^{k+1}$ constructed from $p_{h\tau}^{k+1}$, $\mathbf{u}_{h\tau}^{k+1}$, as proposed in [65, 67], which satisfies:*

$$\boldsymbol{\sigma}_{h\tau}^{k+1} \in P_\tau^0(\mathbf{H}(\mathrm{div}, \Omega)), \tag{3.38}$$

with the local conservation property at each time step n, $0 \le n \le N$:

$$(\tilde{f^n} - \partial_t \tilde{p}_h^{k+1,n} - \nabla\cdot\boldsymbol{\sigma}_h^{k+1,n}, 1)_K = 0, \quad \forall K \in \mathcal{T}_h, \tag{3.39}$$

together with the Neumann condition:

$$-(\boldsymbol{\sigma}_h^{k+1,n} \cdot \boldsymbol{n}_\Omega, 1)_e = (\tilde{g}_\mathrm{N}, 1)_e, \qquad \forall e \in \mathcal{E}_{h,i}^{\Gamma^\mathrm{N}}, \quad \forall i \in [\![1, \mathcal{N}]\!], \tag{3.40}$$

where $\boldsymbol{\sigma}_h^{k+1,n} := \boldsymbol{\sigma}_{h\tau}^{k+1}|_{I_n}$.

3.7 General a posteriori error estimate: fully computable upper bound

Let $X := L^2(0,T;H_0^1(\Omega))$ and $X' = L^2(0,T;H^{-1}(\Omega))$, where we consider $\Gamma^\mathrm{N} = \emptyset$ henceforth for simplicity. Note that in the mixed finite element method, we obtain $p_{h\tau} \in L^2(0,T;L^2(\Omega))$ which is nonconforming in space. Hence, we introduce the broken X-norm where ∇ is the broken gradient operator such that for a piecewise regular function q, then $\nabla q \in L^2(0,T;[L^2(\Omega)]^d)$:

$$|||q|||_X^2 := \sum_{n=1}^N \int_{I_n} ||\boldsymbol{S}^{\frac{1}{2}} \nabla q(\cdot,t)||^2 \mathrm{d}t = \sum_{n=1}^N \int_{I_n} \sum_{K\in\mathcal{T}_h} ||\boldsymbol{S}^{\frac{1}{2}} \nabla q(\cdot,t)||_K^2 \,\mathrm{d}t. \tag{3.41}$$

Let $Y := \{q \in X; \partial_t q \in X'\}$. For $q \in Y$, we introduce the space-time norm proposed in [65]:

$$|||q|||_Y^2 := |||q|||_X^2 + ||\partial_t q||_{X'}^2 + ||q(\cdot,T)||^2, \tag{3.42}$$

where

$$||\partial_t q||_{X'} := \left\{ \int_0^T ||\partial_t q||_{H^{-1}(\Omega)}^2 \,\mathrm{d}t \right\}^{\frac{1}{2}} := \left\{ \int_0^T \left(\sup_{v\in H_0^1(\Omega);\, ||\boldsymbol{S}^{\frac{1}{2}}\nabla v||=1} \langle \partial_t q, v\rangle \right)^2 \mathrm{d}t \right\}^{\frac{1}{2}} \tag{3.43}$$

and we again extend the X-norm and the X' norm to piecewise regular in space functions only since $\tilde{p}_{h\tau} \notin H^1$. Then, the difference between the exact solution p and the approximate solution $\tilde{p}_{h\tau}^{k+1}$ at iteration $k+1$ of the DD algorithm using this space-time norm (3.42) is as follows:

$$|||p - \tilde{p}_{h\tau}^{k+1}|||_Y^2 = |||p - \tilde{p}_{h\tau}^{k+1}|||_X^2 + ||\partial_t(p - \tilde{p}_{h\tau}^{k+1})||_{X'}^2 + ||(p - \tilde{p}_{h\tau}^{k+1})(\cdot, T)||^2. \tag{3.44}$$

Let the norm $|||\cdot|||$ and $|||\cdot|||_\star$ be defined as in Chapter 2 and let $||\cdot||$ be the L^2-norm defined in Chapter 1. Then:

Theorem 3.6 (A posteriori error estimates for the potential, distinguishing space error, time error, and domain decomposition error)**.** *Let p be the weak solution of problem (3.1). Let $\tilde{p}_h^{k+1,n} \in H^1(\mathcal{T}_h)$ be an arbitrary solution at each time step n, $0 \le n \le N$, in particular $\tilde{p}_h^{k+1,n}$ can be the postprocessing (3.33) of the solution $p_h^{k+1,n}$ at iteration $k+1$ of the global-in-time Robin DD algorithm (3.29). Let $\mathbf{u}_h^{k+1,n} = -\boldsymbol{S}\nabla\tilde{p}_h^{k+1,n}$ in each element $K \in \mathcal{T}_h$. Let $s_{h\tau}^{k+1}$ be the potential reconstruction of Definition 3.3, let $\overline{s}_{h\tau,i}^{k+1}$ be the subdomain potential reconstruction of Definition 3.4, and let $\boldsymbol{\sigma}_{h\tau}^{k+1}$ be the equilibrated flux reconstruction of Definition 3.5. We have:*

$$|||p - \tilde{p}_{h\tau}^{k+1}|||_Y \le \tilde{\eta}^{k+1} := \eta_{\mathrm{sp}}^{k+1} + \eta_{\mathrm{tm}}^{k+1} + \eta_{\mathrm{DD}}^{k+1} + \eta_{\mathrm{IC}}^{k+1} + ||f - \tilde{f}||_{X'} + ||s_h^{k+1,N} - \tilde{p}_h^{k+1,N}||, \tag{3.45}$$

where the "subdomain discretization estimator" is:

$$\begin{aligned}\eta_{\mathrm{sp}}^{k+1} :=& \left\{\sum_{n=1}^{N}\tau^n\sum_{K\in\mathcal{T}_h}(\eta_{\mathrm{osc},K}^{k+1,n} + \eta_{\mathrm{DF},1,a,K}^{k+1,n})^2\right\}^{\frac12}\\ &+\left\{\sum_{n=1}^{N}\int_{I_n}\sum_{i=1}^{\mathcal{N}}\sum_{K\in\mathcal{T}_{h,i}}(\eta_{\mathrm{NCP},1,a,K}^{k+1}(t))^2\mathrm{d}t\right\}^{\frac12}\\ &+\left\{\sum_{n=1}^{N}\tau^n\sum_{i=1}^{\mathcal{N}}\sum_{K\in\mathcal{T}_{h,i}}(\eta_{\mathrm{NCP},2,a,K}^{k+1,n})^2\right\}^{\frac12},\end{aligned} \tag{3.46}$$

the "time discretization estimator" is:

$$\eta_{\mathrm{tm}}^{k+1} := \left\{\sum_{n=1}^{N}\sum_{K\in\mathcal{T}_h}\frac{1}{3}\tau^n|||s_h^{k+1,n} - s_h^{k+1,n-1}|||_K^2\right\}^{\frac12}, \tag{3.47}$$

the "domain decomposition estimator" is:

$$\begin{aligned}\eta_{\mathrm{DD}}^{k+1} :=& \left\{\sum_{n=1}^{N}\tau^n\sum_{K\in\mathcal{T}_h}(\eta_{\mathrm{DF},1,b,K}^{k+1,n} + \eta_{\mathrm{NCP},1,b,K}^{k+1,n})^2\right\}^{\frac12}\\ &+\left\{\sum_{n=1}^{N}\int_{I_n}\sum_{i=1}^{\mathcal{N}}\sum_{K\in\mathcal{T}_{h,i}}(\eta_{\mathrm{NCP},1,b,K}^{k+1}(t))^2\mathrm{d}t\right\}^{\frac12}\\ &+\left\{\sum_{n=1}^{N}\tau^n\sum_{i=1}^{\mathcal{N}}\sum_{K\in\mathcal{T}_{h,i}}(\eta_{\mathrm{NCP},2,b,K}^{k+1,n})^2\right\}^{\frac12},\end{aligned} \tag{3.48}$$

and the "initial condition estimator" is:

$$\eta_{\mathrm{IC}}^{k+1} := ||s_h^{k+1,0} - p_0||. \tag{3.49}$$

For all $1 \le n \le N$*, the following terms are the local estimators :*

$$\eta_{\mathrm{osc},K}^{k+1,n} := \frac{h_K}{\pi} c_{\boldsymbol{S},K}^{-\frac{1}{2}} \|\tilde{f}^n - \partial_t s_h^{k+1,n} - \nabla\cdot\boldsymbol{\sigma}_h^{k+1,n}\|_K \quad \text{"data oscillation"}, \tag{3.50a}$$

$$\eta_{\mathrm{DF},1,a,K}^{k+1,n} := |||\boldsymbol{S}\nabla\overline{s}_h^{k+1,n} + \mathbf{u}_h^{k+1,n}|||_{\star,K}, \quad \text{"constitutive relation"}, \tag{3.50b}$$

$$\eta_{\mathrm{DF},1,b,K}^{k+1,n} := |||\mathbf{u}_h^{k+1,n} - \boldsymbol{\sigma}_h^{k+1,n}|||_{\star,K}, \quad \text{"DD flux nonconformity"}, \tag{3.50c}$$

$$\eta_{\mathrm{NCP},1,a,K}^{k+1}(t) := |||(\tilde{p}_{h\tau,i}^{k+1} - \overline{\tilde{s}}_{h\tau,i}^{k+1})(t)|||_K, \ t \in I_n \quad \text{"potential nonconformity"}, \tag{3.50d}$$

$$\eta_{\mathrm{NCP},1,b,K}^{k+1}(t) := |||(\overline{\tilde{s}}_{h\tau,i}^{k+1} - s_{h\tau,i}^{k+1})(t)|||_K, \ t \in I_n \quad \text{"DD potential nonconformity"}, \tag{3.50e}$$

$$\eta_{\mathrm{NCP},1,b,K}^{k+1,n} := |||\overline{\tilde{s}}_{h,i}^{k+1,n} - s_{h,i}^{k+1,n}|||_K, \ \text{"DD potential nonconformity"}, \tag{3.50f}$$

$$\eta_{\mathrm{NCP},2,a,K}^{k+1,n} := \frac{h_K}{\pi} c_{\boldsymbol{S},K}^{-\frac{1}{2}} ||\partial_t(\tilde{p}_{h,i}^{k+1,n} - \overline{\tilde{s}}_{h,i}^{k+1,n})||_K, \ \text{"potential nonconformity"}, \tag{3.50g}$$

$$\eta_{\mathrm{NCP},2,b,K}^{k+1,n} := \frac{h_K}{\pi} c_{\boldsymbol{S},K}^{-\frac{1}{2}} ||\partial_t(\overline{\tilde{s}}_{h,i}^{k+1,n} - s_{h,i}^{k+1,n})||_K, \ \text{"DD potential nonconformity"}, \tag{3.50h}$$

where we recall that $c_{\boldsymbol{S},K}$ *is the smallest eigenvalue of* $\boldsymbol{S}$ *in* K*. We denote* I_{eff}^{k+1} *the effectivity index, which is the ratio of the estimated and the actual error at the iteration* $k+1$ *of the DD algorithm, given as:*

$$I_{\mathrm{eff}} := \frac{\tilde{\eta}^{k+1}}{|||p - \tilde{p}_{h\tau}^{k+1}|||_Y}. \tag{3.51}$$

Proof. Using Theorem 2.1 in [65], for a given $s \in Y$ we have:

$$|||p - s|||_Y^2 = ||\mathscr{R}(s)||_{X'}^2 + ||p_0 - s(\cdot,0)||^2, \tag{3.52}$$

where

$$||\mathscr{R}(s)||_{X'} := \sup_{v\in X,\, |||v|||_X = 1} \langle \mathscr{R}(s), v\rangle_{X',X} \tag{3.53}$$

with

$$\langle \mathscr{R}(s), v\rangle_{X',X} := \int_0^T \left\{(f,v) - (\partial_t s, v) - (\nabla s, \nabla v)\right\}(t)\,\mathrm{d}t. \tag{3.54}$$

In our case, at iteration $k+1$ of the DD algorithm, $\tilde{p}_{h\tau}^{k+1} \notin Y$. For this reason, we can not apply (3.52) to $|||p - \tilde{p}_{h\tau}^{k+1}|||_Y$. Thus, we decompose $|||p - \tilde{p}_{h\tau}^{k+1}|||_Y$ into two parts using the triangle inequality and then apply (3.52) to $|||p - s_{h\tau}^{k+1}|||_Y$ since $s_{h\tau}^{k+1} \in Y$:

$$\begin{aligned} |||p - \tilde{p}_{h\tau}^{k+1}|||_Y &\le |||p - s_{h\tau}^{k+1}|||_Y + |||s_{h\tau}^{k+1} - \tilde{p}_{h\tau}^{k+1}|||_Y \\ &\le ||\mathscr{R}(s_{h\tau}^{k+1})||_{X'} + \eta_{\mathrm{IC}}^{k+1} + |||s_{h\tau}^{k+1} - \tilde{p}_{h\tau}^{k+1}|||_Y. \end{aligned} \tag{3.55}$$

There remains to give a computable upper bound to $||\mathscr{R}(s_{h\tau}^{k+1})||_{X'}$, and $|||s_{h\tau}^{k+1} - \tilde{p}_{h\tau}^{k+1}|||_Y$, and then combine these results.

Computable upper bound for $||\mathscr{R}(s_{h\tau}^{k+1})||_{X'}$

The dual norm $||\mathscr{R}(s_{h\tau}^{k+1})||_{X'}$ is not easily computable. As in Lemma 5.2 in [67]

and the proof of Theorem 3.6 in [67], the computable upper bound on $||\mathscr{R}(s_{h\tau}^{k+1})||_{X'}$ is constructed as below. First, we know that

$$\langle \mathscr{R}(s_{h\tau}^{k+1}), v\rangle_{X',X} := \int_0^T \left\{(f,v) - (\partial_t s_{h\tau}^{k+1}, v) - (\nabla s_{h\tau}^{k+1}, \nabla v)\right\}(t)\,\mathrm{d}t. \tag{3.56}$$

For $v \in X$ with $|||v|||_X = 1$. Then, by adding and subtracting $(\boldsymbol{\sigma}_{h\tau}^{k+1}, \nabla v)$, using the Green theorem, and then adding and subtracting $(\tilde{f}, v)$, we obtain:

$$\begin{aligned}
&\langle \mathscr{R}(s_{h\tau}^{k+1}), v\rangle_{X',X}\\
&:= \int_0^T \left\{(f,v) - (\partial_t s_{h\tau}^{k+1}, v) + (\boldsymbol{\sigma}_{h\tau}^{k+1}, \nabla v) - (\nabla s_{h\tau}^{k+1} + \boldsymbol{\sigma}_{h\tau}^{k+1}, \nabla v)\right\}(t)\,\mathrm{d}t\\
&= \int_0^T \left\{(f,v) - (\partial_t s_{h\tau}^{k+1} + \nabla\cdot\boldsymbol{\sigma}_{h\tau}^{k+1}, v) - (\nabla s_{h\tau}^{k+1} + \boldsymbol{\sigma}_{h\tau}^{k+1}, \nabla v)\right\}(t)\,\mathrm{d}t\\
&= \int_0^T \left\{(f-\tilde{f},v) + (\tilde{f} - \partial_t s_{h\tau}^{k+1} - \nabla\cdot\boldsymbol{\sigma}_{h\tau}^{k+1}, v) - (\nabla s_{h\tau}^{k+1} + \boldsymbol{\sigma}_{h\tau}^{k+1}, \nabla v)\right\}(t)\,\mathrm{d}t\\
&=: R_1 + R_2 + R_3.
\end{aligned} \tag{3.57}$$

First, as $|||v|||_X = 1$, we have $|R_1| \le ||f-\tilde{f}||_{X'}|||v|||_X = ||f-\tilde{f}||_{X'}$. Then, we use the property $s_{h\tau}^{k+1} \in P_\tau^1(H_0^1(\Omega)\cap C^0(\overline{\Omega}))$ (see (3.34)) for the case where $\Gamma^{\mathrm{N}} = \emptyset$, and $\boldsymbol{\sigma}_{h\tau}^{k+1} \in P_\tau^0(\mathbf{H}(\mathrm{div},\Omega))$ (see (3.38)), we have:

$$R_2 = \sum_{n=1}^N \int_{I_n} (\tilde{f}^n - \partial_t s_h^{k+1,n} - \nabla\cdot\boldsymbol{\sigma}_h^{k+1,n}, v(t))\,\mathrm{d}t. \tag{3.58}$$

Lemma 3.1 in [67] which is a consequence of (3.34) and (3.35) gives at each time step n, $1 \le n \le N$:

$$(\partial_t s_h^{k+1,n}, 1)_K = (\partial_t \tilde{p}_h^{k+1,n}, 1)_K, \quad \forall K \in \mathscr{T}_h. \tag{3.59}$$

Then, for all n, $1 \le n \le N$, using (3.59) and (3.39),

$$(\tilde{f}^n - \partial_t s_h^{k+1,n} - \nabla\cdot\boldsymbol{\sigma}_h^{k+1,n}, 1)_K = 0, \quad \forall K \in \mathscr{T}_h. \tag{3.60}$$

Thus, we can write for a.e. $t \in I_n$:

$$\begin{aligned}
(\tilde{f}^n - \partial_t s_h^{k+1,n} - \nabla\cdot\boldsymbol{\sigma}_h^{k+1,n}, v(t))_K &= (\tilde{f}^n - \partial_t s_h^{k+1,n} - \nabla\cdot\boldsymbol{\sigma}_h^{k+1,n}, v(t) - \pi_0 v(t))_K\\
&\le \frac{h_K}{\pi} c_{\boldsymbol{S},K}^{-\frac{1}{2}} ||\tilde{f}^n - \partial_t s_h^{k+1,n} - \nabla\cdot\boldsymbol{\sigma}_h^{k+1,n}||_K |||v|||_K(t),
\end{aligned} \tag{3.61}$$

where the Poincaré inequality given in (2.15) is used on each $K \in \mathscr{T}_h$. Finally,

$$R_3 \le \sum_{n=1}^N \int_{I_n} \sum_{K\in\mathscr{T}_h} |||\boldsymbol{S}\nabla s_{h\tau}^{k+1}(t) + \boldsymbol{\sigma}_h^{k+1,n}|||_{\star,K} |||v|||_K(t). \tag{3.62}$$

The Cauchy–Schwarz inequality gives by collecting the above estimates:

$$|R_2 + R_3| \le \left\{\sum_{n=1}^N \int_{I_n} \sum_{K\in\mathscr{T}_h} (\eta_{\mathrm{osc},K}^{k+1,n} + |||\boldsymbol{S}\nabla s_{h\tau}^{k+1}(t) + \boldsymbol{\sigma}_h^{k+1,n}|||_{\star,K})^2\,\mathrm{d}t\right\}^{\frac{1}{2}}. \tag{3.63}$$

Then,

$$||\mathscr{R}(s_{h\tau}^{k+1})||_{X'} \leq \left\{ \sum_{n=1}^{N} \int_{I_n} \sum_{K\in\mathscr{T}_h} (\eta_{\mathrm{osc},K}^{k+1,n} + |||\boldsymbol{S}\nabla s_{h\tau}^{k+1}(t) + \boldsymbol{\sigma}_h^{k+1,n}|||_{\star,K})^2 \,\mathrm{d}t \right\}^{\frac{1}{2}} + ||f - \tilde{f}||_{X'}. \tag{3.64}$$

Using the triangle inequality, we obtain:

$$|||\boldsymbol{S}\nabla s_{h\tau}^{k+1}(t) + \boldsymbol{\sigma}_h^{k+1,n}|||_{\star,K} \leq |||\boldsymbol{S}(\nabla s_{h\tau}^{k+1}(t) - \nabla s_h^{k+1,n})|||_{\star,K} + |||\boldsymbol{S}\nabla s_h^{k+1,n} + \boldsymbol{\sigma}_h^{k+1,n}|||_{\star,K}, \tag{3.65}$$

which leads to:

$$\begin{aligned}
&\left\{ \sum_{n=1}^{N} \int_{I_n} \sum_{K\in\mathscr{T}_h} (\eta_{\mathrm{osc},K}^{k+1,n} + |||\boldsymbol{S}\nabla s_{h\tau}^{k+1}(t) + \boldsymbol{\sigma}_h^{k+1,n}|||_{\star,K})^2 \,\mathrm{d}t \right\}^{\frac{1}{2}} \\
&\leq \left\{ \sum_{n=1}^{N} \int_{I_n} \sum_{K\in\mathscr{T}_h} (\eta_{\mathrm{osc},K}^{k+1,n} + |||\boldsymbol{S}(\nabla s_{h\tau}^{k+1}(t) - \nabla s_h^{k+1,n})|||_{\star,K} + |||\boldsymbol{S}\nabla s_h^{k+1,n} + \boldsymbol{\sigma}_h^{k+1,n}|||_{\star,K})^2 \,\mathrm{d}t \right\}^{\frac{1}{2}} \\
&\leq \left\{ \sum_{n=1}^{N} \int_{I_n} \sum_{K\in\mathscr{T}_h} (\eta_{\mathrm{osc},K}^{k+1,n} + |||\boldsymbol{S}\nabla s_h^{k+1,n} + \boldsymbol{\sigma}_h^{k+1,n}|||_{\star,K})^2 \,\mathrm{d}t \right\}^{\frac{1}{2}} \\
&\quad + \left\{ \sum_{n=1}^{N} \int_{I_n} \sum_{K\in\mathscr{T}_h} |||\boldsymbol{S}(\nabla s_{h\tau}^{k+1}(t) - \nabla s_h^{k+1,n})|||_{\star,K}^2 \,\mathrm{d}t \right\}^{\frac{1}{2}},
\end{aligned} \tag{3.66}$$

where the last term on the right-hand side can be now integrated in time. Finally we obtain the computable upper bound for $||\mathscr{R}(s_{h\tau}^{k+1})||_{X'}$ as follows:

$$\begin{aligned}
||\mathscr{R}(s_{h\tau}^{k+1})||_{X'} \leq &\left\{ \sum_{n=1}^{N} \tau^n \sum_{K\in\mathscr{T}_h} (\eta_{\mathrm{osc},K}^{k+1,n} + |||\boldsymbol{S}\nabla s_h^{k+1,n} + \boldsymbol{\sigma}_h^{k+1,n}|||_{\star,K})^2 \right\}^{\frac{1}{2}} + \left\{ \sum_{n=1}^{N} (\eta_{\mathrm{tm}}^{k+1,n})^2 \right\}^{\frac{1}{2}} \\
&+ ||f - \tilde{f}||_{X'}.
\end{aligned} \tag{3.67}$$

Computable upper bound for $|||s_{h\tau}^{k+1} - \tilde{p}_{h\tau}^{k+1}|||_Y$

We have from the definition (3.42):

$$|||s_{h\tau}^{k+1} - \tilde{p}_{h\tau}^{k+1}|||_Y^2 = |||s_{h\tau}^{k+1} - \tilde{p}_{h\tau}^{k+1}|||_X^2 + ||\partial_t(s_{h\tau}^{k+1} - \tilde{p}_{h\tau}^{k+1})||_{X'}^2 + ||s_h^{k+1,N} - \tilde{p}_h^{k+1,N}||^2. \tag{3.68}$$

It is clear that

$$|||s_{h\tau}^{k+1} - \tilde{p}_{h\tau}^{k+1}|||_X^2 = \sum_{n=1}^{N} \int_{I_n} \sum_{K\in\mathscr{T}_h} |||(\tilde{p}_{h\tau}^{k+1} - s_{h\tau}^{k+1})(t)|||_K^2 \mathrm{d}t. \tag{3.69}$$

Following Lemma 5.3 in [67], let $v \in X$ and $|||v||| = 1$. As $s_{h\tau}^{k+1}$ and $\tilde{p}_{h\tau}^{k+1}$ are piecewise

affine and continuous in time, we can write:

$$\begin{aligned}||\partial_t(s_{h\tau}^{k+1}-\tilde{p}_{h\tau}^{k+1})||_{X'}^2 &= \int_0^T ||\partial_t(s_{h\tau}^{k+1}-\tilde{p}_{h\tau}^{k+1})||_{H^{-1}(\Omega)}^2 \,\mathrm{d}t \\ &= \int_0^T \sup_{v\in H_0^1(\Omega);\,\|\boldsymbol{S}^{\frac{1}{2}}\nabla v\|=1} (\partial_t(s_{h\tau}^{k+1}-\tilde{p}_{h\tau}^{k+1}),v)^2\,\mathrm{d}t \\ &= \sum_{n=1}^N \int_{I_n} \sup_{v\in H_0^1(\Omega);\,\|\boldsymbol{S}^{\frac{1}{2}}\nabla v\|=1} (\partial_t(s_h^{k+1,n}-\tilde{p}_h^{k+1,n}),v(t))^2\,\mathrm{d}t.\end{aligned} \tag{3.70}$$

Then, for all $1\le n\le N$, and on each element $K\in\mathcal{T}_h$, the quantity $\partial_t(s_h^{k+1,n}-\tilde{p}_h^{k+1,n})$ has zero mean value, see (3.59). Thus,

$$||\partial_t(s_{h\tau}^{k+1}-\tilde{p}_{h\tau}^{k+1})||_{X'}^2 = \sum_{n=1}^N \int_{I_n} \sup_{v\in H_0^1(\Omega);\,\|\boldsymbol{S}^{\frac{1}{2}}\nabla v\|=1} (\partial_t(s_h^{k+1,n}-\tilde{p}_h^{k+1,n}),v(t)-\pi_0 v(t))^2\,\mathrm{d}t. \tag{3.71}$$

Using the Cauchy–Schwarz and Poincaré inequalities:

$$||\partial_t(s_{h\tau}^{k+1}-\tilde{p}_{h\tau}^{k+1})||_{X'}^2 \le \sum_{n=1}^N \int_{I_n} \sum_{K\in\mathcal{T}_h} \left(\frac{h_K}{\pi} c_{\boldsymbol{S},K}^{-\frac{1}{2}} ||\partial_t(s_h^{k+1,n}-\tilde{p}_h^{k+1,n})||_K\right)^2 |||v|||^2, \tag{3.72}$$

where the right-hande side can be easily integrated in time. Finally, using $|||v|||=1$ and from (3.68), (3.69), and (3.72), we obtain:

$$\begin{aligned}|||s_{h\tau}^{k+1}-\tilde{p}_{h\tau}^{k+1}|||_Y^2 \le& \sum_{n=1}^N \int_{I_n} \sum_{K\in\mathcal{T}_h} (|||(\tilde{p}_{h\tau}^{k+1}-s_{h\tau}^{k+1})(t)|||_K)^2\mathrm{d}t \\ &+ \sum_{n=1}^N \tau^n \sum_{K\in\mathcal{T}_h} \left(\frac{h_K}{\pi} c_{\boldsymbol{S},K}^{-\frac{1}{2}} ||\partial_t(\tilde{p}_h^{k+1,n}-s_h^{k+1,n})||_K\right)^2 \\ &+ ||s_h^{k+1,N}-\tilde{p}_h^{k+1,N}||^2.\end{aligned} \tag{3.73}$$

Final bound

Now, combining the previous results (3.55), (3.67), and (3.73), we can write:

$$\begin{aligned}|||p-\tilde{p}_{h\tau}^{k+1}|||_Y \le& \left\{\sum_{n=1}^N \tau^n \sum_{K\in\mathcal{T}_h} (\eta_{\mathrm{osc},K}^{k+1,n} + |||\boldsymbol{S}\nabla s_h^{k+1,n}+\boldsymbol{\sigma}_h^{k+1,n}|||_{\star,K})^2\right\}^{\frac{1}{2}} + \left\{\sum_{n=1}^N (\eta_{\mathrm{tm}}^{k+1,n})^2\right\}^{\frac{1}{2}} \\ &+ \left\{\sum_{n=1}^N \int_{I_n} \sum_{K\in\mathcal{T}_h} |||(\tilde{p}_{h\tau}^{k+1}-s_{h\tau}^{k+1})(t)|||_K^2\mathrm{d}t\right\}^{\frac{1}{2}} \\ &+ \left\{\sum_{n=1}^N \tau^n \sum_{K\in\mathcal{T}_h} \left(\frac{h_K}{\pi} c_{\boldsymbol{S},K}^{-\frac{1}{2}} ||\partial_t(\tilde{p}_h^{k+1,n}-s_h^{k+1,n})||_K\right)^2\right\}^{\frac{1}{2}} \\ &+ \eta_{\mathrm{IC}}^{k+1} + ||f-\tilde{f}||_{X'} + ||s_h^{k+1,N}-\tilde{p}_h^{k+1,N}||.\end{aligned} \tag{3.74}$$

From this inequality and as explained in [67], we can distinghuish the different error components. The error due to the discretization in space:

$$\begin{aligned}&\left\{\sum_{n=1}^{N}\tau^n\sum_{K\in\mathcal{T}_h}(\eta_{\text{osc},K}^{k+1,n}+|||\boldsymbol{S}\nabla s_h^{k+1,n}+\boldsymbol{\sigma}_h^{k+1,n}|||_{\star,K})^2\right\}^{\frac{1}{2}}\\&+\left\{\sum_{n=1}^{N}\int_{I_n}\sum_{K\in\mathcal{T}_h}|||(\tilde{p}_{h\tau}^{k+1}-s_{h\tau}^{k+1})(t)|||_K^2\mathrm{d}t\right\}^{\frac{1}{2}}\\&+\left\{\sum_{n=1}^{N}\tau^n\sum_{K\in\mathcal{T}_h}\left(\frac{h_K}{\pi}c_{\boldsymbol{S},K}^{-\frac{1}{2}}||\partial_t(\tilde{p}_h^{k+1,n}-s_h^{k+1,n})||_K\right)^2\right\}^{\frac{1}{2}},\end{aligned}\tag{3.75}$$

together with $||f-\tilde{f}||_{X'}+||s_h^{k+1,N}-\tilde{p}_h^{k+1,N}||$ and the error due to the initial condition η_{IC}^{k+1}; as well as the error due to the discretization in time:

$$\left\{\sum_{n=1}^{N}(\eta_{\text{tm}}^{k+1,n})^2\right\}^{\frac{1}{2}}.\tag{3.76}$$

This upper bound proposed in [65, 67] is for the one domain case (no DD method was used in [65, 67]). In our case, the global-in-time DD method is used and the domain Ω is decomposed into several subdomains. Therefore, we can distinguish the errors due to the DD method as in Chapter 2.

For the first term in (3.75), using the triangle inequality and the link between the norms $|||\boldsymbol{S}\nabla w|||_{\star,K}=||\boldsymbol{S}^{-\frac{1}{2}}(\boldsymbol{S}\nabla w)||_K=||\boldsymbol{S}^{\frac{1}{2}}\nabla w||_K=|||w|||_K$ (by Definitions (2.13) and (2.14)) for a given $\nabla w\in\mathbf{L}^2(\Omega_i)$ and for $K\in\mathcal{T}_{h,i}$, we have:

$$\begin{aligned}&\sum_{K\in\mathcal{T}_h}|||\boldsymbol{S}\nabla s_h^{k+1,n}+\boldsymbol{\sigma}_h^{k+1,n}|||_{\star,K}^2\\&\leq\sum_{K\in\mathcal{T}_h}\left(|||\boldsymbol{S}\nabla s_h^{k+1,n}+\mathbf{u}_h^{k+1,n}|||_{\star,K}+|||-\mathbf{u}_h^{k+1,n}+\boldsymbol{\sigma}_h^{k+1,n}|||_{\star,K}\right)^2\\&\leq\sum_{i=1}^{\mathcal{N}}\sum_{K\in\mathcal{T}_{h,i}}\left(|||\boldsymbol{S}\nabla s_{h,i}^{k+1,n}-\boldsymbol{S}\nabla\overline{s}_{h,i}^{k+1,n}|||_{\star,K}+|||\boldsymbol{S}\nabla\overline{s}_{h,i}^{k+1,n}+\mathbf{u}_h^{k+1,n}|||_{\star,K}+\eta_{\text{DF},1,b,K}^{k+1,n}\right)^2\\&=\sum_{i=1}^{\mathcal{N}}\sum_{K\in\mathcal{T}_{h,i}}\left(\eta_{\text{NCP},1,b,K}^{k+1,n}+\eta_{\text{DF},1,a,K}^{k+1,n}+\eta_{\text{DF},1,b,K}^{k+1,n}\right)^2.\end{aligned}\tag{3.77}$$

For the second term in (3.75), using the theory of the subdomain potential reconstruction described in Chapter 2, and using the triangle inequality, we obtain:

$$\begin{aligned}\sum_{K\in\mathcal{T}_h}|||(\tilde{p}_{h\tau}^{k+1}-s_{h\tau}^{k+1})(t)|||_K^2&=\sum_{i=1}^{\mathcal{N}}\sum_{K\in\mathcal{T}_{h,i}}|||(\tilde{p}_{h\tau,i}^{k+1}-s_{h\tau,i}^{k+1})(t)|||_K^2\\&\leq\sum_{i=1}^{\mathcal{N}}\sum_{K\in\mathcal{T}_{h,i}}\left(|||(\tilde{p}_{h\tau,i}^{k+1}-\overline{s}_{h\tau,i}^{k+1})(t)|||_K+|||(\overline{s}_{h\tau,i}^{k+1}-s_{h\tau,i}^{k+1})(t)|||_K\right)^2\\&\leq\sum_{i=1}^{\mathcal{N}}\sum_{K\in\mathcal{T}_{h,i}}\left(\eta_{\text{NCP},1,a,K}^{k+1}(t)+\eta_{\text{NCP},1,b,K}^{k+1}(t)\right)^2,\quad t\in I_n,\end{aligned}\tag{3.78}$$

and equally for the third term in (3.75):

$$\begin{aligned}\sum_{K\in\mathcal{T}_h}\left(\frac{h_K}{\pi}c_{\boldsymbol{s},K}^{-\frac{1}{2}}\right)^2||\partial_t(\tilde{p}_h^{k+1,n}-s_h^{k+1,n})||_K^2 &= \sum_{i=1}^{\mathcal{N}}\sum_{K\in\mathcal{T}_{h,i}}\left(\frac{h_K}{\pi}c_{\boldsymbol{s},K}^{-\frac{1}{2}}\right)^2||\partial_t(\tilde{p}_{h,i}^{k+1,n}-s_{h,i}^{k+1,n})||_K^2\\ &\leq \sum_{i=1}^{\mathcal{N}}\sum_{K\in\mathcal{T}_{h,i}}\left(\frac{h_K}{\pi}c_{\boldsymbol{s},K}^{-\frac{1}{2}}\right)^2\Big(||\partial_t(\tilde{p}_{h,i}^{k+1,n}-\overline{s}_{h,i}^{k+1,n})||_K\\ &\quad+||\partial_t(\overline{s}_{h,i}^{k+1,n}-s_{h,i}^{k+1,n})||_K\Big)^2\\ &\leq \sum_{i=1}^{\mathcal{N}}\sum_{K\in\mathcal{T}_{h,i}}\left(\eta_{\mathrm{NCP},2,a,K}^{k+1,n}+\eta_{\mathrm{NCP},2,b,K}^{k+1,n}\right)^2.\end{aligned} \tag{3.79}$$

Finally, from (3.75), (3.77)–(3.79) and Cauchy Schwarz inequality in l^2, we can distinguish the three different error components:

- the error due to the discetization in space:

$$\begin{aligned}\eta_{\mathrm{sp}}^{k+1} =&\left\{\sum_{n=1}^{N}\tau^n\sum_{K\in\mathcal{T}_h}(\eta_{\mathrm{osc},K}^{k+1,n}+\eta_{\mathrm{DF},1,a,K}^{k+1,n})^2\right\}^{\frac{1}{2}}+\left\{\sum_{n=1}^{N}\int_{I_n}\sum_{i=1}^{\mathcal{N}}\sum_{K\in\mathcal{T}_{h,i}}(\eta_{\mathrm{NCP},1,a,K}^{k+1}(t))^2\mathrm{d}t\right\}^{\frac{1}{2}}\\ &+\left\{\sum_{n=1}^{N}\tau^n\sum_{i=1}^{\mathcal{N}}\sum_{K\in\mathcal{T}_{h,i}}(\eta_{\mathrm{NCP},2,a,K}^{k+1,n})^2\right\}^{\frac{1}{2}},\end{aligned} \tag{3.80}$$

- the error due to the discetization in time:

$$\eta_{\mathrm{tm}}^{k+1}:=\left\{\sum_{n=1}^{N}\sum_{K\in\mathcal{T}_h}\frac{1}{3}\tau^n|||s_h^{k+1,n}-s_h^{k+1,n-1}|||_K^2\right\}^{\frac{1}{2}}, \tag{3.81}$$

- the error due to DD method:

$$\begin{aligned}\eta_{\mathrm{DD}}^{k+1} :=&\left\{\sum_{n=1}^{N}\tau^n\sum_{K\in\mathcal{T}_h}(\eta_{\mathrm{DF},1,b,K}^{k+1,n}+\eta_{\mathrm{NCP},1,b,K}^{k+1,n})^2\right\}^{\frac{1}{2}}+\left\{\sum_{n=1}^{N}\int_{I_n}\sum_{i=1}^{\mathcal{N}}\sum_{K\in\mathcal{T}_{h,i}}(\eta_{\mathrm{NCP},1,b,K}^{k+1}(t))^2\mathrm{d}t\right\}^{\frac{1}{2}}\\ &+\left\{\sum_{n=1}^{N}\tau^n\sum_{i=1}^{\mathcal{N}}\sum_{K\in\mathcal{T}_{h,i}}(\eta_{\mathrm{NCP},2,b,K}^{k+1,n})^2\right\}^{\frac{1}{2}},\end{aligned} \tag{3.82}$$

which ends the proof of Theorem 3.6. □

Remark 3.7. *In the follows, we will use the following notations for the restriction of* η_{sp}^{k+1}, η_{tm}^{k+1}, *and* η_{DD}^{k+1} *on the interval* I_n*:*

$$\begin{aligned}\eta_{\mathrm{sp}}^{k+1,n} :=&\left\{\tau^n\sum_{K\in\mathcal{T}_h}(\eta_{\mathrm{osc},K}^{k+1,n}+\eta_{\mathrm{DF},1,a,K}^{k+1,n})^2\right\}^{\frac{1}{2}}+\left\{\int_{I_n}\sum_{i=1}^{\mathcal{N}}\sum_{K\in\mathcal{T}_{h,i}}(\eta_{\mathrm{NCP},1,a,K}^{k+1}(t))^2\mathrm{d}t\right\}^{\frac{1}{2}}\\ &+\left\{\tau^n\sum_{i=1}^{\mathcal{N}}\sum_{K\in\mathcal{T}_{h,i}}(\eta_{\mathrm{NCP},2,a,K}^{k+1,n})^2\right\}^{\frac{1}{2}},\end{aligned} \tag{3.83}$$

$$\eta_{\mathrm{tm}}^{k+1,n} := \left\{ \sum_{K\in\mathscr{T}_h} \frac{1}{3}\tau^n |||s_h^{k+1,n} - s_h^{k+1,n-1}|||_K^2 \right\}^{\frac{1}{2}}, \tag{3.84}$$

$$\begin{aligned}\eta_{\mathrm{DD}}^{k+1,n} :=& \left\{ \tau^n \sum_{K\in\mathscr{T}_h} (\eta_{\mathrm{DF},1,b,K}^{k+1,n} + \eta_{\mathrm{NCP},1,b,K}^{k+1,n})^2 \right\}^{\frac{1}{2}} + \left\{ \int_{I_n} \sum_{i=1}^{\mathscr{N}} \sum_{K\in\mathscr{T}_{h,i}} (\eta_{\mathrm{NCP},1,b,K}^{k+1}(t))^2 \mathrm{d}t \right\}^{\frac{1}{2}} \\ &+ \left\{ \tau^n \sum_{i=1}^{\mathscr{N}} \sum_{K\in\mathscr{T}_{h,i}} (\eta_{\mathrm{NCP},2,b,K}^{k+1,n})^2 \right\}^{\frac{1}{2}}.\end{aligned} \tag{3.85}$$

3.8 Potential and flux reconstructions for the global-in-time DD in the MFE method

3.8.1 Potential reconstruction

In order to build the potential reconstruction $s_h^{k+1,n}$ which is $H^1(\Omega)$-conforming in space at each time step n, for $0 \le n \le N$, as indicated in (3.34), we proceed as in [67]. We first apply the interpolate operator $\mathscr{I}_{\mathrm{av}}$ to $\tilde{p}_h^{k+1,n}$ as in Section 2.5.1 of Chapter 2:

$$\mathscr{I}_{\mathrm{av}}(\tilde{p}_h^{k+1,n}) \in H^1(\Omega). \tag{3.86}$$

Then, $s_h^{k+1,n}$ has to satisfy the second condition (3.35). We need the mean value of $s_h^{k+1,n}$ on each triangle, at time t^n, to be equal to the mean value of the postprocessing $\tilde{p}_{h,i}^{k+1,n}$ of the discrete solution.
In order to obtain (3.35) while maintaining (3.34), we choose $s_h^{k+1,n}$ as follows:

$$s_h^{k+1,n} = \mathscr{I}_{\mathrm{av}}(\tilde{p}_h^{k+1,n}) + \sum_{K\in\mathscr{T}_h} \alpha_K^{k+1,n} b_K, \tag{3.87}$$

where $\alpha_K^{k+1,n}$ is chosen as follows:

$$\alpha_K^{k+1,n} := \frac{1}{(b_K,1)_K} (\tilde{p}_h^{k+1,n} - \mathscr{I}_{\mathrm{av}}(\tilde{p}_h^{k+1,n}), 1)_K, \tag{3.88}$$

and where b_K is the bubble function on the element K. It is a time-independent function defined as the product of the barycentric coordinates of K whose value on the boundary ∂K of K is zero. Note that $\mathscr{I}_{\mathrm{av}}(\tilde{p}_h^{k+1,n}) \in H^1(\Omega)$ as shown in Chapter 2 and we also have $\sum_{K\in\mathscr{T}_h} \alpha_K^{k+1,n} b_K \in H^1(\Omega)$. Hence, $s_h^{k+1,n}$ belongs to $H^1(\Omega)$.
Then, the potential reconstruction $s_{h\tau}^{k+1} \in P_\tau^1(H^1(\Omega) \cap C^0(\overline{\Omega}))$ is defined by the $N+1$ functions $s_h^{k+1,n} \in H^1(\Omega)$ at the discrete times $\{t^n\}_{0\le n\le N}$.

3.8.2 Subdomain potential reconstruction

At each iteration $k+1$ of the DD method and at each time step n, we have to build the subdomain potential reconstruction $\overline{s}_{h,i}^{k+1,n}$ in each subdomain Ω_i which satisfies (3.36a)

and (3.37). For the reason given in Section 2.5.2 of Chapter 2, we first build the subdomain potential reconstruction proposed in (2.55) and denoted here by $\overline{\overline{s}}_{h,i}^{k+1,n}$:

$$\overline{\overline{s}}_{h,i}^{k+1,n}(\mathbf{a}) = w_{i,\mathbf{a}}^{k+1,n} \sum_{K\in\mathscr{T}_\mathbf{a}^i} \tilde{p}_{h,i}^{k+1,n}|_K(\mathbf{a}) + w_{i,\mathbf{a}}^{k+1,n}(1-\overline{w}_\mathbf{a}^{k+1,n}) \sum_{j\in\tilde{B}^i} \sum_{K\in\mathscr{T}_\mathbf{a}^j} \tilde{p}_{h,j}^{k+1,n}|_K(\mathbf{a}), \quad (3.89)$$

where $w_{i,\mathbf{a}}^{k+1,n}$ and $\overline{w}_\mathbf{a}^{k+1,n}$ are constructed as in Section 2.5.2, but now at each time step n. Here, $\overline{\overline{s}}_{h,i}^{k+1,n}$ satifies (3.36a): $\overline{\overline{s}}_{h,i}^{k+1,n} \in H^1(\Omega_i)$ and the boundary condition (3.36b). It remains to verify the condition (3.37) for $\overline{s}_{h\tau,i}^{k+1}$. More precisely, we need the mean value of $\overline{s}_{h,i}^{k+1,n}$ on each triangle, at time t^n, to be equal to the mean value of the postprocessing $\tilde{p}_{h,i}^{k+1,n}$ of the discrete solution. For this purpose and while maintaining (3.36a), $\overline{s}_{h,i}^{k+1}$ is chosen as follows:

$$\overline{s}_{h,i}^{k+1,n} := \overline{\overline{s}}_{h,i}^{k+1,n} + \sum_{K\in\mathscr{T}_h} \overline{\alpha}_K^{k+1,n} b_K, \quad (3.90)$$

where $\overline{\alpha}_K^{k+1,n}$ is chosen in the same spirit as in (3.88):

$$\overline{\alpha}_K^{k+1,n} := \frac{1}{(b_K,1)_K}(\tilde{p}_h^{k+1,n} - \overline{\overline{s}}_{h,i}^{k+1,n}, 1)_K. \quad (3.91)$$

3.8.3 Flux reconstruction

Note that in condition (3.38) we need $\boldsymbol{\sigma}_h^{k+1,n} \in \mathbf{H}(\mathrm{div},\Omega)$ in $\mathscr{T}_h$ at each time step n. As shown in Section 2.6.2.2 for the steady equation, we now construct this flux in $\mathscr{T}_h$ at each time step using the corrections in each band in order to obtain the $\mathbf{H}(\mathrm{div},\Omega)$ property. More precisely, for the unsteady equation and many subdomains, and at each time step n, we need to find corrections $c_{\Gamma_i^b}^{k+1,n}$ and $c_{\Gamma_{i,j}}^{k+1,n}$ to the averaged flux $\{\!\{\mathbf{u}_h^{k+1,n}\cdot\boldsymbol{n}_{\partial\Omega_i^{\mathrm{ext}}}\}\!\}$, which will lead to the equilibrium in each band Ω_i^{ext}, such that:

$$c_{\Gamma_i^b}^{k+1,n} \approx 0 \qquad \text{for } i\in[\![1,\mathscr{N}]\!] \text{ and } b=1,2 \text{ such that } |\partial\Omega_i^{\mathrm{ext}}\cap\partial\Omega|>0, \quad (3.92a)$$

$$c_{\Gamma_{i,j}}^{k+1,n} \approx 0 \qquad \text{for } i,j\in[\![1,\mathscr{N}]\!],\ i<j \text{ such that } j\in B^i. \quad (3.92b)$$

In addition, we keep the same value of the flux $\mathbf{u}_h^{k+1,n}\cdot\boldsymbol{n}_{\partial\Omega_i^{\mathrm{ext}}\cap\partial\Omega_i^{\mathrm{int}}}$ located on the boundary $\partial\Omega_i^{\mathrm{ext}}\cap\partial\Omega_i^{\mathrm{int}}$, for each subdomain Ω_i. Thus, we set:

$$c_{\partial\Omega_i^{\mathrm{ext}}\cap\partial\Omega_i^{\mathrm{int}}}^{k+1,n} := 0 \quad \forall\Omega_i,\ i\in[\![1,\mathscr{N}]\!]. \quad (3.93)$$

There are as many balancing conditions as bands Ω_i^{ext}, and thus as the number of subdomains. The $\mathscr{N}$ balancing conditions that have to be satisfied, $\forall i\in[\![1,\mathscr{N}]\!]$, are:

$$\sum_{\substack{b=1,2/\\ |\partial\Omega_i\cap\partial\Omega|>0}} c_{\Gamma_i^b}^{k+1,n} + \sum_{j\in B^i}(\boldsymbol{n}_{\Gamma_{i,j}}\cdot\boldsymbol{n}_{\partial\Omega_i^{\mathrm{ext}}})c_{\Gamma_{i,j}}^{k+1,n} = (\tilde{f}^n - \partial_t\tilde{p}_h^{k+1,n}, 1)_{\Omega_i^{\mathrm{ext}}} - \langle\{\!\{\mathbf{u}_h^{k+1,n}\cdot\boldsymbol{n}_{\partial\Omega_i^{\mathrm{ext}}}\}\!\}, 1\rangle_{\partial\Omega_i^{\mathrm{ext}}}, \quad (3.94)$$

where

$$(\tilde{f}^n - \partial_t\tilde{p}_h^{k+1,n}, 1)_{\Omega_i^{\mathrm{ext}}} - \langle\{\!\{\mathbf{u}_h^{k+1,n}\cdot\boldsymbol{n}_{\partial\Omega_i^{\mathrm{ext}}}\}\!\}, 1\rangle_{\partial\Omega_i^{\mathrm{ext}}},\ i\in[\![1,\mathscr{N}]\!], \quad (3.95)$$

is the mistfit of mass balance of the averaging in each subdomain for $i \in [\![1, \mathcal{N}]\!]$. At each time step n, equations (3.94), for $i \in [\![1, \mathcal{N}]\!]$ lead to a rectangular linear system which give an infinity of solutions and where we use the least squares algorithm to obtain the closest solution to (3.92), as in Section 2.6.2.2. The resulting boundary fluxes of this method are now:

$$\boldsymbol{\sigma}_h^{k+1,n} \cdot \boldsymbol{n}_e = \begin{cases} \{\!\{ \mathbf{u}_h^{k+1,n} \cdot \boldsymbol{n}_e \}\!\} + \dfrac{1}{|\Gamma_{i,j}|} c_{\Gamma_{i,j}}^{k+1,n}, & \forall e \subset \Gamma_{i,j},\ j \in B^i,\ i < j,\ i \in [\![1, \mathcal{N}]\!], \\ \mathbf{u}_h^{k+1,n} \cdot \boldsymbol{n}_e + \dfrac{1}{|\Gamma_i^b|} c_{\Gamma_i^b}^{k+1,n}, & \forall e \subset \Gamma_i^b \text{ for } i \in [\![1, \mathcal{N}]\!] \text{ and } b = 1,2 \\ & \text{such that } |\partial\Omega_i^{\text{ext}} \cap \partial\Omega| > 0, \\ \mathbf{u}_{h,i}^{k+1,n} \cdot \boldsymbol{n}_e, & \forall e \subset \partial\Omega_i^{\text{ext}} \cap \partial\Omega_i^{\text{int}},\ i = 1, .., \mathcal{N}. \end{cases} \tag{3.96}$$

With these boundary fluxes the mass balance on each domain Ω_i^{ext} is satisfied at each time step n. Then, following Section 2.6.2.3 (for the steady case), a well-posed local Neumann problem in each band is solved at each time step n, wich satify the local conservation property 3.39, see Figure 3.2.

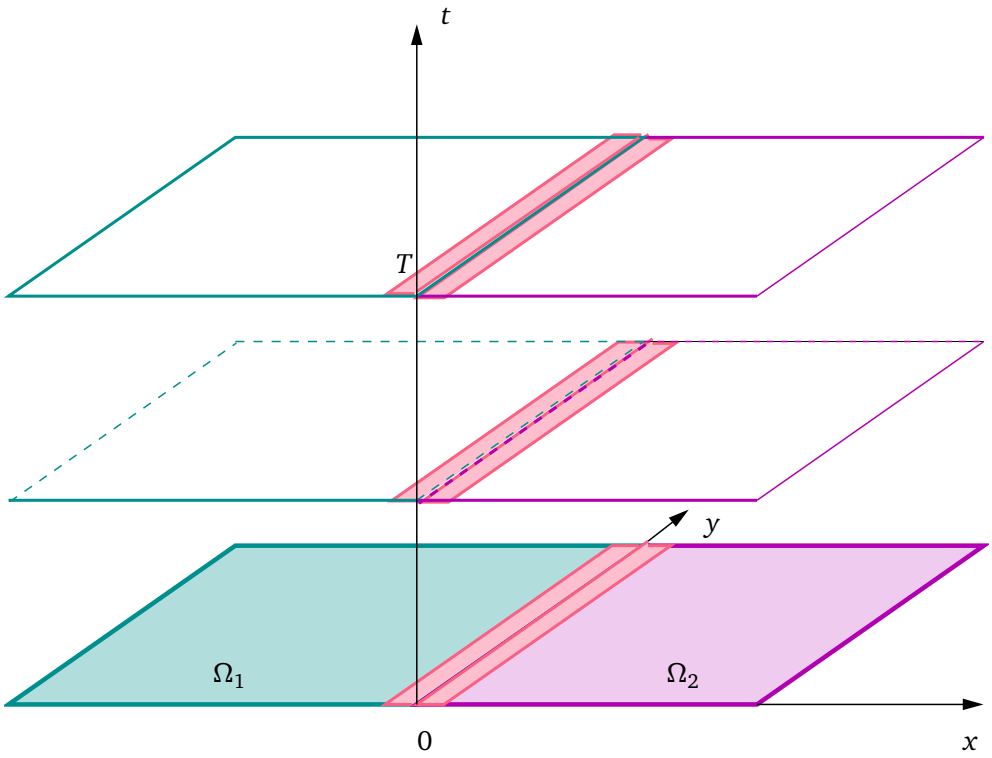

Figure 3.2: Bands in Ω_1 and Ω_2 at each time step

The space of the local Neumann problem is defined at each time step n as follows:

Definition 3.8 (Spaces of local Neumann problem at each time step n)**.** *We define for*

$i \in [\![1, \mathcal{N}]\!]$ the spaces on Ω_i^{ext}:

$$
\begin{aligned}
\mathbf{W}_{h,z,n,\Omega_i^{\text{ext}}} = \Bigg\{ & \mathbf{v}_h^{k+1,n} \in \mathbf{W}_{h,i}(\Omega_i^{\text{ext}}) : \\
& \mathbf{v}_h^{k+1,n} \cdot \boldsymbol{n}_{\Omega_i^{\text{ext}}} = z + \Big\{ \boldsymbol{n}_{\partial\Omega_i^{\text{ext}}} \cdot \boldsymbol{n}_{\Gamma_{i,j}} \frac{c_{\Gamma_{i,j}}^{k+1,n}}{|\Gamma_{i,j}|},\ \textit{if } z \neq 0 \Big\},\ j \in B^i, \\
& \mathbf{v}_h^{k+1,n} \cdot \boldsymbol{n}_{\Omega_i^{\text{ext}}} = z + \Big\{ \frac{c_{\Gamma_i^b}^{k+1,n}}{|\Gamma_i^b|},\ \textit{if } z \neq 0 \Big\}, \textit{ for } b = 1,2 \textit{ such that } |\partial\Omega_i^{\text{ext}} \cap \partial\Omega| > 0, \\
& \mathbf{v}_h^{k+1,n} \cdot \boldsymbol{n}_{\Omega_i^{\text{ext}}} = z \textit{ on } \partial\Omega_i^{\text{ext}} \cap \partial\Omega_i^{\text{int}} \Bigg\}.
\end{aligned}
\tag{3.97}
$$

The local Neumann problem is written as follows:
Find $\boldsymbol{\sigma}_h^{k+1,n}{}_{|\Omega_i^{\text{ext}}} \in \mathbf{W}_{h,\{\!\{\mathbf{u}_h^{k+1,n}\cdot\boldsymbol{n}_{\Omega_i^{\text{ext}}}\}\!\},n,\Omega_i^{\text{ext}}}$ and $q_h^{k+1,n} \in M_{h,i}(\Omega_i^{\text{ext}})$ such that $(q_h^{k+1,n}, 1)_{|\Omega_i^{\text{ext}}} = 0$, which solve the following mixed problem:

$$
(\boldsymbol{S}^{-1}(\boldsymbol{\sigma}_h^{k+1,n} - \mathbf{u}_h^{k+1,n}), \mathbf{v}_h)_{\Omega_i^{\text{ext}}} - (q_h^{k+1,n}, \nabla\cdot\mathbf{v}_h)_{\Omega_i^{\text{ext}}} = 0, \quad \forall \mathbf{v}_h \in \mathbf{W}_{h,0,n,\Omega_i^{\text{ext}}}, \tag{3.98a}
$$

$$
(\nabla\cdot\boldsymbol{\sigma}_h^{k+1,n}, w_h)_{\Omega_i^{\text{ext}}} = (\bar{f}^n, w_h)_{\Omega_i^{\text{ext}}}, \quad \forall w_h \in M_{h,i}(\Omega_i^{\text{ext}}), \quad \text{where } (w_h, 1)_{|\Omega_i^{\text{ext}}} = 0, \tag{3.98b}
$$

with $\bar{f}^n := \tilde{f}^n - \dfrac{p_{h,i}^{k+1,n} - p_{h,i}^{k+1,n-1}}{\tau^n}$.
Then $\boldsymbol{\sigma}_{h\tau}^{k+1}$ is defined by the N functions $\left(\boldsymbol{\sigma}_h^{k+1,n}\right)_{1\le n\le N}$ associated with the time subintervals $\{I_n\}_{1\le n\le N}$. In this section, the time step in the subdomains are supposed to be the same. In Section 3.10, we extend the method to the case of nonconforming time grids.

3.9 Numerical results

In this section, we present some numerical illustrations of the a posteriori error estimators of Theorem 3.6. We consider a domain Ω divided into nine equally sized subdomains and we use an unstructured mesh in space. The Jacobi iterative method and GMRES are used.

3.9.1 Model example with the Jacobi solver

We consider the decomposition of $\Omega =]0,1[\times]0,1[$ into nine subdomains, $\Omega = \bigcup_{i=1}^{9} \Omega_i$, in the case where:

- The diffusion tensor: $\boldsymbol{S} = \begin{pmatrix} 1 & 0 \\ 0 & 1 \end{pmatrix}$,
- The exact solution: $p(\mathbf{x}, t) = \sin(2\pi x)\sin(2\pi y)\cos(2\pi t)$,
- $\partial_t p(\mathbf{x}, t) = -2\pi \sin(2\pi x)\sin(2\pi y)\sin(2\pi t)$,
- $f(\mathbf{x}, t) = 8\pi^2 \sin(2\pi x)\sin(2\pi y)\cos(2\pi t) + \partial_t p$ is the corresponding source term,
- $x = 0$ is the Neumann boundary,
- $x = 1$ is the Robin boundary,
- $y = 0$ and $y = 1$ are the Dirichlet boundaries.

Number of triangles in Ω	76888
Number of subdomains	9
Subdomain solver	Direct
DD solver	Jacobi
Final time	$T = 1$
Time step τ	$1/100$
Original DD stopping criterion	1e-6
A posteriori stopping criterion	$\eta_{\text{DD}} \leq 0.1 \max(\eta_{\text{tm}}, \eta_{\text{sp}})$
Total number of iterations	63
Number of iterations with an a posteriori stopping criterion	18
Unnecessary iterations	45
Spared iteration from the total number of iteration	≈ 71 %

Table 3.1: Example with the Jacobi solver

In this example, the number of triangles in the domain Ω after discretization is 76888. In Figure 3.3, we plot the evolution of η_{DD}, η_{sp}, and η_{tm} presented in Theorem 3.6, as well as their sum, as a function of the number of iterations of the global-in-time Robin DD method with the Jacobi solver (i.e. the OSWR method). As shown in Table 3.1, we fix the original DD stopping citerion at 1e-6. In other words, it corresponds to the case where the residual of the jump of the Robin condition is lower than 1e-6. From Figure 3.3, we can describe what is happening during the iterations of the DD

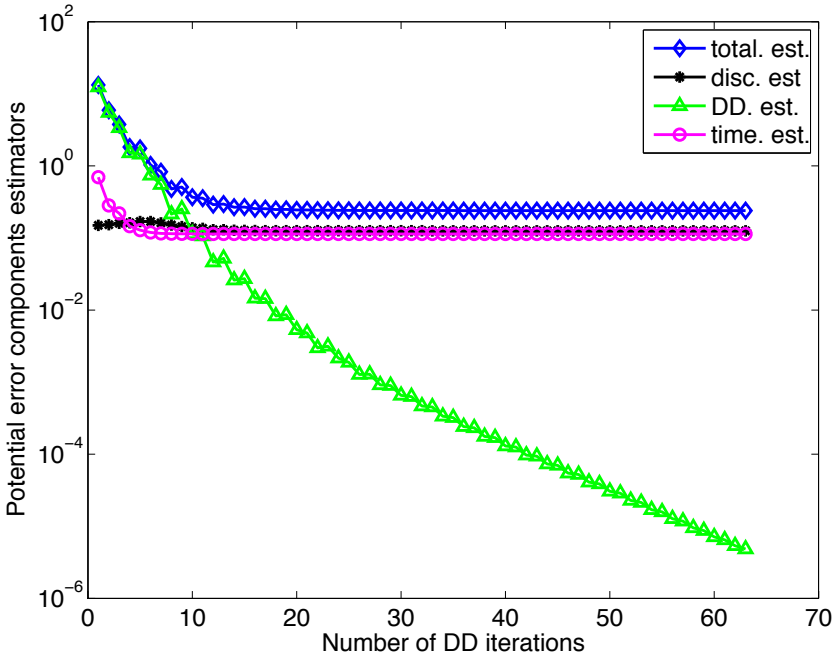

Figure 3.3: Error component estimates with the Jacobi solver

solver. At the beginning, we can remark that η_{DD} dominates up to roughly 10 iterations and then gets smaller compared to η_{sp} and η_{tm}. The original DD stopping criterion is verified after 63 iterations. Instead of this criterion, we can deduce a better criterion

using the a posteriori estimates which is when the domain decomposition error does not contribute significantly to the overall error, i.e.:

$$\eta_{\mathrm{DD}} \leq \gamma \max(\eta_{\mathrm{tm}}, \eta_{\mathrm{sp}}), \quad \gamma \approx 0.1.$$

For the example of Figure 3.3, the new criterion stops the algorithm at iteration 18, and thereby avoid 45 unnecessary iterations. On Figure 3.4, we plot a rough approximation of the error $|||p - \tilde{p}_{h\tau}^{k+1}|||_Y$ which is represented here by $\{|||p - \tilde{p}_{h\tau}^{k+1}|||_X^2 + ||(p - \tilde{p}_{h\tau}^{k+1})(\cdot, T)||^2\}^{\frac{1}{2}}$ without the term $||\partial_t(p - \tilde{p}_{h\tau}^{k+1})||_{X'}$ whose computation would be burden to compute (this term is not expected to be dominant). We also plot the total estimator, versus the number of iterations, see Figure 3.4. The total estimator de-

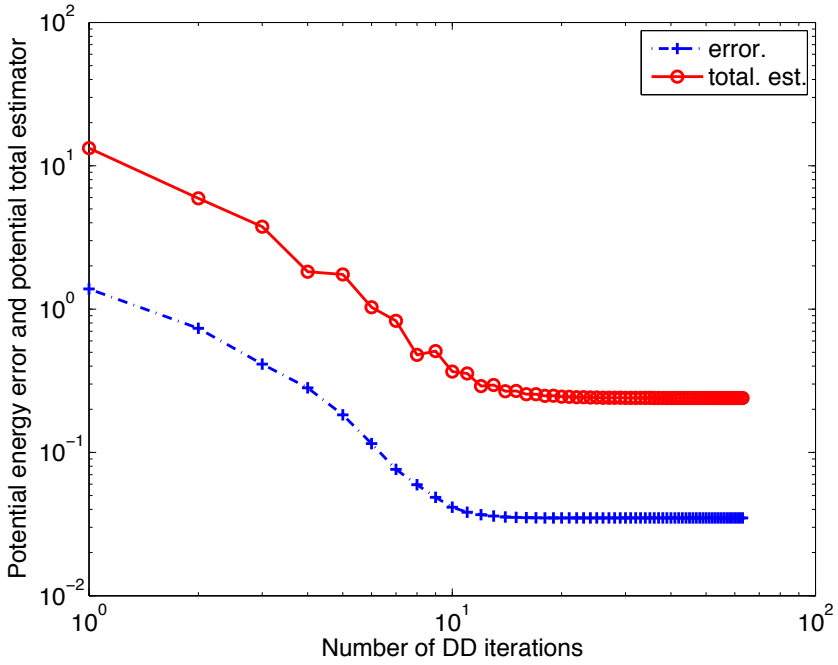

Figure 3.4: Energy error and total estimator with the Jacobi solver

scribed by the red curve is always above the blue curve of the energy norm which gives a numerical indication of the validity of Theorem 3.6. Consequently, we can obtain the effectivity index given in (3.51) at each iteration of the DD algorithm, see Figure 3.5, which starts from the value 9.58 and then decreases until it reaches approximately the value 6.87 at iteration 63. We observe that the effectivity index is not close to the optimal value of 1, as shown in Chapter 2. One of the reasons may be that the negative norms in Theorem 3.6 have not been computed. It could also be lowered further while using directly the bounds (3.63) and (3.73) not separating the different error components. Note that at iteration 18, where the a posteriori stopping criterion is defined, the value of the effectivity index is approximately 7.1, see Figure 3.5. In Figure 3.6, a zoom of the different component estimators is shown, until the 18^{th} iteration of the Jacobi solver, which represents the a posteriori stopping criterion.

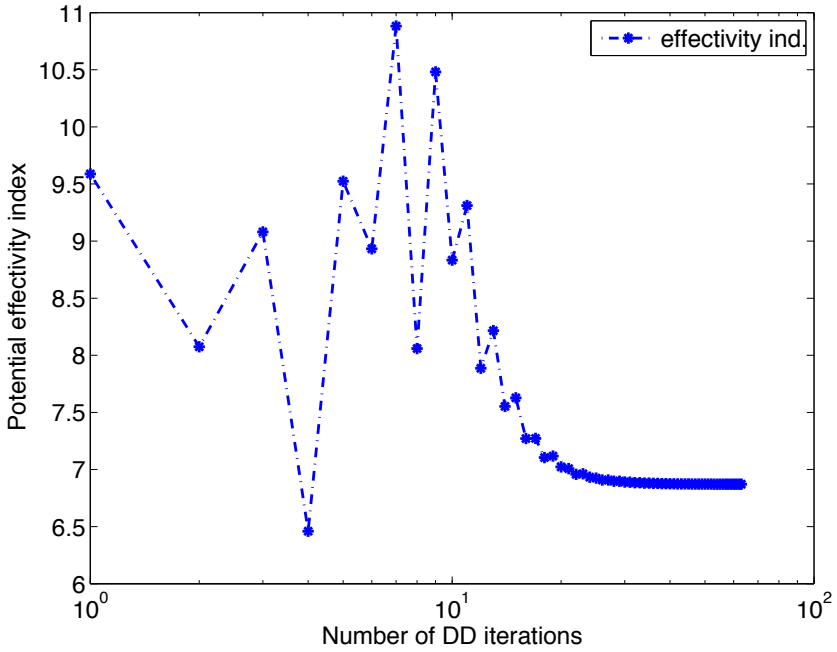

Figure 3.5: Effectivity index with the Jacobi solver

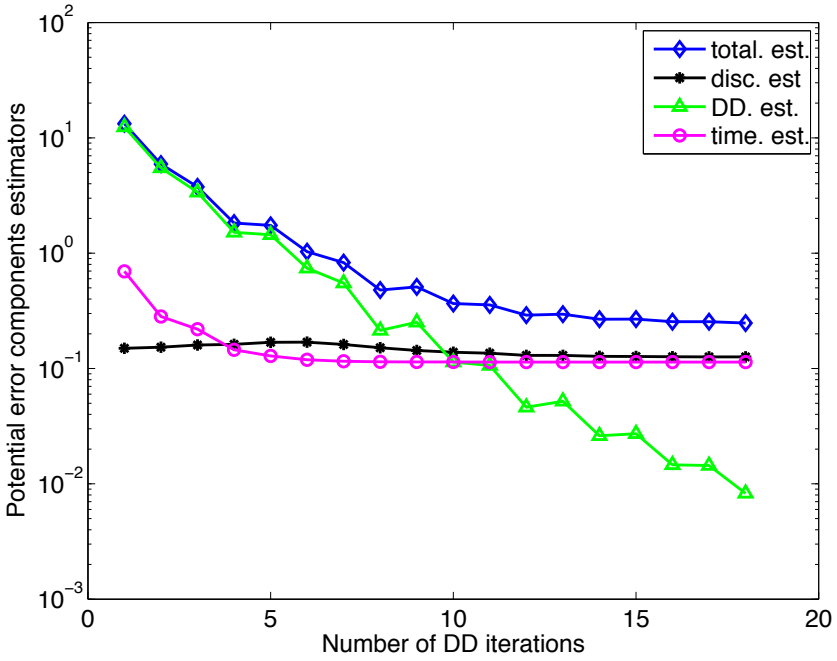

Figure 3.6: Error component estimates with the Jacobi solver

DD estimators at the 18^{th} iteration

In this part, we represent the distributions of the DD estimators on each mesh element of the domain Ω, on the last subinterval $I = I_{100} = [0.99, 1]$, and at iteration 18. In

Figure 3.7, we show the DD potential nonconformity estimators:

$$\left\{\int_{I_{100}} (\eta^{18}_{\mathrm{NCP},1,b,K})^2(t)\,\mathrm{d}t\right\}^{\frac{1}{2}}, \quad \text{(Figure 3.7 on the left)},$$

and

$$\left\{\tau^{100}(\eta^{18,100}_{\mathrm{NCP},2,b,K})^2\right\}^{\frac{1}{2}}, \quad \text{(Figure 3.7 on the right)}.$$

As shown in Chapter 2 and completed for the heat equation in this chapter, these

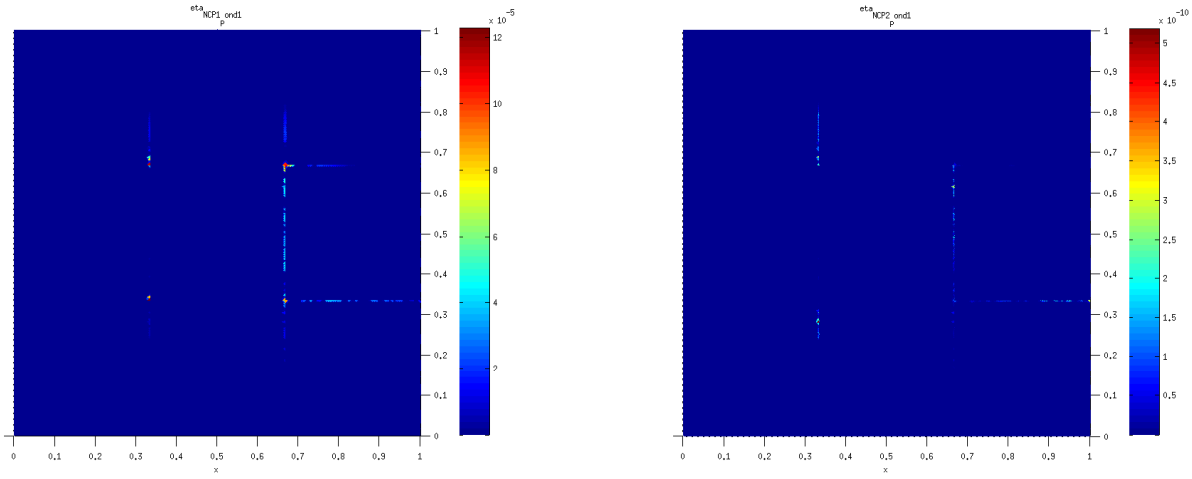

Figure 3.7: Distribution of the estimator $\left\{\int_{I_{100}} (\eta^{18}_{\mathrm{NCP},1,b,K})^2(t)\,\mathrm{d}t\right\}^{\frac{1}{2}}$ on Ω (on the left) and of $\left\{\tau^{100}(\eta^{18,100}_{\mathrm{NCP},2,b,K})^2\right\}^{\frac{1}{2}}$ (on the right) at the final time step 100 and at the 18th iteration of the Jacobi solver

two DD estimators are constructed using the subdomain potential reconstruction on the interface. We remark that the contributions of the elements of $\eta^{18}_{\mathrm{NCP},1,b,K}$ on I_{100} are (in the infinity norm) about 12e-5 and distributed around the interfaces of the 9 subdomains, whereas $\eta^{18,100}_{\mathrm{NCP},2,b,K}$ are about 5e-10 around the interfaces. Then, in Figure 3.8, we plot the DD estimator built using the flux reconstruction coming from the local Neumann problems:

$$\left\{\tau^{100}(\eta^{18,100}_{\mathrm{DF},1,b,K})^2\right\}^{\frac{1}{2}}.$$

In this figure, we can see that the errors (in the infinity norm) are distributed around the interfaces and are about 2.5e-5. Finally, we plot $\eta^{18,100}_{\mathrm{DD}}$ in Figure 3.8 (on the right), which is the sum of these three above estimators, and defined in (3.85). We observe that it follows the same distributions as $\left\{\int_{I_{100}} (\eta^{18}_{\mathrm{NCP},1,b,K})^2(t)\,\mathrm{d}t\right\}^{\frac{1}{2}}$ which has the largest contribution to $\eta^{18,100}_{\mathrm{DD}}$.

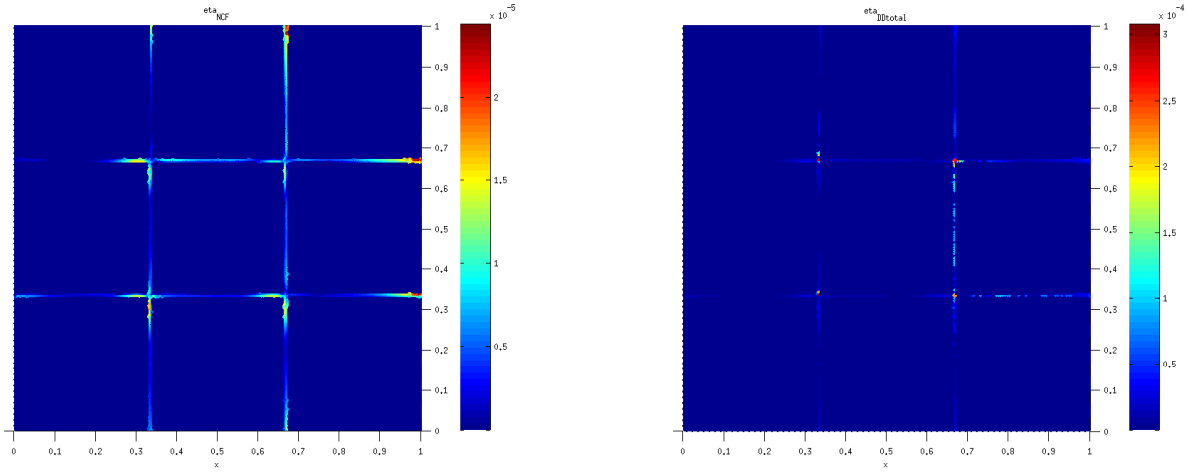

Figure 3.8: Distribution of the estimator $\left\{\tau^{100}(\eta^{18,100}_{\mathrm{DF},1,b,K})^2\right\}^{\frac{1}{2}}$ on Ω (on the left) and of $\eta^{18,100}_{\mathrm{DD}}$ (on the right) at the final time step 100 and at the 18th iteration of the Jacobi solver

Total discretization estimator, time estimator, and global estimator at the 18^{th} iteration

In Figure 3.9 (on the left), we plot the distribution on Ω of the time discretization estimator $\eta^{18,100}_{\mathrm{tm}}$, introduced in (3.84), which is about 5e-6. In Figure 3.9 (on the right), the distribution on Ω of the subdomain discretization estimator $\eta^{18,100}_{\mathrm{sp}}$ introduced in (3.83) is shown and is about 2e-4.

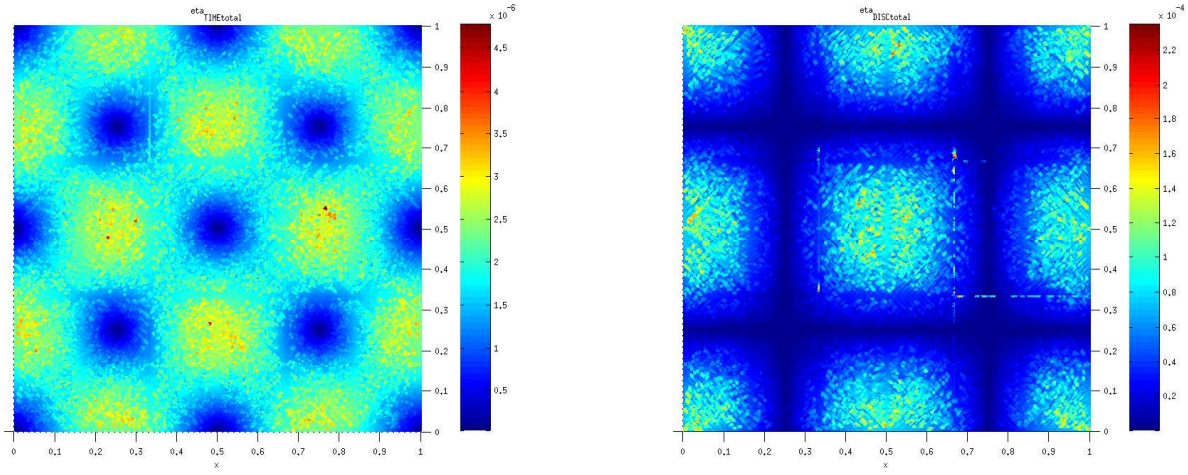

Figure 3.9: Distribution of the estimator $\eta^{18,100}_{\mathrm{tm}}$ on Ω (on the left) and of $\eta^{18,100}_{\mathrm{sp}}$ (on the right) at the final time step 100 and at the 18th iteration of the Jacobi solver

We remark that $\eta^{18,100}_{\mathrm{sp}}$ in Figure 3.9 (on the right) dominates and is close to the total estimator in Figure 3.10 (on the left) that bound the norm $|||p-\tilde{p}_h^{18,100}|||_Y$ in (3.45) at time step 100. Finally, Figure 3.10 (on the right) shows the error between the exact

solution and the approximate solution $\{|||p-\tilde{p}_{h\tau}^{18}|||_X^2+||(p-\tilde{p}_{h\tau}^{18})(\cdot,T)||^2\}^{\frac{1}{2}}$ at the time step 100. We first remark that it is about 9.5e-5, which is smaller than the one of the total estimator in Figure 3.10 left (which is about 3.5e-4). The element contributions do not perfectly match with the total estimator, which may be due to the fact that the error $||\partial_t(p-\tilde{p}_{h\tau}^{k+1})||_{X'}$ in $|||p-\tilde{p}_{h\tau}^{k+1}|||_Y$ has not been computed.

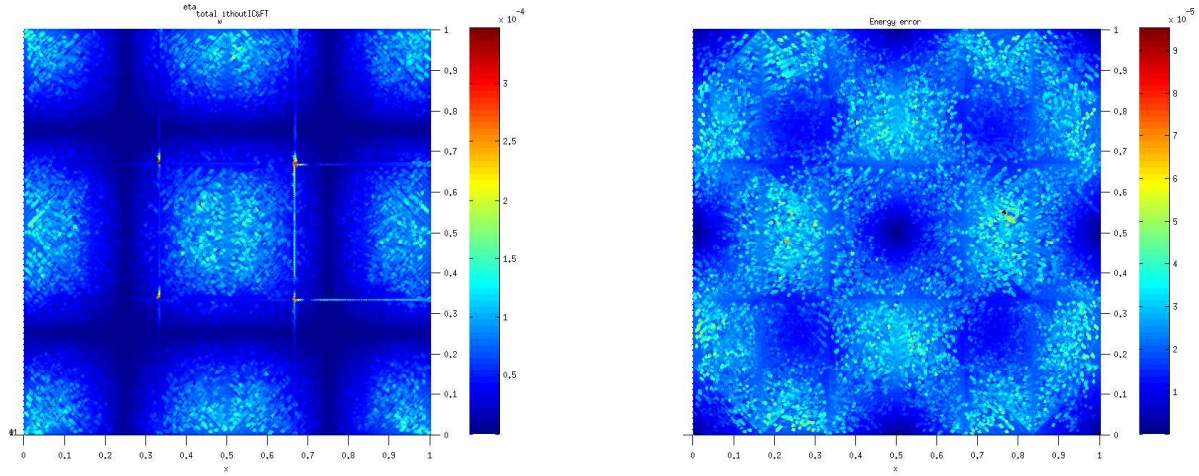

Figure 3.10: Distribution of the total estimator on Ω (on the left) and of the error between the exact solution and the approximate solution (on the right) at the final time step 100 and at the 18th iteration of the Jacobi solver

3.9.2 Model example with the GMRES solver

Number of triangles in Ω	76888
Number of subdomains	9
Subdomain solver	Direct
DD solver	GMRES
Final time	$T=1$
Time step τ	1/100
Original DD stopping criterion	1e-6
A posteriori stopping criterion	$\eta_{\text{DD}} \leq 0.1\max(\eta_{\text{tm}},\eta_{\text{sp}})$
Total number of iterations	41
Number of iterations with an a posteriori stopping criterion	13
Unnecessary iterations	28
Spared iteration from the total number of iteration	$\approx$ 68 %

Table 3.2: Example with the GMRES solver

We consider here the same example as in Section 3.9.1 but using the GMRES solver, see Table 3.2. We fix the original DD stopping citerion at 1e-6 as before in the Jacobi example. Note that the GMRES solver converges faster than the Jacobi solver, as shown in Figure 3.11. We remark that η_{DD} dominates up to roughly 7 iterations and then gets smaller compared to the discretization and time estimators.

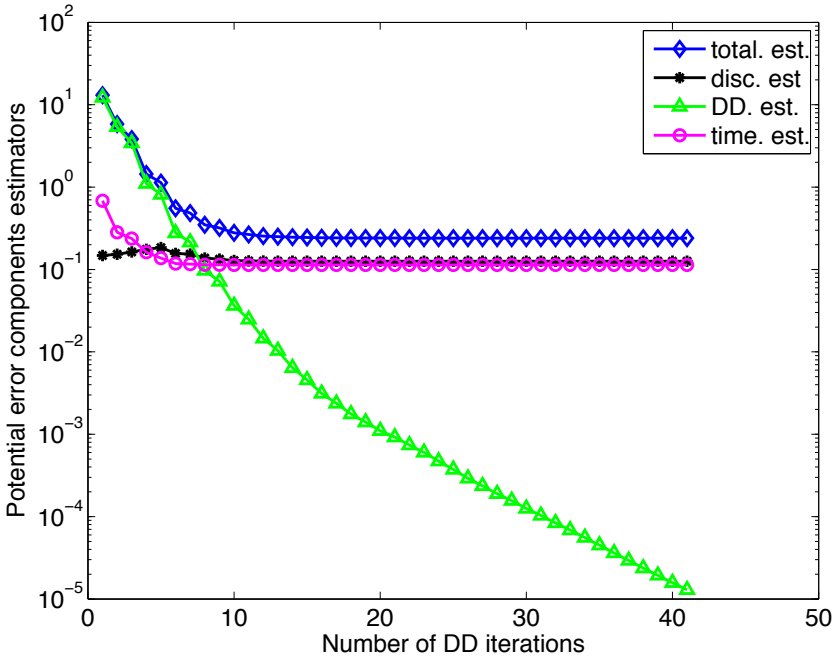

Figure 3.11: Error component estimates with the GMRES solver

Here, we can stop the DD algorithm at iteration 13 when $\eta_{\mathrm{DD}} \leq 0.1 \max(\eta_{\mathrm{tm}}, \eta_{\mathrm{sp}})$, thereby avoid 28 unnecessary iterations, whereas for the Jacobi solver the algorithm is stopped at iteration 18. Thus, we can save another 5 iterations compared to the Jacobi solver.

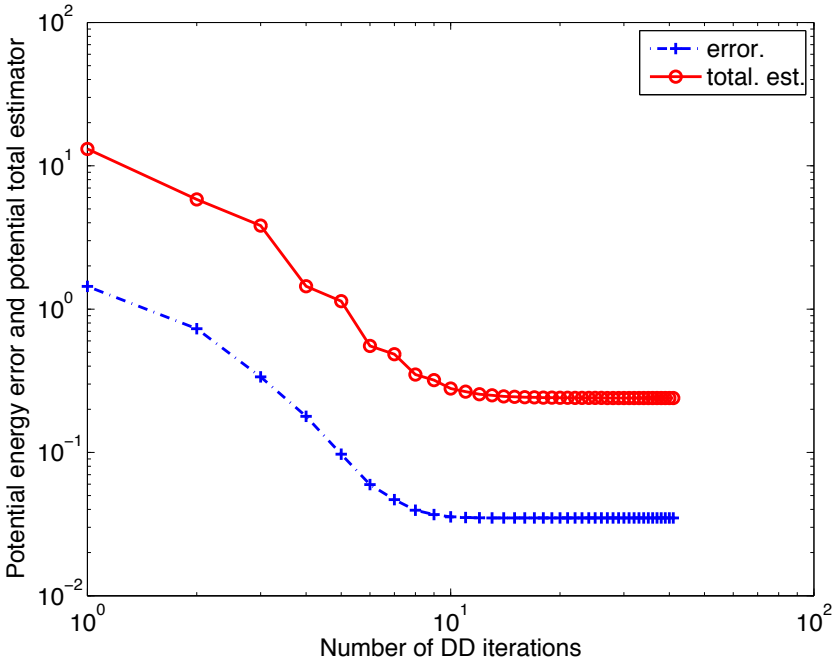

Figure 3.12: Energy error and total estimator with the GMRES solver

In Figure 3.12, we show the energy error and the total estimator versus the num-

ber of iterations. The effectivity index is represented in Figure 3.13 and reaches approximately the value 6.8 at the iteration 41 wheras its value is approximately 7.1 at iteration 13.

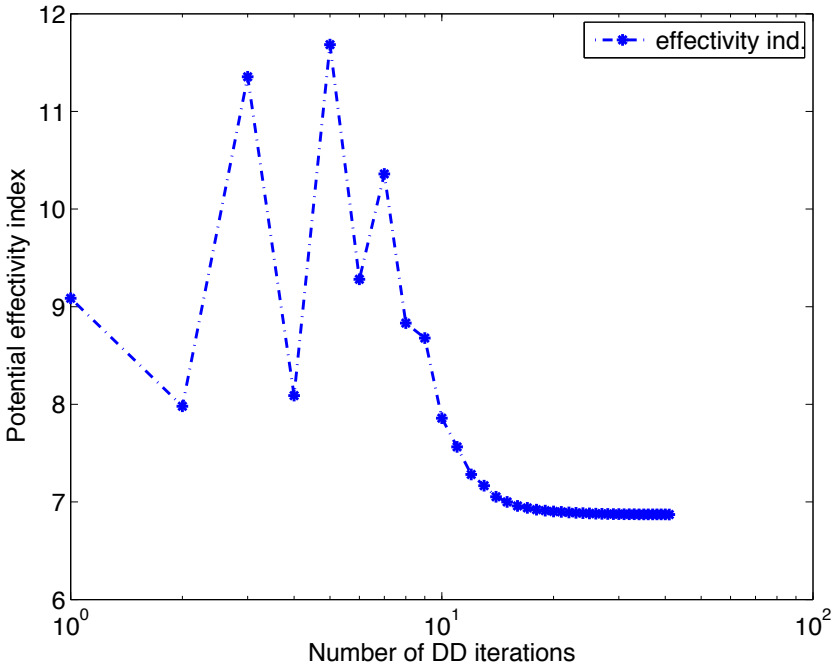

Figure 3.13: Effectivity index with the GMRES solver

3.9.3 Example in an industrial context using conforming time grids

This example, given by ANDRA (see also [95]), is a simplified version of a problem which simulates the transport of contaminant in and around a nuclear waste repository site. The repository (yellow), where the nuclear waste is stored, is a 2950m by 10m rectangle located in the center of a clay domain of 3950m by 140m (light brown), see Figure 3.14 (not to scale). In this example, we consider a more general time-dependent diffusion problem with a discontinuous porosity, $\phi \neq 1$, so the equation is as follows:

$$\mathbf{u} = -\boldsymbol{S}\nabla p \quad \text{in} \quad \Omega \times (0,T), \tag{3.99a}$$

$$\phi \frac{\partial p}{\partial t} + \nabla \cdot \mathbf{u} = f \qquad \text{in} \quad \Omega \times (0,T), \tag{3.99b}$$

where $\Omega = [0,3950] \times [0,140]$, p represents the concentration of the contaminant, f is the source term, ϕ is the porosity, and $\boldsymbol{S}$ is the time-independent diffusion tensor. The initial condition is $p_0 = 0$ and we set homogeneous Dirichlet conditions on the top and the bottom of Ω, and homogeneous Neumann conditions on the other sides of $\partial\Omega$. We decompose Ω into nine subdomains where Ω_5 is the nuclear waste repository domain, see Figure 3.15. For this simulation, we are interested in the long-term behavior of the repository, i.e. over one million years: T=10^6 years. The porosity in Ω is as follows:

$$\phi = \begin{cases} 0.2 & \text{in } \Omega_5, \\ 0.05 & \text{in } \Omega_i, \ i \neq 5, \end{cases} \tag{3.100}$$

the diffusion tensor is:

$$\boldsymbol{S} = \begin{cases} 210^{-9}\boldsymbol{I}\ \mathrm{m}^2/\mathrm{s} & \text{in } \Omega_5, \\ 510^{-12}\boldsymbol{I}\ \mathrm{m}^2/\mathrm{s} & \text{in } \Omega_i,\ i \neq 5, \end{cases} \tag{3.101}$$

where $\boldsymbol{I}$ is the identity matrix, and the source term f is zero in the clay layer and

$$f = \begin{cases} 10^{-5}\text{years}^{-1} & \text{if } t \leq 10^5 \text{ years}, \\ 0 & \text{if } t > 10^5 \text{ years}, \end{cases} \quad \text{in the repository.} \tag{3.102}$$

In order to solve our problem easily, we write the dimensionless form of (3.99).

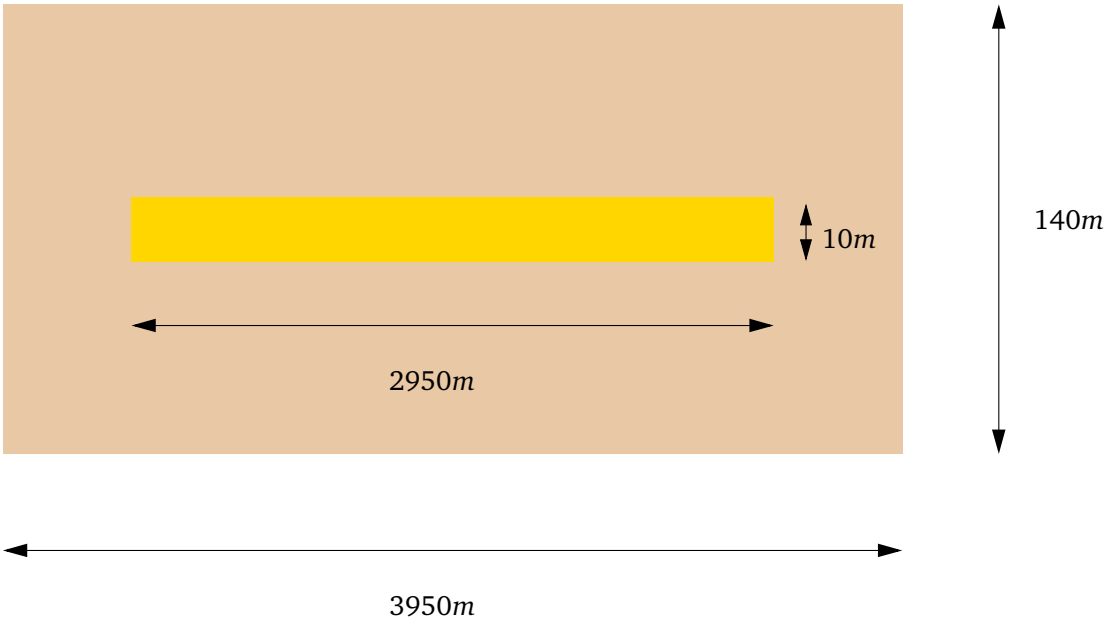

Figure 3.14: Geometry of the nuclear waste repository (yellow) and the clay layer around it (light brown)

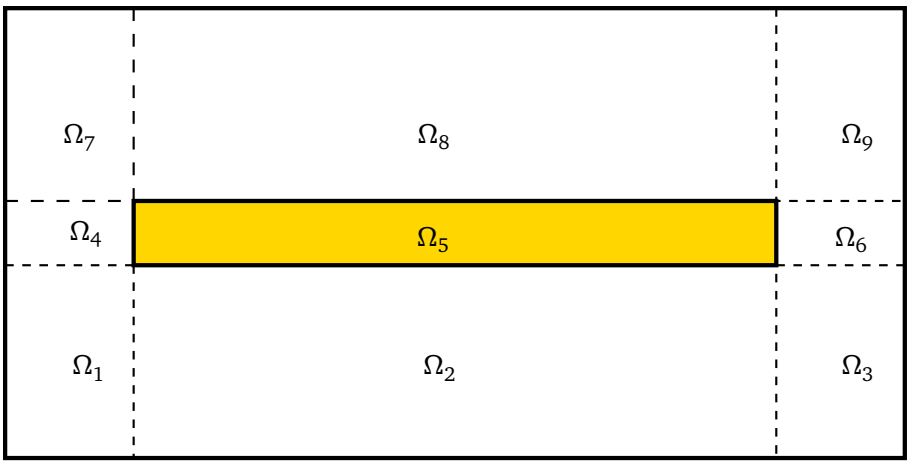

Figure 3.15: The decomposition of the domain Ω into 9 subdomains

Remark 3.9. *Let (3.99) be the equation defined in $\Omega \times [0,T]$, where $\Omega = [0,X] \times [0,Y]$ and where $\boldsymbol{S}$ is a diagonal matrix:*

$$\begin{bmatrix} \boldsymbol{S}_x & 0 \\ 0 & \boldsymbol{S}_y \end{bmatrix} \tag{3.103}$$

Equations (3.99) can be written now as follows:

$$\mathbf{u} = -\left[\boldsymbol{S}_x \frac{\partial p}{\partial x}, \boldsymbol{S}_y \frac{\partial p}{\partial y}\right] \quad in \quad \Omega \times (0,T), \tag{3.104a}$$

$$\phi \frac{\partial p}{\partial t} + \nabla \cdot \mathbf{u} = f \quad in \quad \Omega \times (0,T), \tag{3.104b}$$

where $\nabla \cdot \mathbf{u} = -\boldsymbol{S}_x \frac{\partial^2 p}{\partial x^2} - \boldsymbol{S}_y \frac{\partial^2 p}{\partial y^2}$. We choose characteristic lengths L in x and H in y, a characteristic time t_c, and a characteristic pressure P. The dimensionless variables are:

$$\tilde{x} = \frac{x}{L}, \qquad \tilde{y} = \frac{y}{H}, \qquad \tilde{t} = \frac{t}{t_c}, \tag{3.105}$$

so that

$$\frac{\partial}{\partial x} = \frac{\partial}{\partial \tilde{x}} \frac{\partial \tilde{x}}{\partial x} = \frac{1}{L} \frac{\partial}{\partial \tilde{x}} \quad and \quad \frac{\partial^2}{\partial x^2} = \frac{1}{L^2} \frac{\partial^2}{\partial \tilde{x}^2}, \tag{3.106a}$$

$$\frac{\partial}{\partial y} = \frac{\partial}{\partial \tilde{y}} \frac{\partial \tilde{y}}{\partial y} = \frac{1}{H} \frac{\partial}{\partial \tilde{y}} \quad and \quad \frac{\partial^2}{\partial y^2} = \frac{1}{H^2} \frac{\partial^2}{\partial \tilde{y}^2}, \tag{3.106b}$$

$$\frac{\partial}{\partial t} = \frac{\partial}{\partial \tilde{t}} \frac{\partial \tilde{t}}{\partial t} = \frac{1}{t_c} \frac{\partial}{\partial \tilde{t}}. \tag{3.106c}$$

Thus, (3.99) becomes:

$$\mathbf{u} = -\left[\frac{\boldsymbol{S}_x}{L} \frac{\partial p}{\partial \tilde{x}}, \frac{\boldsymbol{S}_y}{H} \frac{\partial p}{\partial \tilde{y}}\right] \quad in \quad \Omega \times (0, \frac{T}{t_c}), \tag{3.107a}$$

$$\phi \frac{\partial p}{\partial \tilde{t}} + t_c \nabla \cdot \mathbf{u} = t_c f \quad in \quad \Omega \times (0, \frac{T}{t_c}), \tag{3.107b}$$

where $\nabla \cdot \mathbf{u} = -\tilde{\boldsymbol{S}}_x \frac{\partial^2 p}{\partial \tilde{x}^2} - \tilde{\boldsymbol{S}}_y \frac{\partial^2 p}{\partial \tilde{y}^2}$, with $\tilde{\boldsymbol{S}}_x = \frac{\boldsymbol{S}_x}{L^2}$ and $\tilde{\boldsymbol{S}}_y = \frac{\boldsymbol{S}_y}{H^2}$.

To cope with the anisotropy of the domain, as well as a better visualization of the solution and the error distribution in the estimators, we decide to choose $L = 14$, $H = 1$, whereas $t_c = 1$ years $\approx 3.16e^7$ s. Figure 3.16 shows an example of the discretization in space for $\Omega = [0, \frac{3950}{14}] \times [0, 140]$, where the refinement in and around the subdomain Ω_5 containing the nuclear waste, is high compared to the other domains. In our example, the number of triangles in Ω is 106638, see Table 3.3. For the time discretization, we use a conforming time grids with $\tau^n = 4000$ years, $\forall n = 1, ..., N$, and for all Ω_i, $i = 1, ..., 9$. In Figure 3.17, the evolution of the solution at the iteration 44, when the original DD stopping criterion is 1e-8, is presented at different times. We remark that the contaminant slowly migrates from the repository, with a blow up in the y-direction, to the area arround Ω_5. Moreover, its concentration increases until injection stops (i.e. after 1e5 years) and then decreases.

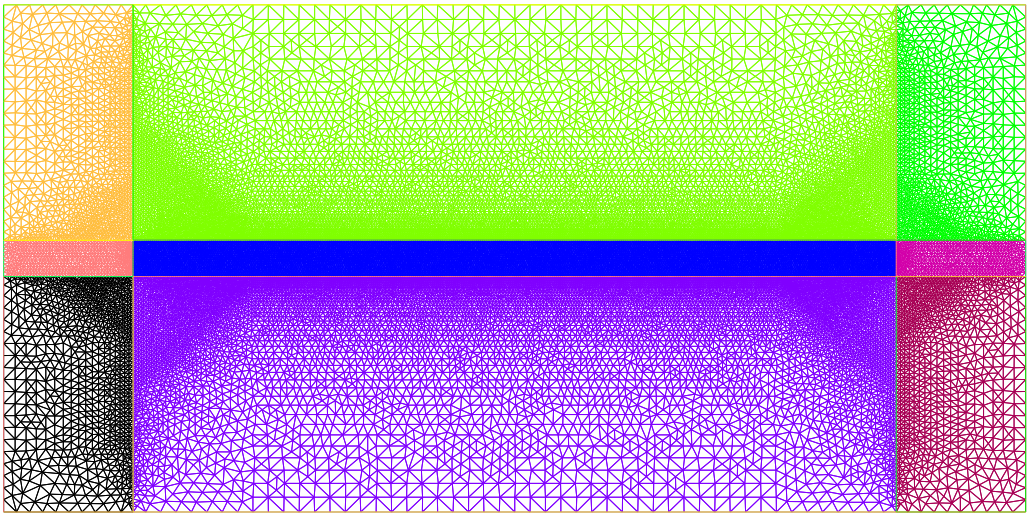

Figure 3.16: Example of a discretization used in and around a nuclear waste repository site

A posteriori estimates

Figure 3.18 shows the evolution of η_{DD} in green, η_{sp} in black, η_{tm} in magenta, and their sum in blue as a function of the number of iterations of the global-in-time DD method with the GMRES solver. These estimators are computed every 6 iterations to decrease the computational cost. We remark that η_{DD} dominates until iteration 5 and then decreases and reaches 1e-6 at iteration 44. As shown in Figure 3.18, η_{sp} and η_{tm} are roughly constant after iteration 7 and until the iteration 44. An a posteriori stopping criterion of this iterative method is when $\eta_{\mathrm{DD}} \leq \gamma \max(\eta_{\mathrm{tm}}, \eta_{\mathrm{sp}})$, $\gamma \approx 0.1$, i.e., at iteration 11. Note that, for this example, the effectivity index is not computed because the exact solution p is unknown.

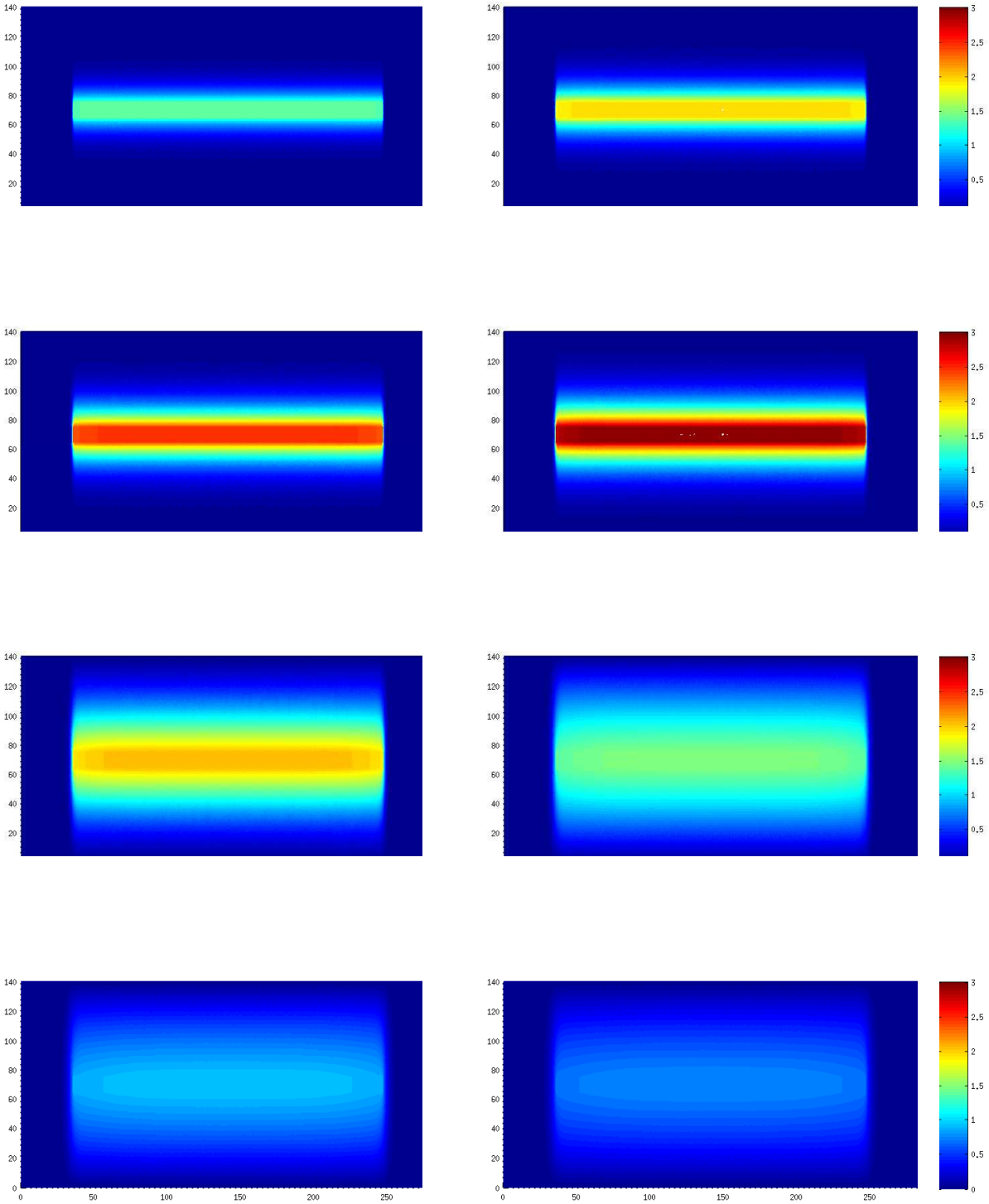

Figure 3.17: Domain decomposition solution after 20000, 60000, 80000, 100000, 200000, 400000, 800000, and 1000000 years going from the left to the right and from the top to the bottom

Number of triangles in Ω	106638
Number of subdomains	9
Subdomain solver	Direct
DD solver	GMRES
Final time	T=1e6
Time step τ	1e6/250 = 4000
Original DD stopping criterion	1e-8
A posteriori stopping criterion	$\eta_{\mathrm{DD}} \leq 0.1 \max(\eta_{\mathrm{tm}}, \eta_{\mathrm{sp}})$
Total number of iterations	44
Number of iterations with an a posteriori stopping criterion	11
Unnecessary iterations	33
Spared iteration from the total number of iteration	$\approx$ 75 %

Table 3.3: Industrial example with the GMRES solver

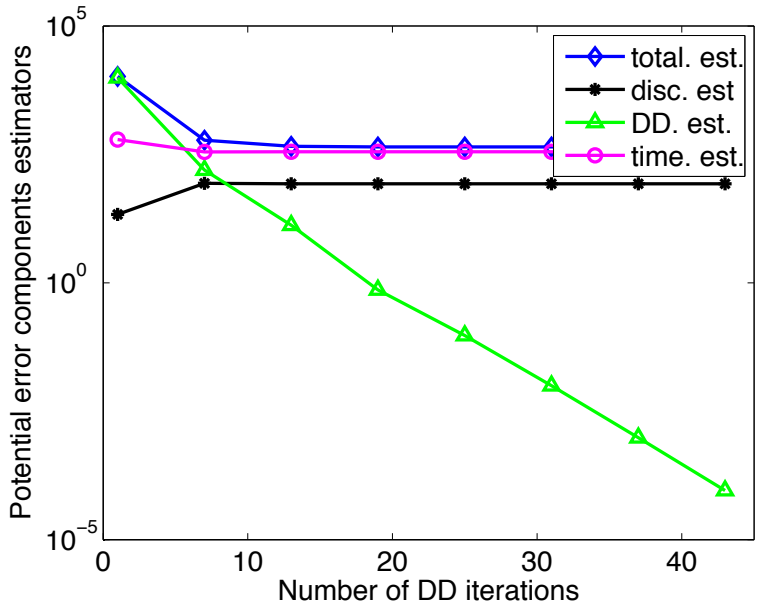

Figure 3.18: Error component estimates of the industrial example with the GMRES solver

Figures of DD and total error estimators at the final time 1e6 and at iterations 11 and 44 of the DD GMRES solver

At iteration 11 of the DD solver, corresponding to the a posteriori stopping criterion, the error contributions of the elements of η_{DD} in Figure 3.19 (on the left) are distributed on the interfaces but still have a non-negligible influence on the total estimator in Figure 3.19 (on the right). At iteration 44, the error contributions of the elements of η_{DD} in Figure 3.20 (on the left) are very small and do not have any noticeable influence on the total estimator in Figure 3.20 (on the right).

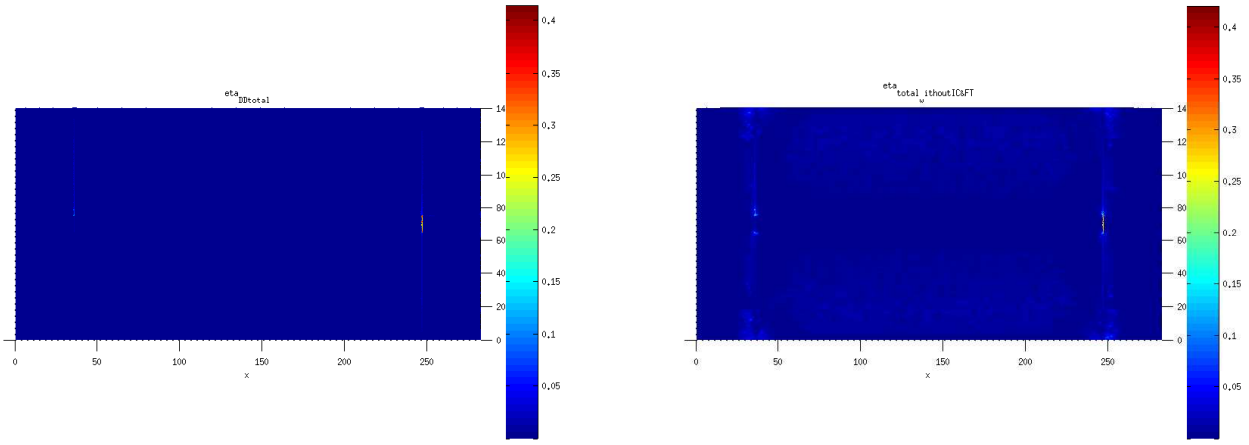

Figure 3.19: Distribution of $\eta_{\mathrm{DD}}^{11,250}$ on Ω (on the left) and the total estimator (on the right) at the final time step 250 (i.e. T=1e6) and at iteration 11 of the GMRES solver

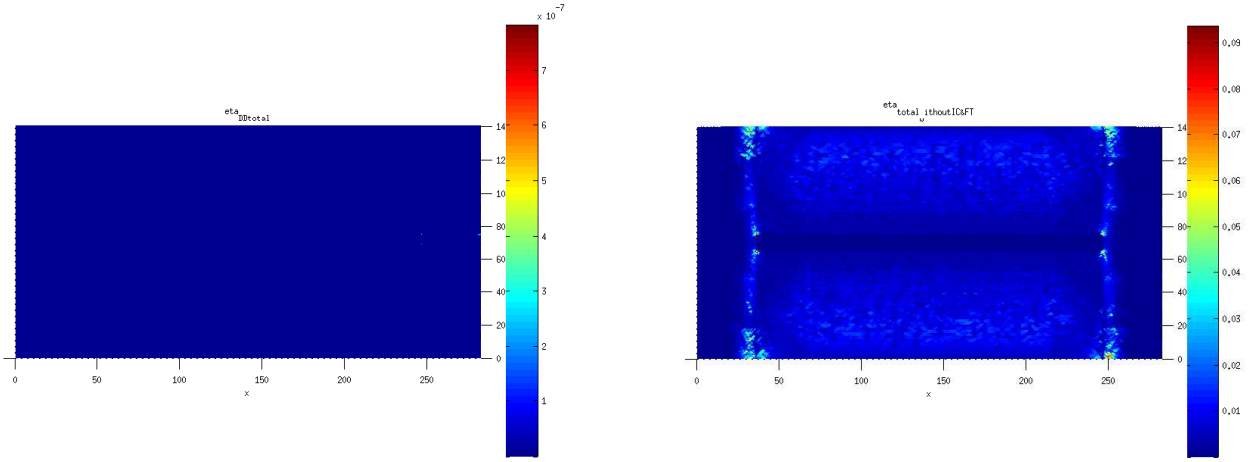

Figure 3.20: Distribution of $\eta_{\mathrm{DD}}^{44,250}$ on Ω (on the left) and the total estimator (on the right) at the final time step 250 (i.e. T=1e6) and at iteration 44 of the GMRES solver

3.10 Global-in-time domain decomposition using nonconforming time grids

The domain decomposition method presented in the previous section is global in time. Thus, it enables the use of different time discretizations in the subdomains based on L^2 projections in time [26, 29, 74, 92, 93, 95]. The time projection between subdomains is obtained by a projection algorithm with linear complexity and without any additional grid, see [77, 78].
For $i \in [\![1, \mathcal{N}]\!]$, let $\{t^{n,i}\}_{0 \leq n \leq N_i}$ be a sequence of discrete times of the subdomain Ω_i such that:

$$t^{0,i} = 0 < t^{1,i} < \cdots < t^{n,i} < \cdots < t^{N_i-1,i} < t^{N_i,i} = T.$$

Let $\mathscr{T}_{\tau,i}$ be the partition of the time interval $(0,T)$ into subintervals $I_{n,i} := (t^{n-1,i}, t^{n,i}]$ where $\tau^{n,i} := t^{n,i} - t^{n-1,i}$ for all $1 \le n \le N_i$. Here the partition $\mathscr{T}_{\tau,i}$ of Ω_i is possibly different from the partition $\mathscr{T}_{\tau,j}$ of the neighboring subdomain, $j \in B^i$, see Figure 3.21.

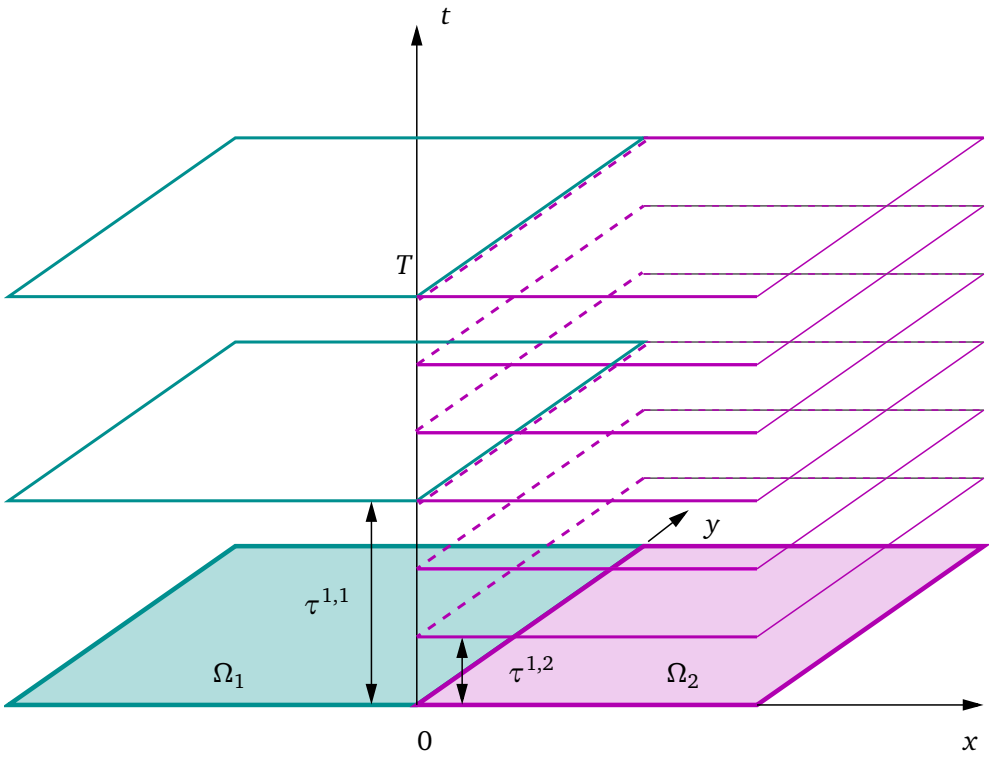

Figure 3.21: Nonconforming time grids for Ω_1 and Ω_2

Let $P^0_{\mathscr{T}_{\tau,i}}(L^2(\Gamma))$, $1 \le i \le \mathscr{N}$, be the space of piecewise constant functions in time on grid $\mathscr{T}_{\tau,i}$ with values on $L^2(\Gamma)$:

$$P^0_{\mathscr{T}_{\tau,i}}(L^2(\Gamma)) = \{\phi_\tau : (0,T) \to L^2(\Gamma),\ \ \phi_\tau \text{ is constant on } I_{n,i},\ \ \forall 1 \le n \le N_i\}. \quad (3.108)$$

Let $\Pi_{i,j}$ be the L^2 projection from $P^0_{\mathscr{T}_{\tau,j}}(L^2(\Gamma))$ onto $P^0_{\mathscr{T}_{\tau,i}}(L^2(\Gamma))$, i.e. for the given interface Γ, for $\phi_\tau \in P^0_{\mathscr{T}_{\tau,j}}(L^2(\Gamma))$, $(\Pi_{i,j}\phi_\tau)|_{I_{n,i}}$ is the average value of ϕ_τ on $I_{n,i}$, for $n = 1, ..., N_i$:

$$(\Pi_{i,j}\phi_\tau)|_{I_{n,i}} = \frac{1}{|I_{n,i}|} \sum_{l=1}^{N_j} \int_{I_{l,j} \cap I_{n,i}} \phi_\tau. \quad (3.109)$$

The semi-discrete counterpart in time of (3.9) with possibly different time grids in the subdomains can be written as follows:

Find $(\xi_{\tau,1}, \ldots, \xi_{\tau,\mathscr{N}}) \in L_{\mathscr{T}_{\tau,1}} \times \ldots \times L_{\mathscr{T}_{\tau,\mathscr{N}}}$, where $L_{\mathscr{T}_{\tau,i}} = P^0_{\mathscr{T}_{\tau,i}}\left(\prod_{j \in B^i} L^2(\Gamma_{i,j})\right)$ such that:

For $\boldsymbol{\xi}_{\tau,i} = \left(\xi_{\tau,i,j}\right)_{j\in B^i}$ where $\xi_{\tau,i,j} \in P^0_{\mathscr{T}_{\tau,i}}(L^2(\Gamma_{i,j}))$:

$$\left((\boldsymbol{\xi}_{\tau,i})_j - \Pi_{i,j}\left(\boldsymbol{S}_j^{\mathrm{RtR}}(\boldsymbol{\xi}_{\tau,j}, \boldsymbol{\mathscr{F}}_j)\right)_i\right)\Big|_{I_{n,i}} = 0, \quad \forall n = 1,...,N_i, \quad \forall j \in B^i, \quad \forall i \in [\![1,\mathscr{N}]\!]. \tag{3.110}$$

This space-time interface problem is solved by the Jacobi method or GMRES.

Remark 3.10. *In the case where the time grid is the same for all the subdomains, Π_{ij} is the identity operator and (3.110) reduces to (3.24). In the case of different time meshes in different subdomains, due to the use of projection operators, the discrete interface problem (3.110) is different from the problem in the conforming case (3.24). Applying the Jacobi method or GMRES (3.110) leads at convergence to a semi-discrete in time scheme which is different from the monodomain MFE scheme. This semi-discrete in time scheme is analyzed in [92, 93] where it is shown that the method preserves the order of the discontinuous Galerkin method. This result is shown numerically in the context of the MFE method in [95].*

For the sake simplicity, the Jacobi algorithm for solving (3.110) is presented below.

Local problem at iteration $k+1$ with nonconforming time grids

For the subdomain Ω_i, $\forall i \in [\![1,\mathscr{N}]\!]$, we introduce the following notations for $n = 1,..,N_i$:

$$\tilde{f}^{n,i} := \frac{1}{\tau^{n,i}}\int_{I_{n,i}} f(\cdot,t)\mathrm{d}t, \quad \tilde{g}_{\mathrm{D}}^{n,i} := \frac{1}{\tau^{n,i}}\int_{I_{n,i}} g_{\mathrm{D}}(\cdot,t)\mathrm{d}t, \text{ and } \quad \tilde{g}_{\mathrm{N}}^{n,i} := \frac{1}{\tau^{n,i}}\int_{I_{n,i}} g_{\mathrm{N}}(\cdot,t)\mathrm{d}t$$

The fully discrete problem at iteration $k+1$, in the subdomain Ω_i, $\forall i \in [\![1,\mathscr{N}]\!]$, is:

Find $\mathbf{u}_{h,i}^n \in \mathbf{W}_{h,i}^{\tilde{g}_{h,\mathrm{N}}^{n,i}}$ and $p_{h,i}^n \in M_{h,i}$ on the interval $I_{n,i}$, for $n = 1,..,N_i$, such that:

$$\mathbf{a}_i(\mathbf{u}_{h,i}^{k+1,n}, \mathbf{v}_{h,i}) - \mathbf{b}_i(\mathbf{v}_{h,i}, p_{h,i}^{k+1,n}) = \tilde{\boldsymbol{\ell}}_i^{k,n}(\mathbf{v}_{h,i}), \ \forall \mathbf{v}_{h,i} \in \mathbf{W}_{h,i}^0, \tag{3.111a}$$

$$(p_{h,i}^{k+1,n}, q_{h,i})_{\Omega_i} + \tau^{n,i}\mathbf{b}_i(\mathbf{u}_{h,i}^{k+1,n}, q_{h,i}) = \tau^{n,i}(\tilde{f}^n, q_{h,i})_{\Omega_i} + (p_{h,i}^{k+1,n-1}, q_{h,i})_{\Omega_i}, \ \forall q_{h,i} \in M_{h,i}, \tag{3.111b}$$

$$\left(p_{h,i}^{k+1,0}, q_{h,i}\right)_{\Omega_i} = (p_0, q_{h,i}), \ \forall q_{h,i} \in M_i, \tag{3.111c}$$

where the linear form $\tilde{\boldsymbol{\ell}}_i^{k,n}$ is defined as:

$$\tilde{\boldsymbol{\ell}}_i^{k,n} : \mathbf{W}_{h,i}^0 \longmapsto \mathbb{R}, \quad \tilde{\boldsymbol{\ell}}_i^{k,n}(\mathbf{v}_{h,i}) = -\langle \tilde{g}_{\mathrm{D}}^{n,i}, \mathbf{v}_{h,i}\cdot\boldsymbol{n}_i\rangle_{\Gamma_i^{\mathrm{D}}} - \sum_{j\in B^i}\Pi_{i,j}\langle \tilde{g}_{\mathrm{R},\tau,j}^k, \mathbf{v}_{h,i}\cdot\boldsymbol{n}_i\rangle_{\Gamma_{i,j}}\Big|_{I_{n,i}}. \tag{3.112}$$

For the first iteration, $\tilde{g}_{\mathrm{R},\tau,j}^0$ is a given initial guess on $\Gamma_{i,j}$, $j \in B^i$, $i = 1,...,\mathscr{N}$, and for iterations $k \geq 1$ and for $e' \in \Gamma_{i,j}$:

$$\Pi_{i,j}\langle \tilde{g}_{\mathrm{R},\tau,j}^k, \psi_{e'}\cdot\boldsymbol{n}_i\rangle_{\Gamma_{i,j}}\Big|_{I_{n,i}} =$$

$$\sum_{m=1}^{N_j}\Pi_{i,j}\left(\int_{\Gamma_{i,j}}\beta_{i,j}(\mathbf{u}_{h,j}^{k,n}\cdot\boldsymbol{n}_j)\psi_{e'}\cdot\boldsymbol{n}_i\,\mathrm{d}\gamma + \int_{\Gamma_{i,j}}(\beta_{j,i}\mathbf{u}_{h,j}^{k,n}\cdot\boldsymbol{n}_j + \Pi_{j,i}\tilde{g}_{\mathrm{R},\tau,i}^{k-1})\mathrm{d}\gamma\right)\Big|_{I_{n,i}\cap I_{m,j}},$$

and equal to zero when $e' \notin \Gamma_{i,j}$.

3.11 A posteriori error estimates for nonconforming time grids

At the iteration $k+1$ of the DD algorithm using different time grids, we obtain $\forall i \in [\![1, \mathcal{N}]\!]$ the couple $(p_{h,i}^{k+1,n}, \mathbf{u}_{h,i}^{k+1,n})$ at each time step $t^{n,i}$, $1 \leq n \leq N_i$. Here, $t^{n,i} \neq t^{n,j}$ for $j \in B^i$ in general. We actually suppose that we treat a situation as in Figure 3.21, i.e., the time grids in the individual subdomains are not completely independent but rather stem from subrefinement of some common time grid. Thus, the couples $(p_{h,i}^{k+1,n}, \mathbf{u}_{h,i}^{k+1,n})$ for $1 \leq n \leq N_i$ are not approximations at the same times as $(p_{h,j}^{k+1,n}, \mathbf{u}_{h,j}^{k+1,n})$, $1 \leq n \leq N_j$. Thus, we cannot immediately build the potential, subdomain potential, and flux reconstructions at each time step in order to use the a posteriori estimates of Theorem 3.6 introduced in the case of conforming time grids.

To adapt the present methodology to this case as well, we first need to introduce some new notation. Let $\{t_{\text{new}}^n\}_{0 \leq n \leq N_{\text{new}}}$ be the sequence of discrete times, for all Ω_i $i \in [\![1, \mathcal{N}]\!]$, such that:

$$t_{\text{new}}^0 = 0 < t_{\text{new}}^1 < \cdots < t_{\text{new}}^n < \cdots < t_{\text{new}}^{N_{\text{new}}} = T.$$

This new sequence is defined as follows:

$$\{t_{\text{new}}^n\}_{0 \leq n \leq N_{\text{new}}} = \bigcup_{i=1}^{\mathcal{N}} \{t^{n,i}\}_{0 \leq n \leq N_i}. \tag{3.113}$$

We will call $\mathcal{T}_{\tau,\text{new}}$ the partition of the time interval $(0,T)$ into subintervals $I_{n,\text{new}} := (t_{\text{new}}^{n-1}, t_{\text{new}}^n]$ and where $\tau^{n,\text{new}} := t_{\text{new}}^n - t_{\text{new}}^{n-1}$ for all $1 \leq n \leq N_{\text{new}}$. We then construct the potential and the flux for the subdomain Ω_i at each time step t_{new} which is not defined in the $\{t^{n,i}\}_{0 \leq n \leq N_i}$ as follows:
We first compute the number R of the new time step between $t^{n-1,i}$ and $t^{n,i}$. Let $t_{\text{new}}^{m-1} = t^{n-1,i}$ and $t_{\text{new}}^{m+R} = t^{n,i}$ be the two successive time steps in $\{t^{n,i}\}_{0 \leq n \leq N_i}$ where the couples $(p_{h,i}^{k+1,m-1}, \mathbf{u}_{h,i}^{k+1,m-1})$ and $(p_{h,i}^{k+1,m+R}, \mathbf{u}_{h,i}^{k+1,m+R})$ are known.
We then compute the couple $(p_{h,i}^{k+1,m-1+r}, \mathbf{u}_{h,i}^{k+1,m-1+r})$ for $r = 1, .., R$ by:

$$\begin{aligned} \mathbf{u}_{h,i}^{k+1,m-1+r} &= \mathbf{u}_{h,i}^{k+1,m-1} + \frac{r}{R+1}(\mathbf{u}_{h,i}^{k+1,m+R} - \mathbf{u}_{h,i}^{k+1,m-1}), \\ p_{h,i}^{k+1,m-1+r} &= p_{h,i}^{k+1,m-1} + \frac{r}{R+1}(p_{h,i}^{k+1,m+R} - p_{h,i}^{k+1,m-1}). \end{aligned} \tag{3.114}$$

This construction of the potential and the flux is done on the union of nested grids. Note that this construction is easier to do than returning to the conforming time grids, applying the MFE at each time step, and then doing the constructions of potentials and flux.

Remark 3.11. *The construction of the potential and the flux in* (3.114) *is presented for nested grids. Note that* (3.114) *can be extended and adapted to the non-nested grids according to each case of the non-nested grids.*

We present in Figure 3.22 the case of two subdomains where we have just to construct the potential and the flux in the subdomain Ω_1. This figure presents the construction of the potential and the flux between $t_{\text{new}}^{m-1} = t^{n-1,i}$ and $t_{\text{new}}^{m+R} = t^{n,i}$ where

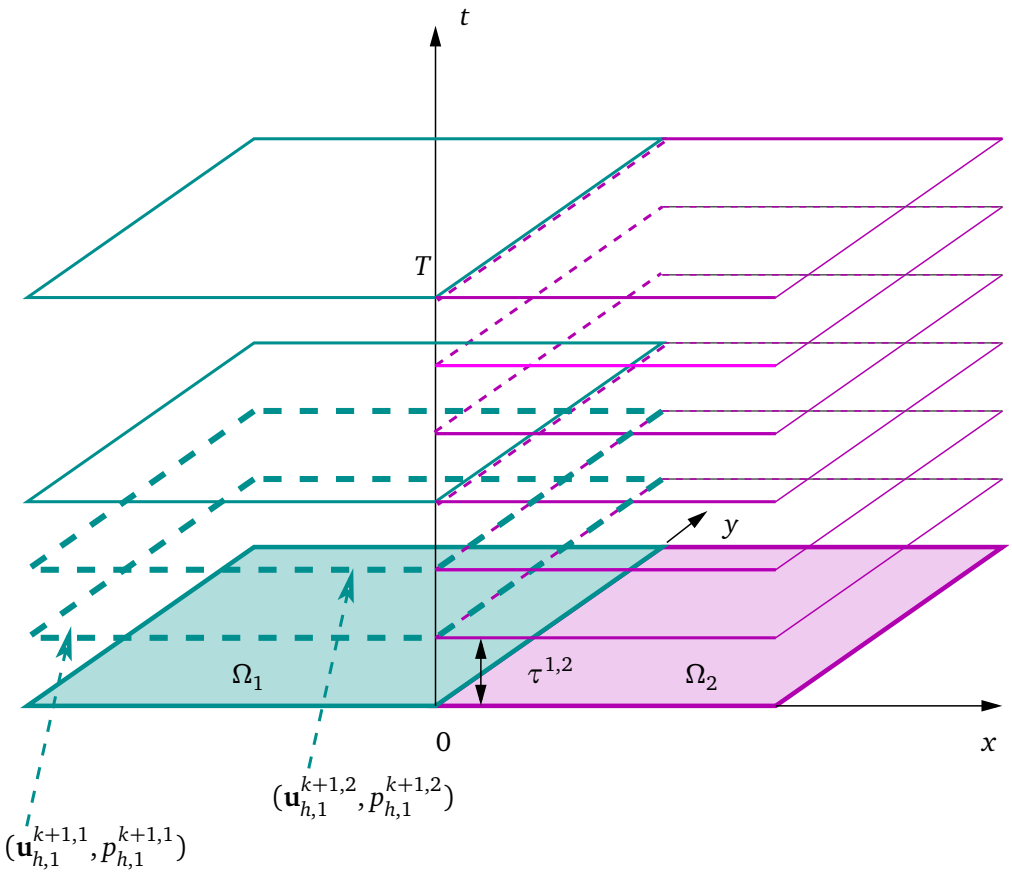

Figure 3.22: Construction of the potential and the flux between $t^{0,1}$ and $t^{1,1}$ in Ω_1 at the iteration $k+1$ of the DD algorithm

$m = 1$, $n = 1$ and $R = 2$. Then, Theorem 3.6 holds by replacing N by N_{new} in η_{sp}^{k+1}, η_{tm}^{k+1}, and η_{DD}^{k+1} (see (3.46) (3.47), and (3.48)):

$$|||p - \tilde{p}_{h\tau}^{k+1}|||_Y \leq \eta_{\text{sp}}^{k+1} + \eta_{\text{tm}}^{k+1} + \eta_{\text{DD,NC}_{\text{tm}}}^{k+1} + \eta_{\text{IC}}^{k+1} + ||f - \tilde{f}||_{X'} + ||s_h^{k+1,N_{\text{new}}} - \tilde{p}_h^{k+1,N_{\text{new}}}||, \tag{3.115}$$

where $\tilde{f}$ is defined as in 3.19 but in the new grid $\mathcal{T}_{\tau,\text{new}}$.

Here $\eta_{\text{DD,NC}_{\text{tm}}}$ is equal to the estimator η_{DD} defined in (3.48) in Theorem 3.6. This other notation of η_{DD} is given here because this estimator is not only a domain decomposition estimator, but it mixes the error due to the nonconformity discretization in time and the domain decomposition method. Indeed, $\eta_{\text{DF},1,b,K}^{k+1,n}$ given in (3.50c), which is part of $\eta_{\text{DD,NC}_{\text{tm}}}^{k+1,n}$, is the source of this new nonconformity discretization error in time. There is no reason for $\boldsymbol{\sigma}_h^{k+1,n}$ to converge to $\mathbf{u}_h^{k+1,n}$, as $\boldsymbol{\sigma}_h^{k+1,n}$ satisfies the local conservation (3.39) on each element K in space, but $\mathbf{u}_h^{k+1,n}$ in general not (the MFE scheme now faces the conformity of the temporal meshes).
Consequently, $\eta_{\text{DD,NC}_{\text{tm}}}$ can not reach an arbitrary small value since it is not only a DD estimator. It rather reaches a certain value and then becomes constant, see Figure 3.24. We choose an adaptative refinement in space and in time in order to obtain the curve of η_{tm} and η_{sp} close to each other. Thus, when $\eta_{\text{DD,NC}_{\text{tm}}}^{k+1,n}$ reaches a

values smaller than η_{tm} and η_{sp} we can stop the DD algorithm. In other word, an a posteriori stopping criterion is for example when $\eta_{\text{DD,NC}_{\text{tm}}} \leq 0.5\min(\eta_{\text{tm}}, \eta_{\text{sp}})$, as indicated in the numerical results below.

Remark 3.12. *At each time step n, $0 \leq n \leq N_{\text{new}}$, we now need to solve a well-posed local Neumann problem in each band, see Figure 3.23. This means that we can easily take into account different time grids on different subdomains, for the price of introducing a same time grid in the whole domain Ω where only local problems in the bands depicted in Figure 3.23 are solved.*

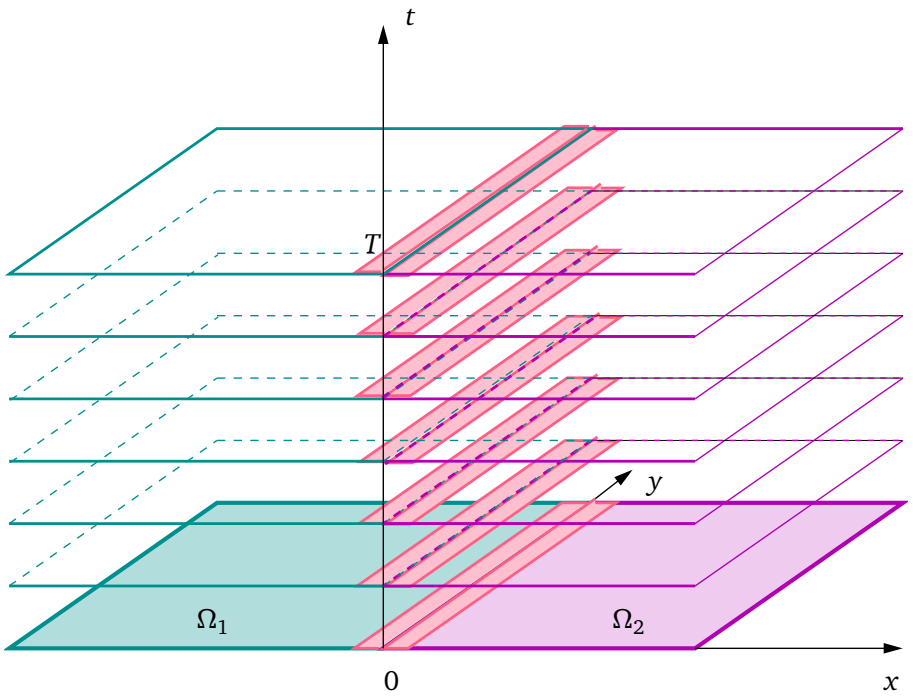

Figure 3.23: Bands in Ω_1 and Ω_2 at each time step

3.12 Numerical results

3.12.1 Example in an industrial context using nonconforming time grids

We take the same industrial example as in Section 3.9.3. Here, nonconforming time grids are used such that $\tau^{n,5} = 1000$ years in Ω_5 for all $1 \leq n \leq N_5 = 1000$ and $\tau^{n,i} = 5000$ years for all $1 \leq n \leq N_i = 200$, for $i \neq 5$. Here, the ratio of the time discretization between the subdomains $\dfrac{N_5}{N_i}$ is 5, for $i \neq 5$. The evolution of η_{DD} in green, η_{sp} in black, η_{tm} in magenta, and their sum in blue as a function of the number of iterations of the DD GMRES solver is presented in Figure 3.24. These estimators are computed every 9 iterations to decrease the calculation cost. We remark that η_{DD} dominates until iteration 8 and then decreases again until iteration 10, then becomes constant and stagnate. As shown in Figure 3.24, η_{sp} and η_{tm} are constant after iteration 7 and until the iteration 28. An a posteriori stopping criterion of this iterative method is when $\eta_{\text{DD}} \leq \gamma \min(\eta_{\text{tm}}, \eta_{\text{sp}})$, $\gamma \approx 0.5$, i.e., at iteration 11. A more detailed evolution of the estimators is given in Figure 3.25.

Number of triangles in Ω	34984
Number of subdomains	9
Subdomain solver	Direct
DD solver	GMRES
Final time	T=1e6
Time step $\tau^{n,i}$, $i \neq 5$	1e6/200 = 5000
Time step $\tau^{n,i}$, $i = 5$	1e6/1000 = 1000
Original DD stopping criterion	1e-6
A posteriori stopping criterion	$\eta_{\mathrm{DD}} \leq 0.5 \min(\eta_{\mathrm{tm}}, \eta_{\mathrm{sp}})$
Total number of iterations	28
Number of iterations with an a posteriori stopping criterion	10
Unnecessary iterations	18
Spared iteration from the total number of iteration	$\approx$ 64.2 %

Table 3.4: Industrial example with nonconforming time grids and using the GMRES solver

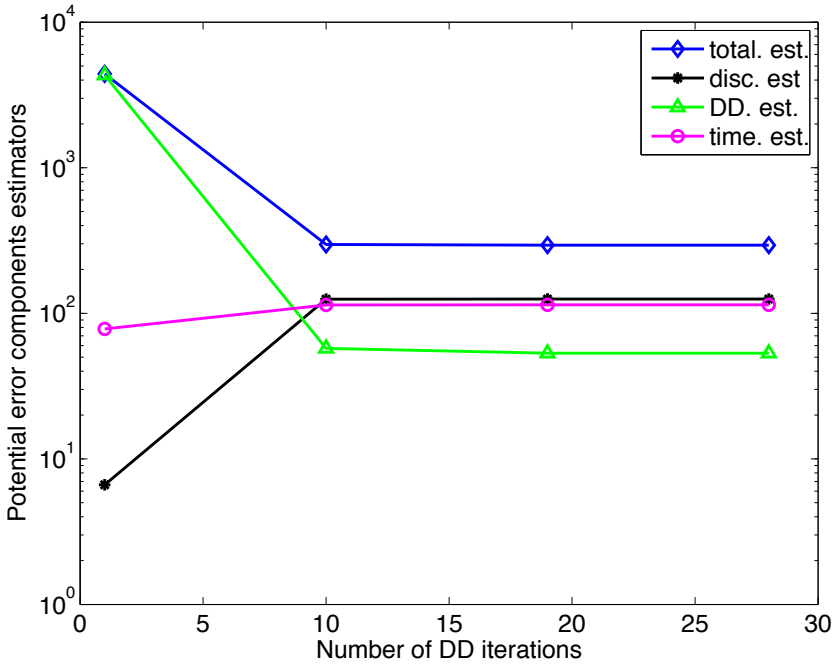

Figure 3.24: Error component estimates of the industrial example using different time grids and with the GMRES solver

Figure 3.26 presents the error contributions of the elements of $\eta_{\mathrm{DD,NC_{tm}}}$ at the final time T =1e6 years and at the iteration 11 of the DD algorithm. Then, Figure 3.27 presents the error contributions of the elements of $\eta_{\mathrm{DD,NC_{tm}}}$ at the final time T =1e6 years and at the iteration 28 of the DD algorithm. We remark that the error decreases slightly but the error still exit around the interfaces at the iteration 28. As explained before, $\eta_{\mathrm{DD,NC_{tm}}}$ now estimates simultaneously the error due to the domain decomposition and nonconforming time grids; in the first iterations, the DD part dominates, whereas later the nonconforming time grids part remains.

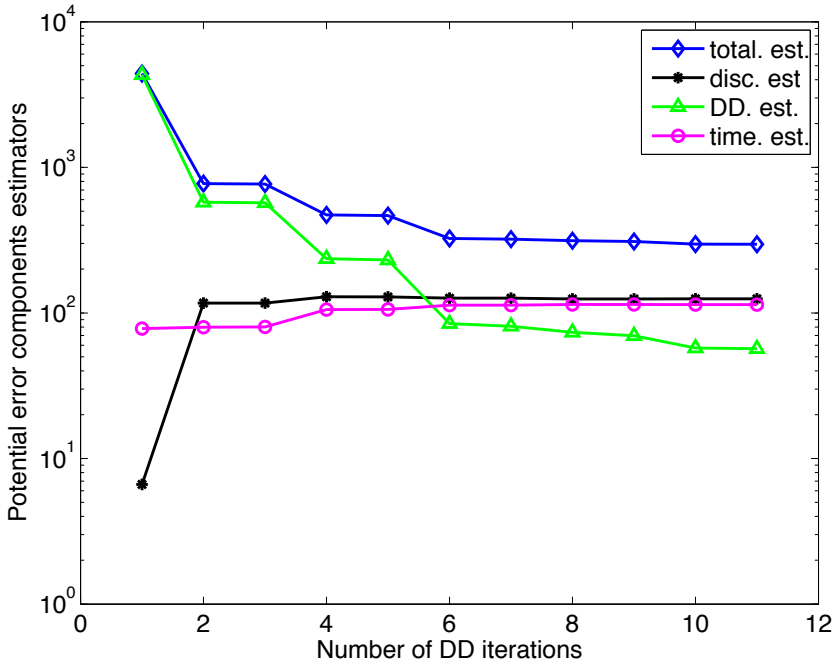

Figure 3.25: Zoom of Figure 3.24 until iteration 10 where the a posteriori stopping criterion is satisfied

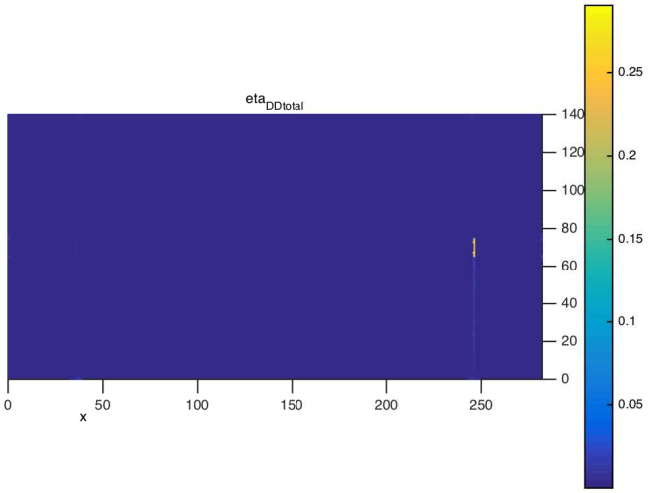

Figure 3.26: Distribution of $\eta_{\mathrm{DD,NC_{tm}}}$ on Ω at the final time T =1e6 years and at iteration 11 of the DD algorithm

To shed more light on the choice of nonconformity of the time grids, we plot in Figure 3.28, the error component estimates for different ratios of the time discretization between the central subdomain and the surrounding subdomains. Figure 3.28 illustrates the following ratios:

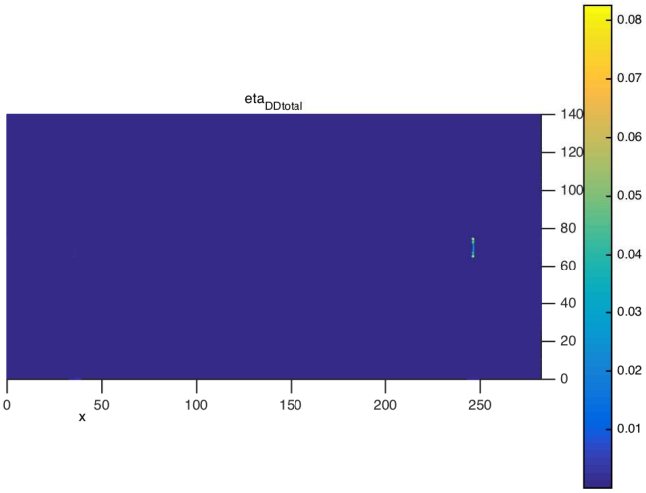

Figure 3.27: Distribution of $\eta_{\mathrm{DD,NC_{tm}}}$ on Ω at the final time T =1e6 years and at iteration 28 of the DD algorithm

- the ratio is $\dfrac{N_5}{N_i} = \dfrac{1000}{100} = 10$ in Figure 3.28 (top left),
- the ratio is $\dfrac{N_5}{N_i} = \dfrac{1000}{200} = 5$ in Figure 3.28 (top right),
- the ratio $\dfrac{N_5}{N_i} = \dfrac{1000}{250} = 4$ in Figure 3.28 (middle left),
- the ratio $\dfrac{N_5}{N_i} = \dfrac{400}{200} = 2$ in Figure 3.28 (middle right),
- the ratio is $\dfrac{N_5}{N_i} = \dfrac{250}{250} = 1$ in Figure 3.28 (bottom).

We can observe that in all cases, the discretization in space estimator (black) remains the same, which confirms numerically that it is indeed given by the space discretization error. The discretization in time estimator (magenta) goes up when the number of time steps in the central subdomain decreases; it is relatively stable otherwise. This confirms numerically both that it is connected with the time discretization error and that it is the number of time steps in the central subdomain that is the most important. Most importantly, the curve for $\eta_{\mathrm{DD,NC_{tm}}}$ estimator (green), goes down when the ratio decrease from 10 to 2 but for each ratio it becomes stable after a certain number of iteration. Finally, when the ratio is 1, we come back to the case of a conforming time grid, and, as expected, the green curve declines and decreases to a small value because no time discretization error is included in this curve. We can thus conclude it represents well the error from the time-nonconforming grids (in addition to the DD error) and that $\dfrac{N_5}{N_i} = 10$ is the highest reasonable nonconformity in time.

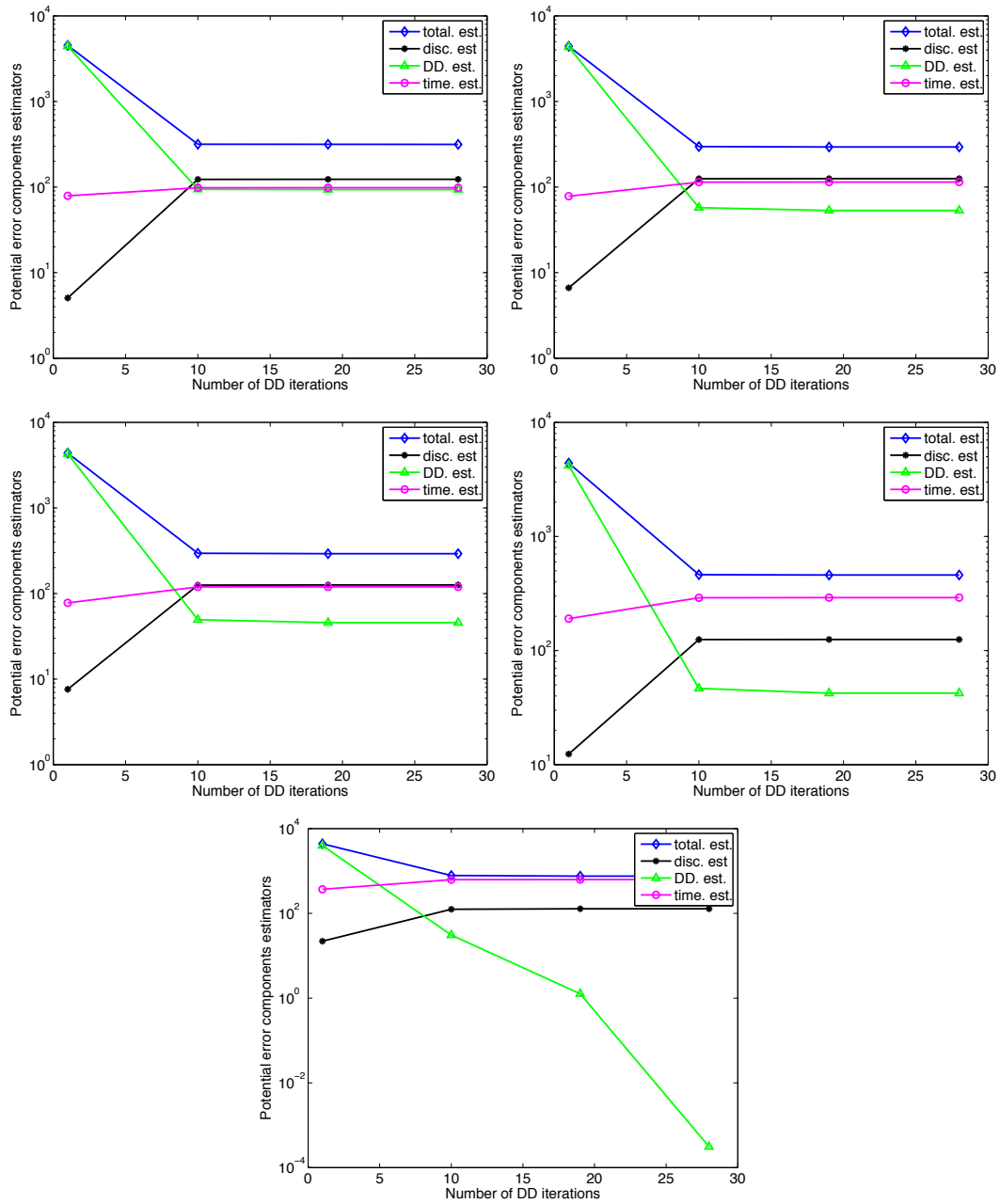

Figure 3.28: Error component estimates of the industrial example with the GMRES solver for different ratios discretization in time $\frac{N_5}{N_i}$, for $i \neq 5$: 10, 5, 4, 2, 1 starting from the left to the right and from the top to the bottom

Chapter 4

A posteriori error estimates and stopping criteria for space–time domain decomposition for two-phase flow between different rock types

Contents

Authors: Elyes Ahmed, Sarah Ali Hassan, Caroline Japhet, Michel Kern,

and Martin Vohralík

This work is the result of a collaboration that took place during the CEMRACS 2016. This work was supported by the French ANR DEDALES, Labex MME-DII, and the French Agency for Nuclear Waste Management (ANDRA). It also received funding from the European Research Council (ERC) under the European Union's Horizon 2020 research and innovation program (grant agreement No 647134 GATIPOR).

Abstract We consider two-phase flow in a porous medium composed of two different rock types, so that the capillary pressure field is discontinuous at the interface between the rocks. This is a nonlinear and degenerate parabolic problem with nonlinear and discontinuous transmission conditions on the interface. We first describe a space-time domain decomposition method based on the optimized Schwarz waveform relaxation algorithm (OSWR) with Robin or Ventcell transmission conditions. Full numerical approximation is achieved by a finite volume scheme in space and the backward Euler scheme in time. We then derive a guaranteed and fully computable a posteriori error estimate which in particular takes into account the domain decomposition error. Precisely, at each iteration of the OSWR algorithm and on each linearization step, the estimate delivers a guaranteed upper bound on an energy-type error between the exact and the approximate solution. Furthermore, to make the OSWR algorithm efficient, the different error components given by the spatial discretization, the temporal discretization, the linearization, and the domain decomposition are distinguished. These ingredients are then used to design a stopping criterion for the OSWR algorithm as well as for the linearization iterations, which together lead to important computational savings. Numerical experiments illustrate the efficiency of our estimates and the performance of the OSWR algorithm with adaptive stopping criteria on a model problem in three space dimensions. Additionally, the results show how a posteriori error estimates can help determine the free Robin or Ventcell parameters.

Keywords: two-phase Darcy flow, discontinuous capillary pressure, finite volume scheme, domain decomposition method, optimized Schwarz waveform relaxation,

Robin and Ventcell transmission conditions, linearization, a posteriori error estimate, stopping criteria

4.1 Introduction

Two-phase flows in porous media are of interest in a number of situations, such as CO2 sequestration in saline aquifers, description of oil reservoirs, or gas migration around a nuclear waste repository in the subsurface, where natural and engineered barriers are used to isolate the radionuclides and to slow down their release from the storage site into the environment. In fact, one of the problems encountered when designing nuclear waste repositories is that of gas produced from the corrosion of metallic components and from the nuclear waste itself. The numerical simulation of such flows is a challenging task, in particular because of the heterogeneity of the permeability, as well as the relative permeability and the capillary pressure that are functions of the saturation.

We consider in this paper a two-phase flow model introduced in [63] to study the phenomenon of oil or gas trapping in a porous medium with several rock types. This model, in which the convection is neglected, takes into account discontinuous capillary pressure functions across the interface between rock types. In particular, the existence of two different capillary pressure curves, discontinuous across the interface between the rock types, may play a role in preventing and isolating the radionuclide in the nuclear waste (see e.g. [151] and references therein). The effects of space-depending capillarities have been widely studied during the last years, see [63, 39, 41, 40, 35] for more details. The resulting problem is a nonlinear and degenerate parabolic equation for the saturation of the non-wetting phase, with nonlinear and discontinuous transmission conditions at the interface between the rocks. The numerical analysis of this problem has been considered in [63] for the model considered here, and in [35] for the full two-phase flow case. Existence of a weak solution was proved using the convergence of a finite volume scheme. In [39], Cancès proved the uniqueness of a weak solution for this model for a particular choice of functions characterizing the porous medium. In [41, 40], Cancès et al. proved the uniqueness of the full two-phase problem with convection terms in the one-dimensional case.

This model is formulated in [7] as a space-time transmission problem, which is solved with a non-overlapping space-time domain decomposition method. In the literature, few works exist for domain decomposition problems with jumping nonlinearities, although one can see for example [24, 25, 131] and the references therein. Domain decomposition methods for two phase flow problems were proposed in [163, 164], see also [81, 145, 146]. In such numerical approximations where the physics is quite complex, it is important to look at the quality of the resulting solution, as well as on the efficiency of the used algorithms. A practical tool is provided by a posteriori error estimates and adaptive stopping criteria for the different iterative methods involved in the calculation.

Some questions concerning a posteriori error estimates and stopping criteria in the context of Robin–Schwarz domain decomposition in combination with mixed finite element discretization for linear problems are treated in S. Ali Hassan's Ph.D. thesis [11]. Previous contributions include [20, 16, 106, 68] for general techniques taking into account inexact algebraic solvers, [130] for multiscale mortar techniques in a unified

treatment of various discretizations, [141, 140] for FETI and BDD algorithms combined with conforming finite element discretizations, and [46, 158, 42, 55] for a posteriori error estimates for two-phase flows, see also the reference therein. In these works, it is shown how a posteriori error estimates can distinguish between the various components of the error (space discretization, time discretization, domain decomposition, and the nonconformity error due to space-time domain decomposition with different time steps in the subdomains), thus leading to efficient stopping criteria for the (domain decomposition) iterations. To the best of our knowledge, contrarily to the case of linear problems, no results are available for a posteriori error estimates for the nonlinear problem with discontinuous transmission conditions.

The purpose of the present paper is threefold: first, to extend the work in [7] to a more general Schwarz method, with time-dependent Ventcell transmission conditions; second, to derive a posteriori error estimates for its finite volume–backward Euler approximation; and third, to address the question of when to stop the domain decomposition iterations as well as the iterations of the nonlinear solver used for the subdomain problems. With respect to the first point, our method is a space-time domain decomposition method for solving time-dependent PDEs, in which at each OSWR iteration, space-time subdomain problems across the time interval are solved. The exchange between the subdomains is here ensured using time-dependent, higher-order transmission operators. Thus physically more valuable information is exchanged between the subdomains and hence a better convergence behavior can be expected (numerically observed in our experiments) for the resulting method, see [21, 38, 71, 86, 89, 98, 103, 124] and the references therein. All the derived results also naturally hold in the Robin case, obtained by setting one of the Ventcell parameters to zero. With respect to the second and third points, we build on the a posteriori methodology derived in [127, 152, 109, 67, 42, 56] for nonlinear, time-dependent problems, see also the references therein; we will in particular rely on [56, Theorem 5.2] for our error upper bound.

We measure the error between the unknown exact solution and the currently available approximate solution in energy-type norm introduced in [56]. At each iteration of the OSWR algorithm and on each linearization step, our estimates give a guaranteed and easily computable upper bound. This is achieved by introducing $\mathbf{H}(\mathrm{div})$-conforming and locally conservative flux reconstructions, piecewise constant in time, following [67], and a saturation reconstruction, H^1-conforming in each subdomain, which is continuous and piecewise affine in time and satisfies the nonlinear discontinuous interface condition. The derived estimates are then splitted to the components corresponding to the space error, time error, linearization error, and the domain decomposition error. The benefits of such a procedure are to spare numerous iterations of the OSWR algorithm as well as of the linearization iterations used for the subdomain problems and to ensure tight overall error control at any point.

The outline of the paper is as follows: Section 4.2 recalls the physical model and defines weak solutions as well as the relevant functions spaces. Section 4.3 presents the space-time domain decomposition method with optimized Ventcell transmission conditions. In Section 4.4, we present the discrete OSWR algorithm, by combining a finite volume scheme for the discretization in the individual subdomains and the backward Euler time stepping with the Ventcell–Schwarz method. We subsequently construct the needed ingredients for the a posteriori error estimates: Section 4.5 defines the

postprocessing as well as the H^1-(subdomain by subdomain) and $\mathbf{H}(\mathrm{div})$-conforming reconstructions. Section 4.6 puts the pieces together by presenting a guaranteed and fully computable error estimate that bounds the energy-type error between the unknown exact solution and the approximate solution. In Section 4.7 we decompose this estimate into estimators characterizing the space, time, domain decomposition, and linearization error components. This is next used in Section 4.8 to propose stopping criteria for the OSWR algorithm and for the nonlinear iterations. The method is finally numerically validated on an example in three space dimensions in Section 4.9.

4.2 Presentation of the problem

Let Ω be an open bounded domain of $\mathbb{R}^d$ ($d = 2$ or 3) which is assumed to be polygonal if $d = 2$ and polyhedral if $d = 3$. We denote by $\partial\Omega$ its boundary (supposed to be Lipschitz-continuous) and by $\mathbf{n}$ the unit normal to $\partial\Omega$, outward to Ω. Let a time interval $(0, T)$ be given with $T > 0$. We consider a simplified model of a two-phase flow through a heterogeneous porous medium, in which the convection is neglected. Assuming that there are only two phases occupying the porous medium Ω, say gas and water, and that each phase is composed of a single component, the mathematical form of this problem as it is exposed in [63, 39] is as follows: given initial and boundary gas saturations u_0 and g, as well as a source term f, find $u : \Omega \times [0, T] \to [0, 1]$ such that

$$\partial_t u - \nabla\cdot(\lambda(u, \mathbf{x})\nabla\pi(u, \mathbf{x})) = f, \quad \text{in } \Omega \times (0, T), \tag{4.1a}$$

$$u(\cdot, 0) = u_0, \quad \text{in } \Omega, \tag{4.1b}$$

$$u = g, \quad \text{on } \partial\Omega \times (0, T). \tag{4.1c}$$

Here u is the gas saturation (and therefore $(1 - u)$ is the water saturation), $\pi(u, \mathbf{x}) : [0, 1] \times \Omega \to \mathbb{R}$ is the capillary pressure, and $\lambda(u, \mathbf{x}) : [0, 1] \times \Omega \to \mathbb{R}$ is the global mobility of the gas. For simplicity, we consider only Dirichlet boundary conditions on $\partial\Omega$. Other types of boundary conditions could be dealt with the same way as in [39, 63, 158]. The model problem given by (4.1a) is a nonlinear degenerate parabolic problem as the global mobility $\lambda(u) \to 0$ for $u \to 0$ and 1, and, moreover, $\pi'(u) \to 0$ for $u \to 0$ (see [18, 44]).

4.2.1 Flow between two rock types

In this part, we particularize the model problem (4.1a) to a porous medium with discontinuous capillary pressure which has been introduced in [63]. We suppose that Ω is composed of two disjoint subdomains Ω_i, $i = 1, 2$, which are both open polygonal subsets of $\mathbb{R}^d$ with Lipschitz-continuous boundary. We denote by Γ the interface between Ω_1 and Ω_2, i.e., $\overline{\Gamma} = \partial\Omega_1 \cap \partial\Omega_2$. Let $\Gamma_i^{\mathrm{D}} = \partial\Omega_i \cap \partial\Omega$. Both data λ and π, that can in general depend on the physical characteristics of the rock, are henceforth supposed to be homogeneous in each subdomain Ω_i, $i = 1, 2$, i.e., $\lambda_i(\cdot) := \lambda_{|\Omega_i}(\cdot) = \lambda(\cdot, \mathbf{x})$, $\forall \mathbf{x} \in \Omega_i$, and similarly for π_i. The equations (4.1a) in each subdomain Ω_i then read as

$$\partial_t u_i - \nabla\cdot\big(\lambda_i(u_i)\nabla\pi_i(u_i)\big) = f_i, \quad \text{in } \Omega_i \times (0, T), \tag{4.2a}$$

$$u_i(\cdot, 0) = u_0, \quad \text{in } \Omega_i, \tag{4.2b}$$

$$u_i = g_i, \quad \text{on } \Gamma_i^{\mathrm{D}} \times (0, T). \tag{4.2c}$$

Before transcribing the transmission conditions on the interface Γ, we make precise the assumptions on the data:

Assumption 4.2.1 (Data). *1. For $i \in \{1,2\}$, $\pi_i \in C^1([0,1],\mathbb{R})$ can be extended in a continuous way to a function (still denoted by π_i) such that $\pi_i(u) = \pi_i(0)$ for all $u \leq 0$ and $\pi_i(u) = \pi_i(1)$ for all $u \geq 1$. Moreover, $\pi_i|_{[0,1]}$ is a strictly increasing function.*

2. For $i \in \{1,2\}$, $\lambda_i \in C^0([0,1],\mathbb{R}^+)$ is bounded and can be extended in a continuous way to a function (still denoted by λ_i) such that $\lambda_i(u) = \lambda_i(0)$ for all $u \leq 0$ and $\lambda_i(u) = \lambda_i(1)$ for all $u \geq 1$. We denote by C_λ an upper bound of $\lambda_i(u)$, $u \in \mathbb{R}$.

3. The initial condition is such that $u_0 \in L^\infty(\Omega)$ with $0 \leq u_0 \leq 1$ a.e. in Ω.

4. The boundary conditions g_i are at most piecewise second-order polynomials with respect to the boundary faces of the spatial mesh introduced in Section 4.4.1.1 below, continuous on Γ_i^D, and constant in time. Moreover, they match in the sense that $\pi_1(g_1(\mathbf{x})) = \pi_2(g_2(\mathbf{x}))$ for all $\mathbf{x} \in \Gamma \cap \Gamma_1^D$ and all $\mathbf{x} \in \Gamma \cap \Gamma_2^D$.

5. The source term is such that $f \in L^2(0,T;L^2(\Omega))$. For simplicity we further assume that f is piecewise constant in time with respect to the temporal mesh introduced in Section 4.4.1.2 below.

We give now the transmission conditions needed to connect the subdomain problems (4.2), for $i = 1,2$. We consider two cases. The first case is when

$$\pi_1(0) = \pi_2(0) \qquad \text{and} \qquad \pi_1(1) = \pi_2(1), \tag{4.3}$$

the same way as in [39]. If the functions π_i satisfy the above condition, the capillarity curves are said to be matching and the resulting transmission conditions on the interface are given by

$$\pi_1(u_1) = \pi_2(u_2), \qquad \text{on } \Gamma \times (0,T), \tag{4.4a}$$

$$\lambda_1(u_1)\nabla\pi_1(u_1)\cdot\mathbf{n}_1 = -\lambda_2(u_2)\nabla\pi_2(u_2)\cdot\mathbf{n}_2, \quad \text{on } \Gamma \times (0,T). \tag{4.4b}$$

These conditions yield a discontinuous saturation across the interface, i.e., we find that in general $u_1 \neq u_2$ on Γ.

In the second case, i.e., in the case when

$$\pi_1(0) \neq \pi_2(0) \qquad \text{or} \qquad \pi_1(1) \neq \pi_2(1), \tag{4.5}$$

the capillarity pressure curves are said to be non-matching. Consequently, not only the saturation is discontinuous at the medium interface, but also the capillary pressure field. The condition (4.5), studied in [63], has direct consequences on the behavior of the capillary pressures on both sides of the interface Γ. Indeed, suppose that $\pi_1(0) \leq \pi_2(0) < \pi_1(1) \leq \pi_2(1)$, and that u_1^* is the unique real in $[0,1]$ satisfying $\pi_1(u_1^*) = \pi_2(0)$, and u_2^* is the unique real in $[0,1]$ satisfying $\pi_2(u_2^*) = \pi_1(1)$. Then, if $u_1 \geq u_1^*$ and $u_2 \leq u_2^*$, we can still on the interface Γ prescribe the connection of the capillary pressures $\pi_1(u_1) = \pi_2(u_2)$ as in (4.4a). If $0 \leq u_1 \leq u_1^*$, we impose $u_2 = 0$, and the gas phase is entrapped in the rock Ω_1, and the water flows across Γ. In the same way, if $u_2^* \leq u_2 \leq 1$, we set $u_1 = 1$, and the water phase is captured in Ω_2 as a discontinuous

phase, and the gas flows across Γ (see Figure 4.1 left). Following [63], these conditions on the gas-water saturations on the interface Γ are simply given by

$$\overline{\pi}_1(u_1) = \overline{\pi}_2(u_2), \qquad \text{on } \Gamma \times (0,T), \tag{4.6a}$$

$$\lambda_1(u_1)\nabla\pi_1(u_1)\cdot\mathbf{n}_1 = -\lambda_2(u_2)\nabla\pi_2(u_2)\cdot\mathbf{n}_2, \quad \text{on } \Gamma \times (0,T), \tag{4.6b}$$

where $\overline{\pi}_i$, for $i = 1,2$, are truncated capillary pressure functions given on $[0,1]$ respectively by $\overline{\pi}_1 : u \mapsto \max(\pi_1(u), \pi_2(0))$ and $\overline{\pi}_2 : u \mapsto \min(\pi_2(u), \pi_1(1))$ (see Figure 4.1 right). In [63], it has been established that the model problem (4.2) together with the transmission conditions (4.6) has the necessary mathematical properties to explain the phenomena of gas trapping (see also [14, 41]).

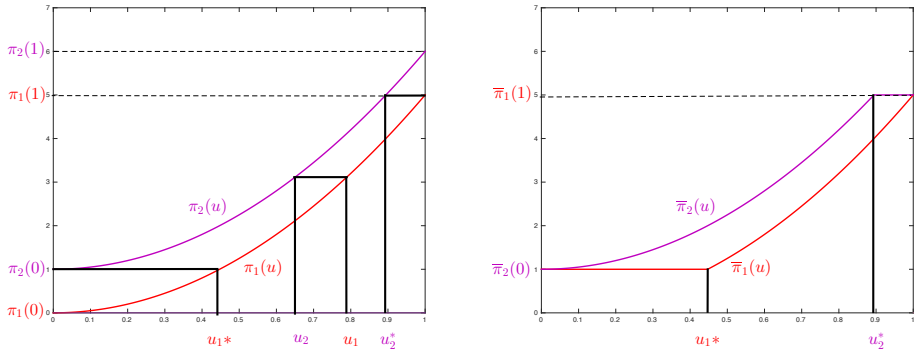

Figure 4.1: Capillary pressure curves (left) and truncated capillary pressures curves (right)

4.2.2 Transformation of the equations and weak formulation

Still following [63], we present here the mathematical quantities and function spaces used to characterize the weak solution to the multidomain problem (4.2) with the conditions (4.6). That of the problem (4.2) with the conditions (4.4) can be deduced straightforwardly from this later, see [39]. As Ω_i is a homogeneous rock type, so that π_i and λ_i do not depend on $\mathbf{x}$, one can define the Kirchhoff transform

$$\varphi_i : \begin{cases} [0,1] & \longrightarrow & \mathbb{R}^+ \\ s & \longmapsto & \displaystyle\int_0^s \lambda_i(a)\pi_i'(a)\mathrm{d}a. \end{cases} \tag{4.7}$$

The function φ_i is Lipschitz-continuous and increasing on $[0,1]$, and we denote by $L_{\varphi,i}$ its Lipschitz constant, i.e., $L_{\varphi,i} := \max_{s\in[0,1]} \lambda_i(s)\pi_i'(s)$, so that

$$|\varphi_i(a) - \varphi_i(b)| \le L_{\varphi,i}|a-b|, \quad \forall (a,b) \in [0,1]^2,$$

and we let $L_\varphi := \max\left(L_{\varphi,1}, L_{\varphi,2}\right)$. We extend the function φ_i from $[0,1]$ to $\mathbb{R}$ so that $\varphi_i(u) = \varphi_i(0)$ for all $u \le 0$ and $\varphi_i(u) = \varphi_i(1)$ for all $u \ge 1$. We now introduce the strictly increasing function ϕ by

$$\phi : \begin{cases} [\pi_2(0), \pi_1(1)] & \longrightarrow & \mathbb{R}^+ \\ s & \longmapsto & \displaystyle\int_{\pi_2(0)}^s \min_{j\in\{1,2\}} (\lambda_j \circ \pi_j^{-1}(a))\,\mathrm{d}a, \end{cases}$$

and let $\Pi_i = \phi \circ \overline{\pi}_i$, for $i \in \{1,2\}$. The functions $\Pi_i|_{[0,1]}$ are differentiable and increasing and we let $\Pi_i(u) = \Pi_i(0)$ for all $u \leq 0$ and $\Pi_i(u) = \Pi_i(1)$ for all $u \geq 1$. We also define the function Π by

$$\Pi(u, \mathbf{x}) = \Pi_i(u), \quad \text{for } \mathbf{x} \in \Omega_i.$$

The function Π introduced first in [63, Lemma 2.1] and used in [39, 41, 7] is more regular than $\overline{\pi}_1$ and $\overline{\pi}_2$ and allows to connect Π_1 and Π_2 instead of $\overline{\pi}_1$ and $\overline{\pi}_2$, that is, for all $(u_1, u_2) \in \mathbb{R}^2$, we have

$$\overline{\pi}_1(u_1) = \overline{\pi}_2(u_2) \Leftrightarrow \Pi_1(u_1) = \Pi_2(u_2).$$

Finally, under Assumption 4.2.1, the function $\Pi_i \circ \varphi_i^{-1}$ is Lipschitz-continuous with a Lipschitz constant lower than 1 (see [63]), i.e.

$$|\Pi_i(a) - \Pi_i(b)| \leq |\varphi_i(a) - \varphi_i(b)|, \quad \forall (a,b) \in [0,1]^2. \tag{4.8}$$

This inequality will be used in Remark 4.6.3 below.

We now apply the Kirchhoff transformation (4.7) separately in each subdomain, giving

$$\partial_t u_i - \Delta \varphi_i(u_i) = f_i, \qquad \text{in } \Omega_i \times (0,T), \tag{4.9a}$$
$$u_i(\cdot, 0) = u_0, \qquad \text{in } \Omega_i, \tag{4.9b}$$
$$\varphi_i(u_i) = \varphi_i(g_i), \quad \text{on } \Gamma_i^{\mathrm{D}} \times (0,T), \tag{4.9c}$$

together with the new expression of the conditions at the interface

$$\Pi_1(u_1) = \Pi_2(u_2), \qquad \text{on } \Gamma \times (0,T), \tag{4.10a}$$
$$\nabla \varphi_1(u_1) \cdot \mathbf{n}_1 = -\nabla \varphi_2(u_2) \cdot \mathbf{n}_2, \quad \text{on } \Gamma \times (0,T). \tag{4.10b}$$

Let us recall that some smoothness of the solutions u_i is required in order to ensure that the condition (4.10b) is well-defined on the interface Γ. In the general case, the multidomain problem (4.9)–(4.10) does not have any strong solution. This leads us to introduce the notion of a weak solution. To this aim, we define

$$X_{\varphi_i(g_i)} := L^2(0,T; H^1_{\varphi_i(g_i)}(\Omega_i)),$$
$$X_{\Pi(g,\cdot)} := L^2(0,T; H^1_{\Pi(g,\cdot)}(\Omega)), \qquad X := L^2(0,T; H^1_0(\Omega)),$$

where $H^1_{\varphi_i(g_i)}(\Omega_i) := \{v \in H^1(\Omega_i), v = \varphi_i(g_i) \text{ on } \Gamma_i^{\mathrm{D}}\}$ and similarly $H^1_{\Pi(g,\cdot)}(\Omega) := \{v \in H^1(\Omega), v = \Pi(g,\cdot) \text{ on } \partial\Omega\}$.

We equip the space X with the norm

$$||\psi||_X := \left\{ \int_0^T ||\nabla \psi(\cdot, t)||^2_{L^2(\Omega)} \, \mathrm{d}t \right\}^{\frac{1}{2}}.$$

The dual space of X is

$$X' := L^2(0,T; H^{-1}(\Omega)).$$

We will use the notation $\langle \cdot, \cdot \rangle_{H^{-1}(\Omega), H^1_0(\Omega)}$ to denote the duality pairing between $H^{-1}(\Omega)$ and $H^1_0(\Omega)$. We will also need the space

$$Z := H^1(0,T; H^{-1}(\Omega)).$$

We now define a weak solution to problem (4.9)–(4.10).

Definition 4.2.2 (Weak solution). *We say that a function u is a weak solution to problem* (4.9)–(4.10) *if it satisfies:*

1. $u \in Z \cap L^\infty(0,T;L^\infty(\Omega))$, $0 \le u \le 1$ *a.e. in* $\Omega \times (0,T)$;
2. $u(\cdot,0) = u_0$;
3. $\varphi_i(u_i) \in X_{\varphi_i(g_i)}$, *where* $u_i := u|_{\Omega_i}$, $i = 1,2$;
4. $\Pi(u,\cdot) \in X_{\Pi(g,\cdot)}$;
5. *For all* $\psi \in X$, *the following integral equality holds:*

$$\int_0^T \Big\{ \langle \partial_t u, \psi \rangle_{H^{-1}(\Omega),H_0^1(\Omega)} + \sum_{i=1}^{2} \big(\nabla \varphi_i(u_i), \nabla \psi\big)_{\Omega_i} - \big(f,\psi\big) \Big\} \mathrm{d}t = 0.$$

In this paper, we assume that a weak solution given by Definition 4.2.2 exists. One can then easily show that Π has sufficient regularity to impose the condition (4.10a). Indeed, since $\Pi_i \circ \varphi_i^{-1}$ is a Lipschitz-continuous function, the third point of Definition 4.2.2 ensures that $\Pi_i(u_i)$ belongs to $L^2(0,T;H^1(\Omega_i))$, $i = 1,2$. Thus, the point 4 of Definition 4.2.2 implies the continuity condition (4.10a). Finally, when supposing additionally that the weak solution u is sufficiently regular so that $\partial_t u \in L^2(0,T;L^2(\Omega))$, condition (4.10b) is satisfied weakly using point 5 of Definition 4.2.2.

Remark 4.2.3 (Existence and uniqueness of a weak solution). *In [63], the existence of a weak solution to problem* (4.9)–(4.10) *was proved using integration by parts for the time term which requires a stronger test function space. In fact, in [63] (see also [39]), the derived weak solution is given as the limit of a finite volume approximation of the solution refining the space and time discretization, and requires a stronger test function space for the application of the Kolmogorov's compactness criterion in L^∞. For the uniqueness, a first result was obtained in [39] for the case of matching capillary pressures curves. For the more general case, the uniqueness is demonstrated only for the one-dimensional case in [40]. However, homogeneous Neumann boundary conditions were needed to prove this result.*

4.3 Space-Time Domain Decomposition Methods with Ventcell Transmission Conditions

Under sufficient regularity, an equivalent formulation to the model problem (4.9)–(4.10) can be obtained by solving, for $i = 1,2$, equations (4.9) together with optimized Ventcell transmission conditions on $\Gamma \times (0,T)$

$$\nabla \varphi_1(u_1)\cdot \mathbf{n}_1 + \mathscr{L}_1(\Pi_1(u_1)) = -\nabla \varphi_2(u_2)\cdot \mathbf{n}_2 + \mathscr{L}_1(\Pi_2(u_2)), \tag{4.11a}$$
$$\nabla \varphi_2(u_2)\cdot \mathbf{n}_2 + \mathscr{L}_2(\Pi_2(u_2)) = -\nabla \varphi_1(u_1)\cdot \mathbf{n}_1 + \mathscr{L}_2(\Pi_1(u_1)), \tag{4.11b}$$

where $\mathscr{L}_i$, $i = 1,2$, is a second-order (or Ventcell) boundary operator defined by

$$\mathscr{L}_i(v) := \alpha_{i,j} v + \gamma_{i,j}(\partial_t v - \Delta_\Gamma v), \quad j = (3-i), \tag{4.12}$$

for a sufficiently regular function v defined on $\Gamma \times (0,T)$, where Δ_Γ represents the Laplace operator on Γ (Laplace–Beltrami operator). The Robin transmission conditions are easily obtained by taking in (4.12) the parameters $\gamma_{i,j} = 0$.

One can easily show that the operators $\mathscr{L}_i$ involve not only the continuity of the function Π as for the Robin case, but also the continuity of the time derivative and of the second-order derivatives of Π along the interface. As a result, this formulation can be seen as a coupling problem between a d-dimensional PDE in the rock Ω_i and a $(d-1)$-dimensional PDE on the interface Γ between the rock types, which greatly enhances the information exchange between the solutions in the subdomains, see [103, 71, 38, 89]. The Robin–Schwarz algorithm applied to this problem has been addressed in [7] and the existence of a weak solution of the local Robin problem (with $\gamma_{i,j} = 0$) in a multidimensional domain was obtained by proving the convergence of a finite volume scheme. Work underway addresses the Ventcell case using the same techniques. When the above multidomain problem is solved iteratively, the coefficients $\alpha_{i,j}$ and $\gamma_{i,j}$ can be chosen so as to minimize the convergence factor of the linearized algorithm as in [103, 71, 38, 89, 95, 98].

The Ventcell-OSWR algorithm is defined as follows: the solution u in the whole domain Ω given by $u_i = u|_{\Omega_i}$ is approximated by a sequence of solutions u_i^k, $k \geq 1$, defined recursively by

$$\partial_t u_i^{(k)} - \Delta \varphi_i(u_i^{(k)}) = f_i, \qquad \text{in } \Omega_i \times (0,T), \tag{4.13a}$$

$$u_i^k(\cdot,0) = u_0, \qquad \text{in } \Omega_i, \tag{4.13b}$$

$$\varphi_i(u_i^k) = \varphi_i(g_i), \qquad \text{on } \Gamma_i^{\mathrm{D}} \times (0,T), \tag{4.13c}$$

$$\nabla \varphi_i(u_i^{(k)}) \cdot \mathbf{n}_i + \mathscr{L}_i(\Pi_i(u_i^{(k)})) = \Psi_i^{k-1}, \qquad \text{on } \Gamma \times (0,T), \tag{4.13d}$$

with

$$\Psi_i^{k-1} := -\nabla \varphi_j(u_j^{(k-1)}) \cdot \mathbf{n}_j + \mathscr{L}_i(\Pi_j(u_j^{(k-1)})), \quad j = (3-i),\ k \geq 2, \tag{4.14}$$

and Ψ_i^0 is an initial Ventcell guess on $\Gamma \times (0,T)$.

Remark 4.3.1 (Interface operators)**.** *The multidomain problem* (4.9) *together with the transmission conditions* (4.11) *can be formulated through the use of Ventcell-to-Ventcell interface operators as a problem posed on the space-time interface, see [7]. This interface problem can be solved iteratively by using fixed point iterations (which corresponds to the OSWR algorithm above) or via a Newton–Krylov method.*

4.4 The cell-centered finite volume scheme

We present in this section the OSWR algorithm (4.13)–(4.14) discretized by a finite volume method.

4.4.1 Space-time discretization, notations, and function spaces

We introduce here the partitions of Ω and Γ, time discretization, notation, and function spaces; see [69, 63, 67] for the standard part of the notation.

4.4.1.1 Partitions of Ω and Γ

Let $\mathcal{T}_{h,i}$ be a partition of the subdomain Ω_i into elements K, such that $\overline{\Omega_i} = \cup_{K\in\mathcal{T}_{h,i}} K$; here we suppose that they are either simplices or rectangular parallelepipeds but general elements can be treated via submeshes, see [55] and the references therein. Moreover, we assume that the partition is conforming in the sense that if K, $L \in \mathcal{T}_{h,i}$, $K \neq L$, then $K \cap L$ is either an empty set, a common face, edge, or vertex of K and L.

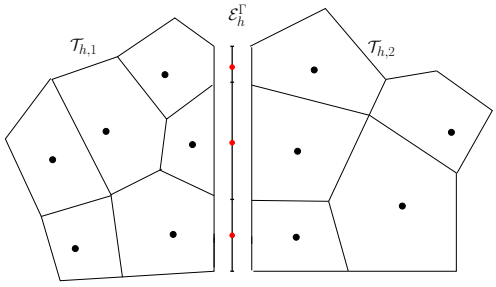

Figure 4.2: Compatible meshes in the subdomains in two space dimensions

We then set $\mathcal{T}_h = \cup_{i=1}^2 \mathcal{T}_{h,i}$ and denote by h the maximal element diameter in $\mathcal{T}_h$. The meshes are supposed to be matching on the interface Γ (see Figure 4.2). For all $K \in \mathcal{T}_h$, h_K denotes the diameter of the mesh element K and $|K|$ its volume. The interior mesh faces in $\mathcal{T}_{h,i}$ are collected into the set $\mathcal{E}_{h,i}^{\rm int}$, hence $\mathcal{E}_{h,i}^{\rm int}$ contains neither the subdomain interfaces nor the outer boundary of Ω. The faces of $\mathcal{T}_{h,i}$ lying on $\Gamma_i^{\rm D}$ are collected in the set $\mathcal{E}_{h,i}^{\rm D}$. We denote by $\mathcal{E}_{h,i}$ all the faces of $\mathcal{T}_{h,i}$ and we set $\mathcal{E}_h = \cup_{i=1}^2 \mathcal{E}_{h,i}$. The notation $\mathcal{E}_K$ stands for all the faces of an element $K \in \mathcal{T}_h$. Let $\mathcal{E}_h^\Gamma$ be a partition of Γ given by the faces of $\mathcal{T}_h$ on Γ. We use also $\mathcal{F}_{h,i}^{\rm int}$ to denote the interior sides (these are the points (if $d = 2$) or edges (if $d = 3$)) of $\mathcal{E}_h^\Gamma$. We denote by $\mathcal{F}_{h,i}^{\rm D}$ the sides of $\mathcal{E}_h^\Gamma$ on $\Gamma_i^{\rm D}$. The sides of a face $\sigma \in \mathcal{E}_h$ are collected in the set $\mathcal{F}_\sigma$. The volume of a face σ is denoted by $|\sigma|$ and that of a side e by $|e|$. Finally, we use the notation $\mathbf{x}_K$ to denote the "center" of the cell $K \in \mathcal{T}_h$. If $\sigma = K|L \in \mathcal{E}_h$ separates the cells K and L, $d_{K,L}$ denotes the Euclidean distance between $\mathbf{x}_K$ and $\mathbf{x}_L$, and $d_{K,\sigma}$ for $\sigma \in \mathcal{E}_K$ denotes the distance from $\mathbf{x}_K$ to σ. Similarly, we let $\mathbf{x}_\sigma$ be the "center" of the face σ and $\mathbf{x}_e$ the "center" of the edge e and denote respectively by $d_{\sigma,\tilde\sigma}$ and $d_{\sigma,e}$ the distance between $\mathbf{x}_\sigma$ and $\mathbf{x}_{\tilde\sigma}$ for $e = \sigma|\tilde\sigma \in \mathcal{F}_{h,i}^{\rm int}$ and the distance from $\mathbf{x}_\sigma$ to e for $e \in \mathcal{F}_\sigma$.

We assume that the composite mesh $\mathcal{T}_h$ satisfies the following orthogonality condition: for an interface $\sigma = K|L$, the line segment $\mathbf{x}_K\mathbf{x}_L$ is orthogonal to this interface (see [69]). The same condition should be satisfied for a side $e = \sigma|\tilde\sigma \in \mathcal{F}_{h,i}^{\rm int}$ due to the discretization of the Ventcell operator (see Figure 4.3).

4.4.1.2 Time discretization

For an integer $N \geq 0$, let $(\tau^n)_{0\leq n\leq N}$ denote a sequence of positive real numbers corresponding to the discrete time steps such that $T = \displaystyle\sum_{n=1}^{N} \tau^n$. Let $t_0 = 0$, and $t^n = \displaystyle\sum_{j=1}^{n} \tau^j$, $1 \leq n \leq N$, be the discrete times. Let $I^n = (t^{n-1}, t^n]$, $1 \leq n \leq N$. For simplicity, we consider only conforming time grids. The analysis remains valid if we

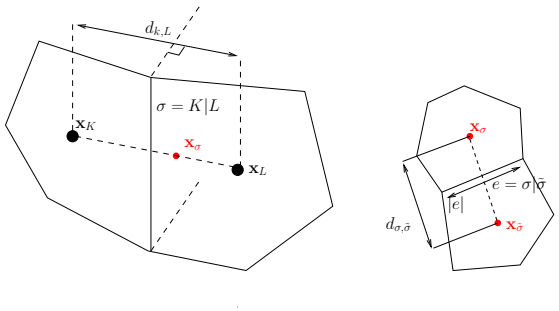

Figure 4.3: Notation for admissible meshes in three space dimensions

use different time steps in the subdomains, as was done in [11] for a linear diffusion problem.

4.4.1.3 Notation and function spaces

We denote by $\mathbb{P}_l(S)$ the space of polynomials on a subdomain $S \subset \Omega$ of total degree less than or equal to l and by

$$\mathbb{P}_l(\mathscr{T}_h) := \{p_h \in L^2(\Omega);\ p_h|_K \in \mathbb{P}_l(K),\ \forall K \in \mathscr{T}_h\},$$

the space of piecewise l-degree polynomials on $\mathscr{T}_h$. We use the notation $\|\cdot\|_K$ for the norm in $L^2(K)$, $K \in \mathscr{T}_h$. The corresponding inner product is $(\cdot,\cdot)_K$. We also denote by $(\cdot,\cdot)_\sigma$ the inner product in $L^2(\sigma)$ for $\sigma \in \mathscr{E}_h$. Let $|S|$ be the Lebesgue measure of S, and $|\sigma|$ the $(d-1)$-dimensional Lebesgue measure of $\sigma \in \mathbb{R}^{d-1}$. We define the broken Sobolev space $H^1(\mathscr{T}_h)$ as the space of all functions $v \in L^2(\Omega)$ such that $v|_K \in H^1(K)$, for all $K \in \mathscr{T}_h$. We will use the sign ∇ to denote the elementwise gradient, i.e., the gradient of a function restricted to a mesh element $K \in \mathscr{T}_h$. We define $P^1_\tau(H^1(\mathscr{T}_h))$ and $P^1_\tau(H^1_0(\Omega))$ as the space of continuous and piecewise affine in-time functions $v_{h\tau}$ with values in $H^1(\mathscr{T}_h)$ and in $H^1_0(\Omega)$, respectively. In both these situations, for every time step $1 \le n \le N$, we will use the abridged notations

$$v_h^n := v_{h\tau}(\cdot, t^n),$$
$$\partial_t^n v_{h\tau}^n := \partial_t v_{h\tau}|_{I^n} = \frac{(v_h^n - v_h^{n-1})}{\tau^n}.$$

By Assumption 4.2.1, the source function f is piecewise constant in time, i.e., constant on each time interval I^n, $1 \le n \le N$. Its value on I^n is denoted by $f^n := f|_{I^n}$.

The domain decomposition method we consider is global in time. Thus, at the space-time interface $\Gamma \times (0,T)$, data should be transferred from one space-time subdomain to the neighboring subdomain. Then, we denote by $P^0_\tau(L^2(\Gamma))$ the space of functions piecewise constant in time and with values in $L^2(\Gamma)$. Let $\mathbf{H}(\mathrm{div},\Omega)$ be the space of vector-valued functions from $\left[L^2(\Omega)\right]^d$ that admit a weak divergence $L^2(\Omega)$. Consequently, all functions in $\mathbf{H}(\mathrm{div},\Omega)$ have a continuous normal trace across the interface Γ. As above, $P^0_\tau(\mathbf{H}(\mathrm{div},\Omega))$ is the space of functions piecewise constant in time with values in $\mathbf{H}(\mathrm{div},\Omega)$. We use $\mathbf{RTN}_0(\Omega)$ to denote the lowest-order Raviart–Thomas–Nédélec finite-dimensional subspace of $\mathbf{H}(\mathrm{div},\Omega)$; any $\mathbf{v}_h \in \mathbf{RTN}_0(\Omega)$ takes on each element $K \in \mathscr{T}_h$ the form $[\mathbb{P}_0(K)]^d + \mathbb{P}_0(K)\mathbf{x}$ for the example of simplices.

Finally, given a function v that is double-valued on the interface Γ, the jump and the average of v on a face $\sigma \in \mathscr{E}_h^\Gamma$, $\sigma = K|L$, $K \in \mathscr{T}_{h,1}$, $L \in \mathscr{T}_{h,2}$, are defined as

$$[\![v]\!] = (v_K)|_\sigma - (v_L)|_\sigma, \qquad \{\!\{v\}\!\} = \frac{(v_K)|_\sigma + (v_L)|_\sigma}{2}.$$

Here $v_K = v|_K$ is the restriction of v to the element $K \in \mathscr{T}_h$.

4.4.2 A space-time fully discrete scheme based on finite volumes in space and the backward Euler scheme in time

For the iteration $k \geq 1$ of the OSWR algorithm, subdomain Ω_i, $i = 1, 2$, and the time steps $0 \leq n \leq N$, let the discrete saturation $u_{h,i}^{k,n} \in \mathbb{P}_0(\mathscr{T}_{h,i}) \times \mathbb{P}_0(\mathscr{E}_h^\Gamma)$ be identified with the vector of unknowns

$$u_{h,i}^{k,n} := \left((u_K^{k,n})_{K \in \mathscr{T}_{h,i}}, (u_{K,\sigma}^{k,n})_{\sigma \in \mathscr{E}_K \cap \mathscr{E}_h^\Gamma, K \in \mathscr{T}_{h,i}} \right).$$

Note that there are two interface unknowns for each face of $\mathscr{E}_h^\Gamma$.

We then define the discrete flux $F_{K,\sigma}$ over a face $\sigma \in \mathscr{E}_h \cap \mathscr{E}_K$, $K \in \mathscr{T}_{h,i}$, by

$$F_{K,\sigma}(u_{h,i}^{k,n}) := \begin{cases} \dfrac{\varphi_i(u_K^{k,n}) - \varphi_i(u_L^{k,n})}{d_{K,L}}, & \text{if } \sigma = K|L \in \mathscr{E}_{h,i}^{\mathrm{int}}, \\ \dfrac{\varphi_i(u_K^{k,n}) - \varphi_i(g_i(\mathbf{x}_\sigma))}{d_{K,\sigma}}, & \text{if } \sigma \in \mathscr{E}_K \cap \mathscr{E}_{h,i}^{\mathrm{D}}, \\ \dfrac{\varphi_i(u_K^{k,n}) - \varphi_i(u_{K,\sigma}^{k,n})}{d_{K,\sigma}}, & \text{if } \sigma \in \mathscr{E}_K \cap \mathscr{E}_h^\Gamma, \end{cases} \tag{4.15a}$$

and the discrete $(d-1)$-dimensional flux $\bar{F}_{\sigma,e}$ over a side $e \in \mathscr{F}_\sigma$, $\sigma \in \mathscr{E}_K \cap \mathscr{E}_h^\Gamma$, by

$$\bar{F}_{\sigma,e}(u_{h,i}^{k,n}) := \begin{cases} \dfrac{\Pi_i(u_{K,\sigma}^{k,n}) - \Pi_i(u_{K,\tilde{\sigma}}^{k,n})}{d_{\sigma,\tilde{\sigma}}}, & \text{if } e = \sigma|\tilde{\sigma} \in \mathscr{F}_\sigma \cap \mathscr{F}_{h,i}^{\mathrm{int}}, \\ \dfrac{\Pi_i(u_{K,\sigma}^{k,n}) - \Pi_i(g_i(\mathbf{x}_e))}{d_{\sigma,e}}, & \text{if } e \in \mathscr{F}_\sigma \cap \mathscr{F}_{h,i}^{\mathrm{D}}. \end{cases} \tag{4.15b}$$

Using (4.15), the finite volume approximation of the solution u^k in the OSWR algorithm (4.13)–(4.14) is: at each iteration $k \geq 1$, the initial condition is given by

$$u_K^{k,0} = \frac{1}{|K|}(u_0, 1)_K, \qquad \forall K \in \mathscr{T}_h, \tag{4.16a}$$

and for $n = 1, \ldots, N$, the discrete saturation $u_{h,i}^{k,n} \in \mathbb{P}_0(\mathscr{T}_{h,i}) \times \mathbb{P}_0(\mathscr{E}_h^\Gamma)$, $i = 1, 2$, is given by the following scheme:

$$\begin{aligned} &\frac{u_K^{k,n} - u_K^{k,n-1}}{\tau^n}|K| + \sum_{\sigma \in \mathscr{E}_K} |\sigma| F_{K,\sigma}(u_{h,i}^{k,n}) = (f_i^n, 1)_K, \\ &\qquad\qquad \forall K \in \mathscr{T}_{h,i}, \end{aligned} \tag{4.16b}$$

$$-F_{K,\sigma}(u_{h,i}^{k,n}) + \gamma_{i,j} \frac{\Pi_i(u_{K,\sigma}^{k,n}) - \Pi_i(u_{K,\sigma}^{k,n-1})}{\tau^n}|\sigma| + \left(\Lambda_{K,\Gamma}(u_{h,i}^{k,n}) \right)_\sigma = \Psi_{L,\sigma}^{k-1,n},$$

$$\forall \sigma = K|L \in \mathscr{E}_h^\Gamma, \tag{4.16c}$$

where, for $K \in \mathscr{T}_{h,i}$,

$$\left(\Lambda_{K,\Gamma}(u_{h,i}^{k,n})\right)_\sigma := \alpha_{i,j}|\sigma|\Pi_i(u_{K,\sigma}^{k,n}) + \gamma_{i,j}\sum_{e\in\mathscr{F}_\sigma}|e|\bar{F}_{\sigma,e}(u_{h,i}^{k,n}), \quad \sigma \in \mathscr{E}_K \cap \mathscr{E}_h^\Gamma \tag{4.16d}$$

and, for $L \in \mathscr{T}_{h,j}$, $j = 3-i$, and $\sigma = K|L \in \mathscr{E}_h^\Gamma$, the Ventcell information from Ω_j is

$$\Psi_{L,\sigma}^{k-1,n} := F_{L,\sigma}(u_{h,j}^{k-1,n}) + \gamma_{i,j}\frac{\Pi_j(u_{L,\sigma}^{k-1,n}) - \Pi_j(u_{L,\sigma}^{k-1,n-1})}{\tau^n}|\sigma| + \left(\Lambda_{L,\Gamma}(u_{h,j}^{k-1,n})\right)_\sigma. \tag{4.17}$$

4.4.3 Newton linearization

At each OSWR domain decomposition step $k \geq 1$ and each time step $n \geq 1$, the equations (4.16b)–(4.16c) constitute a block 2×2 system of nonlinear algebraic equations. Solving this system requires an iterative linearization procedure on each subdomain. We use for this purpose the Newton–Raphson method. We obtain at linearization step $m \geq 1$ the following scheme: find $u_{h,i}^{k,n,m} \in \mathbb{P}_0(\mathscr{T}_{h,i}) \times \mathbb{P}_0(\mathscr{E}_h^\Gamma)$, $u_{h,i}^{k,n,m} := \left((u_K^{k,n,m})_{K\in\mathscr{T}_{h,i}}, (u_{K,\sigma}^{k,n,m})_{\sigma\in\mathscr{E}_K\cap\mathscr{E}_h^\Gamma, K\in\mathscr{T}_{h,i}}\right)$, such that

$$\frac{u_K^{k,n,m} - u_K^{k,n-1}}{\tau^n}|K| + \sum_{\sigma\in\mathscr{E}_K}|\sigma|F_{K,\sigma}^{m-1}(u_{h,i}^{k,n,m}) = (f_i^n, 1)_K, \quad \forall K \in \mathscr{T}_{h,i}, \tag{4.18a}$$

$$-F_{K,\sigma}^{m-1}(u_{h,i}^{k,n,m}) + \gamma_{i,j}\frac{\Pi_i^{m-1}(u_{K,\sigma}^{k,n,m}) - \Pi_i(u_{K,\sigma}^{k,n-1})}{\tau^n}|\sigma| + \left(\Lambda_{K,\Gamma}^{m-1}(u_{h,i}^{k,n,m})\right)_\sigma = \Psi_{L,\sigma}^{k-1,n}, \quad \forall \sigma = K|L \in \mathscr{E}_h^\Gamma, \tag{4.18b}$$

where $F_{K,\sigma}^{m-1}(u_{h,i}^{k,n,m})$ are the linearized face fluxes given by

$$F_{K,\sigma}^{m-1}(u_{h,i}^{k,n,m}) := F_{K,\sigma}(u_{h,i}^{k,n,m-1}) + \sum_{M=K,L}\frac{\partial F_{K,\sigma}}{\partial u_M}(u_{h,i}^{k,n,m-1})\cdot(u_M^{k,n,m} - u_M^{k,n,m-1}) + \frac{\partial F_{K,\sigma}}{\partial u_{K,\sigma}}(u_{h,i}^{k,n,m-1})\cdot(u_{K,\sigma}^{k,n,m} - u_{K,\sigma}^{k,n,m-1}),$$

where the linearization of the function Π_i is

$$\Pi_i^{m-1}(u_{K,\sigma}^{k,n,m}) := \Pi_i(u_{K,\sigma}^{k,n,m-1}) + \frac{\partial \Pi_i}{\partial u_{K,\sigma}}(u_{K,\sigma}^{k,n,m-1})\cdot(u_{K,\sigma}^{k,n,m} - u_{K,\sigma}^{k,n,m-1}),$$

and where finally

$$\left(\Lambda_{K,\Gamma}^{m-1}(u_{h,i}^{k,n,m})\right)_\sigma := \left(\Lambda_{K,\Gamma}(u_{h,i}^{k,n,m-1})\right)_\sigma + \alpha_{i,j}|\sigma|\frac{\partial \Pi_i}{\partial u_{K,\sigma}}(u_{K,\sigma}^{k,n,m-1})\cdot(u_{K,\sigma}^{k,n,m} - u_{K,\sigma}^{k,n,m-1}) + \gamma_{i,j}\sum_{e\in\mathscr{F}_\sigma}|e|\sum_{A=\sigma,\tilde{\sigma}}\frac{\partial \bar{F}_{\sigma,e}}{\partial u_A}(u_{h,i}^{k,n,m-1})\cdot(u_A^{k,n,m} - u_A^{k,n,m-1}).$$

The equations (4.18a)–(4.18b) form a system of linear algebraic equations that is solved at each domain decomposition iteration k, at time step n, at each Newton iteration m and this independently in each of the subdomains Ω_i.

4.5 Postprocessing and H^1- and H(div)-conforming reconstructions

At each OSWR iteration $k \geq 1$ and linearization step $m \geq 1$ of our method, let $u_{h\tau,i}^{k,m}$, $i = 1,2$, be a piecewise constant in space and in time approximation given by the values $u_K^{k,n,m}$, $K \in \mathcal{T}_{h,i}$, $0 \leq n \leq N$. Thus also the approximate quantities $\varphi_i(u_{h\tau,i}^{k,m})$ and $\Pi_i(u_{h\tau,i}^{k,m})$, $i = 1,2$, are piecewise constant. These approximations are not appropriate for an energy a posteriori error estimate. Following [156, 67, 130], our basic tools for the a posteriori error analysis will be:

(i) To construct a local postprocessing $\tilde{\varphi}_{h\tau,i}^{k,m}$ of the subdomain quantities $\varphi_i(u_{h\tau,i}^{k,m})$, $i = 1,2$, using the known fluxes. This will be discontinuous piecewise quadratic in space and continuous piecewise affine in time. Therefrom, the postprocessed discontinuous saturation $\tilde{u}_{h,i}^{k,n,m}$ will be obtained by $\varphi_i^{-1}(\tilde{\varphi}_{h,i}^{k,n,m})$.

(ii) To construct from $\tilde{\varphi}_{h\tau,i}^{k,m}$ by averaging a function $\hat{\varphi}_{h\tau,i}^{k,m}$, piecewise quadratic in space and continuous in each Ω_i, and continuous piecewise affine in time. Therefrom, the postprocessed saturation $s_{h\tau}^{k,m}$ will be defined in the spirit of $\varphi_i^{-1}(\tilde{\varphi}_{h,i}^{k,n,m})$; it will be continuous in each Ω_i and we will moreover ensure that $\Pi_1(s_{h\tau}^{k,m}|_{\Omega_1}) = \Pi_2(s_{h\tau}^{k,m}|_{\Omega_2})$ on the interface $\Gamma \times (0,T)$.

(iii) To construct a piecewise constant in-time and $\mathbf{RTN}_0(\Omega)$-conforming flux $\boldsymbol{\sigma}_{h\tau}^{k,m}$, locally conservative on the mesh $\mathcal{T}_h$.

4.5.1 Discontinuous piecewise quadratic $\tilde{\varphi}_{h,i}^{k,n,m}$ and postprocessed saturation $\tilde{u}_{h,i}^{k,n,m}$

Consider an OSWR iteration $k \geq 1$, a time step $1 \leq n \leq N$, and a linearization step $m \geq 1$. Let $\mathbf{u}_{h,i}^{k,n,m} \in \mathbf{RTN}_0(\Omega_i) \subset \mathbf{H}(\mathrm{div}, \Omega_i)$ be prescribed by the fluxes $F_{K,\sigma}(u_{h,i}^{k,n,m})$ in each subdomain Ω_i, $i = 1,2$, i.e., on each $K \in \mathcal{T}_{h,i}$ and each face $\sigma \in \mathcal{E}_K$:

$$(\mathbf{u}_{h,i}^{k,n,m} \cdot \mathbf{n}_i, 1)_\sigma = (F_{K,\sigma}(u_{h,i}^{k,n,m}), 1)_\sigma. \tag{4.19}$$

Following [70, 156] and the references therein, we define the postprocessed approximation $\tilde{\varphi}_{h,i}^{k,n,m} \in \mathbb{P}_2(\mathcal{T}_{h,i})$ in each element $K \in \mathcal{T}_{h,i}$ as the solution of

$$-\nabla \tilde{\varphi}_{h,i}^{k,n,m}|_K = \mathbf{u}_{h,i}^{k,n,m}|_K, \quad \forall K \in \mathcal{T}_{h,i}, \tag{4.20a}$$

$$\frac{(\varphi^{-1}(\tilde{\varphi}_{h,i}^{k,n,m}), 1)_K}{|K|} = u_K^{k,n,m}, \quad \forall K \in \mathcal{T}_{h,i}. \tag{4.20b}$$

Remark 4.5.1 (Approximation)**.** *In practice, the condition* (4.20b) *will be approximated by a quadrature rule by* $\tilde{\varphi}_{h,i}^{k,n,m}(\mathbf{x}_K) = \varphi_i(u_K^{k,n,m})$ $\forall K \in \mathcal{T}_{h,i}$.

This procedure is local in each element and its cost is negligible. The postprocessed approximation $\tilde{\varphi}_{h,i}^{k,n,m}$ is, however, not $H^1(\Omega_i)$-conforming, with jumps over the interior faces. We therefrom construct the corresponding postprocessed saturation by

$$\tilde{u}_{h,i}^{k,n,m} := \varphi_i^{-1}(\tilde{\varphi}_{h,i}^{k,n,m}). \tag{4.21}$$

Remark 4.5.2 (Practice). *The postprocessed saturation $\tilde{u}_{h,i}^{k,n,m}$ will only be used for the theoretical analysis. In practice, the estimators in Theorem 4.6.1 below involving $\tilde{u}_{h,i}^{k,n,m}$ will be neglected and only the postprocessed $\tilde{\varphi}_{h,i}^{k,n,m}$ will be used to compute the error estimators. A practical approximate way to calculate the estimators involving $\tilde{u}_{h,i}^{k,n,m}$ is to use corresponding quadrature rules and to let (4.21) be satisfied at the quadrature nodes.*

We define the continuous, piecewise affine in-time functions $\tilde{u}_{h\tau,i}^{k,m}$ and $\tilde{\varphi}_{h\tau,i}^{k,m}$ by

$$\tilde{u}_{h\tau,i}^{k,m}(\cdot,t_n)=\tilde{u}_{h,i}^{k,n,m},\qquad \tilde{\varphi}_{h\tau,i}^{k,m}(\cdot,t_n)=\tilde{\varphi}_{h,i}^{k,n,m},\qquad 1\le n\le N, \tag{4.22}$$

and define as usually $\tilde{u}_{h\tau}^{k,m}$ such that $\tilde{u}_{h\tau}^{k,m}|_{\Omega_i}:=\tilde{u}_{h\tau,i}^{k,m}$.

4.5.2 Continuous piecewise quadratic $\hat{\varphi}_{h,i}^{k,n,m}$ and H^1-conforming reconstruction $s_{h\tau}^{k,m}$

Consider an OSWR iteration $k\ge 1$ and a linearization step $m\ge 1$. In this section, we define a reconstructed saturation $s_{h\tau}^{k,m}\in Z$ with $\varphi_i(s_{h\tau,i}^{k,m})\in X_{\varphi_i(g_i)}$ and $\Pi(s_{h\tau}^{k,m},\cdot)\in X_{\Pi(g,\cdot)}$ to be a conforming discrete counterpart of the weak solution of Definition 4.2.2. Practically, we in particular require that, at each time step $1\le n\le N$,

$$s_h^{k,n,m}|_{\Omega_i}\in H^1(\Omega_i), \tag{4.23a}$$

$$s_h^{k,n,m}|_{\Gamma_i^{\mathrm{D}}}=g_i, \tag{4.23b}$$

$$\Pi_1(s_h^{k,n,m}|_{\Omega_1})=\Pi_2(s_h^{k,n,m}|_{\Omega_2}) \text{ on } \Gamma, \tag{4.23c}$$

$$\frac{1}{|K|}(s_h^{k,n,m},1)_K=u_K^{k,n,m},\quad \forall K\in\mathcal{T}_h. \tag{4.23d}$$

Then the continuous piecewise affine in-time function $s_{h\tau}^{k,m}$ is prescribed by

$$s_{h\tau}^{k,m}(\cdot,t_n)=s_h^{k,n,m},\qquad 1\le n\le N. \tag{4.24}$$

As usually, $s_{h\tau,i}^{k,m}:=s_{h\tau}^{k,m}|_{\Omega_i}$.

Remark 4.5.3 (Conditions (4.23a)–(4.23c)). *Conditions (4.23b)–(4.23c) together with (4.24) and the smoothness of the functions Π_i imply, at least for $0\le s_h^{k,n,m}\le 1$, the more abstract condition $\Pi(s_{h\tau}^{k,m},\cdot)\in X_{\Pi(g,\cdot)}$ (cf. point 4 of Definition 4.2.2).*

4.5.2.1 Continuous piecewise quadratic $\hat{\varphi}_{h,i}^{k,n,m}$

For a given postprocessed function $\tilde{\varphi}_{h,i}^{k,n,m}\in\mathbb{P}_2(\mathcal{T}_{h,i})$ defined by (4.20), we now prescribe at the degrees of freedom of $\mathbb{P}_2(\mathcal{T}_{h,i})\cap H^1(\Omega_i)$ a piecewise continuous polynomial $\hat{\varphi}_{h,i}^{k,n,m}\in\mathbb{P}_2(\mathcal{T}_{h,i})\cap H^1(\Omega_i)$. If $\mathbf{x}$ is a Lagrange node situated in the interior of Ω_i or at the interface Γ, we set

$$\hat{\varphi}_{h,i}^{k,n,m}(\mathbf{x}):=\mathcal{I}_{\mathrm{av}}(\tilde{\varphi}_{h,i}^{k,n,m})(\mathbf{x}),$$

where $\mathcal{I}_{\mathrm{av}}:\mathbb{P}_2(\mathcal{T}_{h,i})\to\mathbb{P}_2(\mathcal{T}_{h,i})\cap H^1(\Omega_i)$ is the interpolation operator given by

$$\mathcal{I}_{\mathrm{av}}(\phi_h)(\mathbf{x})=\frac{1}{|\mathcal{T}_{\mathbf{x}}|}\sum_{K\in\mathcal{T}_{\mathbf{x}}}\phi_h|_K(\mathbf{x}),$$

with $\mathcal{T}_{\mathbf{x}}$ the set of all the elements of $\mathcal{T}_{h,i}$ sharing the node $\mathbf{x}$. At the Lagrangian nodes $\mathbf{x}$ situated at the boundary Γ_i^{D}, we set $\hat{\varphi}_{h,i}^{k,n,m}(\mathbf{x}):=\varphi_i(g_i(\mathbf{x}))$.

4.5.2.2 H^1-conforming reconstruction $s_{h\tau}^{k,m}$

We now consider $\varphi_i^{-1}(\hat{\varphi}_{h,i}^{k,n,m})$ and modify them at the interface Γ in order to satisfy (4.23c), as well as on the boundaries Γ_i^{D} to satisfy (4.23b). In order to satisfy the mean value condition (4.23d), we proceed as in [67, Section 3.2.2] and employ the bubble functions b_K over each element $K \in \mathcal{T}_h$ (the product of the barycentric coordinates for a simplex), multiplied by suitable constants α_K.

Remark 4.5.4 (Practice)**.** *In practice, we only arrive at satisfying the condition* (4.23c) *in the sense of quadrature. Indeed, for* $1 \le n \le N$, $1 \le i \le 2$, *and any node* $\mathbf{x}_\Gamma$ *of the chosen quadrature rule lying at the interface* Γ, *we can request*

$$\Pi_i(s_h^{k,n,m}|_{\Omega_i}(\mathbf{x}_\Gamma)) = \frac{\Pi_i(\varphi_i^{-1}(\hat{\varphi}_{h,i}^{k,n,m}(\mathbf{x}_\Gamma))) + \Pi_j(\varphi_j^{-1}(\hat{\varphi}_{h,j}^{k,n,m}(\mathbf{x}_\Gamma)))}{2}.$$

Similarly, equation (4.23d) *will also typically only be satisfied up to a quadrature error.*

4.5.3 Equilibrated flux reconstruction $\boldsymbol{\sigma}_{h\tau}^{k,m}$

Because of the domain decomposition formulation with Robin or Ventcell transmission conditions, the finite volume fluxes $F_{K,\sigma}(u_{h,i}^{k,n,m})$ (or their linearizations $F_{K,\sigma}^{m-1}(u_{h,i}^{k,n,m})$) do not match from the two sides of the interface Γ. Consequently, $\mathbf{u}_h^{k,n,m}$ given by (4.19) is not $\mathbf{H}(\mathrm{div},\Omega)$-conforming, i.e., it does not lie in the space $\mathbf{RTN}_0(\Omega)$. We now present, following [11], a procedure allowing to construct an equilibrated flux $\boldsymbol{\sigma}_{h\tau}^{k,m}$ that satisfies

$$\boldsymbol{\sigma}_{h\tau}^{k,m} \in P_\tau^0(\mathbf{RTN}_0(\Omega)), \tag{4.25a}$$

$$\left(f^n - \frac{u_K^{k,n,m} - u_K^{k,n-1}}{\tau^n} - \nabla\cdot\boldsymbol{\sigma}_h^{k,n,m}, 1\right)_K = 0, \quad \forall K \in \mathcal{T}_h. \tag{4.25b}$$

For each subdomain Ω_i, we consider a subset B_i of Ω_i, termed a band, which contains all the elements of $\mathcal{T}_{h,i}$ that share a face with the interface Γ. We denote by $\mathcal{T}_{h,i}^B$ the resulting submesh. We start by setting

$$\boldsymbol{\sigma}_h^{k,n,m}|_K := \mathbf{u}_h^{k,n,m}|_K, \quad \forall K \in \mathcal{T}_{h,i} \text{ s.t. } K \subset \Omega_i \backslash B_i. \tag{4.26}$$

In the bands, we will modify $\mathbf{u}_h^{k,n,m}$ so as to arrive at (4.25); note that simply prescribing the normal components of $\boldsymbol{\sigma}_h^{k,n,m}$ by $\{\!\{\mathbf{u}_{h,i}^{k,n,m}\cdot\mathbf{n}_{B_i}\}\!\}$ at the interface would lead to (4.25a) but not to (4.25b).

We first calculate the mass balance misfit by

$$err_i^{k,n,m} = \left(f_i^n - \frac{u_K^{k,n,m} - u_K^{k,n-1}}{\tau^n}, 1\right)_{B_i} - (\{\!\{\mathbf{u}_{h,i}^{k,n,m}\cdot\mathbf{n}_{B_i}\}\!\}, 1)_{\partial B_i}, \quad i = 1,2,$$

where $\mathbf{n}_{B_i}$ is the outward unit vector normal to ∂B_i. We next denote by Γ_i^b, $b = 1,2,3,4$, the four boundaries (in 3D) of ∂B_i that intersect $\partial\Omega$, for $i = 1,2$. We denote also by Γ_i^{int} the boundary of ∂B_i that is inside Ω_i, $i = 1,2$, see Figure 4.4. We then identify nine corrections $\left(c_{\Gamma_1^b}^{k,n,m}\right)_{1\le b\le 4}$, $\left(c_{\Gamma_2^b}^{k,n,m}\right)_{1\le b\le 4}$, and $c_\Gamma^{k,n,m}$ to the averaged flux

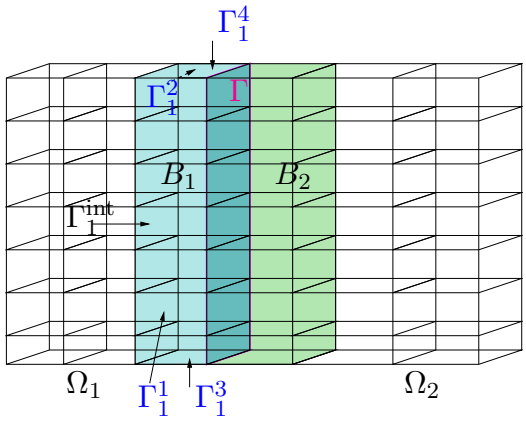

Figure 4.4: Bands B_1 and B_2 surrounding the interface Γ in three space dimensions

$\{\!\{\mathbf{u}_{h,i}^{k,n,m}\cdot\mathbf{n}_{B_i}\}\!\}$ that will lead to equilibrium in each band B_i, $i=1,2$. In other words, we seek to satisfy the two balancing conditions:

$$\sum_{b=1}^{4} c_{\Gamma_i^b}^{k,n,m} + (\mathbf{n}_\Gamma\cdot\mathbf{n}_{B_i})c_\Gamma^{k,n,m} = err_i^{k,n,m}, \quad i=1,2. \tag{4.27}$$

Here $\mathbf{n}_\Gamma$ is a unit vector normal to Γ, pointing either from Ω_1 to Ω_2, or from Ω_2 to Ω_1.

The interface problem (4.27) is a rectangular linear system of nine unknowns and two equations and is solved via the least squares minimization; it may be seen as a coarse-grid balancing solve in a simplified version of [49], tailored to Robin or Ventcell boundary conditions. Finally, the corrections are distributed from the boundary of the bands to their interiors by approximating, using the mixed finite element or the finite volume method, the following local Neumann problems: find $(q_{h,i}^{k,n,m},\boldsymbol{\sigma}_{h,i}^{k,n,m}) \in \mathbb{P}_0(\mathscr{T}_{h,i}^B)\times\mathbf{RTN}_0(B_i)$ with $(q_{h,i}^{k,n,m},1)_{B_i}=0$ such that

$$\begin{cases} \nabla\cdot\boldsymbol{\sigma}_{h,B_i}^{k,n,m}|_K = f_i^n|_K - \dfrac{u_K^{k,n,m}-u_K^{k,n-1,m}}{\tau^n} & \forall K\in\mathscr{T}_{h,i}^B,\\ \boldsymbol{\sigma}_{h,B_i}^{k,n,m} - \mathbf{u}_{h,i}^{k,n,m} = -\nabla q_{h,i}^{k,n,m}, & \text{in } B_i,\\ \boldsymbol{\sigma}_{h,B_i}^{k,n,m}\cdot\mathbf{n}_\Gamma = \mathbf{u}_{h,i}^{k,n,m}\cdot\mathbf{n}_\Gamma, & \text{on } \Gamma_i^{\text{int}},\\ \boldsymbol{\sigma}_{h,B_i}^{k,n,m}\cdot\mathbf{n}_\Gamma = \{\!\{\mathbf{u}_h^{k,n,m}\cdot\mathbf{n}_\Gamma\}\!\} + \dfrac{1}{|\Gamma|}c_\Gamma^{k,n,m}, & \text{on } \Gamma,\\ \boldsymbol{\sigma}_{h,B_i}^{k,n,m}\cdot\mathbf{n}_\Gamma = \mathbf{u}_{h,i}^{k,n,m}\cdot\mathbf{n}_\Gamma + \dfrac{1}{|\Gamma_i^b|}c_{\Gamma_i^b}^{k,n,m}, & \text{on } \Gamma_i^b. \end{cases}$$

We finally complement (4.26) by setting $\boldsymbol{\sigma}_h^{k,n,m}|_{B_i} := \boldsymbol{\sigma}_{h,B_i}^{k,n,m}$.

4.6 A posteriori error estimate

Relying on the developments of the previous sections, we derive here a posteriori error estimates that include the domain decomposition error. More precisely, at each OSWR iteration $k\geq 1$ and at each linearization step $m\geq 1$, we bound an energy error

between the postprocessed saturation $\tilde{u}_{h\tau}^{k,m}$ defined in Section 4.5.1 and the weak solution u of Definition 4.2.2 by a guaranteed and fully computable upper bound. Before formulating the a posteriori error estimates, we recall the Poincaré inequality:

$$\|q - q_K\| \le C_{\mathrm{P},K} h_K \|\nabla q\|_K, \quad \forall q \in H^1(K),$$

where q_K is the mean value of the function q on the element K and $C_{\mathrm{P},K} = 1/\pi$ whenever the element K is convex.

It is important to stress that the result below applies to all functions $s_{h\tau}^{k,m} \in Z$, such that $\varphi_i(s_{h\tau,i}^{k,m}) \in X_{\varphi_i(g_i)}$ and $\Pi(s_{h\tau}^{k,m},\cdot) \in X_{\Pi(g,\cdot)}$. For all times $t \in (0,T)$, let

$$Q_{t,i} := L^2(0,t;L^2(\Omega_i)), \qquad X_t := L^2(0,t;H_0^1(\Omega)), \qquad X_t' := L^2(0,t;H^{-1}(\Omega)).$$

Because of the assumptions on the weak solution u in Definition 4.2.2 and since $\varphi_i(\tilde{u}_{h\tau,i}^{k,m}) = \tilde{\varphi}_{h\tau,i}^{k,m} \in L^2(0,T;L^2(\Omega_i))$ by (4.21)–(4.22), $\tilde{u}_{h\tau}^{k,m} \in X'$, and $\tilde{u}_{h\tau}^{k,m}(\cdot,T) \in H^{-1}(\Omega)$, we can define two energy-type error measures, following [56], as

$$\begin{aligned}\|u - \tilde{u}_{h\tau}^{k,m}\|_\star^2 := \sum_{i=1}^2 \|\varphi_i(u_i) - \varphi_i(\tilde{u}_{h\tau,i}^{k,m})\|_{Q_{T,i}}^2 + \frac{L_\varphi}{2}\|u - \tilde{u}_{h\tau}^{k,m}\|_{X'}^2 \\ + \frac{L_\varphi}{2}\|(u - \tilde{u}_{h\tau}^{k,m})(\cdot,T)\|_{H^{-1}(\Omega)}^2\end{aligned} \tag{4.28}$$

and

$$\begin{aligned}&\|u - \tilde{u}_{h\tau}^{k,m}\|_\sharp^2 := \|u - \tilde{u}_{h\tau}^{k,m}\|_\star^2 \\ &+ 2\sum_{i=1}^2 \int_0^T \left(\|\varphi_i(u_i) - \varphi_i(\tilde{u}_{h\tau,i}^{k,m})\|_{Q_{t,i}}^2 + \int_0^t \|\varphi_i(u_i) - \varphi_i(\tilde{u}_{h\tau,i}^{k,m})\|_{Q_{s,i}}^2 e^{t-s}\mathrm{d}s \right)\mathrm{d}t;\end{aligned} \tag{4.29}$$

recall that L_φ is the maximal Lipschitz constant of the functions φ_i defined by (4.7). We will also need the weaker distance

$$\begin{aligned}\|u - s_{h\tau}^{k,m}\|_\flat := \sqrt{\frac{L_\varphi}{2}} \Bigg\{ (2e^T - 1)\|u_0 - s_{h\tau}^{k,m}(\cdot,0)\|_{H^{-1}(\Omega)}^2 + \|\mathscr{R}(s_{h\tau}^{k,m})\|_{X'}^2 \\ + 2\int_0^T \left(\|\mathscr{R}(s_{h\tau}^{k,m})\|_{X_t'}^2 + \int_0^t \|\mathscr{R}(s_{h\tau}^{k,m})\|_{X_s'}^2 e^{t-s}\mathrm{d}s \right)\mathrm{d}t \Bigg\}^{\frac{1}{2}}\end{aligned} \tag{4.30}$$

featuring the residual $\mathscr{R}(s_{h\tau}^{k,m})$ of $s_{h\tau}^{k,m}$, given for $\psi \in X$, by

$$\begin{aligned}&\langle \mathscr{R}(s_{h\tau}^{k,m}), \psi\rangle_{X',X} \\ &:= \int_0^T \Big\{ (f,\psi) - \langle \partial_t s_{h\tau}^{k,m}, \psi\rangle_{H^{-1}(\Omega),H_0^1(\Omega)} - \sum_{i=1}^2 (\nabla\varphi_i(s_{h\tau,i}^{k,m}), \nabla\psi)_{\Omega_i} \Big\}(s)\mathrm{d}s,\end{aligned}$$

and its dual norm given by

$$\|\mathscr{R}(s_{h\tau}^{k,m})\|_{X'} := \sup_{\psi\in X,\, \|\psi\|_X = 1} \langle \mathscr{R}(s_{h\tau}^{k,m}), \psi\rangle_{X',X}.$$

Our main result is summarized in the following theorem:

Theorem 4.6.1 (A posteriori error estimate). *Let u be the weak solution of the multidomain problem (4.9)–(4.10) in the sense of Definition 4.2.2. Let $\tilde{u}_{h\tau}^{k,m}$ be the postprocessed saturation at the iteration $k \geq 1$ and the linearization step $m \geq 1$, prescribed by (4.21)–(4.22) from the finite volume OSWR scheme of Section 4.4.3. Let $s_{h\tau}^{k,m}$ and $\boldsymbol{\sigma}_{h\tau}^{k,m}$ be the reconstructed functions as obtained in Sections 4.5.2 and 4.5.3. If*

$$\bar{\varphi} \in X, \quad \text{where} \quad \bar{\varphi}|_{\Omega_i} := \varphi_i(u_i) - \varphi_i(s_{h\tau,i}^{k,m}), \quad i = 1,2, \tag{4.31}$$

then there holds

$$\|u - \tilde{u}_{h\tau}^{k,m}\|_\sharp \leq \eta^{k,m} + \|\tilde{u}_{h\tau}^{k,m} - s_{h\tau}^{k,m}\|_\sharp, \tag{4.32}$$

and there always holds

$$\|u - s_{h\tau}^{k,m}\|_\flat \leq \eta^{k,m}, \tag{4.33}$$

where

$$\begin{aligned} \eta^{k,m} := \sqrt{\frac{L_\varphi}{2}} \Bigg\{ & (2e^T - 1)\big(\eta_{\mathrm{IC}}^{k,m}\big)^2 + \sum_{n=1}^{N} \big(\eta^{k,n,m}\big)^2 \\ & + 2\sum_{n=1}^{N} \tau^n \sum_{l=1}^{n} \big(\eta^{k,l,m}\big)^2 + 2\sum_{n=1}^{N}\sum_{l=1}^{n} J_{nl} \Big(\sum_{q=1}^{l} \big(\eta^{k,q,m}\big)^2 \Big) \Bigg\}^{\frac{1}{2}}, \end{aligned} \tag{4.34a}$$

where the initial condition estimator $\eta_{\mathrm{IC}}^{k,m}$ and the estimators $\eta^{k,n,m}$ are respectively defined by:

$$\eta_{\mathrm{IC}}^{k,m} := \|u_0 - s_{h\tau}^{k,m}(\cdot,0)\|_{H^{-1}(\Omega)}, \tag{4.34b}$$

$$\eta^{k,n,m} := \left\{ \int_{I^n} \sum_{i=1}^{2} \sum_{K \in \mathcal{T}_{h,i}} \Big(\eta_{\mathrm{R},K}^{k,n,m} + \eta_{\mathrm{disc},K,i}^{k,n,m}(t) \Big)^2 \mathrm{d}t \right\}^{\frac{1}{2}}, \quad 1 \leq n \leq N, \tag{4.34c}$$

with the residual and the discretization estimators given respectively by

$$\eta_{\mathrm{R},K}^{k,n,m} := C_{\mathrm{P},K} h_K \|f^n - \partial_t^n s_{h\tau}^{k,m} - \nabla\cdot\boldsymbol{\sigma}_h^{k,n,m}\|_K, \quad K \in \mathcal{T}_h, \tag{4.34d}$$

$$\eta_{\mathrm{disc},K,i}^{k,n,m}(t) := \|\boldsymbol{\sigma}_h^{k,n,m} + \nabla\varphi_i(s_{h\tau}^{k,m}(\cdot,t))\|_K, \quad K \in \mathcal{T}_{h,i},\ t \in I^n, \tag{4.34e}$$

and where we have set, for $1 \leq n, l \leq N$,

$$J_{nl} := \int_{I^n}\int_{I^l} e^{t-s}\mathrm{d}s\mathrm{d}t.$$

Proof. We have set $s_{h\tau}^{k,m}$ so that $\varphi_i(s_{h\tau,i}^{k,m}) \in X_{\varphi_i(g_i)}$, $\Pi(s_{h\tau}^{k,m},\cdot) \in X_{\Pi(g,\cdot)}$, and

$$(f^n - \partial_t^n s_{h\tau}^{k,m} - \nabla\cdot\boldsymbol{\sigma}_h^{k,n,m}, 1)_K = 0 \qquad \forall K \in \mathcal{T}_h,\ 1 \leq n \leq N. \tag{4.35}$$

Indeed, (4.35) follows from (4.25b) and from the requirement (4.23d) as in [67, Lemma 3.1]. Thus we can proceed as in [56, Theorem 5.3] to see (4.33). Next, it follows by inspection of the proof of [56, Theorem 5.2] that, under assumption (4.31), we have

$$\|u - s_{h\tau}^{k,m}\|_\sharp \leq \|u - s_{h\tau}^{k,m}\|_\flat. \tag{4.36}$$

Thus, (4.32) follows by the triangle inequality

$$\|u - \tilde{u}_{h\tau}^{k,m}\|_\sharp \leq \|u - s_{h\tau}^{k,m}\|_\sharp + \|\tilde{u}_{h\tau}^{k,m} - s_{h\tau}^{k,m}\|_\sharp.$$

□

Remark 4.6.2 (Condition (4.31))**.** *Condition* (4.31) *seems unfortunately necessary to apply [56, Theorem 5.2] so as to obtain* (4.36)*, and is indeed rather restrictive for the complete problem* (4.9)–(4.10)*. One may, though, typically expect that it will be satisfied when the global mobilities of the gas λ_i are the same in the two subdomains (no jump of λ over the interface Γ), so that both $\varphi_i(u_i)$ and $\varphi_i(s_{h\tau,i}^{k,m})$ are continuous over the space-time interface $\Gamma\times(0,T)$ in the sense of traces.*

Remark 4.6.3 (A posteriori estimate of the saturation and capillary pressure errors)**.** *Applying* (4.8)*, the above estimators bound also the saturation and the capillary pressure errors. More precisely, replacing the functions φ_i by the functions Π_i everywhere in* (4.28)–(4.29)*, the estimate* (4.32) *still holds.*

4.7 An a posteriori error estimate distinguishing the space, time, linearization, and the DD errors

In this section, we distinguish the different error components, proceeding as in [68, 42, 56, 11] and the references therein. The aim is in particular to separate the domain decomposition error from the estimated space, time, and linearization errors.

For the iteration $k\geq 1$ of the OSWR algorithm, for all time steps $0\leq n\leq N$, a linearization step $m\geq 1$, and both subdomains Ω_i, $i=1,2$, we define a vector function $\boldsymbol{\ell}_{h,i}^{k,n,m}\in\mathbf{RTN}(\Omega_i)$ that approximates the available flux used in the Newton iterations in Section 4.4.3, i.e.,

$$(\boldsymbol{\ell}_{h,i}^{k,n,m}\cdot\mathbf{n}_i,1)_\sigma=(F_{K,\sigma}^{m-1}(u_{h,i}^{k,n,m}),1)_\sigma,\quad\forall\sigma\in\mathscr{E}_K,\ \forall K\in\mathscr{T}_{h,i}. \tag{4.37}$$

The vector function $\boldsymbol{\ell}_{h,i}^{k,n,m}$ is called the linearized flux. It tends to $\mathbf{u}_{h,i}^{k,n,m}$ defined in (4.19) at convergence of the Newton algorithm. For all $K\in\mathscr{T}_{h,i}$, we then define the local *spatial*, *temporal*, *domain decomposition*, and *linearization* estimators by:

$$\eta_{\mathrm{sp},K,i}^{k,n,m}:=\eta_{\mathrm{R},K}^{k,n,m}+\|\nabla\varphi_i(s_{h\tau}^{k,m}(\cdot,t_n))+\boldsymbol{\ell}_{h,i}^{k,n,m}\|_K, \tag{4.38a}$$

$$\eta_{\mathrm{tm},K,i}^{k,n,m}(t):=\|\nabla\big(\varphi_i(s_{h\tau}^{k,m}(\cdot,t))-\varphi_i(s_{h\tau}^{k,m}(\cdot,t_n))\big)\|_K, \tag{4.38b}$$

$$\eta_{\mathrm{dd},K,i}^{k,n,m}:=\|\nabla\varphi_i(\tilde{u}_{h,i}^{k,n,m})+\boldsymbol{\sigma}_h^{k,n,m}\|_K, \tag{4.38c}$$

$$\eta_{\mathrm{lin},K,i}^{k,n,m}:=\|\nabla\varphi_i(\tilde{u}_{h,i}^{k,n,m})+\boldsymbol{\ell}_{h,i}^{k,n,m}\|_K; \tag{4.38d}$$

note that from (4.21) and (4.20a), $-\nabla\varphi_i(\tilde{u}_{h,i}^{k,n,m})=\mathbf{u}_{h,i}^{k,n,m}$, so that (4.38c) and (4.38d) only work with lowest-order Raviart–Thomas–Nédélec polynomials, so that they can be evaluated without numerical quadrature error and fast. Set, like in (4.34c), for $\mathrm{a}=\mathrm{sp},\mathrm{tm},\mathrm{dd},\mathrm{lin}$,

$$(\eta_{\mathrm{a},i}^{k,n,m})^2:=\int_{I^n}\sum_{K\in\mathscr{T}_{h,i}}(\eta_{\mathrm{a},K,i}^{k,n,m})^2\mathrm{d}t\quad\text{and}\quad(\eta_{\mathrm{a}}^{k,n,m})^2:=\sum_{i=1}^2(\eta_{\mathrm{a},i}^{k,n,m})^2, \tag{4.39}$$

and note that except for $\mathrm{a}=\mathrm{tm}$, $(\eta_{\mathrm{a},i}^{k,n,m})^2=\tau^n\sum_{K\in\mathscr{T}_{h,i}}(\eta_{\mathrm{a},K,i}^{k,n,m})^2$; for $\mathrm{a}=\mathrm{tm}$, the dependence of the estimators on time is left implicit. The global versions, like in (4.34a) but

without the initial condition, are

$$\begin{aligned}\eta_{\mathrm{a}}^{k,m} :=& \sqrt{\frac{L_\varphi}{2}}\Bigg(\Bigg\{\sum_{n=1}^{N}\Big(\eta_{\mathrm{a}}^{k,n,m}\Big)^2\Bigg\}^{\frac{1}{2}} + \sqrt{2}\Bigg\{\sum_{n=1}^{N}\tau^n\sum_{l=1}^{n}\Big(\eta_{\mathrm{a}}^{k,l,m}\Big)^2\Bigg\}^{\frac{1}{2}} \\ &+ \sqrt{2}\Bigg\{\sum_{n=1}^{N}\sum_{l=1}^{n}J_{nl}\sum_{q=1}^{l}\Big(\eta_{\mathrm{a}}^{k,q,m}\Big)^2\Bigg\}^{\frac{1}{2}}\Bigg) + \delta_{\mathrm{a}}\|\tilde{u}_{h\tau}^{k,m} - s_{h\tau}^{k,m}\|_\sharp,\end{aligned} \tag{4.40}$$

where $\delta_{\mathrm{a}} = 0$ for $\mathrm{a} = \mathrm{tm}, \mathrm{dd}, \mathrm{lin}$ and δ_{sp} is set to 0 or 1. Then using estimates (4.32) and (4.33) together with the triangle inequality gives:

corollary 4.7.1 (A posteriori error estimate distinguishing the error components)**.** *Let the assumptions of Theorem 4.6.1 be satisfied. Let the linearized flux $\boldsymbol{\ell}_h^{k,n,m}$ be given by (4.37) and the estimators by (4.34b) and (4.38)–(4.40). Then, under condition (4.31) and with $\delta_{\mathrm{sp}} = 1$,*

$$\|u - \tilde{u}_{h\tau}^{k,m}\|_\sharp \le \sqrt{\frac{L_\varphi}{2}}\sqrt{2e^T - 1}\,\eta_{\mathrm{IC}}^{k,m} + \eta_{\mathrm{sp}}^{k,m} + \eta_{\mathrm{tm}}^{k,m} + \eta_{\mathrm{dd}}^{k,m} + \eta_{\mathrm{lin}}^{k,m},$$

whereas

$$\|u - s_{h\tau}^{k,m}\|_\flat \le \sqrt{\frac{L_\varphi}{2}}\sqrt{2e^T - 1}\,\eta_{\mathrm{IC}}^{k,m} + \eta_{\mathrm{sp}}^{k,m} + \eta_{\mathrm{tm}}^{k,m} + \eta_{\mathrm{dd}}^{k,m} + \eta_{\mathrm{lin}}^{k,m}$$

without any assumption and with $\delta_{\mathrm{sp}} = 0$.

4.8 Stopping criteria and optimal balancing of the different error components

We provide here stopping criteria for the OSWR algorithm and the nonlinear solver for the subdomain problems as in [68, 42, 56, 11] and the references therein.

Let two real parameters δ_{lin} and δ_{dd} be given in $(0, 1)$. The stopping criteria for the linearization step (inner loop in m) in each subdomain i, at each time step n, and each OSWR iteration k is chosen as, employing the estimates (4.39)

$$\eta_{\mathrm{lin},i}^{k,n,m} \le \delta_{\mathrm{lin}} \max\Big\{\eta_{\mathrm{sp},i}^{k,n,m}, \eta_{\mathrm{tm},i}^{k,n,m}, \eta_{\mathrm{dd},i}^{k,n,m}\Big\}, \quad i = 1, 2. \tag{4.41}$$

Similarly, the stopping criteria for the OSWR algorithm (outer loop in k) is set as, employing the estimates (4.40),

$$\eta_{\mathrm{dd}}^{k,m} \le \delta_{\mathrm{dd}} \max\Big\{\eta_{\mathrm{sp}}^{k,m}, \eta_{\mathrm{tm}}^{k,m}\Big\}. \tag{4.42}$$

The first criterion (4.41) stipulates that there is no need to continue with the linearization iterations if the overall error is dominated by the other components. That of the second criterion (4.42) decides that we stop the OSWR algorithm if the domain decomposition error is dominated by one of the other components. The entire procedure of the approach is then described by the following algorithm:

Data: Enter T, u_0, and Ω_i, π_i, λ_i, and f_i, $i = 1,2$.
Result: The saturations $u^{k,m}_{h\tau,i}$.
Give the initial Ventcell guess $\Psi_i^{0,1}$, $i = 1,2$, on Γ;
$k := 0$;
repeat
  $k \longleftarrow k+1$;
  for *i=1,2* **do**
    $j := (3-i)$;
    $n := 0$;
    while $t^n \leq T$ **do**
      $n \longleftarrow n+1$;
      $m := 0$;
      repeat
        $m \longleftarrow m+1$;
        $u^{k,n,m}_{h,i} := \Upsilon_i(u^{k,n,m-1}_{h,i}, \Psi^{k-1,n}_j, f^n_i, u^{k,n-1}_{h,i})$ by (4.18);
        Compute $\eta^{k,n,m}_{\mathrm{sp},i}$, $\eta^{k,n,m}_{\mathrm{tm},i}$, $\eta^{k,n,m}_{\mathrm{dd},i}$, and $\eta^{k,n,m}_{\mathrm{lin},i}$;
      until $\eta^{k,n,m}_{\mathrm{lin},i} \leq \delta_{\mathrm{lin}} \max\left\{\eta^{k,n,m}_{\mathrm{sp},i}, \eta^{k,n,m}_{\mathrm{tm},i}, \eta^{k,n,m}_{\mathrm{dd},i}\right\}$;
      Set $u^{k,n}_{h,i} := u^{k,n,m}_{h,i}$;
      Set $\Psi^{k-1,n}_i := \{\Psi^{k-1,n}_{L,\sigma}\}_{\sigma=K|L, K\in\mathcal{T}_{h,i}, L\in\mathcal{T}_{h,j}}$ with, by (4.17), $\Psi^{k-1,n}_{L,\sigma} :=$
      $F_{L,\sigma}(u^{k-1,n}_{h,j}) + \gamma_{i,j}\dfrac{\Pi_j(u^{k-1,n}_{L,\sigma}) - \Pi_j(u^{k-1,n-1}_{L,\sigma})}{\tau^n}|\sigma| + \left(\Lambda_{L,\Gamma}(u^{k-1,n}_{h,j})\right)_\sigma$;
    end
  end
  Compute $\eta^{k,m}_{\mathrm{sp}}$, $\eta^{k,m}_{\mathrm{tm}}$, $\eta^{k,m}_{\mathrm{dd}}$;
until $\eta^{k,m}_{\mathrm{dd}} \leq \delta_{\mathrm{dd}} \max\left\{\eta^{k,m}_{\mathrm{sp}}, \eta^{k,m}_{\mathrm{tm}}\right\}$;

Algorithm 1: Complete solution algorithm with adaptive stopping criteria

Remark 4.8.1 (Space and time adaptivity)**.** *The above local-in-time estimators are calculated on each element of the mesh and on each time step, and could also be used as indicators in order to refine adaptively the time steps τ^n and/or the space meshes $\mathcal{T}_{h,i}$, see [56, 42, 158] and the references therein.*

4.9 Numerical experiments

In this section we illustrate the efficiency of our theoretical results on a numerical experiment with the finite volume OSWR algorithm of Section 4.4. We take $\Omega = [0,1]^3$ and $T = 15$. The subdomains are $\Omega_1 = \{0 < x < 1/2\}$ and $\Omega_2 = \{1/2 < x < 1\}$, with $\Gamma = \{x = 1/2\}$. We consider the capillary pressure functions and the global mobilities from [63] given respectively by

$$\pi_1(u) = 5u^2, \qquad \pi_2(u) = 5u^2 + 1, \qquad \lambda_i(u) = u(1-u),\ i \in \{1,2\}.$$

We impose Dirichlet conditions on two subsets of the boundary $\partial\Omega$. A saturation is set equal to 0.9 on $\Gamma_{\mathrm{D,in}} = \{(x,y,z) \in \partial\Omega \mid x = 0 \text{ and } 0.4 \leq y \leq 0.6\}$. On the outflow boundary $\Gamma_{\mathrm{out}} = \{(x,y,z) \in \partial\Omega \mid x = 1\}$, the saturation at time t^{n+1} is set equal to that inside the closest cell at time t^n (see [6]). We assume homogeneous Neumann

boundary conditions on the remaining part of the boundary. The initial condition is taken to be zero everywhere and fitting the condition (4.10a) at the interface between the rocks. We take $f = 0$ in Ω_1 and Ω_2. The gas is moving through the interface Γ before penetrating the subdomain Ω_2. Note that the gas cannot enter the subdomain Ω_2 if the capillary pressure $\pi_1(u_1)$ is lower than the entry pressure $\pi_1(u_1^*)$, with $u_1^* = \dfrac{1}{\sqrt{5}}$.

For the spatial discretization, we use uniform meshes in the subdomains consisting of rectangular parallelepipeds matching on the interface Γ. The implementation is based on the Matlab Reservoir Simulation Toolbox [115], and makes use of its automatic differentiation feature to compute the Jacobian matrices for solving the nonlinear subdomain problems by Newton's method. The optimized (Robin or Ventcell) parameters are computed by numerically minimizing the continuous convergence factor corresponding to a linearized version of the problem (see [7] for details).

In the rest of this section, we denote the method defined by using the OSWR method with Robin transmission conditions by Robin-OSWR, while the method using full Ventcell transmission conditions will be denoted by Ventcell-OSWR. When appropriate, we qualify the Robin conditions as one-sided ($\alpha_{12} = \alpha_{21}$) or two-sided in the more general case.

4.9.1 The performance of the OSWR method with adaptive stopping criteria

We start by analyzing the performance of the OSWR algorithm with adaptive stopping criteria of Section 4.8. We in particular compare (4.42) with the common approach in which the OSWR algorithm is continued until the residual on the interface becomes smaller than a threshold taken as 10^{-6}, i.e.,

$$\|\Psi_1^k - \Psi_1^{k-1}\|_\infty + \|\Psi_2^k - \Psi_2^{k-1}\|_\infty \leq 10^{-6}. \tag{4.43}$$

The Newton iterations are first stopped when the residual

$$\leq 10^{-8}. \tag{4.44}$$

In this first experiment, we consider the OSWR algorithm with Robin transmission conditions, i.e. $\gamma_{12} = \gamma_{21} = 0$ and $\alpha = \alpha_{1,2} = \alpha_{2,1}$. Four snapshots of the saturation are shown in Fig. 4.5, together with two snapshots of the capillary pressure in Fig. 4.6. As expected, the saturation of the gas in Ω_1, as well as the capillary pressure, increase until the capillary pressure reaches the entry pressure. We can see that the capillary pressure field becomes continuous when the entry pressure is reached, then Ω_2 is infiltrated by the gas, but the saturation remains discontinuous across the interface and some quantity of gas remains trapped under the rock discontinuity.

Next we verify the performance of the optimized parameters. Fig. 4.7 (left) shows the domain decomposition estimator $\eta_{\text{dd}}^{k,m}$ after $k = 25$ OSWR iterations as a function of the Robin parameter α. The estimator behaves very similarly to what is usually observed for the DD error (see e.g. [71]). Moreover, the optimized parameter (marked by a square) is close to the numerically optimal value. This result points the way to the possibility of finding the optimal Robin parameter by minimizing the DD estimator. It also confirms the efficiency of the DD estimator to separate the domain decomposition error from the other components of the global error.

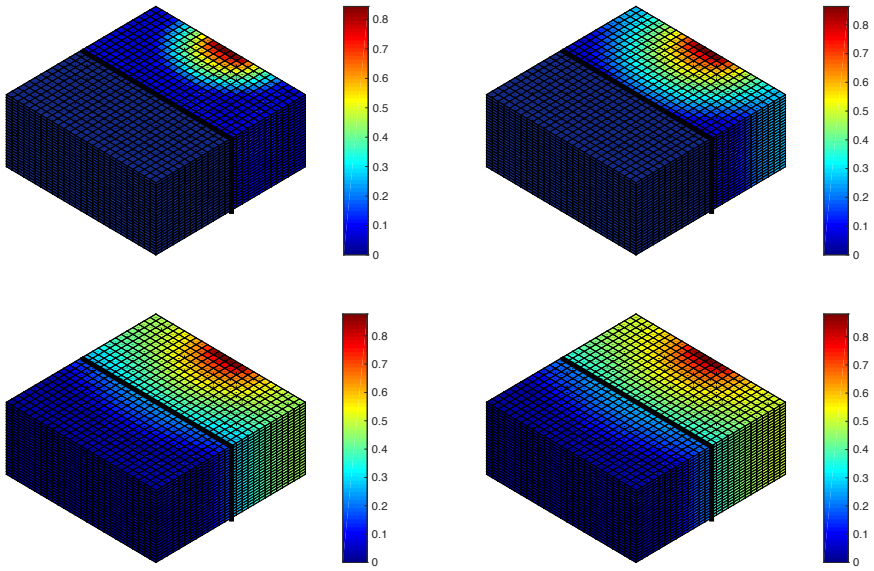

Figure 4.5: Robin interface conditions: saturation $u(t)$ for $t = 2.9$, $t = 6.6$, $t = 13$, and $t = 15$

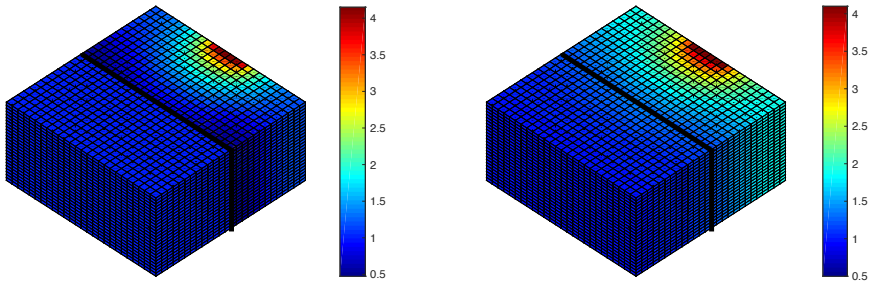

Figure 4.6: Robin interface conditions: capillary pressure field $\pi(u(t), \cdot)$ for $t = 6.6$ and $t = 15$

In Fig. 4.7 (right), we plot the dependence of the different estimators on the OSWR iterations. The adaptive stopping criterion (4.42) needs only 10 iterations, while the classical stopping criterion (4.43) requires 25 iterations.

Fig. 4.8 depicts the evolution of the estimated error after using the stopping criteria (4.42) with $\delta_{\text{dd}} = 0.1$ and (4.41) with $\delta_{\text{lin}} = 0.1$. We notice that the error distribution follows the saturation front but also that some error near the interface is still detected. In Fig. 4.9, the domain decomposition error is shown at two different time steps, and clearly one can remark that the DD error is not affecting the global error, in agreement with (4.42). The results, from a practical viewpoint, coincide with the results obtained using classical stopping criteria (4.44) and (4.43).

Fig. 4.10 plots the different estimators in each subdomain, as a function of the Newton iteration at the final iteration of OSWR algorithm. Only three iterations are required to reach (4.41) for the subdomain solvers, where 13 iterations for the solves in Ω_1 and 7 iterations for the solves in Ω_2 are needed to reach the classical criteria (4.44).

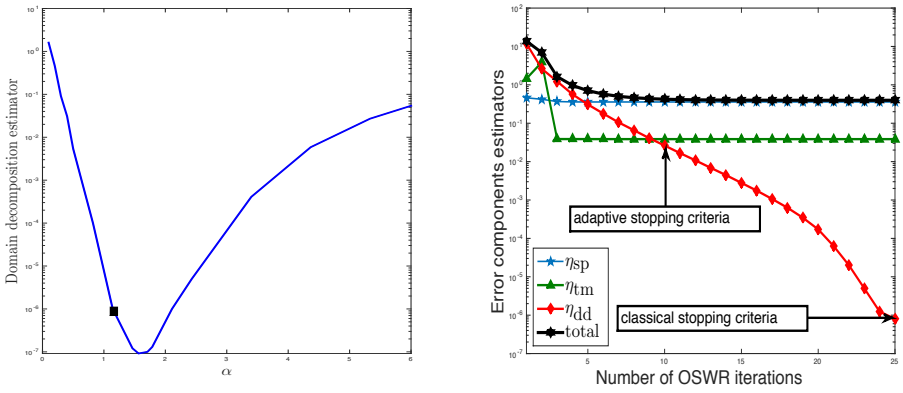

Figure 4.7: Domain decomposition error estimator $\eta_{\text{dd}}^{k,m}$ after $k = 25$ Robin-OSWR iterations as a function of the parameter α (left) and evolution of the spatial, temporal, and domain decomposition error estimators as a function of the number of Robin-OSWR iterations (right)

4.9.2 Comparison of Robin- and Ventcell-OSWR algorithm with adaptive stopping criteria

We now consider the OSWR algorithm with two-sided Robin transmission conditions (i.e. $\gamma_{12} = \gamma_{21} = 0$ and $\alpha_{12} \neq \alpha_{21}$) on the one hand, and Ventcell transmission conditions (i.e. $\gamma = \gamma_{12} = \gamma_{21}$ and $\alpha = \alpha_2 = \alpha_{21}$) on the other hand. Fig. 4.11 shows, for each method, the dependence of the different estimators on the number of DD iterations. We observe that the estimated space and time errors coincide for the two methods and that they are also very close to those obtained with the one-sided Robin-OSWR algorithm (see Fig. 4.7), as expected. For the DD error, both methods are faster than the one-sided Robin-OSWR method. The usual stopping criteria are reached after 14 and 9 iterations respectively, whereas only 4 iterations are needed with the adaptive stopping criteria 4.42. Fig. 4.12 shows contour lines of the DD estimator $\eta_{\text{dd}}^{k,m}$ as a function of the parameters, at the final OSWR iteration. The square marks the parameters obtained via the optimization procedure described previously. It is worth noting that this optimized parameter is close to the parameter that numerically minimizes the error estimate $\eta_{\text{dd}}^{k,m}$.

We have also checked the efficiency of the adaptive linearization stopping criterion (4.41) for both methods. The results (not shown here) are similar to the Robin-OSWR case, which allows to stop the Newton algorithm after 4 iterations for most of the solves, instead of 8 and 15 for the classical criterion.

The results confirm that the domain decomposition estimator is a practical tool to estimate the domain decomposition error component and that combining optimized parameters and adaptive stopping criteria results in efficient OSWR algorithms.

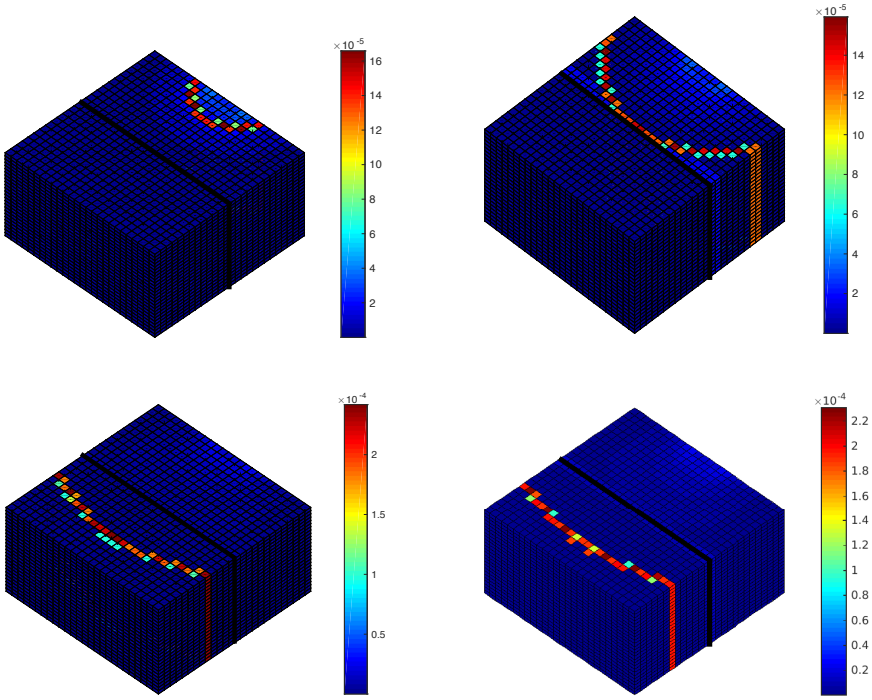

Figure 4.8: Robin interface conditions: estimated error for $t = 2.9$, $t = 6.6$, $t = 13$, and $t = 15$

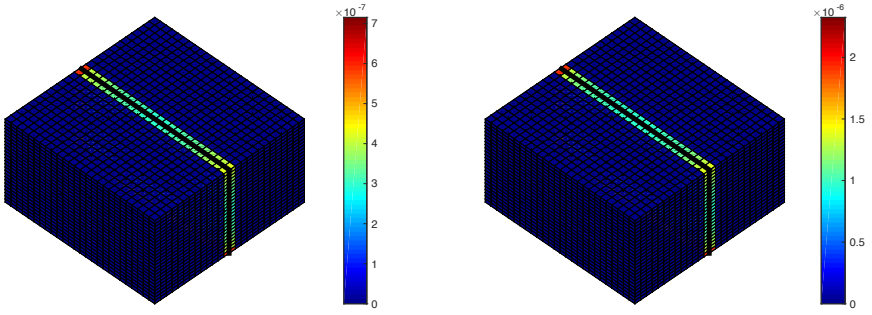

Figure 4.9: Robin interface conditions: estimated DD error for $t = 6.6$ and $t = 15$

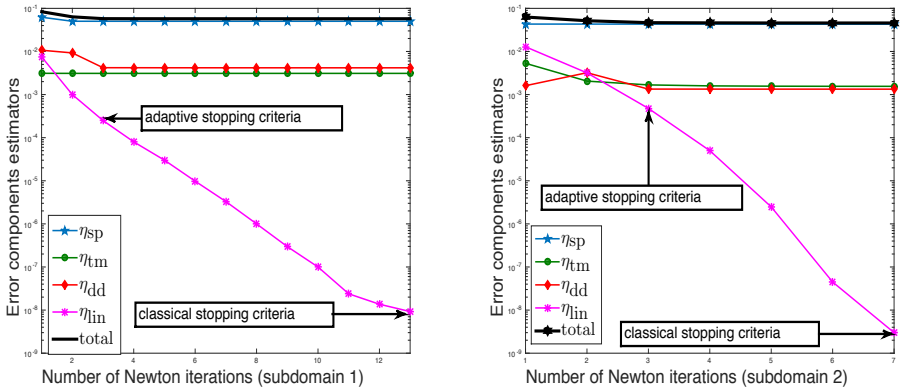

Figure 4.10: Robin interface conditions: evolution of the spatial, temporal, domain decomposition, and linearization error estimators as a function of Newton iterations for the final iteration of OSWR algorithm for $t = 6.6$; subdomain 1 (left) and subdomain 2 (right)

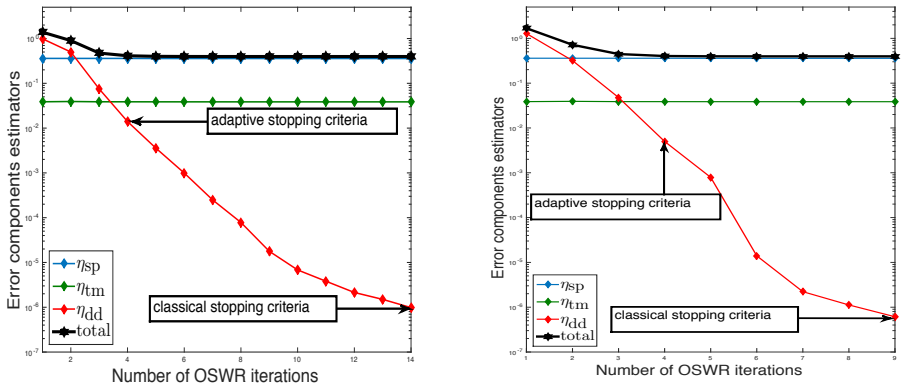

Figure 4.11: Evolution of the spatial, temporal, and domain decomposition error estimators as a function of OSWR iterations for the two-sided Robin-OSWR method (left) and the Ventcell-OSWR method (right)

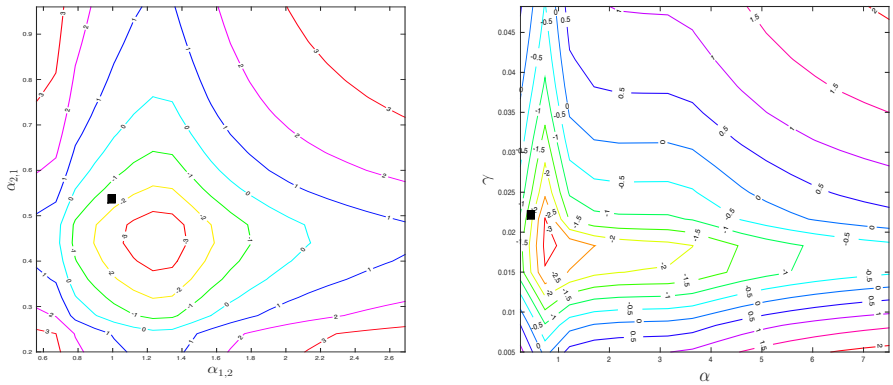

Figure 4.12: Domain decomposition error estimator $\eta_{dd}^{k,m}$ as a function of the free parameters after 4 iterations of the OSWR of the two-sided Robin-OSWR method (left) and 3 iterations of the optimized Ventcell-OSWR method (right)

Conclusions and future work

In this thesis, we have developed a posteriori analysis for:

- the optimized Schwarz (Robin-to-Robin) domain decomposition method using the mixed finite element discretization in space for the steady diffusion equation,
- the global-in-time optimized Schwarz method using the mixed finite element discretization in space and the discontinuous Galerkin scheme in time for the unsteady diffusion case,
- the global-in-time optimized Schwarz method using the finite volume discretization in space and the backward Euler scheme in time for the two-phase flow case.

For the heat equation, a global-in-time domain decomposition method is used for both conforming and nonconforming time grids allowing for different time steps in different subdomains. At the space-time interface, data is transferred between two subdomains using a suitable projection. Domain decomposition method is specially used when different geological properties are involved, which leads to strong heterogeneity in space. Then, nonconforming discretization in time is used because of the various physical or chemical processes independently in each subdomain.

We have succeeded in bounding the error between the exact solution of the partial differential equation and the approximate numerical solution at each iteration of the domain decomposition algorithm by fully computable estimators using the theory of a posteriori estimates. Moreover, different components of the error were distinguished. For the diffusion equation, these are: estimators due to the discretization in space using the lowest-order mixed finite element scheme and estimators due to the domain decomposition method. For the heat equation there appear in addition a discretization in time estimator. Finally, for the two-phase flow, in addition to discretization in space, discretization in time, and domain decomposition estimators, a linearization estimator appears as well. This distinguishing of different error components allows us to define efficient stopping criteria for the domain decomposition algorithm (linearization possible as well). All the derived error bounds are guaranteed and enable the actual error control. Numerical experiments are carried out for different test cases, including industrial test for nuclear waste storage.

Through this work, it was shown that:

- The quality of the resulting approximation can be assessed by controlling the error between the approximate solution and the exact solution.

- The proposed methodology has been mathematically justified and applied on problems ranging from linear, steady model and unsteady Darcy flow to a two-phase porous media flow with disappearing phase and nonlinear and discontinuous transmission condition with an important industrial application.
- The overestimation factors (effectivity indices) are very close to the optimal value of one for the linear, steady Darcy equation and still very reasonable also for the heat equation.
- We obtain an efficient criterion to stop the domain decomposition iterations. Often, as much as 70% of the usually performed domain decomposition iterations can be spared.
- Thus a large portion of the computing time can be saved.
- The proposed estimators enable to design of adaptive strategies with equilibration of all the domain decomposition error, the space discretization error, and the time discretization error (linearization error in the two-phase flow case).

This work can be taken further in various directions, one of which is the extention to the advection-diffusion equation in the operator splitting context. We use operator splitting introduced in [100] to treat the advection and the diffusion separately and differently. The a posteriori estimates can then be easily extended from the unsteady diffusion equation to this case. We can also study the local efficiency (9) for each problem presented in this work. Another perspective is to develop the a posteriori error estimates for the Robin domain decomposition method in the conforming finite element discretization context. In this case, the potential is locally conforming in each subdomain but the available flux is not $\mathbf{H}(\mathrm{div},\Omega)$-conforming even in the subdomains. Applying the averaging operator at each Lagrangian node of the interface between two subdomains, we can obtain a potential reconstruction which is globally conforming, and flux in each subdomain can be easily obtained by the equilibration procedures derived in the context of exact linear solvers. The challenge here would thus be to obtain a globally $\mathbf{H}(\mathrm{div},\Omega)$-conforming flux.

Appendix A

Vectorisation in MATLAB

In this chapter, we will briefly present an efficient way to implement the a posteriori estimates in MATLAB that has been used to carry out the numerical experiments of this thesis.

To assemble finite element matrices using vector languages (e.g. Matlab, Octave, Python, R, Julia, Scilab, C++ with STL,...), a simple vectorized algorithms have been proposed recently, see e.g. [52] and the references therein. Inspiried by these vectorized algorithms, the numerical method, the mixed finite element in this thesis, is implemented in MATLAB in order to solve subdomain problems. The algorithm in MATLAB can be optimized and accelerated by avoiding the big loops such as the loop over the mesh elements using the vectorization (vector and matrix operations). Note that if we do not avoid the loop over large systems, the computing time can quickly increase significantly since each line has to be computed at each iteration of the loop.

Let Ω be the computational domain and let $\mathcal{T}_h = \{K_1, K_2, K_3, K_4, K_5, K_6\}$ be an example of triangulation of Ω, see Figure A.1.

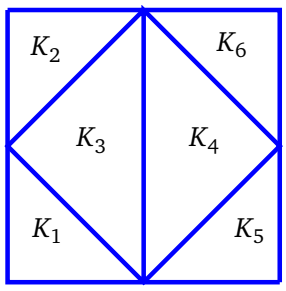

Figure A.1: Triangulation mesh of the domain Ω

In order to compute the estimators proposed in this thesis, for example the domain decomposition estimator (2.19) given in Chapter 2, we first recall how to compute the L^2-norm:

$$
\begin{aligned}
||u||^2 &= \Big(\sum_{a=1}^{M}\mu_a w_a(\mathbf{x}), \sum_{a=1}^{M}\mu_a w_a(\mathbf{x})\Big)_\Omega \\
&= \sum_{a=1}^{M}\sum_{b=1}^{M}\mu_a\mu_b\big(w_a(\mathbf{x}), w_b(\mathbf{x})\big)_\Omega \\
&= X'QX
\end{aligned}
\tag{A.1}
$$

where w_a, for $a = 1, ..., M$, are the M basis functions and μ_a is the components of u in the basis w_a, $X = (\mu_a)_{a=1,..,M}$, and where the components of the square matrix Q are as follows:

$$
(Q)_{a,b} = \big(w_a(\mathbf{x}), w_b(\mathbf{x})\big)_\Omega. \tag{A.2}
$$

In the context of the lowest-order mixed finite element method, $\mathbf{u}_h$ is decomposed in the RT0 basis on each mesh element K as follows:

$$
\mathbf{u}_h(\mathbf{x}) = \sum_{e\in\mathscr{E}_K} u_e\psi_e(\mathbf{x}), \tag{A.3}
$$

where $\psi_e(\mathbf{x})$ is the RT0 basis function associated with the edge e and where $\mathscr{E}_K$ is the set of egdes of K. In two dimension, $|\mathscr{E}_K|$ is equal to 3, the number of egdes of a triangle. Then the DD estimator $\eta^2_{\mathrm{DDF},K}$ on a mesh element K, given by (2.19), is written as follows:

$$
\begin{aligned}
\eta^2_{\mathrm{DDF},K} &:= |||\mathbf{u}_h^{k+1} - \boldsymbol{\sigma}_h^{k+1}|||^2_{\star,K} \\
&= ||\boldsymbol{S}^{\frac{1}{2}}(\mathbf{u}_h^{k+1} - \boldsymbol{\sigma}_h^{k+1})||^2_K \\
&= \big(\boldsymbol{S}^{-1}(\mathbf{u}_h^{k+1} - \boldsymbol{\sigma}_h^{k+1}), \mathbf{u}_h^{k+1} - \boldsymbol{\sigma}_h^{k+1}\big)_K \\
&= (\boldsymbol{S}^{-1}\mathbf{u}_h^{k+1}, \mathbf{u}_h^{k+1})_K - 2(\boldsymbol{S}^{-1}\mathbf{u}_h^{k+1}, \boldsymbol{\sigma}_h^{k+1})_K + (\boldsymbol{S}^{-1}\boldsymbol{\sigma}_h^{k+1}, \boldsymbol{\sigma}_h^{k+1})_K \\
&= \big(\boldsymbol{S}^{-1}\sum_{e\in\mathscr{E}_K} u_e^{k+1}\psi_e(\mathbf{x}), \sum_{e\in\mathscr{E}_K} u_e^{k+1}\psi_e(\mathbf{x})\big)_K - 2\big(\boldsymbol{S}^{-1}\sum_{e\in\mathscr{E}_K} u_e^{k+1}\psi_e(\mathbf{x}), \sum_{e\in\mathscr{E}_K} \sigma_e^{k+1}\psi_e(\mathbf{x})\big)_K \\
&\quad + \big(\boldsymbol{S}^{-1}\sum_{e\in\mathscr{E}_K} \sigma_e^{k+1}\psi_e(\mathbf{x}), \sum_{e\in\mathscr{E}_K} \sigma_e^{k+1}\psi_e(\mathbf{x})\big)_K \\
&= \sum_{e\in\mathscr{E}_K}\sum_{y\in\mathscr{E}_K} u_e^{k+1}u_y^{k+1}\big(\boldsymbol{S}^{-1}\psi_e(\mathbf{x}), \psi_y(\mathbf{x})\big)_K - 2\sum_{e\in\mathscr{E}_K}\sum_{y\in\mathscr{E}_K} u_e^{k+1}\sigma_y^{k+1}\big(\boldsymbol{S}^{-1}\psi_e(\mathbf{x}), \psi_y(\mathbf{x})\big)_K \\
&\quad + \sum_{e\in\mathscr{E}_K}\sum_{y\in\mathscr{E}_K} \sigma_e^{k+1}\sigma_y^{k+1}\big(\boldsymbol{S}^{-1}\psi_e(\mathbf{x}), \psi_y(\mathbf{x})\big)_K \\
&= \sum_{e\in\mathscr{E}_K}\sum_{y\in\mathscr{E}_K} \mathbf{U}_K(e,1)\mathbb{M}_K(e,y)\mathbf{U}_K(y,1) - 2\sum_{e\in\mathscr{E}_K}\sum_{y\in\mathscr{E}_K} \mathbf{U}_K(e,1)\mathbb{M}_K(e,y)\mathbf{V}_K(y,1) \\
&\quad + \sum_{e\in\mathscr{E}_K}\sum_{y\in\mathscr{E}_K} \mathbf{V}_K(e,1)\mathbb{M}_K(e,y)\mathbf{V}_K(y,1) \\
&= \mathbf{U}_K^{'}\mathbb{M}_K\mathbf{U}_K - 2\mathbf{U}_K^{'}\mathbb{M}_K\mathbf{V}_K + \mathbf{V}_K^{'}\mathbb{M}_K\mathbf{V}_K
\end{aligned}
\tag{A.4}
$$

where, in two space dimensions, $\mathbf{U}_K = [u_{e1}; u_{e2}; u_{e3}]$ is a 3×1 vector, $\mathbf{V}_K = [v_{e1}; v_{e2}; v_{e3}]$ is a 3×1 vector, and $\mathbb{M}_K$ is a 3×3 matrix defined as follows:

$$
(\mathbb{M}_K)_{e,e'} = \big(\boldsymbol{S}^{-1}\psi_e(\mathbf{x}), \psi_{e'}(\mathbf{x})\big)_K. \tag{A.5}
$$

Then,

$$\eta^2_{\mathrm{DDF}} := \sum_{K\in|\mathscr{T}_h|} \eta^2_{\mathrm{DDF},K} \tag{A.6}$$

In MATLAB, we have to compute $\eta^2_{\mathrm{DDF},K}$ for all the elements in $\mathscr{T}_h$. It is not optimal and not efficient if there is a loop with the size of the number of elements, where in each step, $\mathbf{U}_K^{'}\mathbb{M}_K\mathbf{U}_K$ is computed. For this reason, we build a three-dimensional matrix $\overline{\mathbb{M}}$, as presented in Figure A.2. Let NT=$|\mathscr{T}_h|$ be the cardinality of $\mathscr{T}_h$. The dimension of $\overline{\mathbb{M}}$ is $3\times 3\times|\mathscr{T}_h|$ and the dimension of the matrices $\overline{\mathbf{U}}$ and $\overline{\mathbf{V}}$ are $|\mathscr{T}_h|\times 3$, where:

$$\overline{\mathbf{U}}(l,:)=\mathbf{U}^{'}_{K_l} \quad \text{and} \quad \overline{\mathbf{V}}(l,:)=\mathbf{V}^{'}_{K_l}, \qquad l=1,..,\mathrm{NT}. \tag{A.7}$$

Then,

$$\begin{aligned}
\eta^2_{\mathrm{DDF}} &= \sum_{l=1}^{\mathrm{NT}} \eta^2_{\mathrm{DDF},K_l} \\
&= \sum_{l=1}^{\mathrm{NT}} \sum_{e\in\mathscr{E}_{K_l}} \sum_{y\in\mathscr{E}_{K_l}} \overline{\mathbf{U}}(l,y)\overline{\mathbb{M}}(y,e,l)\overline{\mathbf{U}}(l,e) \\
&\quad - 2\sum_{l=1}^{\mathrm{NT}} \sum_{e\in\mathscr{E}_{K_l}} \sum_{y\in\mathscr{E}_{K_l}} \overline{\mathbf{U}}(l,y)\overline{\mathbb{M}}(y,e,l)\overline{\mathbf{V}}(l,e) \\
&\quad + \sum_{l=1}^{\mathrm{NT}} \sum_{e\in\mathscr{E}_{K_l}} \sum_{y\in\mathscr{E}_{K_l}} \overline{\mathbf{V}}(l,y)\overline{\mathbb{M}}(y,e,l)\overline{\mathbf{V}}(l,e).
\end{aligned} \tag{A.8}$$

In the vectorized form, we only do a small double loop in order to compute η^2_{DDF}:

1. eta1=zeros(NT,1);
2. eta2=zeros(NT,1);
3. eta3=zeros(NT,1);
4. for e=1:3
5. for y=1:3
6. eta1= eta1 + $\overline{\mathbf{U}}$(:,y).*$\overline{\mathbb{M}}$(y,e,:).*$\overline{\mathbf{U}}$(:,e);
7. eta2 = eta2+$\overline{\mathbf{U}}$(:,y).*$\overline{\mathbb{M}}$(y,e,:).*$\overline{\mathbf{V}}$(:,e);
8. eta3 = eta3+ $\overline{\mathbf{V}}$(:,y).*$\overline{\mathbb{M}}$(y,e,:).*$\overline{\mathbf{V}}$(:,e);
9. end
10. end
11. η^2_{DDF} = sum(eta1 -2* eta2 + eta3);

where oparation .* in $\overline{\mathbf{U}}$(:,y).*$\overline{\mathbb{M}}$(y,e,:), which multiplies vectors $\overline{\mathbf{U}}$(:,y) and $\overline{\mathbb{M}}$(y,e,:) element by element and returns a vector, is faster then a loop on the size of $\overline{\mathbf{U}}$(:,y). An illustration of $\overline{\mathbb{M}}$(y,e,:) for y=1,..,3 and for e=1,..,3 is given in Figure A.3.

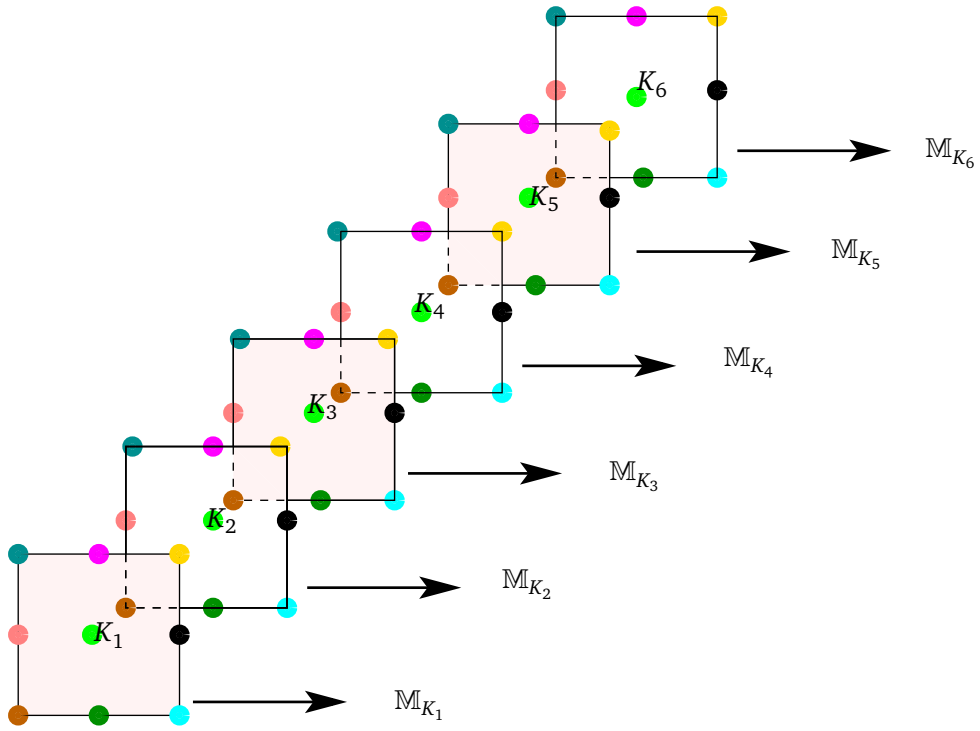

Figure A.2: The 3D matrix $\overline{\mathbb{M}}$

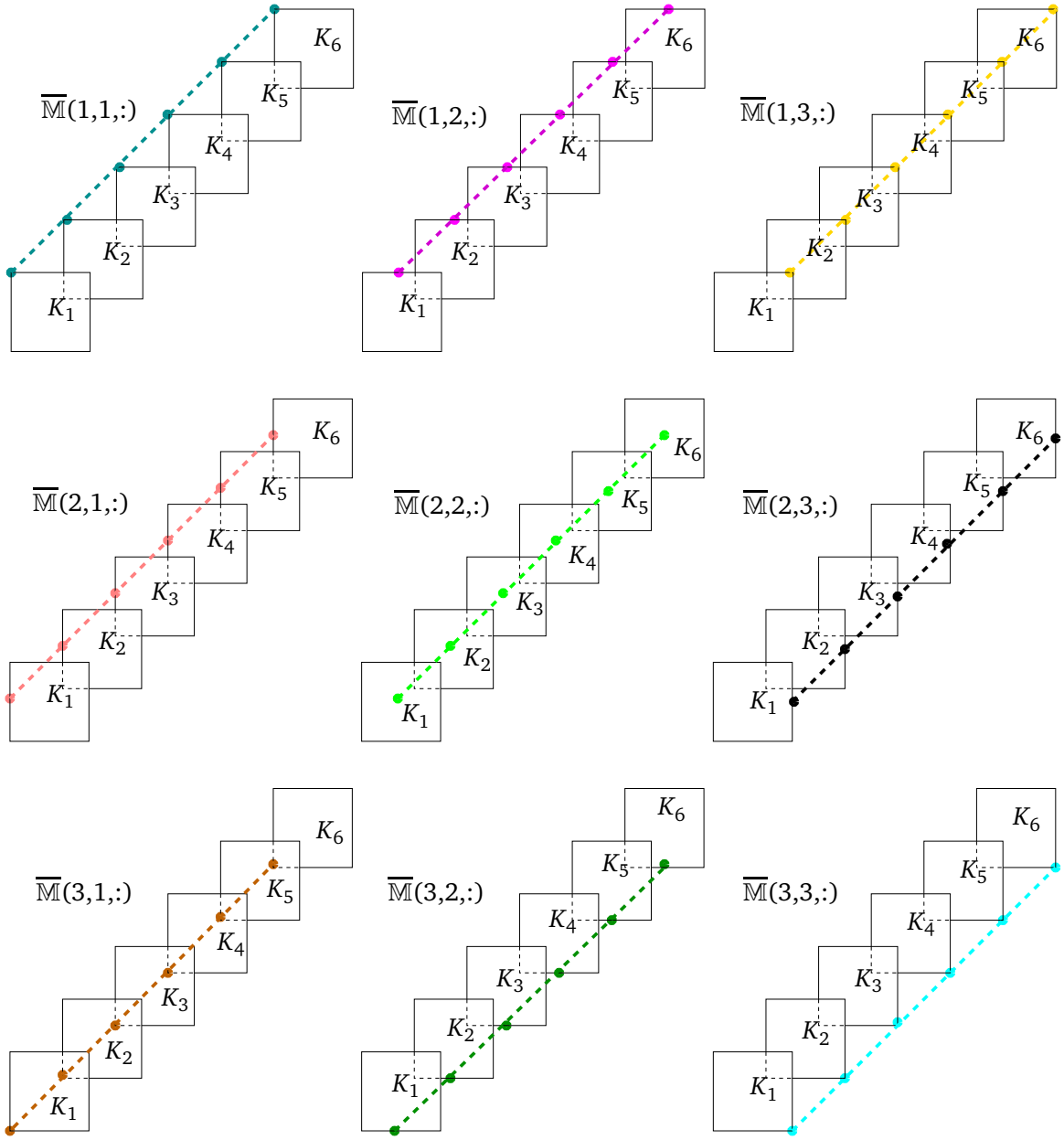

Figure A.3: $\overline{\mathbb{M}}$(y,e,:) for y=1,..,3 and for e=1,..,3

Bibliography

[1] J. E. Aarnes and Y. Efendiev, *An adaptive multiscale method for simulation of fluid flow in heterogeneous porous media*, Multiscale Model. Simul., 5 (2006), pp. 918–939.

[2] B. Achchab, A. Agouzal, J. Baranger, and J.-F. Maître, *Estimateur d'erreur a posteriori hiérarchique. Application aux éléments finis mixtes*, Numer. Math., 80 (1998), pp. 159–179.

[3] Y. Achdou, C. Bernardi, and F. Coquel, *A priori and a posteriori analysis of finite volume discretizations of Darcy's equations*, Numer. Math., 96 (2003), pp. 17–42.

[4] R. A. Adams, *Sobolev spaces*, Academic Press [A subsidiary of Harcourt Brace Jovanovich, Publishers], New York-London, 1975. Pure and Applied Mathematics, Vol. 65.

[5] V. I. Agoshkov and V. I. Lebedev, *Poincaré-Steklov operators and methods of partition of the domain in variational problems*, in Computational processes and systems, No. 2, "Nauka", Moscow, 1985, pp. 173–227.

[6] E. Ahmed, J. Jaffré, and J. E. Roberts, *A reduced fracture model for two-phase flow with different rock types*, Math. Comput. Simulation, 137 (2017), pp. 49–70.

[7] E. Ahmed, C. Japhet, and M. Kern, *A finite volume Schwarz algorithm for two-phase immiscible flow with different rock types*. In preparation.

[8] M. Ainsworth, *A posteriori error estimation for lowest order Raviart–Thomas mixed finite elements*, SIAM J. Sci. Comput., 30 (2007), pp. 189–204.

[9] M. Ainsworth and J. T. Oden, *A posteriori error estimation in finite element analysis*, Pure and Applied Mathematics (New York), Wiley-Interscience [John Wiley & Sons], New York, 2000.

[10] M. Ainsworth and R. Rankin, *Fully computable error bounds for discontinuous Galerkin finite element approximations on meshes with an arbitrary number of levels of hanging nodes*, SIAM J. Numer. Anal., 47 (2010), pp. 4112–4141.

[11] S. Ali Hassan, *A posteriori error estimates and stopping criteria for solvers using domain decomposition method and with local time stepping*. Submitted Ph.D. thesis, University Paris 6, 2017.

[12] G. Allaire, *Analyse numérique et optimisation*, Editions Ecole Polytechnique, Palaiseau, France, 2005.

[13] A. ALONSO, *Error estimators for a mixed method*, Numer. Math., 74 (1996), pp. 385–395.

[14] B. ANDREIANOV, K. BRENNER, AND C. CANCÈS, *Approximating the vanishing capillarity limit of two-phase flow in multi-dimensional heterogeneous porous medium*, ZAMM Z. Angew. Math. Mech., 94 (2014), pp. 655–667.

[15] T. ARBOGAST AND Z. CHEN, *On the implementation of mixed methods as nonconforming methods for second-order elliptic problems*, Math. Comp., 64 (1995), pp. 943–972.

[16] M. ARIOLI, D. LOGHIN, AND A. J. WATHEN, *Stopping criteria for iterations in finite element methods*, Numer. Math., 99 (2005), pp. 381–410.

[17] D. N. ARNOLD AND F. BREZZI, *Mixed and nonconforming finite element methods: implementation, postprocessing and error estimates*, RAIRO Modél. Math. Anal. Numér., 19 (1985), pp. 7–32.

[18] K. AZIZ AND A. SETTARI, *Petroleum Reservoir Simulation*, Applied Science Publishers, 1979.

[19] J. BEAR, *Dynamics of fluids in porous media*, Dover, New York, 1988.

[20] R. BECKER, C. JOHNSON, AND R. RANNACHER, *Adaptive error control for multigrid finite element methods*, Computing, 55 (1995), pp. 271–288.

[21] D. BENNEQUIN, M. J. GANDER, AND L. HALPERN, *A homographic best approximation problem with application to optimized Schwarz waveform relaxation*, Math. Comp., 78 (2009), pp. 185–223.

[22] C. BERNARDI AND F. HECHT, *Error indicators for the mortar finite element discretization of the Laplace equation*, Math. Comp., 71 (2002), pp. 1371–1403.

[23] C. BERNARDI, T. C. REBOLLO, F. HECHT, AND Z. MGHAZLI, *Mortar finite element discretization of a model coupling Darcy and Stokes equations*, M2AN Math. Model. Numer. Anal., 42 (2008), pp. 375–410.

[24] H. BERNINGER, S. LOISEL, AND O. SANDER, *The 2-Lagrange multiplier method applied to nonlinear transmission problems for the Richards equation in heterogeneous soil with cross points*, SIAM J. Sci. Comput., 36 (2014), pp. A2166–A2198.

[25] H. BERNINGER AND O. SANDER, *Substructuring of a Signorini-type problem and Robin's method for the Richards equation in heterogeneous soil*, Comput. Vis. Sci., 13 (2010), pp. 187–205.

[26] P. M. BERTHE, C. JAPHET, AND P. OMNES, *Space-Time Domain Decomposition with Finite Volumes for Porous Media Applications*, in Domain decomposition methods in science and engineering XXI, J. Erhel, M. Gander, L. Halpern, G. Pichot, T. Sassi, and O. Widlund, eds., vol. 98 of Lect. Notes Comput. Sci. Eng., Springer, 2014, pp. 483–490.

[27] P. E. BJØRSTAD, J. BRÆKHUS, AND A. HVIDSTEN, *Parallel substructuring algorithms in structural analysis, direct and iterative methods*, in Fourth International Symposium on Domain Decomposition Methods for Partial Differential Equations (Moscow, 1990), SIAM, Philadelphia, PA, 1991, pp. 321–340.

[28] E. BLAYO, L. DEBREU, AND F. LEMARIÉ, *Toward an optimized global-in-time Schwarz algorithm for diffusion equations with discontinuous and spatially variable coefficients. Part 1: the constant coefficients case*, ETNA, Kent State University Library, 40 (2013), pp. 170–186.

[29] E. BLAYO, L. HALPERN, AND C. JAPHET, *Optimized Schwarz waveform relaxation algorithms with nonconforming time discretization for coupling convection-diffusion problems with discontinuous coefficients*, in Domain decomposition methods in science and engineering XVI, vol. 55 of Lect. Notes Comput. Sci. Eng., Springer, Berlin, 2007, pp. 267–274.

[30] J.-F. BOURGAT, R. GLOWINSKI, P. LE TALLEC, AND M. VIDRASCU, *Variational formulation and algorithm for trace operator in domain decomposition calculations*, in Domain decomposition methods (Los Angeles, CA, 1988), SIAM, Philadelphia, PA, 1989, pp. 3–16.

[31] D. BRAESS AND J. SCHÖBERL, *Equilibrated residual error estimator for edge elements*, Math. Comp., 77 (2008), pp. 651–672.

[32] D. BRAESS AND R. VERFÜRTH, *A posteriori error estimators for the Raviart–Thomas element*, SIAM J. Numer. Anal., 33 (1996), pp. 2431–2444.

[33] J. H. BRAMBLE, J. E. PASCIAK, AND A. H. SCHATZ, *The construction of preconditioners for elliptic problems by substructuring. I*, Math. Comp., 47 (1986), pp. 103–134.

[34] J. H. BRAMBLE AND J. XU, *A local post-processing technique for improving the accuracy in mixed finite-element approximations*, SIAM J. Numer. Anal., 26 (1989), pp. 1267–1275.

[35] K. BRENNER, C. CANCÈS, AND D. HILHORST, *Finite volume approximation for an immiscible two-phase flow in porous media with discontinuous capillary pressure*, Comput. Geosci., 17 (2013), pp. 573–597.

[36] F. BREZZI AND M. FORTIN, *Mixed and hybrid finite element methods*, vol. 15 of Springer Series in Computational Mathematics, Springer-Verlag, New York, 1991.

[37] E. BURMAN AND A. ERN, *Continuous interior penalty hp-finite element methods for advection and advection-diffusion equations*, Math. Comp., 76 (2007), pp. 1119–1140.

[38] F. CAETANO, M. J. GANDER, L. HALPERN, AND J. SZEFTEL, *Schwarz waveform relaxation algorithms for semilinear reaction-diffusion equations*, Netw. Heterog. Media, 5 (2010), pp. 487–505.

[39] C. CANCÈS, *Nonlinear parabolic equations with spatial discontinuities*, NoDEA Nonlinear Differential Equations Appl., 15 (2008), pp. 427–456.

[40] ——, *Finite volume scheme for two-phase flows in heterogeneous porous media involving capillary pressure discontinuities*, M2AN Math. Model. Numer. Anal., 43 (2009), pp. 973–1001.

[41] C. CANCÈS, T. GALLOUËT, AND A. PORRETTA, *Two-phase flows involving capillary barriers in heterogeneous porous media*, Interfaces Free Bound., 11 (2009), pp. 239–258.

[42] C. CANCÈS, I. S. POP, AND M. VOHRALÍK, *An a posteriori error estimate for vertex-centered finite volume discretizations of immiscible incompressible two-phase flow*, Math. Comp., 83 (2014), pp. 153–188.

[43] C. CARSTENSEN, *A posteriori error estimate for the mixed finite element method*, Math. Comp., 66 (1997), pp. 465–476.

[44] G. CHAVENT AND J. JAFFRÉ, *Mathematical models and finite elements for reservoir simulation*, North-Holland, Amsterdam, 1986. Studies in Mathematics and Its Applications, Vol. 17.

[45] G. CHAVENT AND J. ROBERTS, *A unified physical presentation of mixed, mixed-hybrid finite elements and standard finite difference approximations for the determination of velocities in waterflow problems*, Advances in Water Resources, 14 (1991), pp. 329–348.

[46] Y. CHEN AND W. LIU, *A posteriori error estimates of mixed methods for miscible displacement problems*, Internat. J. Numer. Methods Engrg., 73 (2008), pp. 331–343.

[47] Z. CHEN, *Analysis of mixed methods using conforming and nonconforming finite element methods*, RAIRO Modél. Math. Anal. Numér., 27 (1993), pp. 9–34.

[48] Z. CHEN, G. HUAN, AND Y. MA, *Computational methods for multiphase flows in porous media*, Society for Industrial and Applied Mathematics, Philadelphia, 2006.

[49] L. C. COWSAR, J. MANDEL, AND M. F. WHEELER, *Balancing domain decomposition for mixed finite elements*, Math. Comp., 64 (1995), pp. 989–1015.

[50] E. CREUSÉ AND S. NICAISE, *A posteriori error estimations of a coupled mixed and standard Galerkin method for second order operators*, J. Comput. Appl. Math., 213 (2008), pp. 35–55.

[51] F. CUVELIER, C. JAPHET, AND G. SCARELLA, *Personal communication*.

[52] ——, *An efficient way to assemble finite element matrices in vector languages*, BIT, 56 (2016), pp. 833–864.

[53] T. A. DAVIS, *Direct methods for sparse linear systems*, vol. 2 of Fundamentals of Algorithms, Society for Industrial and Applied Mathematics (SIAM), Philadelphia, PA, 2006.

[54] Y.-H. DE ROECK AND P. LE TALLEC, *Analysis and test of a local domain-decomposition preconditioner*, in Fourth International Symposium on Domain Decomposition Methods for Partial Differential Equations (Moscow, 1990), SIAM, Philadelphia, PA, 1991, pp. 112–128.

[55] D. A. Di Pietro, E. Flauraud, M. Vohralík, and S. Yousef, *A posteriori error estimates, stopping criteria, and adaptivity for multiphase compositional Darcy flows in porous media*, J. Comput. Phys., 276 (2014), pp. 163–187.

[56] D. A. Di Pietro, M. Vohralík, and S. Yousef, *Adaptive regularization, linearization, and discretization and a posteriori error control for the two-phase Stefan problem*, Math. Comp., 84 (2015), pp. 153–186.

[57] V. Dolean, P. Jolivet, and F. Nataf, *An introduction to domain decomposition methods*, Society for Industrial and Applied Mathematics (SIAM), Philadelphia, PA, 2015. Algorithms, theory, and parallel implementation.

[58] V. Dolejší, A. Ern, and M. Vohralík, *hp-adaptation driven by polynomial-degree-robust a posteriori error estimates for elliptic problems*, SIAM J. Sci. Comput., 38 (2016), pp. A3220–A3246.

[59] J. J. Douglas, P. J. Paes-Leme, J. E. Roberts, and J. P. Wang, *A parallel iterative procedure applicable to the approximate solution of second order partial differential equations by mixed finite element methods*, Numer. Math., 65 (1993), pp. 95–108.

[60] M. Dryja, *Substructuring methods for parabolic problems*, in Fourth International Symposium on Domain Decomposition Methods for Partial Differential Equations (Moscow, 1990), SIAM, Philadelphia, PA, 1991, pp. 264–271.

[61] R. Durán and C. Padra, *An error estimator for nonconforming approximations of a nonlinear problem*, in Finite element methods (Jyväskylä, 1993), vol. 164 of Lecture Notes in Pure and Appl. Math., Dekker, New York, 1994, pp. 201–205.

[62] L. El Alaoui and A. Ern, *Residual and hierarchical a posteriori error estimates for nonconforming mixed finite element methods*, M2AN Math. Model. Numer. Anal., 38 (2004), pp. 903–929.

[63] G. Enchéry, R. Eymard, and A. Michel, *Numerical approximation of a two-phase flow problem in a porous medium with discontinuous capillary forces*, SIAM J. Numer. Anal., 43 (2006), pp. 2402–2422.

[64] A. Ern, S. Nicaise, and M. Vohralík, *An accurate* $\mathbf{H}(\mathrm{div})$ *flux reconstruction for discontinuous Galerkin approximations of elliptic problems*, C. R. Math. Acad. Sci. Paris, 345 (2007), pp. 709–712.

[65] A. Ern, I. Smears, and M. Vohralík, *Guaranteed, locally space-time efficient, and polynomial-degree robust a posteriori error estimates for high-order discretizations of parabolic problems*. HAL Preprint 01377086, submitted for publication, 2016.

[66] A. Ern, A. F. Stephansen, and M. Vohralík, *Guaranteed and robust discontinuous Galerkin a posteriori error estimates for convection-diffusion-reaction problems*, J. Comput. Appl. Math., 234 (2010), pp. 114–130.

[67] A. Ern and M. Vohralík, *A posteriori error estimation based on potential and flux reconstruction for the heat equation*, SIAM J. Numer. Anal., 48 (2010), pp. 198–223.

[68] ——, *Adaptive inexact Newton methods with a posteriori stopping criteria for nonlinear diffusion PDEs*, SIAM J. Sci. Comput., 35 (2013), pp. A1761–A1791.

[69] R. EYMARD, T. GALLOUËT, AND R. HERBIN, *Finite volume methods*, in Handbook of Numerical Analysis, Vol. VII, , North-Holland, Amsterdam, 2000, pp. 713–1020.

[70] R. EYMARD, T. GALLOUËT, AND R. HERBIN, *Finite volume approximation of elliptic problems and convergence of an approximate gradient*, Appl. Numer. Math., 37 (2001), pp. 31–53.

[71] M. J. GANDER, *Optimized Schwarz methods*, SIAM J. Numer. Anal., 44 (2006), pp. 699–731.

[72] M. J. GANDER AND O. DUBOIS, *Optimized Schwarz methods for a diffusion problem with discontinuous coefficient*, Numer. Algorithms, 69 (2015), pp. 109–144.

[73] M. J. GANDER AND L. HALPERN, *Optimized Schwarz waveform relaxation methods for advection reaction diffusion problems*, SIAM J. Numer. Anal., 45 (2007), pp. 666–697.

[74] M. J. GANDER, L. HALPERN, AND M. KERN, *A Schwarz waveform relaxation method for advection-diffusion-reaction problems with discontinuous coefficients and nonmatching grids*, in Domain decomposition methods in science and engineering XVI, vol. 55 of Lect. Notes Comput. Sci. Eng., Springer, Berlin, 2007, pp. 283–290.

[75] M. J. GANDER, L. HALPERN, AND F. NATAF, *Optimal Convergence for Overlapping and Non-Overlapping Schwarz Waveform Relaxation*, in Proceedings of the 11th International Conference on Domain Decomposition Methods, C.-H. Lai, P. Bjørstad, M. Cross, and O. Widlund, eds., 1999, pp. 27–36.

[76] ——, *Optimal Schwarz waveform relaxation for the one dimensional wave equation*, SIAM J. Numer. Anal., 41 (2003), pp. 1643–1681.

[77] M. J. GANDER AND C. JAPHET, *Algorithm 932: PANG: software for nonmatching grid projections in 2D and 3D with linear complexity*, ACM Trans. Math. Software, 40 (2013), pp. Art. 6, 25.

[78] M. J. GANDER, C. JAPHET, Y. MADAY, AND F. NATAF, *A new cement to glue nonconforming grids with Robin interface conditions: the finite element case*, in Domain decomposition methods in science and engineering, vol. 40 of Lect. Notes Comput. Sci. Eng., Springer, Berlin, 2005, pp. 259–266.

[79] M. J. GANDER AND A. M. STUART, *Space-time continuous analysis of waveform relaxation for the heat equation*, SIAM J. Sci. Comput., 19 (1998), pp. 2014–2031.

[80] M. J. GANDER AND X. TU, *On the Origins of Iterative Substructuring Method*, in Domain decomposition methods in science and engineering XXI, J. Erhel, M. Gander, L. Halpern, G. Pichot, T. Sassi, and O. Widlund, eds., vol. 98 of Lect. Notes Comput. Sci. Eng., Springer, 2014, pp. 597–605.

[81] B. GANIS, K. KUMAR, G. PENCHEVA, M. F. WHEELER, AND I. YOTOV, *A global Jacobian method for mortar discretizations of a fully implicit two-phase flow model*, Multiscale Model. Simul., 12 (2014), pp. 1401–1423.

[82] L. GASTALDI, *A domain decomposition for the transport equation*, in Domain decomposition methods in science and engineering (Como, 1992), vol. 157 of Contemp. Math., Amer. Math. Soc., Providence, RI, 1994, pp. 97–102.

[83] S. GHANEMI, P. JOLY, AND F. COLLINO, *Domain decomposition method for harmonic wave equations*, in Third international conference on mathematical and numerical aspect of wave propagation, 1995, pp. 663–672.

[84] E. GILADI AND H. B. KELLER, *Space-time domain decomposition for parabolic problems*, Numer. Math., 93 (2002), pp. 279–313.

[85] F. HAEBERLEIN, *Time Space Domain Decomposition Methods for Reactive Transport — Application to CO2 Geological Storage*, Ph.D. thesis, Université Paris-Nord - Paris XIII, 2011.

[86] F. HAEBERLEIN, L. HALPERN, AND A. MICHEL, *Newton-Schwarz optimised waveform relaxation Krylov accelerators for nonlinear reactive transport*, in Domain decomposition methods in science and engineering XX, vol. 91 of Lect. Notes Comput. Sci. Eng., Springer, Heidelberg, 2013, pp. 387–394.

[87] H. HAJIBEYGI AND P. JENNY, *Adaptive iterative multiscale finite volume method*, J. Comput. Phys., 230 (2011), pp. 628–643.

[88] L. HALPERN, *Artificial Boundary Conditions for the Advection-Diffusion Equations*, Math. Comp., 174 (1986), pp. 425–438.

[89] L. HALPERN AND F. HUBERT, *A finite volume Ventcell-Schwarz algorithm for advection-diffusion equations*, SIAM J. Numer. Anal., 52 (2014), pp. 1269–1291.

[90] L. HALPERN AND C. JAPHET, *Discontinuous Galerkin and Nonconforming in Time Optimized Schwarz Waveform Relaxation for Heterogeneous Problems*, in Decomposition Methods in Science and Engineering XVII, U. Langer, M. Discacciati, D. Keyes, O. Widlund, and W. Zulehner, eds., vol. 60 of Lecture Notes in Computational Science and Engineering, Springer, 2008, pp. 211–219.

[91] L. HALPERN, C. JAPHET, AND P. OMNES, *Nonconforming in time domain decomposition method for porous media applications.*, in Proceedings of the 5th European Conference on Computational Fluid Dynamics ECCOMAS CFD 2010., J. C. F. Pereira and A. Sequeira, eds., Lisbon, Portugal, 2010.

[92] L. HALPERN, C. JAPHET, AND J. SZEFTEL, *Discontinuous Galerkin and nonconforming in time optimized Schwarz waveform relaxation*, in Domain Decomposition Methods in Science and Engineering XIX, vol. 78 of Lect. Notes Comput. Sci. Eng., Springer, Heidelberg, 2011, pp. 133–140.

[93] ——, *Optimized Schwarz waveform relaxation and discontinuous Galerkin time stepping for heterogeneous problems*, SIAM J. Numer. Anal., 50 (2012), pp. 2588–2611.

[94] T. T. P. HOANG, *Space-time domain decomposition methods for mixed formulations of flow and transport problems in porous media*, Ph.D. thesis, University Paris 6, 2013.

[95] T.-T.-P. HOANG, J. JAFFRÉ, C. JAPHET, M. KERN, AND J. E. ROBERTS, *Space-time domain decomposition methods for diffusion problems in mixed formulations*, SIAM J. Numer. Anal., 51 (2013), pp. 3532–3559.

[96] T. T. P. HOANG, C. JAPHET, M. KERN, AND J. E. ROBERTS, *Space-time domain decomposition for advection-diffusion problems in mixed formulations*, Mathematics and Computers in Simulation, (2016).

[97] ——, *Space-time domain decomposition for reduced fracture models in mixed formulation*, SIAM J. Numer. Anal., 54 (2016), pp. 288–316.

[98] ——, *Ventcell conditions with mixed formulations for flow in porous media*, in Decomposition Methods in Science and Engineering XXII, T. Dickopf, M. Gander, L. Halpern, R. Krause, and L. F. Pavarino, eds., vol. 104 of Lecture Notes in Computational Science and Engineering, Springer, 2016, pp. 531–540.

[99] U. HORNUNG, ed., *Homogenization and porous media*, vol. 6 of Interdisciplinary Applied Mathematics, Springer-Verlag, New York, 1997.

[100] W. HUNDSDORFER AND J. VERWER, *Numerical solution of time-dependent advection-diffusion-reaction equations*, Springer, Berlin Heidelberg New York etc, 2010.

[101] C. JAPHET, *Méthode de décomposition de domaine et conditions aux limites artificielles en mécanique des fluides: méthode optimisée d'ordre 2*, Ph.D. thesis, Université Paris-Nord - Paris XIII, 1998.

[102] ——, *Optimized Krylov-Ventcell Method. Application to convection-diffusion problems*, in Domain Decomposition Methods in Science and Engineering IX, P. Bjørstad, M. Espedal, and D. Keyes, eds., John Wiley & Sons Ltd, 1998, pp. 382–389.

[103] C. JAPHET AND F. NATAF, *The best interface conditions for domain decomposition methods: absorbing boundary conditions*, in Absorbing Boundaries and Layers, Domain Decomposition Methods, Nova Sci. Publ., Huntington, NY, 2001, pp. 348–373.

[104] C. JAPHET, F. NATAF, AND F. ROGIER, *The optimized order 2 method. Application to convection-diffusion problems*, Future Gener. Comp. Sy., 18 (2001), pp. 17–30.

[105] C. JAPHET AND P. OMNES, *Optimized Schwarz waveform relaxation for porous media applications*, in Domain decomposition methods in science and engineering XX, vol. 91 of Lect. Notes Comput. Sci. Eng., Springer, Heidelberg, 2013, pp. 585–592.

[106] P. JIRÁNEK, Z. STRAKOŠ, AND M. VOHRALÍK, *A posteriori error estimates including algebraic error and stopping criteria for iterative solvers*, SIAM J. Sci. Comput., 32 (2010), pp. 1567–1590.

[107] O. A. KARAKASHIAN AND F. PASCAL, *A posteriori error estimates for a discontinuous Galerkin approximation of second-order elliptic problems*, SIAM J. Numer. Anal., 41 (2003), pp. 2374–2399.

[108] K. Y. KIM, *A posteriori error analysis for locally conservative mixed methods*, Math. Comp., 76 (2007), pp. 43–66.

[109] ——, *A posteriori error estimators for locally conservative methods of nonlinear elliptic problems*, Appl. Numer. Math., 57 (2007), pp. 1065–1080.

[110] V. KIPPE, J. E. AARNES, AND K.-A. LIE, *A comparison of multiscale methods for elliptic problems in porous media flow*, Comput. Geosci., 12 (2008), pp. 377–398.

[111] R. KIRBY, *Residual a posteriori error estimates for the mixed finite element method*, Comput. Geosci., 7 (2003), pp. 197–214.

[112] P. LADEVÈZE AND D. LEGUILLON, *Error estimate procedure in the finite element method and applications*, SIAM J. Numer. Anal., 20 (1983), pp. 485–509.

[113] M. G. LARSON AND A. MÅLQVIST, *Adaptive variational multiscale methods based on a posteriori error estimation: energy norm estimates for elliptic problems*, Comput. Methods Appl. Mech. Engrg., 196 (2007), pp. 2313–2324.

[114] ——, *A posteriori error estimates for mixed finite element approximations of elliptic problems*, Numer. Math., 108 (2008), pp. 487–500.

[115] K.-A. LIE, S. KROGSTAD, I. S. LIGAARDEN, J. R. NATVIG, H. M. NILSEN, AND B. SKAFLESTAD, *Open source matlab implementation of consistent discretisations on complex grids*, Comput. Geosci., 16 (2012), pp. 297–322.

[116] J.-L. LIONS AND E. MAGENES, *Problèmes aux limites non homogènes et applications. Vol. 1*, Travaux et Recherches Mathématiques, No. 17, Dunod, Paris, 1968.

[117] P.-L. LIONS, *On the Schwarz alternating method. I*, in First International Symposium on Domain Decomposition Methods for Partial Differential Equations, G. H. G. G. A. M. R. Glowinski and J. Périaux, eds., Philadelphia, PA, SIAM, 1988, pp. 1–42.

[118] ——, *On the Schwarz alternating method. II*, in Second International Symposium on Domain Decomposition Methods for Partial Differential Equations, R. G. J. P. T. Chan and O. Widlund, eds., Philadelphia, PA, SIAM, 1989, pp. 47–70.

[119] ——, *On the Schwarz alternating method. III: a variant for nonoverlapping subdomains*, in Third International Symposium on Domain Decomposition Methods for Partial Differential Equations, held in Houston, Texas, March 20-22, 1989, R. G. J. P. T. F. Chan and O. Widlund, eds., Philadelphia, PA, SIAM, 1990, pp. 202–223.

[120] C. LOVADINA AND R. STENBERG, *Energy norm a posteriori error estimates for mixed finite element methods*, Math. Comp., 75 (2006), pp. 1659–1674.

[121] R. LUCE AND B. I. WOHLMUTH, *A local a posteriori error estimator based on equilibrated fluxes*, SIAM J. Numer. Anal., 42 (2004), pp. 1394–1414.

[122] J. MANDEL, *Balancing domain decomposition*, Comm. Numer. Methods Engrg., 9 (1993), pp. 233–241.

[123] J. MANDEL AND M. BREZINA, *Balancing domain decomposition for problems with large jumps in coefficients*, Math. Comp., 65 (1996), pp. 1387–1401.

[124] V. MARTIN, *An optimized Schwarz waveform relaxation method for the unsteady convection diffusion equation in two dimensions*, Appl. Numer. Math., 52 (2005), pp. 401–428.

[125] T. MATHEW, *Domain Decomposition Methods for the Numerical Solution of Partial Differential Equations*, vol. 61 of Lecture Notes in Computational Science and Engineering, Springer, 2008.

[126] F. NATAF, F. ROGIER, AND E. DE STURLER, *Domain Decomposition Methods for Fluid Dynamics*, in Navier-Stokes Equations and Related Nonlinear Analysis, A. Sequeira, ed., Plenum Press Corporation, 1995, pp. 367–376.

[127] R. H. NOCHETTO, A. SCHMIDT, AND C. VERDI, *A posteriori error estimation and adaptivity for degenerate parabolic problems*, Math. Comp., 69 (2000), pp. 1–24.

[128] M. OHLBERGER, *A posteriori error estimates for the heterogeneous multiscale finite element method for elliptic homogenization problems*, Multiscale Model. Simul., 4 (2005), pp. 88–114.

[129] J. E. PASCIAK, *Domain decomposition preconditioners for elliptic problems in two and three dimensions: first approach*, in First International Symposium on Domain Decomposition Methods for Partial Differential Equations (Paris, 1987), SIAM, Philadelphia, PA, 1988, pp. 62–72.

[130] G. V. PENCHEVA, M. VOHRALÍK, M. F. WHEELER, AND T. WILDEY, *Robust a posteriori error control and adaptivity for multiscale, multinumerics, and mortar coupling*, SIAM J. Numer. Anal., 51 (2013), pp. 526–554.

[131] I. S. POP, J. BOGERS, AND K. KUMAR, *Analysis and upscaling of a reactive transport model in fractured porous media with nonlinear transmission condition*, Vietnam J. Math., 45 (2017), pp. 77–102.

[132] W. PRAGER AND J. L. SYNGE, *Approximations in elasticity based on the concept of function space*, Quart. Appl. Math., 5 (1947), pp. 241–269.

[133] J. PRZEMIENIECKI, *Matrix structural analysis of substructures*, Am. Inst. Aero. Astro., 1 (1963), pp. 138–147.

[134] A. QUARTERONI AND A. VALLI, *Theory and application of Steklov-Poincaré operators for boundary-value problems: the heterogeneous operator case*, in Fourth International Symposium on Domain Decomposition Methods for Partial Differential Equations (Moscow, 1990), SIAM, Philadelphia, PA, 1991, pp. 58–81.

[135] A. QUARTERONI AND A. VALLI, *Domain decomposition methods for partial differential equations*, Numerical Mathematics and Scientific Computation, The Clarendon Press, Oxford University Press, New York, 1999. Oxford Science Publications.

[136] P.-A. RAVIART AND J.-M. THOMAS, *Introduction à l'analyse numérique des équations aux dérivées partielles*, Collection Mathématiques Appliquées pour la Maîtrise. [Collection of Applied Mathematics for the Master's Degree], Masson, Paris, 1983.

[137] S. Repin, S. Sauter, and A. Smolianski, *Two-sided a posteriori error estimates for mixed formulations of elliptic problems*, SIAM J. Numer. Anal., 45 (2007), pp. 928–945.

[138] S. I. Repin, *A posteriori estimates for partial differential equations*, vol. 4 of Radon Series on Computational and Applied Mathematics, Walter de Gruyter GmbH & Co. KG, Berlin, 2008.

[139] S. I. Repin and A. Smolianski, *Functional-type a posteriori error estimates for mixed finite element methods*, Russian J. Numer. Anal. Math. Modelling, 20 (2005), pp. 365–382.

[140] V. Rey, P. Gosselet, and C. Rey, *Strict lower bounds with separation of sources of error in non-overlapping domain decomposition methods*, Internat. J. Numer. Methods Engrg., 108 (2016), pp. 1007–1029.

[141] V. Rey, C. Rey, and P. Gosselet, *A strict error bound with separated contributions of the discretization and of the iterative solver in non-overlapping domain decomposition methods*, Comput. Methods Appl. Mech. Engrg., 270 (2014), pp. 293–303.

[142] J. E. Roberts and J.-M. Thomas, *Mixed and hybrid methods*, in Handbook of Numerical Analysis, Vol. II, , North-Holland, Amsterdam, 1991, pp. 523–639.

[143] Y. Saad, *Iterative methods for sparse linear systems*, Society for Industrial and Applied Mathematics, Philadelphia, PA, second ed., 2003.

[144] H. A. Schwarz, *Gesammelte mathematische Abhandlungen. Band I, II*, Chelsea Publishing Co., Bronx, N.Y., 1972. Nachdruck in einem Band der Auflage von 1890.

[145] J. O. Skogestad, E. Keilegavlen, and J. M. Nordbotten, *Domain decomposition strategies for nonlinear flow problems in porous media*, J. Comput. Phys., 234 (2013), pp. 439–451.

[146] ——, *Two-scale preconditioning for two-phase nonlinear flows in porous media*, Transp. Porous Media, 114 (2016), pp. 485–503.

[147] R. Stenberg, *Postprocessing schemes for some mixed finite elements*, RAIRO Modél. Math. Anal. Numér., 25 (1991), pp. 151–167.

[148] J.-M. Thomas, *Sur l'analyse numérique des méthodes d'éléments finis hybrides et mixtes*, Ph.D. thesis, University Paris 6, 1977.

[149] V. Thomee, *Galerkin Finite Element Methods for Parabolic Problems*, Springer, 1997.

[150] A. Toselli and O. Widlund, *Domain decomposition methods—algorithms and theory*, vol. 34 of Springer Series in Computational Mathematics, Springer-Verlag, 2005.

[151] C. J. Van Duijn, J. Molenaar, and M. J. De Neef, *The effect of capillary forces on immiscible two-phase flow in heterogeneous porous media*, Transport in Porous Media, 21 (1995), pp. 71–93.

[152] R. VERFÜRTH, *A posteriori error estimates for finite element discretizations of the heat equation*, Calcolo, 40 (2003), pp. 195–212.

[153] R. VERFÜRTH, *A posteriori error estimation techniques for finite element methods*, Numerical Mathematics and Scientific Computation, Oxford University Press, Oxford, 2013.

[154] M. VOHRALÍK, *A posteriori error estimates for lowest-order mixed finite element discretizations of convection-diffusion-reaction equations*, SIAM J. Numer. Anal., 45 (2007), pp. 1570–1599.

[155] ——, *Residual flux-based a posteriori error estimates for finite volume and related locally conservative methods*, Numer. Math., 111 (2008), pp. 121–158.

[156] ——, *Unified primal formulation-based a priori and a posteriori error analysis of mixed finite element methods*, Math. Comp., 79 (2010), pp. 2001–2032.

[157] ——, *Guaranteed and fully robust a posteriori error estimates for conforming discretizations of diffusion problems with discontinuous coefficients*, J. Sci. Comput., 46 (2011), pp. 397–438.

[158] M. VOHRALÍK AND M. F. WHEELER, *A posteriori error estimates, stopping criteria, and adaptivity for two-phase flows*, Comput. Geosci., 17 (2013), pp. 789–812.

[159] M. F. WHEELER AND I. YOTOV, *A posteriori error estimates for the mortar mixed finite element method*, SIAM J. Numer. Anal., 43 (2005), pp. 1021–1042.

[160] O. B. WIDLUND, *Iterative substructuring methods: algorithms and theory for elliptic problems in the plane*, in First International Symposium on Domain Decomposition Methods for Partial Differential Equations (Paris, 1987), SIAM, Philadelphia, PA, 1988, pp. 113–128.

[161] B. I. WOHLMUTH, *A residual based error estimator for mortar finite element discretizations*, Numer. Math., 84 (1999), pp. 143–171.

[162] B. I. WOHLMUTH AND R. H. W. HOPPE, *A comparison of a posteriori error estimators for mixed finite element discretizations by Raviart–Thomas elements*, Math. Comp., 68 (1999), pp. 1347–1378.

[163] I. YOTOV, *A mixed finite element discretization on non-matching multiblock grids for a degenerate parabolic equation arising in porous media flow*, East-West J. Numer. Math., 5 (1997), pp. 211–230.

[164] I. YOTOV, *Interface solvers and preconditioners of domain decomposition type for multiphase flow in multiblock porous media*, in Scientific computing and applications (Kananaskis, AB, 2000), vol. 7 of Adv. Comput. Theory Pract., Nova Sci. Publ., Huntington, NY, 2001, pp. 157–167.